



Durham E-Theses

Langmuir-Blodgett films for non-linear optics

Neal, D. B.

How to cite:

Neal, D. B. (1987) *Langmuir-Blodgett films for non-linear optics*, Durham theses, Durham University.
Available at Durham E-Theses Online: <http://etheses.dur.ac.uk/9527/>

Use policy

The full-text may be used and/or reproduced, and given to third parties in any format or medium, without prior permission or charge, for personal research or study, educational, or not-for-profit purposes provided that:

- a full bibliographic reference is made to the original source
- a [link](#) is made to the metadata record in Durham E-Theses
- the full-text is not changed in any way

The full-text must not be sold in any format or medium without the formal permission of the copyright holders.

Please consult the [full Durham E-Theses policy](#) for further details.

The copyright of this thesis rests with the author.
No quotation from it should be published without
his prior written consent and information derived
from it should be acknowledged.

LANGMUIR-BLODGETT FILMS
FOR NON-LINEAR OPTICS

by

D. B. Neal, B.Sc.

A Thesis submitted for the Degree of
Doctor of Philosophy in the
University of Durham

March 1987



21 MAY 1987

DECLARATION

I hereby declare that the work carried out in this thesis has not previously been submitted for any degree and is not being currently submitted in candidature for any other degree.

Signed David Neal

The work carried out in this thesis was carried out by the candidate.

Signed McCarthy

.....
Directors of Studies

..... David Neal

Candidate

ACKNOWLEDGEMENTS

During the course of my research at Durham I have become indebted to numerous people, to whom I would now like to express my gratitude. Primarily, I wish to thank my supervisors, Dr. Mike Petty and Professor Gareth Roberts, for the time and effort they have devoted to directing and encouraging my studies. I have found working with them to be a highly rewarding and pleasurable experience. I am also grateful to everyone in the Department of Applied Physics and Electronics for their constant friendship and sharing of ideas, and in particular to the technical staff, headed by Mr. Frank Spence, who have contributed their skills and knowledge. My thanks also go to Mrs. Pauline Morrell for her patience in typing this thesis and to Mr. Norman Thompson for his proficiency in preparing the diagrams.

I would like to thank Dr. Graham Russell for his assistance in the electron diffraction studies, and Dr. Jonathan Lloyd for his advice and the use of his SPR equipment. I greatly appreciate the efforts made by Dr. Munir Ahmad and Dr. James Feast in synthesising the many compounds described in this thesis, without which the project could not have been undertaken. The measurements of second harmonic generation from LB films were performed in collaboration with Drs. I. R. Peterson, I. R. Girling, P. V. Kolinsky, and N. A. Cade of GEC Hirst Research Laboratories, whose co-operation has been invaluable to the success of this research. I would also like to thank Dr. Julian Hill of British Telecom Research Laboratories for supplying the theoretical hyperpolarizability data, and Dr. Martin Goodwin of Plessey Research (Caswell) Ltd. for the use of his powder SHG equipment. I gratefully acknowledge the financial support given to me by the SERC and Plessey Research (Caswell) Ltd.; the work was partly funded under a Joint Opto-Electronics Research Scheme (JOERS).

A great many close personal friends have helped me in recent years; I am particularly indebted to Mr. M. Lyons for his constant support in times of crisis. Lastly, but most importantly, thanks to my mother, brother and sister for their unwavering faith and encouragement over the years.

ABSTRACT

In recent years there has been considerable interest in media which display significant non-linear optical properties; the telecommunications industry may exploit thin films of such materials for signal processing applications. The Langmuir-Blodgett (LB) technique provides a means of depositing organic layers of a precisely defined thickness. Moreover, by alternating layers of different materials, supermolecular arrays may be fabricated in which there is no centrosymmetry, and therefore the second-order non-linearity of the constituent molecules may be exploited.

An investigation of the properties of water-surface monolayers of a number of novel materials with potentially large non-linearities is described. Several of these compounds are shown to form high quality homogeneous or heterogeneous LB films. The optical and electrical properties of the layers are characterized by optical absorption spectroscopy, surface plasmon resonance, and measurements of capacitance, whilst their structure is examined by electron diffraction. Monolayers of a nitrostilbene dye are shown to exhibit an exceptionally high degree of crystalline order. Data are also given for theoretical calculations of non-linear coefficients and for the relative efficiency of second harmonic generation from bulk samples of various materials.

Studies of second harmonic generation from monolayer and alternate multilayer films are reported. Optical non-linearity in an alternating donor-acceptor: inverted donor-acceptor dye system is demonstrated for the first time; the results are analysed in terms of second harmonic surface susceptibilities, and the value of the second-order hyperpolarizability determined for the first bilayer is found to be much superior to that expected by the simple addition of the hyperpolarizabilities of the separate layers. Monolayers containing a mixture of hemicyanine and cadmium arachidate are found to give rise to second harmonic generation which is enhanced relative to that obtained from a pure monolayer of the dye. Corresponding changes in the absorption spectra of the layers can be observed. These findings may have important implications for improving the efficiencies of any non-linear optical device which utilises LB films.

CONTENTS

	<u>Page</u>
<u>CHAPTER 1 - INTRODUCTION</u>	1
<u>CHAPTER 2 - NON-LINEAR OPTICAL EFFECTS</u>	
2.0 Introduction	3
2.1 Origin and Classification of Non-Linear Optical Effects	3
2.1.0 Background	
2.1.1 Physical origins	
2.1.2 Linear polarization	
2.1.3 Quadratic polarization	
2.1.4 Cubic polarization	
2.2 A Comparison of Available Materials	10
2.3 Optimization of Organic Materials	12
2.3.1 General	
2.3.2 Optimization of molecular structure	
2.3.3 Crystal structure considerations	
2.3.4 Implementation of the principles for the optimization of non-linear response	
2.4 Applications of Non-Linear Optical Phenomena	24
<u>CHAPTER 3 - LB FILM TECHNOLOGY</u>	
3.0 Introduction	27
3.1 Basic Concepts	27
3.2 Materials	28
3.2.1 Classical materials	
3.2.2 Novel materials from the literature	
3.2.3 Novel materials used in this project	
3.3 The Conventional Langmuir Trough	32
3.3.1 Mechanical construction	
3.3.2 Instrumentation	
3.3.3 Reduction of contamination	
3.4 The Alternate Layer Langmuir Trough	36
3.4.1 Mechanical construction	
3.4.2 Instrumentation	
3.4.3 Cross-contamination	

	<u>Page</u>
3.5 Properties of the Water-Surface Monolayer	38
3.5.1 Pressure-area isotherms	
3.5.2 Decay in surface area with time	
3.5.3 Monolayer mobility	
3.6 Experimental Techniques	41
3.6.1 Monolayer spreading	
3.6.2 Monolayer compression	
3.6.3 LB film deposition	
3.7 Quality Assessment	44
3.8 Possible Applications for LB Films	46
3.9 Non-Linear Optical Effects in LB Films	48
3.10 Summary	52

CHAPTER 4 - EXPERIMENTAL TECHNIQUES

4.0 Introduction	53
4.1 Device Fabrication	53
4.1.1 Substrate preparation	
4.1.2 Electrode deposition	
4.2 Measurement of the Relative Permittivity of LB Films	56
4.2.1 Experimental technique	
4.2.2 Interpretation of results	
4.3 Measurement of Optical Absorption Spectra	58
4.4 Surface Plasmon Resonance	58
4.5 Electron Diffraction	60
4.6 Kurtz Powder Technique	61
4.7 Second Harmonic Generation from LB Films	62

<u>CHAPTER 5 - MONOLAYER CHARACTERIZATION : RESULTS AND DISCUSSION</u>	<u>Page</u>
5.0 Introduction	64
5.1 Materials	64
5.1.1 Modified commercially available materials	
5.1.2 Anthracene derivatives	
5.1.3 Dipolar chromophores	
5.2 The Interpretation of Pressure - Area Isotherms and Monolayer Stability Studies	67
5.2.1 Pressure-area isotherms	
5.2.2 Monolayer stability studies	
5.3 Monolayer Characterization : Results	71
5.3.1 Modified commercially available materials	
5.3.2 Anthracene derivatives	
5.3.3 Dipolar chromophores	
5.4 Film Transfer	81
5.5 Summary	83
<u>CHAPTER 6 - SOME TECHNIQUES FOR THE CHARACTERIZATION OF LB FILMS AND MATERIALS : RESULTS AND DISCUSSIONS</u>	
6.0 Introduction	85
6.1 Optical Absorption	86
6.1.0 Background	
6.1.1 Merocyanine (compound D1)	
6.1.2 Amidonitrostilbene (compound D5)	
6.1.3 Aminonitrostilbene (compound D6)	
6.1.4 Tertiary aminonitrostilbene (compound D7)	
6.1.5 Hemicyanine (compound D2)	
6.1.6 The alternate layer hemicyanine/ amidonitrostilbene system	
6.1.7 The hemicyanine/cadmium arachidate system of mixed monolayers	
6.2 Determination of the Relative Permittivity	101
6.3 Surface Plasmon Resonance Studies of Amidonitrostilbene Multilayers	103
6.4 The Kurtz Powder Technique	105
6.5 Theoretical Values for β	107
6.6 Summary	109

	<u>Page</u>
<u>CHAPTER 7 - ELECTRON DIFFRACTION STUDIES OF LB FILMS :</u>	
<u>RESULTS AND DISCUSSION</u>	
7.0 Introduction	112
7.1 Calibration of Electron Diffraction Patterns	113
7.2 C4 Anthracene (Compound A1)	115
7.2.1 Background	
7.2.2 Results	
7.2.3 Discussion and conclusions	
7.3 Amidonitrostilbene (Compound D5)	118
7.3.1 Background	
7.3.2 Effect of film thickness	
7.3.3 Effect of different substrates	
7.3.4 Effect of deposition conditions	
7.3.5 Chromophore orientation in monolayers	
7.3.6 Conclusions	
7.4 Other Materials	126
7.4.1 Aminonitrostilbene (Compound D6)	
7.4.2 Merocyanine (Compound D1)	
7.4.3 Hemicyanine (Compound D2)	
7.4.4 The hemicyanine/amidonitrostilbene alternate layer system	
7.5 Summary	129
<u>CHAPTER 8 - SECOND HARMONIC GENERATION FROM LB FILMS : RESULTS AND DISCUSSION</u>	
8.0 Introduction	131
8.1 Calibration of Experimental System	132
8.1.1 Signals normalised with respect to photodiode response	
8.1.2 Signals normalised with respect to total incident energy	
8.1.3 Signals normalised with respect to quartz	
8.2 Second Harmonic Generation from Homogeneous Monolayers	140
8.2.1 A comparison of materials	
8.2.2 Effect of in-plane anisotropy on SHG from amidonitrostilbene monolayers	

	<u>Page</u>
8.3 SHG from Alternating Layer Structures Containing Active and Passive Components	144
8.3.1 Effect of thickness	
8.3.2 Effect of angle of incidence	
8.3.3 Interference effects	
8.4 SHG from Alternating Layer Structures Containing Two Different Active Components	148
8.4.0 Background	
8.4.1 Comparison of the D2/D5 and D2/D6 systems	
8.4.2 A detailed study of the D2/D5 system	
8.4.3 Conclusions	
8.5 SHG from Heterogeneous Monolayers	162
8.5.1 The D2/cadmium arachidate system	
8.5.2 Other heterogeneous monolayer systems	
8.6 Summary	168
<u>CHAPTER 9 - CONCLUSIONS AND SUGGESTIONS FOR FURTHER WORK</u>	170
<u>APPENDICES</u>	
A1 - A5 Publications	

CHAPTER 1

INTRODUCTION

Non-linear optical phenomena, in which electromagnetic fields interact to produce new waves with a different phase, frequency, amplitude, or other propagation characteristics, may form the basis of high bandwidth optical switching and processing devices for telecommunications systems⁽¹⁾. Intense interest is being focussed onto the media which display these effects particularly strongly; not only are their non-linear optical properties important, but other characteristics, such as stability, ease of preparation, and compatibility with microelectronic processing techniques, will ultimately define the extent of their application in useful devices.

A great deal of the work on new non-linear materials has centred on bulk materials coupled to high-power lasers. However, in order to make the transition from the mere observation of non-linear effects to their actual utilization in relatively low-power semiconductor laser-driven systems, fully optimized structures must be developed, such as those employing waveguiding in thin films or fibres⁽²⁾. One particularly elegant technique, pioneered by Langmuir and Blodgett⁽³⁾, enables amphiphilic organic molecules to be assembled into layers of a very precisely defined symmetry and thickness. Moreover, by alternately depositing monomolecular layers of two different materials, supermolecular arrays may be fabricated possessing the non-centrosymmetric crystal structure requisite for a medium to exhibit second-order optical non-linearity. In this thesis the production and subsequent characterization of Langmuir-Blodgett (LB) films of some novel materials, whose molecular structures were engineered to give large non-linear effects, is described.



A general introduction to non-linear effects, their origins, classification, and applications, is given in chapter 2. Furthermore, a comparison of materials which exhibit significant second-order non-linearities is presented, together with some guidelines for the synthesis of highly efficient organic materials. LB film technology is reviewed in chapter 3; this includes a description of the materials, experimental methods, basic characterization techniques, and equipment associated with the process. A discussion of the possible applications of the deposited films, particularly in non-linear optical devices, is also given. Other experimental techniques, such as those employed in the study of the optical, dielectric, structural, or non-linear optical properties of the layers, are detailed in chapter 4.

Most of the experimental results appear in chapters 5-8. The first of these deals with the screening of new materials for LB film formation and the optimization of deposition conditions, whilst the next is concerned with the initial characterization of these films and the bulk materials from which they were derived. Details of the structural characteristics of monolayer and multilayer arrays of various materials, as revealed by electron diffraction studies, are given in chapter 7. Data obtained from the investigation of second harmonic generation from different acentric LB film structures are compared and discussed in chapter 8. Finally, the closing chapter contains a summary of the conclusions of this thesis, and some suggestions for further work.

CHAPTER 2

NON-LINEAR OPTICAL EFFECTS

2.0 Introduction

This chapter is concerned with a general discussion of non-linear optical effects and materials. Following a brief introduction, in which the roots of non-linear behaviour in electromagnetic theory are examined, together with the technological progress which has made such effects significant, the physical origins of non-linearity are discussed. The various non-linear optical phenomena are then classified according to the order of the polarization field associated with them. A comparison of the organic and inorganic materials in current use is given in section 2.2, whilst section 2.3 details the molecular and structural features required for an organic material to display highly non-linear behaviour, and how they can be obtained in practice. Finally, section 2.4 deals with the applications of non-linear optical phenomena.

2.1 Origin and Classification of Non-Linear Optical Effects

2.1.0 Background

Advances in non-linear optics have relied heavily on the development of Q-spoiled lasers⁽⁴⁾. Such lasers have outputs consisting of a series of intense coherent pulses, typically 30-100 ns long, in which the power density is a few MW cm^{-2} . For a power density of 1 MW cm^{-2} , the peak electric field strength in a pulse is $E_1 = 30 \text{ kV cm}^{-1}$, a figure which is still very small when compared to typical atomic field strengths: $E_a \sim 3 \times 10^5 \text{ kV cm}^{-1}$. However, under ideal conditions the characteristic length for significant second harmonic generation (SHG) or parametric amplification is⁽⁴⁾ $L \sim \lambda E_a/E_1$ where $\lambda \sim 10^{-4} \text{ cm}$ is the

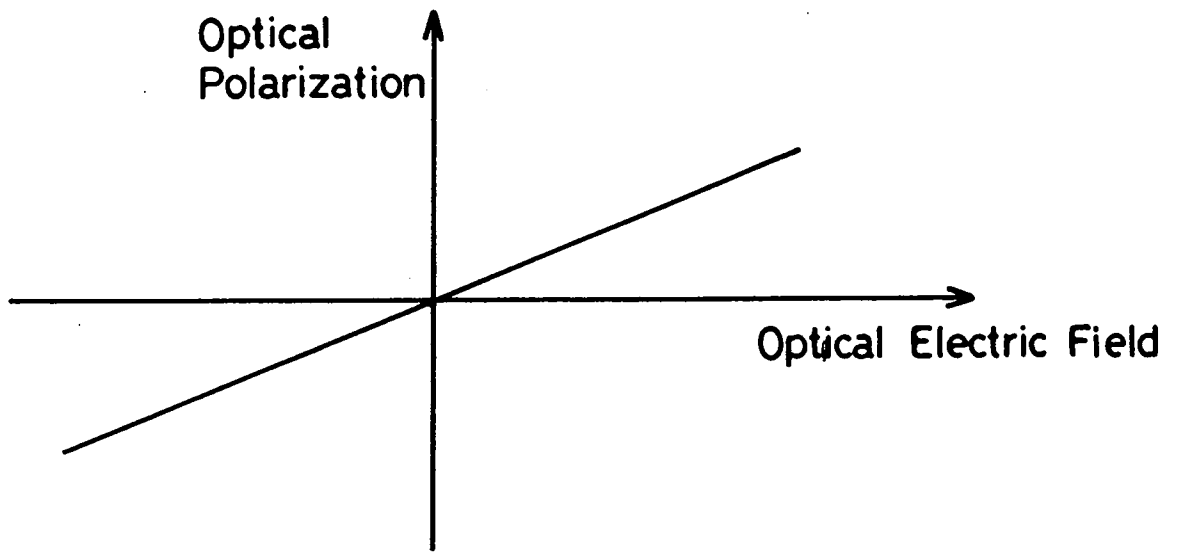
wavelength of the light. Thus $L \sim 1 \text{ cm}$ for a power density of 1 MW cm^{-2} , and since much higher power densities than this can be achieved either by focussing the pulse with a lens system or by amplifying it with a laser amplifier it is now possible to achieve significant non-linear optical effects in samples of suitable materials with dimensions smaller than a centimetre.

2.1.1 Physical Origins

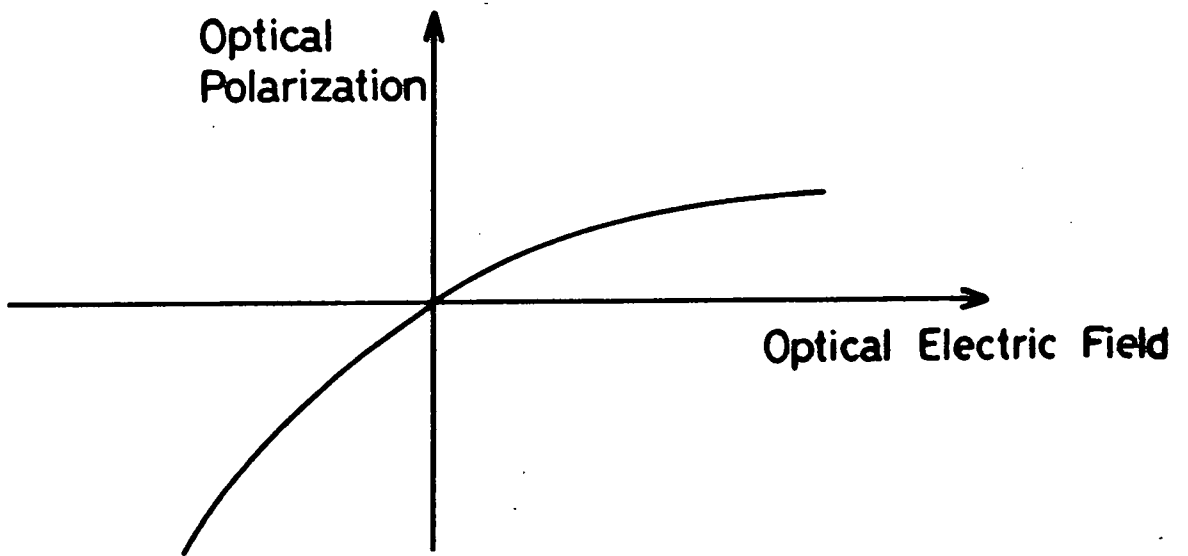
Maxwell's equations are a set of perfectly linear equations which, when taken with a set of "constitutive" relations, form the basis of electromagnetic theory. The constitutive relations connect the moment of the charge and current distributions in the medium to the electric and magnetic fields in order to describe the response of the medium to an electromagnetic wave, and they are not linear⁽¹⁾. However, in conventional optics the relations are linearized and, for example, the superposition principle can be applied. In linear optics, waves do not interact and change their frequencies. Alternatively, when the constitutive relations are retained in their full form, the origins of non-linear optical processes become apparent. A rigorous theoretical treatment will not be given here; instead a more simplistic approach will be taken which yields the same important equations for describing the effects.

The propagation of electromagnetic radiation through linear media produces a polarization, P , which is proportional to the electric field, E , that induces it (figure 2.1a). However, this linear polarization is really only the first term in the power series⁽²⁾ given in equation 2.1:

$$P - P_0 = \epsilon_0 \chi^{(1)} E + \epsilon_0 \chi^{(2)} E E + \epsilon_0 \chi^{(3)} E E E + \dots \quad (2.1)$$



(a) Linear dielectric



(b) Nonlinear dielectric

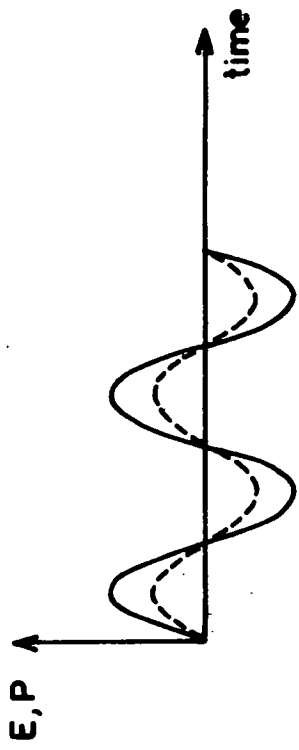
Figure 2.1

Relation between induced polarization and the electric field causing it.

where P_0 is the polarization with zero applied field, ϵ_0 is the permittivity of free space, $\chi^{(1)}$ is the linear susceptibility, and $\chi^{(n)}$ is the n^{th} order susceptibility tensor of the medium. The higher order terms in this equation are only significant in materials with large non-linear susceptibilities and at high optical fields. Figure 2.1b illustrates the relationship between the polarization and the optical field in a non-linear medium. The oscillations in the polarization of linear and non-linear dielectrics as a result of an applied sinusoidal electric field are illustrated in figure 2.2.

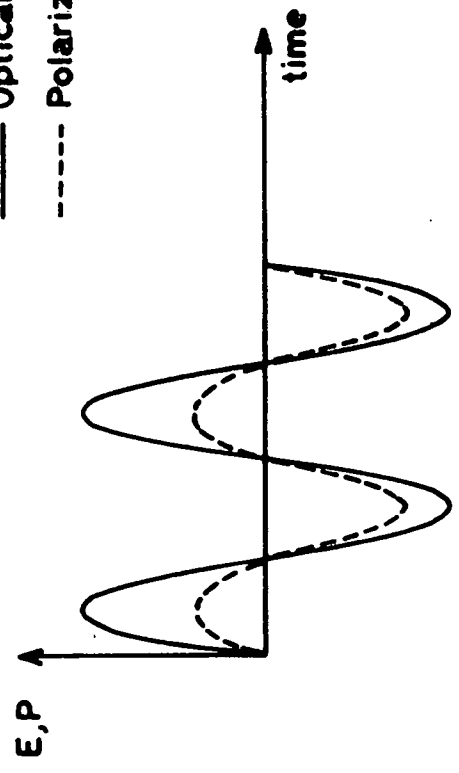
The optical polarization of dielectric crystals is due mostly to the outer, loosely bound valence electrons that are displaced by the optical field⁽³⁾. This displacement is governed by the restoring force acting on the electrons, which in turn is determined by their potential energy. Using a one-dimensional analogue, the potential energy (V) of an electron in a dielectric crystal may be written as a power series in terms of displacement (x) of the electron from its equilibrium position, and it is the higher order terms in this series which give rise to the non-linear susceptibilities. Terms in $V(x)$ which contain even powers of x give rise to the odd-order susceptibilities (such as linear and cubic) whilst those containing odd powers of x give rise to the even-order susceptibilities (such as quadratic). In symmetric crystals the potential energy of an electron must reflect the crystal symmetry i.e. $V(x) = V(-x)$, therefore $V(x)$ contains only even powers of x and the crystal has zero even-order susceptibilities. This is not the case in noncentrosymmetric crystals where $V(x) \neq V(-x)$ and the even-order susceptibilities are finite.

In sections 2.1.2 - 2.1.4 a variety of effects arising from each term in equation 2.1 are introduced in turn. For the moment, the vector



(a) Linear dielectric

— Optical field (E)
 - - - Polarization (P)



(b) Nonlinear dielectric

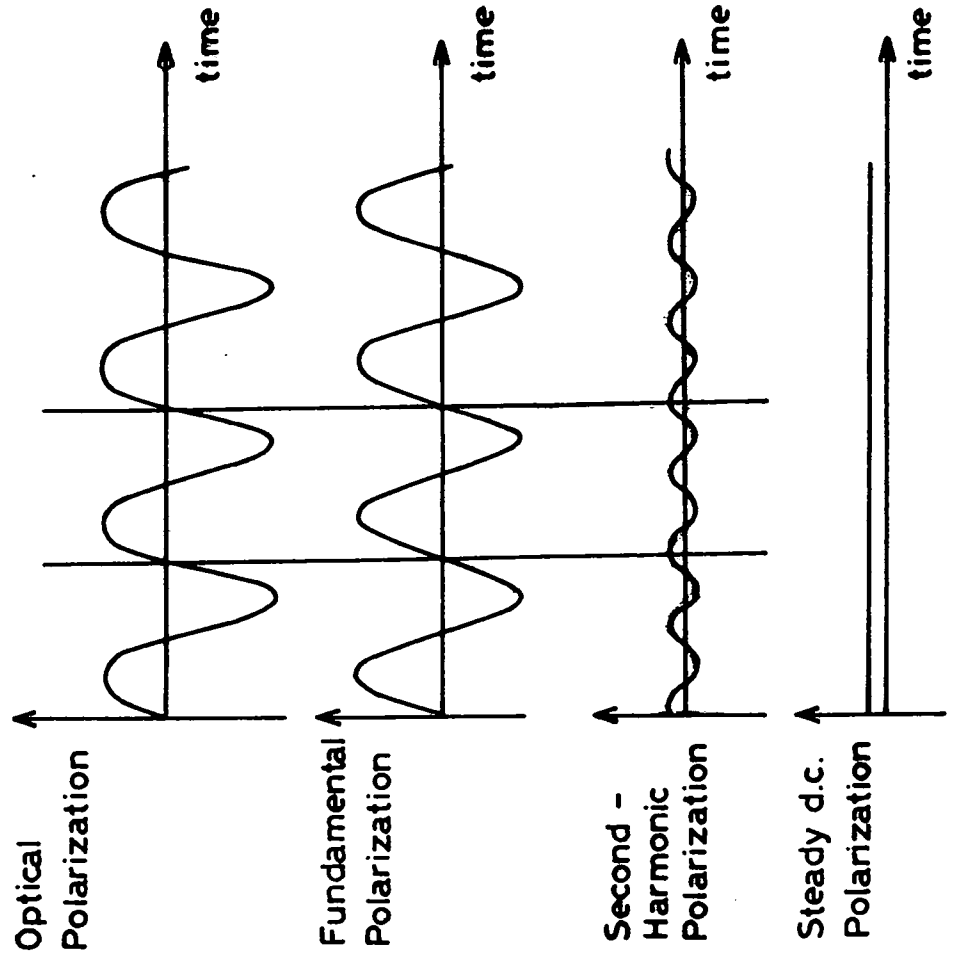


Figure 2.3

Components of the non-linear polarization wave of figure 2.2b.

Figure 2.2

Polarization resulting from an applied sinusoidal electric field.

character of the electric field and the polarization, and the tensor character and frequency dependence of the susceptibilities, will be ignored. Most of the more useful and practically realisable effects involve the quadratic polarization (section 2.1.3) and therefore the bulk of later discussions are restricted to this term.

2.1.2 Linear Polarization : $P^{(1)} = \epsilon_0 \chi^{(1)} E$

The linear polarization is responsible for refraction and attenuation. When the applied optical field is a wave with a frequency ω , the linear polarization also has frequency ω , radiating into the medium and modifying the way in which the wave propagates.

The electric flux density, D , is given by

$$D = \epsilon_0 E + P^{(1)} = \epsilon_0 \epsilon_r E$$

where ϵ_r is the dielectric constant. It therefore follows that $\epsilon_r = 1 + \chi^{(1)}$. Now, the refractive index, n , is given by

$$n = \frac{c}{v} = \left(\frac{\epsilon \mu}{\epsilon_0 \mu_0} \right)^{\frac{1}{2}} = (\epsilon_r \mu_r)^{\frac{1}{2}}$$

where v , c are the velocities of light in the medium and in vacuum, respectively. If a relative permeability (μ_r) of unity is assumed then the refractive index will be $(1 + \chi^{(1)})^{\frac{1}{2}}$ and the propagation constant, k , is $(1 + \chi^{(1)})^{\frac{1}{2}} \omega/c$. In practice $\chi^{(1)}$ is a complex quantity and the component of $P^{(1)}$ in quadrature with the field results in losses and hence attenuation.

When the optical field contains several waves at different frequencies they propagate independently of one another in the linear regime.

2.1.3 Quadratic Polarization : $P^{(2)} = \epsilon_0 \chi^{(2)} EE$

The effects arising from the quadratic polarization are basically all mixing phenomena, involving the generation of sum and difference frequencies, but they take a variety of different forms.

- (i) When the applied optical field contains only one frequency, such as in figure 2.2b, a Fourier analysis of the non-linear polarization wave shows that it contains an average (d.c.) term and a term oscillating at twice the applied frequency (see figure 2.3). This can readily be seen for a light wave of the form $E = E_0 \sin \omega t$, giving a quadratic polarization of the form

$$P^{(2)} = \epsilon_0 \chi^{(2)} E_0^2 \sin^2 \omega t$$

which can be rewritten as

$$P^{(2)} = \frac{\epsilon_0 \chi^{(2)}}{2} E_0^2 (1 - \cos 2\omega t)$$

The d.c. polarization produces a d.c. electric field in the medium (optical rectification), and the polarization at twice the applied frequency radiates into the medium (second harmonic generation).

- (ii) When the optical field contains two frequencies a new range of effects occur.

(a) The simplest case is where one of the frequencies is zero (monochromatic wave propagated through the medium in the presence of a d.c. electric field). $P^{(2)}$ then contains a term which is proportional to the product of the d.c. and optical fields, leading to an extra term in the total polarization which is linear in the optical field and whose magnitude is proportional to the d.c. field. The effect of this extra term on the optical wave is equivalent to changing $\chi^{(1)}$ by an amount proportional to the d.c. field. The refractive index at the optical frequency is thus dependent on the d.c. field; this is the linear electrooptic or Pockels effect.

(b) If a small optical signal (frequency ω_s) is propagated through the medium in the presence of a powerful "pump" optical field (at a higher frequency ω_p) the phenomenon of parametric amplification occurs. The pump and signal beat together to produce an "idler field" proportional to the product of the pump and signal fields and having the difference frequency $\omega_i = \omega_p - \omega_s$. A further beating action then takes place between the idler and pump to produce a term in the polarization (at the difference frequency $\omega_p - \omega_i = \omega_s$) which is proportional to the product of the signal field and the pump intensity. Thus, as a result of this double beating action, there is an extra term in the total polarization which is linear in the signal field and whose effect on the latter is equivalent to changing $\chi^{(1)}$ by an amount proportional to the pump intensity. Hence the propagation constant at

the signal frequency depends on the pump intensity. This effect is called parametric interaction because the pump field may be regarded as modulating the parameter $\chi^{(1)}$ at the pump frequency. The phenomenon is maximised when the linear propagation constants k_s , k_i and k_p at the frequencies ω_s , ω_i and ω_p , respectively, satisfy the "phase-matching" condition given in equation (2.2).

$$k_s + k_i = k_p \quad (2.2)$$

The concept of phase-matching arises in connection with a range of optical mixing phenomena, and a more detailed discussion is given in section 2.3.3 with second harmonic generation being taken as an example.

2.1.4 Cubic Polarization: $P^{(3)} = \epsilon_0 \chi^{(3)} EEE$

For a monochromatic wave of the form $E = E_0 \sin \omega t$ we have

$$\begin{aligned} P^{(3)} &= \epsilon_0 \chi^{(3)} E_0^3 \sin^3 \omega t \\ &= \frac{\epsilon_0 \chi^{(3)}}{4} E_0^3 (3 \sin \omega t - \sin 3\omega t) \end{aligned}$$

Thus the cubic polarization gives rise to third harmonic generation and related mixing phenomena. An example of such a phenomenon is the change in refractive index which occurs when a monochromatic wave propagates through the medium in the presence of a d.c. field. This change is proportional to the square of the d.c. field and is the quadratic

electrooptic or Kerr effect frequently used in the electronic shutter in Q-spoiled lasers.

As well as the low frequency, essentially classical, mixing phenomena, $P^{(3)}$ also gives rise to some quantal effects which arise for certain frequency combinations when a small signal wave of frequency ω_s propagates through the medium in the presence of a strong pump wave at frequency ω_p . If ω_s and ω_p are selected such that $\omega_p + \omega_s = \omega_t$, where ω_t is some transition frequency of the medium, then the transition can take place through the simultaneous absorption of a pump and a signal photon. This process of two-photon absorption produces signal attenuation even though the signal frequency itself is not equal to a transition frequency of the medium, unlike one-photon absorption processes which arise from $\chi^{(1)}$ and which disappear when $\omega_s \neq \omega_t$. Conversely, if ω_s and ω_p are chosen such that $\omega_p - \omega_s = \omega_t$, then the transition can take place by the simultaneous absorption of a pump photon and emission of a signal photon, resulting in signal amplification. In this stimulated Raman effect the signal field stimulates the emission of signal photons, unlike the incoherent Raman effect where the transitions are spontaneous. The two-photon effects both arise from the term in $P^{(3)}$ which is proportional to the product of the signal field and the pump intensity. The effect of this term on the signal wave is equivalent to changing $\chi^{(1)}$ by an amount proportional to the pump intensity, the propagation constant at the signal frequency being similarly modified.

2.2 A Comparison of Available Materials

Most of the non-linear optical materials in current use are inorganic solids, such as lithium niobate and potassium dihydrogen

phosphate (KDP). Their use has primarily stemmed from earlier work on the piezoelectric, ferroelectric, and semiconductor transport properties of inorganic dielectric insulators and semiconductors. However, much interest has recently been directed to organic molecular and polymeric solids⁽⁵⁾ due to their exceptionally large second-order susceptibilities and the potentially wide range of crystal structures which they could adopt (see section 2.3.4). A comparison of non-linear optical figures of merit for organic and inorganic solids is given in figure 2.4. The quantities compared are Miller's delta (δ) for second harmonic generation and the polarization optic coefficient (f) for the linear electrooptic effect. Miller's delta is defined⁽⁶⁾ by equation 2.3:

$$d_{ijk} = \epsilon_o \chi_{ii}^{(1)} \chi_{jj}^{(1)} \chi_{kk}^{(1)} \delta_{ijk} \quad (2.3)$$

where terms such as $\chi_{ii}^{(1)}$ are the linear susceptibility components, and the second harmonic coefficient, d_{ijk} , is defined through equation 2.4.

$$\chi_{ijk}^{(2)}(-2\omega; \omega, \omega) = 2 d_{ijk}(-2\omega; \omega, \omega) \quad (2.4)$$

The general notation used when describing $\chi^{(2)}$ coefficients for particular non-linear optical effects can be summarized as follows⁽⁷⁾: if the coefficient is written as $\chi_{ijk}^{(2)}(-\omega_3; \omega_2, \omega_1)$, then i, j, k refer to the principal axes of the medium and indicate the tensorial characteristics of $\chi^{(2)}$; the frequency arguments refer to the production of a field of frequency ω_3 from input frequencies ω_1 and ω_2 ; the minus sign is included by convention to indicate that momentum is conserved i.e. $\underline{k}_3 + \underline{k}_2 + \underline{k}_1 = 0$ where the wave vectors point in the direction of propagation of the wave. The polarization optic coefficient is defined by equation 2.5 :

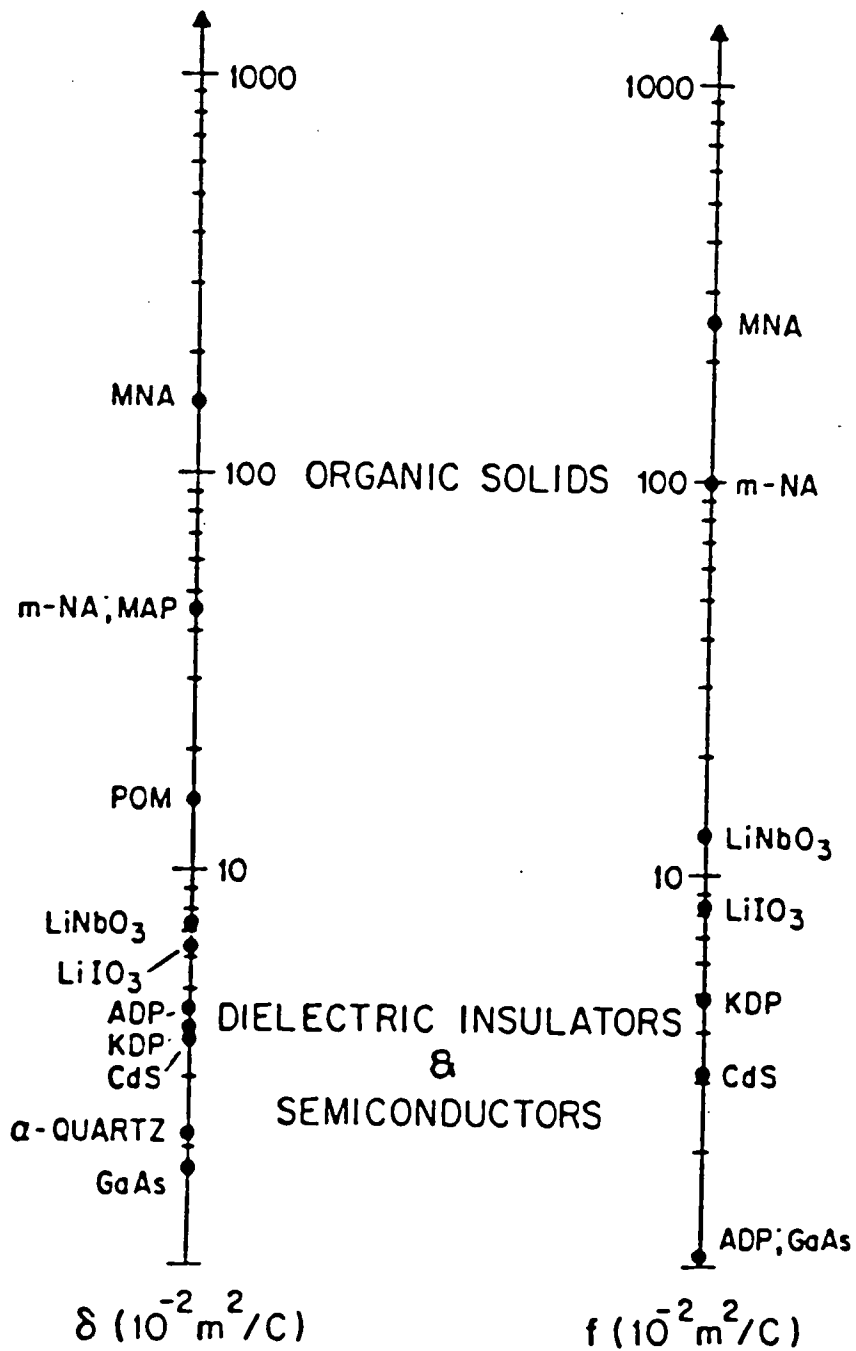


Figure 2.4

Comparative quantities for selected tensor components of second harmonic generation (δ) and the linear electro-optic effect (f). (After reference 5)

$$r_{ijk} = \epsilon_0 (\epsilon_k - 1) f_{ijk} \quad (2.5)$$

where ϵ_k is the dielectric constant, and the linear electrooptic coefficient, r_{ijk} , is defined by equation 2.6 :

$$\chi_{ijk}^{(2)}(-\omega; \omega, 0) = \frac{1}{2} n_{ii}^2 n_{jj}^2 r_{ijk}(-\omega; \omega, 0) \quad (2.6)$$

where n_{ii} is the refractive index. Although dispersion and the possible contribution of atomic and molecular distortions to the electro-optic $\chi^{(2)}$ tensor means that in principle it is not equal to the second harmonic generation $\chi^{(2)}$ tensor, in practice the predominance of electronic contributions in organic materials causes them to be nearly the same.

Organic materials have been found to have the highly desirable property of high optical damage thresholds at the high optical power densities employed in non-linear optical devices⁽⁸⁾.

Section 2.3 will deal exclusively with the optimization of the molecular and crystal structures of organic materials, in view of their exceptional advantages over the conventional inorganics for non-linear optical applications. Particular emphasis will be given to second-order non-linear effects, especially second harmonic generation, for which the crystal structure requirements are particularly demanding.

2.3 Optimization of Organic Materials

2.3.1 General

The molecules within a molecular crystal are located at geometrically equivalent sites and the intermolecular forces between

them are very weak (one or two orders of magnitude smaller) compared to the intramolecular covalent bonds which bind the atoms within each molecule. This scaling of forces allows each molecule within the crystal, to a first approximation, to be treated as an individual centre of non-interacting polarization. The molecular dipole can then be described by equation (2.7), and clear correspondence can be seen between terms in this equation and terms in equation (2.1) describing the bulk polarization of the crystal.

$$\Delta\mu = \mu_e - \mu_g = \alpha E_1 + \beta E_1 E_1 + \gamma E_1 E_1 E_1 + \dots \quad (2.7)$$

(μ_g and μ_e are the ground and excited state dipole moments, respectively; E_1 is the local field, α is the linear polarizability, and β, γ are molecular hyperpolarizabilities).

Taking the example of the second harmonic generation coefficient, d_{IJK} , one can make use of the fact that non-linear processes are basically intramolecular in nature in order to relate corresponding terms in the macroscopic and microscopic dipoles expansions via tensorial summations⁽⁹⁻¹¹⁾ such as that given in equation 2.8:

$$d_{IJK} = N f_I^{2\omega} f_J^\omega f_K^\omega b_{IJK} \quad (2.8)$$

where N is the number of molecules per unit volume (packing density factor); the Lorentz local field correction appropriate for crystal axis L at frequency ν is $f_L^\nu = \frac{[(n_L^\nu)^2 + 2]}{3}$; and the crystalline non-linearity

per molecule, b_{IJK} , can be related to the second-order molecular hyperpolarizability, β_{ijk} , by equation 2.9:

$$b_{IJK} = \frac{1}{n(g)} \sum_{ijk} \sum_{s=1}^{n(g)} C_{Ii}^{(s)} C_{Jj}^{(s)} C_{Kk}^{(s)} \beta_{ijk} \quad (2.9)$$

where IJK (ijk) are axis denominations of the crystalline (molecular) reference frames; n(g) is the number of equivalent positions in the unit cell for the crystal point symmetry group g; and the $C_{Li}^{(s)}$ coefficients are the scalar products $\hat{L} \cdot \hat{l}(s)$ of unit vectors along the crystal axis \hat{L} and molecular axis $\hat{l}(s)$. The tensor b_{IJK} is a useful quantity, being independent of the actual number of molecules within the unit cell, which could be a (sub) multiple of n(g).

The combined influences of molecular and crystalline structure on the enhancement of the macroscopic optical non-linearity are evidenced by equation 2.9. The molecules should be designed to contain specific features which will maximize β_{ijk} , but the projection factors of equation 2.9 imply that the molecules must also be arranged in a crystalline structure which can promote the optimum responses of the individual molecules on a macroscopic level.

2.3.2 Optimization of molecular structure

This section is devoted to the molecular engineering required to optimize β for a molecule and neglects any additional constraints arising from crystal structure considerations.

The dipole moment of a molecule is defined by equation 2.10 :

$$\underline{\mu} = e \underline{l} \quad (2.10)$$

where e is the magnitude of the charge separated by the vectorial distance \underline{l} . Equation 2.7 shows that a large value of $\Delta\mu$ is desirable for non-linear effects, and since molecules with large ground state

dipole moments tend to have correspondingly large excited state dipole moments, the treatment of ground state dipoles is usually sufficient.

In aliphatic systems the dipole moments are usually small and the β values correspondingly low. However, large dipole moments can result from the partial charge transfer between donor and acceptor groups terminating a conjugated chain, and molecules possessing these features exhibit very large optical non-linearities. The major polarisable medium in these materials is the π -electron system, and the origin of the non-linear behaviour lies in the excited π -electron states, particularly those possessing large charge correlations⁽⁶⁾.

It is often convenient to split the contributions to the molecular (hyper)polarizabilities into those made by the length, L , of the conjugated system, and those arising from the substituent perturbations on it. It is well known that $\alpha \propto L^3$, and theory predicts⁽¹²⁾ that $\beta \propto L^3$ and $\gamma \propto L^5$. More qualitative relationships between conjugation length and β have been found; for example, the β values for substituted stilbenes are consistently an order of magnitude larger than those for comparably substituted benzene analogues. It is interesting to note that conjugated systems can be either one dimensional (as in the case of polyenes) or two dimensional (as formed by benzene-type hexagonal rings) but not three dimensional, since the conjugation arises from the electrons in p-orbitals which are not participating in sp hybridization to form the skeleton of the saturated bonds and so cannot be present if all of the four electrons are involved in four different bonding directions. The optical properties of two dimensional conjugated systems will be very different across the plane compared to parallel to it.

There have been several models proposed to explain the enhanced optical non-linearities of polarized conjugated molecules. In one such

model Oudar and Chemla relate the β of a molecule to an equivalent electric field due to the substituents which biases the hyperpolarizabilities⁽¹³⁾. The dominance of the π -electron contribution to β can be illustrated by considering a series of monosubstituted aromatic molecules such as those given in figure 2.5, which clearly demonstrates the relationship between a component of β and the π -electron dipole moment. When both donor and acceptor groups are present simultaneously and are spaced by a conjugated system, their effects are superadditive due to the phenomenon of charge transfer which involves the entire disubstituted molecule. The contribution of this effect to the optical non-linearity can be quantified⁽¹⁴⁾, and figure 2.6 demonstrates its origins. Quantum mechanical models for β have been described by various authors⁽¹¹⁾.

In order for a material to be of practical use for second harmonic generation it must be closely matched to the laser it is to double; the absorption edge should be near the wavelength of the second harmonic but must not include it⁽¹²⁾. Now, as the length of conjugation is increased there is a gradual bathochromic shift in the absorption edge (from 200nm in ethylene to a maximum in the range of 600-700 nm for an infinite series of double bonds), and the addition of donor and acceptor substituents produces a further dramatic bathochromic shift as a result of stabilization due to the mixing of nonbonded and charge-transfer states⁽¹⁵⁾. Thus there has to be a trade-off between transparency and efficiency when selecting the appropriate donor and acceptor groups and conjugated systems for a material destined to be used as a frequency doubler.

In order to select the best combinations of donors and acceptors one must consider the relative strengths of the range of available

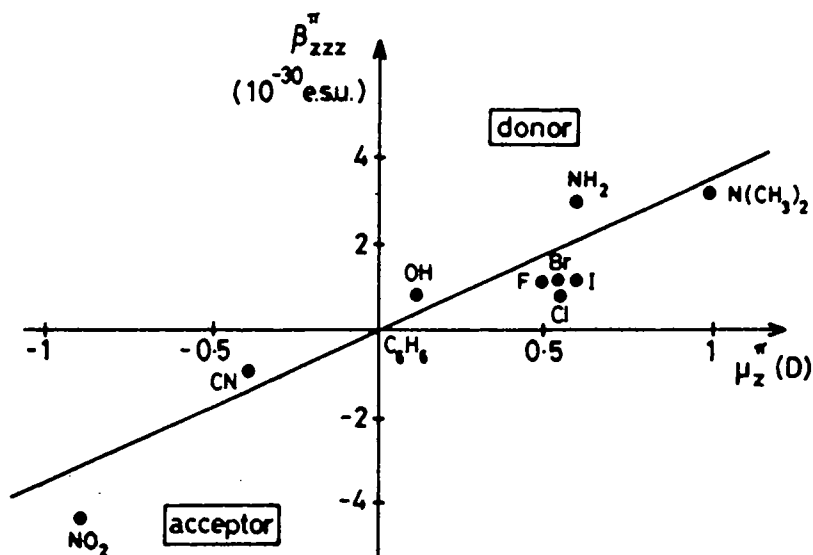


Figure 2.5

Non-linearity of some monosubstituted aromatic molecules in terms of dipole moments (π electron contributions). (After reference 11)

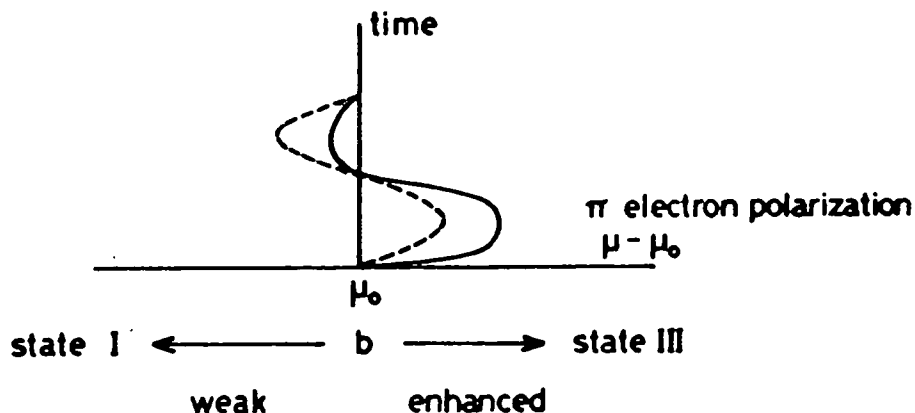
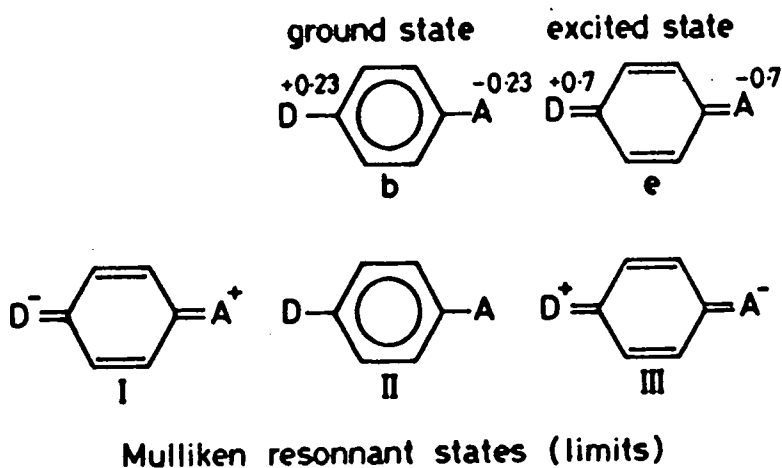


Figure 2.6

Origin of the non-linearity of charge-transfer molecules for a two-level-like disubstituted aromatic molecule. The donor (D) and acceptor (A) cooperate to distort the linear response (dotted lines) of a nonsubstituted benzene ring. (After reference 11)

groups. An approximate measure of donor strength is given by the first ionization potential of a simple, nonconjugated molecule containing the relevant group, since this represents the ease with which it releases electrons. Any atom possessing lone pair electrons in a high energy orbital, such as oxygen, nitrogen and sulphur, can act as an electron donor, provided that this lone pair is available for efficient overlap with the π -electron system of the chromophore. Table 2.1 gives the ionization potentials of the most frequently encountered neutral groupings containing these atoms⁽¹⁶⁾. From this table it can be seen that electron donating ability depends not only on the heteroatom concerned, but also on the nature of the substituents attached to it (for example electron withdrawing groups will decrease the overall strength of the donor). Imparting a negative charge to the atom, as in $-O^-$, $-S^-$, and $-NR^-$, for example by deprotonation, can greatly enhance the donor strength of a particular group.

The effectiveness of acceptor groups tends to be more variable than is the case with donor groups, and the nature of the rest of the chromophore can have an important influence. Simple acceptor groups contain at least two multiple bonded atoms, and the terminal atoms of such groupings are always more electronegative than carbon. The Hammett para σ -constant for a group gives an indication of acceptor strength, and values of this quantity for some typical acceptors are given in table 2.2⁽¹⁶⁾.

2.3.3 Crystal structure considerations

In section 2.1.1 it was pointed out that only noncentrosymmetric crystals have finite second-order susceptibilities; this is because the β tensors of the constituent molecules are orientationally averaged to zero in random ^{media} or centrosymmetric crystals. Even noncentrosymmetric

TABLE 2.1

Relative effectiveness and ionization potentials of some typical electron donor groups (taken from reference 16).

Donor group, X	Ionization Potential of CH ₃ X (eV)	Relative Effectiveness
-OAc	11.0	Least effective Most effective
-OH	10.8	
-NHAc	10.2	
-OMe	10.0	
-SH	9.4	
-NH ₂	9.0	
-SMe	8.7	
-NHMe	8.2	
-NMe ₂	7.9	

TABLE 2.2

Relative effectiveness and Hammett para σ -constants of some typical electron acceptor groups (taken from reference 16).

Acceptor Group	σ -para	Relative Effectiveness
$-\text{CO}_2^-$	0.0	Least effective
$-\text{NO}$	0.12	
$-\text{CHO}$	0.36	
$-\text{CONH}_2$	0.36	
$-\text{CO}_2\text{Me}$	0.39	
$-\text{CO}_2\text{H}$	0.41	
$-\text{SOMe}$	0.49	
$-\text{COMe}$	0.50	
$-\text{CN}$	0.66	
$-\text{SOCF}_3$	0.69	
$-\text{SO}_2\text{Me}$	0.72	
$-\text{NO}_2$	0.78	
$-\text{SO}_2\text{CF}_3$	0.93	Most Effective

crystals usually do not take full advantage of the intrinsic non-linearities of their constituent molecules, due to non-ideal packing arrangements. The molecular parameters which determine crystal structure are very subtle and mutually interactive, which makes them extremely difficult to separate. Thus it is very difficult to predict the crystal structure solely from the molecular structure, and apparently very slight changes to a molecule can result in drastic changes in the bulk packing and consequently in huge differences in non-linear efficiencies.

The crystal structure of organic materials is influenced by a variety of factors, such as molecular shape (close-packing principle), Van der Waal's forces, hydrogen bonding (if present) and multipolar interactions. These forces are all associated with much smaller energies than those involved in intramolecular bonding. Dipolar interaction energies are proportional to the square of the ground state dipole moment and are dependent on the crystal space group. The dipole energy contribution to the total intermolecular binding energy in a crystal varies slowly with structural parameters and, in general, will not bring structures out of a position of minimum energy resulting from Van der Waal's interaction in a close-packed situation⁽¹⁷⁾. However, molecules designed to have large β tensors are atypical in that they often have very large ground state dipole moments so that dipolar interactions tend to favour centrosymmetric crystal structures in which the dipoles are opposed or at least brought out of net alignment. One possible way of overcoming this undesirable influence is by the incorporation of hydrogen bonding groups into the molecules. The energies associated with hydrogen bonding are comparable with those of the dipolar forces, so that the presence of such bonding could help to bring about a favourable molecular orientation.

One way of guaranteeing a finite $\chi^{(2)}$ is to use pure enantiomers, which must crystallize noncentrosymmetrically. However, in practice great differences in efficiency are found between related optically active compounds, and such complications as racemization, optical purity and resolution, which occur in the synthesis of such materials, must be dealt with.

Apart from the enantiomeric ones, only 10 of the 32 classes of crystallographic point group which organic materials can adopt are suitable for such phenomena as second harmonic generation, and most compounds adopt centrosymmetric point groups⁽¹²⁾. In addition, the choice of molecular orientations is further limited by the fact that most of the materials which do adopt useful crystal point groups belong to either of only two space groups. This produces a severe statistical constraint on the number of single crystal organic materials likely to have a useful $\chi^{(2)}$. Another fact to consider is that for a crystal to be of use in non-linear optics it must be capable of being grown to a high degree of perfection.

Further complications arise when single crystals are used for optical mixing, since it is necessary to phase match the interacting waves. For example, a prerequisite for efficient second harmonic generation is that $k^{(2\omega)} = 2k^{(\omega)}$, or equivalently $n^{(2\omega)} = n^{(\omega)}$. If this condition is not met, then the second-harmonic power generated at some plane, say Z_1 , having propagated to some other plane (Z_2), is not in phase with the second-harmonic wave generated at Z_2 , and interference will result. For normally dispersive materials n increases with ω and so $n^{(2\omega)} \neq n^{(\omega)}$. However, in crystals which are naturally birefringent the refractive indices in the ordinary and extraordinary directions are not equal at a given ω , so that by a technique known as "angle

phase-matching" the fundamental and second harmonic can be propagated in such directions that now $n^{(2\omega)} = n^{(\omega)}$. Quasi-phase-matching techniques can be used with materials which are isotropic or which are inadequately birefringent; however, in practice these tend to be difficult to implement and offer only low conversion efficiencies⁽¹⁸⁾.

2.3.4 Implementation of the principles for the optimization of non-linear response

A few examples of organic non-linear optical materials which have been produced following the consideration of the criteria detailed in sections 2.3.2 and 2.3.3 will now be described. Many of these principles can be extended to thin films of organic materials, and their fabrication into waveguiding structures can help to overcome such problems as phase matching (see Chapter 3).

Table 2.3 summarizes most of the organic non-linear materials which have appeared in the literature^(12,19). The relative efficiencies refer to second harmonic generation (SHG) experiments performed on powdered samples using the Kurtz technique (see sections 4.6 and 6.4); the values are only semiquantitative because powder efficiency is a function of particle size distribution, amongst other factors. Where β values are available; they are also given in the table. Urea has been chosen as a reference because it has non-linear properties which are comparable to the best inorganic materials⁽²⁰⁾; the difficulty in growing large high quality crystals is its only drawback.

Compounds 2-6 have received extensive treatment in the past. They all possess donor and acceptor groups linked by a conjugated system, and consequently have quite large values of β ; this is particularly noticeable in 6, in which the conjugation length is greatest. However, 6, like para-nitroaniline (3), crystallizes with a centrosymmetric

TABLE 2.3.

Organic non-linear materials in the literature. Bracketed efficiency factors apply to crystallographically optimal materials. (After reference 12, apart from # 8, which was taken from reference 19 and normalised).

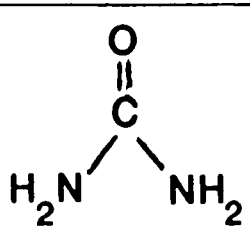
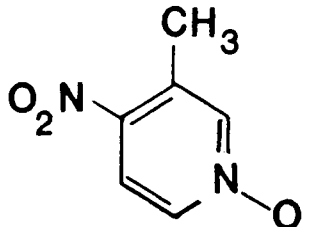
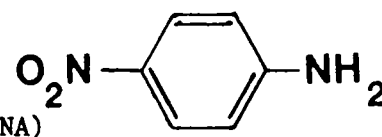
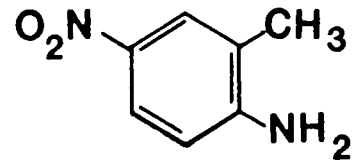
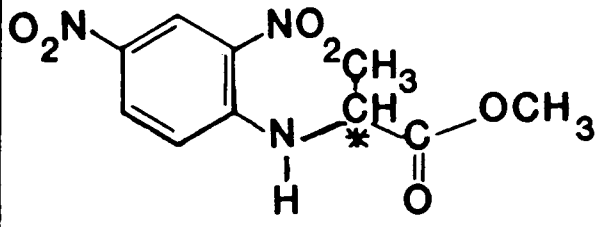
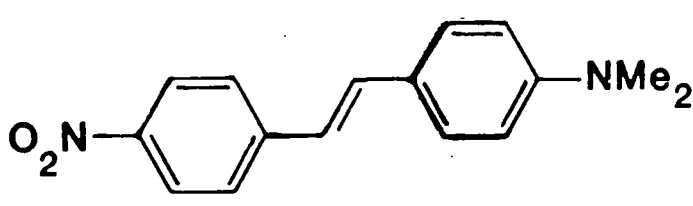
Ref. No.	Structure	$\beta(10^{-50} \text{C}^3 \text{m}^3 \text{J}^{-2})$	Eff (x urea)
1	urea 	0.17	1.0 [x2.5]
2	 3-methyl-4-nitropyridine-1-oxide (POM)	2	13[x4]
3	 p-nitroaniline (p-NA)	13	0.0
4	 2-methyl-4-nitroaniline (MNA)	16	22[x 3.5]
5	 methyl 2-(2',4'-dinitrophenyl)aminopropanoate (MAP)	82	10 [x6.7]
6	 4-dimethylamino-4'-nitrostilbene	170	0.0

TABLE 2.3 (Continued)

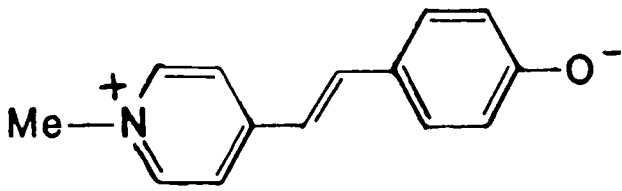
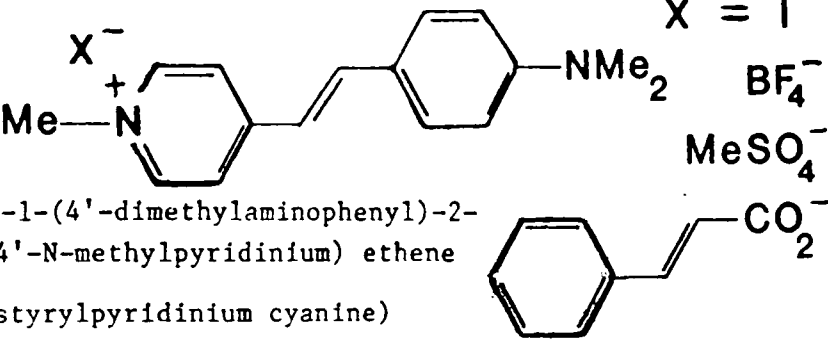
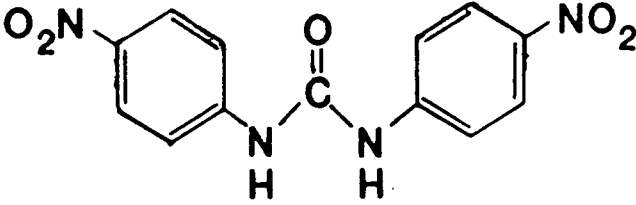
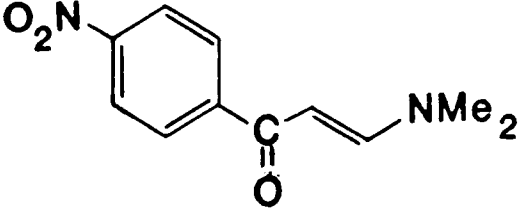
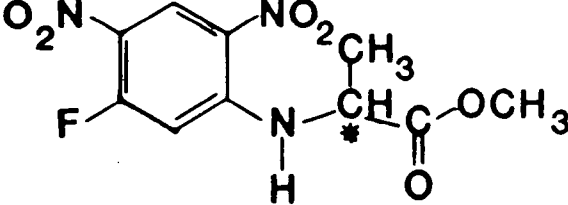
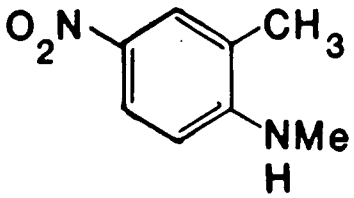
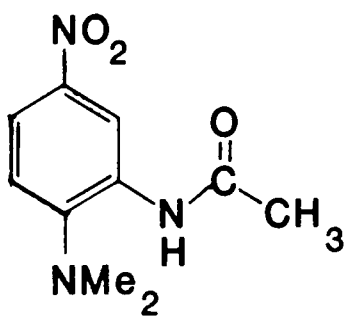
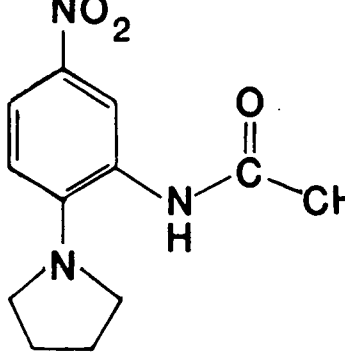
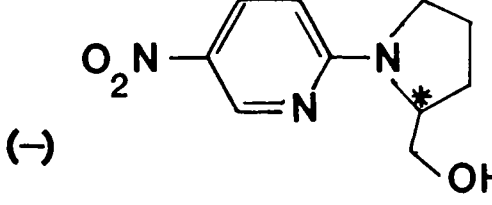
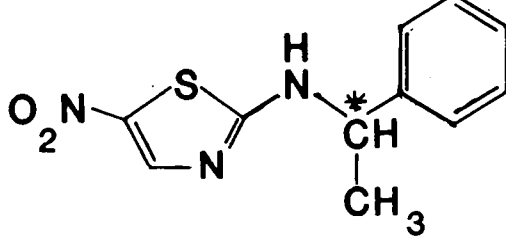
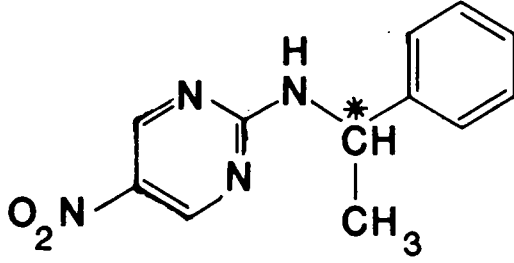
Ref. No.	Structure	B (10^{-50} $C^3m^3J^{-2}$)	Eff (x urea)
7	 <p>E-1-(4'-phenoxy)-2-(4'-N-methylpyridinium) ethene (merocyanine)</p>	370	0.0
8	 <p>E-1-(4'-dimethylaminophenyl)-2-(4'-N-methylpyridinium) ethene (styrylpyridinium cyanine)</p> <p>$X^- = I^-$ BF_4^- $MeSO_4^-$ CO_2^-</p>	0 ~83 ~250 ~13	
9	 <p>N,N'-bis(4'-nitrophenyl)urea (DNPU)</p>	8.8	
10	 <p>2-dimethylamino vinyl-4-nitrophenyl ketone (DMA-NAP)</p>	7.5	
11	 <p>methyl-2-(2',4'-dinitro-5'-fluorophenyl)aminopropanoate</p>	21	
12	 <p>2-methyl-4-nitro-methylaniline (MNMA)</p>	80	

TABLE 2.3 (Continued)

Ref. No.	Structure	Eff (x urea)
13	 <p>2-N,N-dimethylamino-5-nitroacetanilide (DAN)</p>	115
14	 <p>2-N-pyrrolidino-5-nitroacetanilide (PAN)</p>	80
15	 <p>(-) 2-N-prolinol-5-nitropyridine (PNP)</p>	160
16		8
17		4

structure and thus does not display SHG. The addition of a simple methyl group to para-nitroaniline to form MNA⁽²⁰⁾ (4), which has a significant powder efficiency, is an example of how the introduction of an extra substituent can alter the crystal structure. The asymmetrical addition of bulky substituents results in molecules which are less geometrically simple, and such changes can mean that the dipolar forces which favour antiparallel alignment are overcome in order to satisfy the general requirement for dense molecular packing. MAP(5) presents a further example of this principle^(20,21), with the influence of chirality also playing a part in the production of a noncentrosymmetric crystal structure.

The large β value of the merocyanine (7) demonstrates how the presence of charge can enhance the strengths of donors and acceptors, but unfortunately it crystallizes centrosymmetrically. In the series of cationic dyes (8), the importance of the counterion is demonstrated. For such materials, monopolar interactions should be dominant over the deleterious dipolar effects in determining the alignment of the β -enhanced cations. With this particular cation, medium-small, largely pseudo-tetrahedral anions were found to favour the production of an acentric crystal structure⁽¹⁹⁾.

If a molecule could be produced in which dipolar interactions are eliminated, a noncentrosymmetric crystal structure is not guaranteed but at least the structure should be made more sensitive to other influences, such as minor molecular substitutions, which are potentially able to prevent centrosymmetry but which are normally overshadowed by stronger electrostatic forces. This idea has been successfully employed in 3-methyl-4-nitropyridine-1-oxide (POM) (2), which has a vanishing ground state dipole moment and crystallizes

noncentrosymmetrically^(8,20,22). There is an apparent contradiction in the desire for zero dipole moment and conjugated charge transfer, which normally leads to a highly polar structure making a significant resonant contribution to the ground state of the molecule. However, in POM this is not a problem because the localized dipole moment of the N-oxide semi-polar bond opposes and cancels out that of the nitrobenzene, giving a negligible total dipole moment. In a heterocyclic molecule such as this, the N-oxide group may act as a donor or an acceptor depending on the electronic nature of the substituent para to it; in POM, the nitro group is an acceptor and so promotes the donor nature of the N-oxide. The methyl group does not interfere with the basic charge transfer process but does help to dictate the crystal structure. The reduction of the ground state dipole moment is also favourable for the growth of large, high quality crystals from solution, since disruptive molecular associations should be reduced.

Twieg and Jain⁽¹²⁾ have described the assessment of several different groups of materials using the powder technique, and compounds 9-17 represent the best from each class.

- (i) Urea derivatives (e.g. 9). This was an attempt to combine the large non-linearity of nitroaniline molecules with the non-centrosymmetric crystal structure of urea.
- (ii) Polarized enones (e.g. 10). These were related to diethylaminomethylcoumarin, a material studied by other workers⁽²³⁾. Compounds which were identical except that a nitrile group replaced the nitro group all showed zero activity.
- (iii) Analogues of MAP (e.g. 11). Both the amine donor and the substituents on the aromatic ring were changed. A wide range of activity was observed in the series, illustrating the

important effects that slight changes in molecular structure can have on crystal structure.

(iv) Analogues of MNA. Compound 12 was the only achiral derivative studied which showed any activity, and its efficiency was approximately four times that of MNA itself. The origins of this improvement could lie in its stronger donor or in its different crystal space group. Hydrogen bonding between the amide hydrogen and the nitro group of an adjacent molecule is important in determining this crystal structure.

(v) Bifunctional nitrobenzenes (e.g. 13,14). The efficiency of DNPU (9) is limited by the fact that the urea group, required to promote acentric crystallization via hydrogen bonding, is a poor donor. Therefore in this series other nitroaniline derivatives were studied in which a variety of different hydrogen bonding groups were placed at alternative locations in the molecule, and a wide range of efficiencies were observed.

(vi) Nitropyridines. Donor-acceptor substituted benzene derivatives are only a small class in a whole range of non-linear materials, and this section introduces the basis for a whole new class of compounds which have several advantages over the benzene derivatives, including cutoffs at shorter wavelengths and easier synthesis. PNP (15) contains a very strong donor and was found to be highly active, with hydrogen bonding contributing to the production of a favourable molecular alignment in the crystal. NPP, which is the benzene analogue of PNP, is even more active, a property which has been attributed to a structure which is optimal from the standpoint of phase-matching requirements⁽¹¹⁾.

(vii) Thiazoles (e.g. 16) and pyrimidines (e.g. 17). These were selected for their favourable absorption edges and the availability of precursors for synthesis. However, the efficiencies observed so far have been relatively low.

This section has illustrated the great difficulties encountered in obtaining a noncentrosymmetric crystal containing highly non-linear molecules. The subject of this thesis is a novel way of circumventing such problems; the Langmuir-Blodgett (LB) technique can be used to form thin films containing the non-linear species arranged in such a manner as to guarantee the absence of a centre of symmetry. Such films are ideal for applications in integrated optics where single crystals may be inappropriate.

2.4 Applications of Non-Linear Optical Phenomena

The large range of non-linear optical phenomena described in section 2.1 gives rise to a wealth of potential applications. Each application can be classified according to the particular process which it exploits, as in the summary provided in table 2.4. There are two general classes of process : passive and active, the former giving rise to most of the practical applications. In passive processes the non-linear material is effectively acting like a catalyst, and the susceptibilities involved are predominantly real. The imaginary terms in the susceptibilities start to dominate as resonances are approached, giving rise to the active processes such as Raman scattering and two photon absorption⁽¹⁾.

The major interest in non-linear optics stems from the telecommunications industry's need for high-bandwidth optical switching and processing devices to service current information and data

TABLE 2.4

Passive Non-Linear Optical Phenomena and their uses ^(1,7,20)
 ($\omega=0$ refers to a d.c. electric field)

<u>Susceptibility</u>	<u>Process</u>	<u>Application</u>
$\chi^{(1)}$	Linear dispersion, refraction	Optical fibres
$\chi^{(2)}$	Optical rectification (inverse electro-optic effect) $\omega_1 - \omega_1 \rightarrow 0$	Hybrid bistable device
$\chi^{(2)}$	Electro-optic (Pockels) effect $\omega_1 + 0 \rightarrow \omega_1$	Modulators, variable phase retarders
$\chi^{(2)}$	Frequency doubling $\omega_1 + \omega_1 \rightarrow 2\omega_1$	Second harmonic generation
$\chi^{(2)}$	Frequency mixing $\omega_1 \pm \omega_2 \rightarrow \omega_3$	Optical mixers
$\chi^{(2)}$	Parametric amplification $\omega_3 \rightarrow \omega_1 + \omega_2$	Optical parametric oscillators
$\chi^{(3)}$	Frequency tripling $\omega_1 + \omega_1 + \omega_1 \rightarrow 3\omega_1$	Deep U.V. conversion
$\chi^{(3)}$	Quadratic electro-optic effect $\omega_1 + 0 + 0 \rightarrow \omega_1$	Variable phase retardation, liquid-crystal displays
$\chi^{(3)}$	Intensity-dependent refractive index $\omega_1 + \omega_1 - \omega_1 \rightarrow \omega_1$	-
$\chi^{(3)}$	AC electro-optic effect, AC Kerr effect, Brillouin scattering, Raman scattering $\omega_1 + \omega_2 - \omega_2 \rightarrow \omega_3$	Ultra high speed optical gates
$\chi^{(3)}$	AC electro-optic effect, AC Kerr effect, self-focussing, degenerate four-wave mixing $\omega_1 + \omega_1 - \omega_1 \rightarrow \omega_1$	Optical bistability, phase conjugation (image processing), real-time holography, optical transistors, amplifiers, amplitude choppers

transmission needs. In addition, the need for new methods of tailoring individual laser pulses to perform specific functions or to be readily detected in complex experiments has become apparent from the use of a host of sophisticated laser tools.

Second harmonic generation already finds extensive use for doubling the frequency of radiation (see figure 2.7) to take it from the infra-red into the ultra-violet as well as for producing radiation of a suitable wavelength for pumping dyes and for the analysis of short pulses. For example, there should be a variety of applications in such fields as electrophotography, scanning, and optical storage for a device based on a frequency doubled GaAs laser⁽¹²⁾. The frequency modulation of a laser carrier beam, optical parametric oscillation and amplification for solid state infra-red tunable coherent devices⁽¹¹⁾ represent some further applications in the field of integrated optics. Highly efficient non-linear materials can provide such functions on a reduced scale and without a delaying electron-photon conversion process. Two possible forms that a parametric oscillator can take are illustrated in figure 2.8.

One optical element of particular significance is the bistable optical device⁽²⁴⁾. This has an enormous range of optical signal processing capabilities, and could become a key component in future high-speed optical communications repeaters, terminal equipment, data communication systems, and systems for the direct optical processing of visual images. Such a device can be switched between two or more states of transmission of light by temporary changes in the level of light input, and could find applications in memory elements, differential amplifiers, pulse shapers and limiters, optical triodes, and logic elements etc. There are four attractive features of such a device : (i)

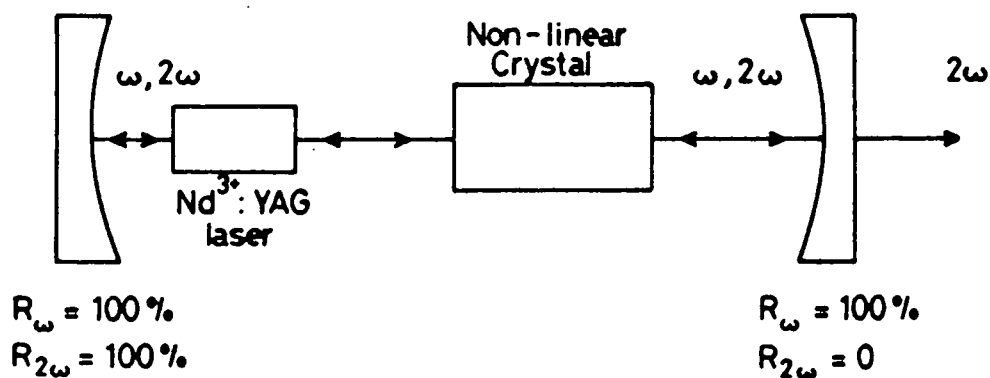


Figure 2.7 Second harmonic conversion inside a laser resonator.

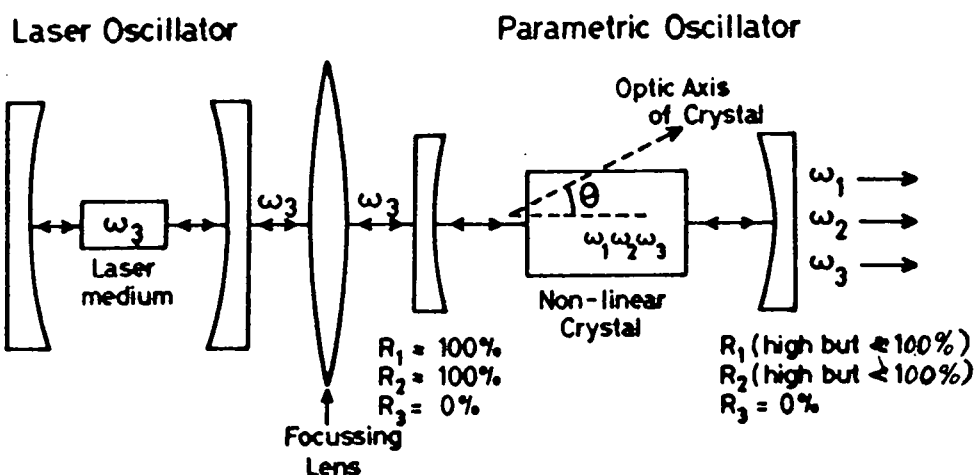


Figure 2.8a Optical parametric oscillator with laser output at ω_3 used as the pump, giving rise to oscillations at ω_1 and ω_2 (where $\omega_3 = \omega_1 + \omega_2$) in an optical cavity that contains the non-linear crystal and resonates at ω_1 and ω_2 .

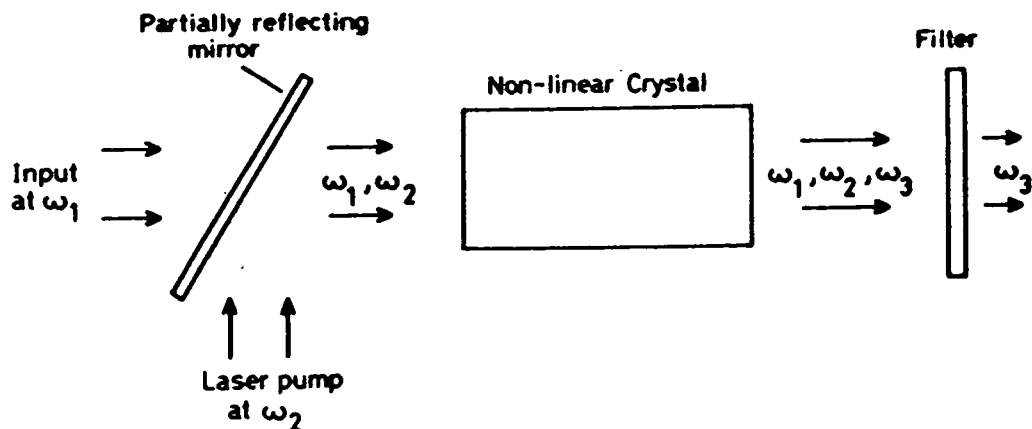


Figure 2.8b Parametric up-conversion in which a signal at ω_1 and a strong laser beam at ω_2 combine in a non-linear crystal to generate a beam at the sum frequency, $\omega_3 = \omega_1 + \omega_2$.

an extremely large bandwidth (greater than 10^{13} Hz); (ii) an ultra-short (subpicosecond) switching time; (iii) capability for parallel processing; (iv) the ability to process light directly. Bistable optical devices can be superior to electronic or Josephson switching devices in terms of both bandwidth and switching time. Figure 2.9 illustrates the form of a very simple bistable optical device.

In devices which employ waveguiding, several different types of structure can be envisaged, such as: a linear guide on a non-linear substrate; a non-linear guide on a linear substrate; or a non-linear guide on a non-linear substrate. Stripe waveguides fabricated by the indiffusion of titanium into a lithium niobate substrate have also been produced. However, an efficient non-linear optical device has yet to be realized using such structures, mainly due to the difficulty encountered in maintaining uniform guide dimensions over the length of the waveguide (in order to maintain phase matching), as well as to scattering losses at the guide-substrate interface and to optical damage as a result of the high optical intensities employed⁽¹⁸⁾. The use of organic materials and lithographic techniques holds great promise for overcoming such problems.

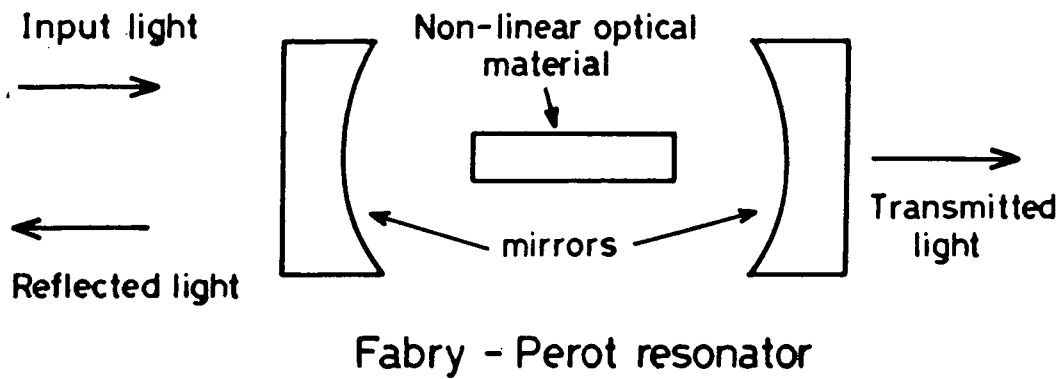


Figure 2.9a Simple bistable optical device

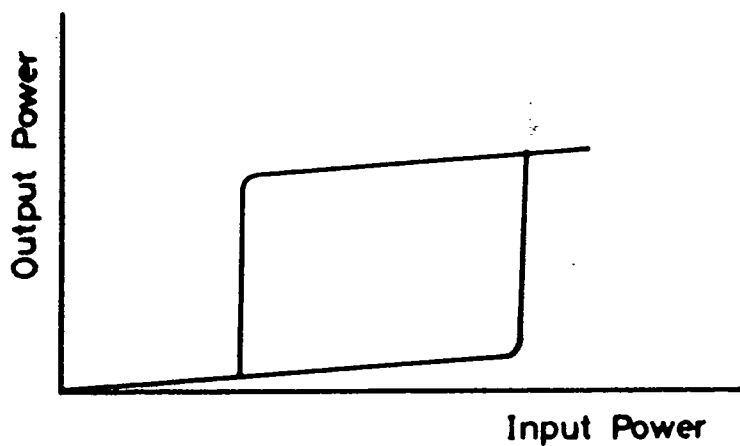


Figure 2.9b Response of the bistable optical device shown in (a) to changes in input power. High light powers within the non-linear material cause large changes in refractive index and thus in the optical path length, thereby tuning the resonator towards or away from resonance.

CHAPTER 3
LB FILM TECHNOLOGY

3.0 Introduction

In this chapter all aspects of Langmuir-Blodgett films are discussed, from the principles involved through to instrumentation and applications. Section 3.1 deals with the basic concepts behind LB film formation, including the formation of water-surface monolayers and their subsequent transfer to solid substrates. An introduction to some of the materials used in LB films, including classical materials such as fatty acids, and some classes of novel chromophoric compounds encountered in this project and in the literature, is given in section 3.2. Two types of Langmuir trough are described; one for the production of multilayer films in which each monolayer has the same composition, and one for the production of supermolecular arrays in which two different monolayer compositions are employed and deposited in an alternating sequence (ABABAB...).

Properties of the water surface monolayer are discussed in section 3.5. Aspects of the deposition and methods for the quality assessment of LB films are also presented. Finally, summaries of the possible applications for LB films in non-linear optics and other fields are given in sections 3.8 and 3.9.

3.1 Basic Concepts

In order for a material to be suitable for deposition onto a substrate using the Langmuir-Blodgett technique it must first be able to form an insoluble monolayer at an air-water interface. For this reason, most LB film materials consist of organic molecules with a hydrophilic

"head" group and a hydrophobic "tail". The material is first dissolved in a volatile organic solvent and the solution dispersed over the water surface; the solvent evaporates, leaving a layer of the material one molecule thick which doesn't dissolve in the water, due to the nature of the tails. Solvation effects favour a molecular orientation within the monolayer such that the polar head groups are in the water. The molecules in such a layer are disorganized, but if the layer is spread in an enclosed area which can subsequently be reduced, then as the surface area available to each molecule gets smaller, the arrangement becomes more ordered. If the monolayer is compressed sufficiently, it forms a quasi two-dimensional solid, although care has to be taken that this process is not taken too far, otherwise the layer will buckle and eventually collapse. If a solid substrate is now dipped vertically through the air-water interface, a monolayer of the material is transferred from the water surface onto the substrate. Further monolayers should then be deposited on each subsequent insertion or withdrawal of the substrate from the subphase (water).

3.2 Materials

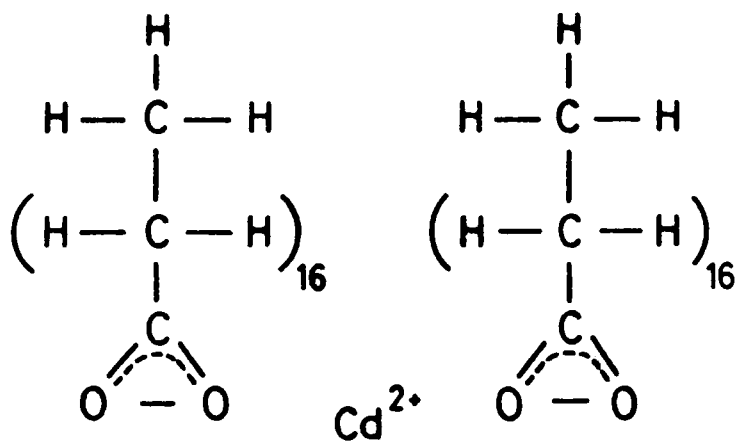
The materials used in LB film formation can be classified as being either 'classical' or 'novel'. The classical materials are those such as the long chain fatty acids which formed the basis of LB film technology; the novel materials are taken to be those selected for study because they contain certain combinations of chemical groups within the molecules which are likely to impart specific properties to the films they form. In this discussion the novel materials have been further subdivided into those reported by other workers in the field and three

categories of material which were either bought or custom synthesized at Durham for their potentially large optical nonlinearities. A much wider range of materials was studied than is reported in this thesis, since subtle variations in the lengths of hydrocarbon chains or their replacement with fluorocarbon chains were investigated. However, only the more interesting results are discussed.

3.2.1 Classical materials.

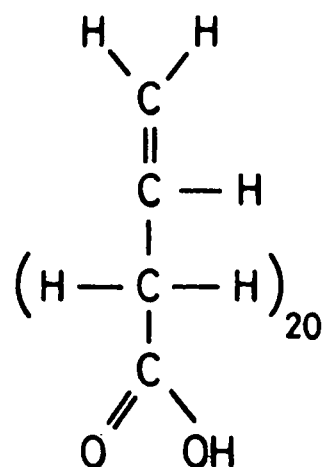
Section 3.1 referred to the use of materials with hydrophilic head groups and hydrophobic tails; perhaps the most commonly encountered molecule of this variety is stearic acid, which possesses a long hydrocarbon chain (hydrophobic) terminated by a carboxyl group (hydrophilic). For a homologous series of saturated aliphatic carboxylic acids, the solubility of the material is dependent on the length of the hydrocarbon chain, approximately 20 carbon atoms being required for negligible solubility. It is hardly surprising that solubility problems are encountered in this field, in view of the very large surface area to volume ratio of a monomolecular film.

The stability and solubility of water-surface monolayers, and the quality of the deposited films, are dependent on a wide range of inter-related variables, such as subphase pH, temperature, and the presence of counterions. For example, the solubility of stearic acid is reduced by the presence of divalent metal cations, such as Cd^{2+} , and control of pH is important in determining the extent of salt formation. Since such salt formation involves two stearic acid molecules for each cadmium ion (figure 3.1a), such a process improves the lateral cohesion of the layer⁽¹⁾ and gives rise to superior film quality. The typical subphase conditions used for the deposition of cadmium stearate are a



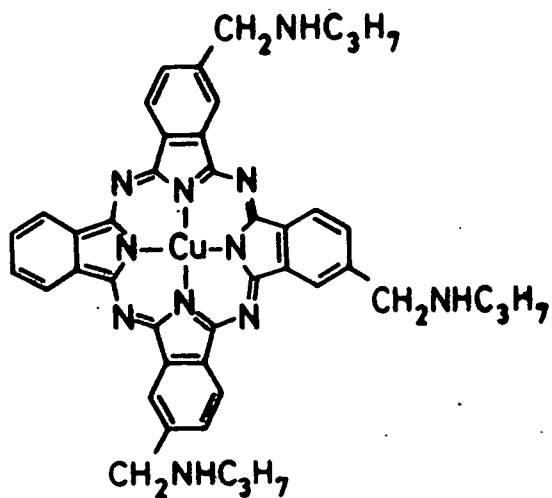
(a)

Cadmium stearate, $\text{Cd}(\text{C}_{17}\text{H}_{35}\text{CO}_2)_2$



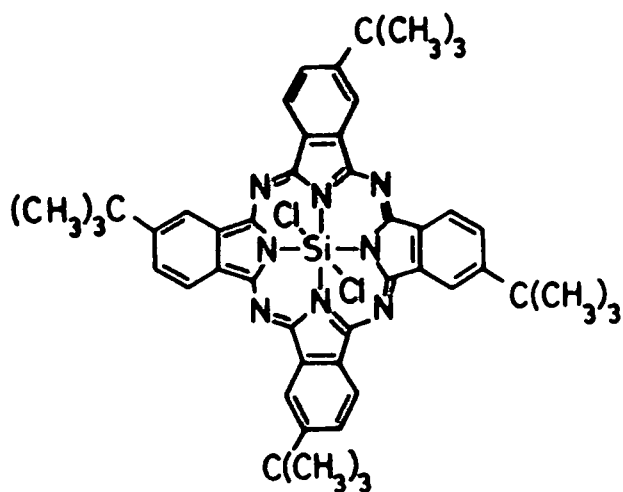
(b)

ω -tricosenoic acid (ω -TA),
 $\text{CH}_2\text{CH}(\text{CH}_2)_{20}\text{COOH}$



(c)

Asymmetric copper phthalocyanine



(d)

Symmetric silicon phthalocyanine

Figure 3.1

Structural formulae of some classical and novel LB film materials in the literature.

10^{-4} M cadmium chloride solution with pH = 5.6. A closely related material to this is ω -tricosenoic acid⁽²⁾ (ω -TA), whose structural formula is given in figure 3.1b. The unsaturated terminal carbon-carbon bond renders the material susceptible to polymerisation by such means as an electron beam, and the resulting cross-linking of bonds gives rise to a linear polymer. This feature had led to the proposed use of ω -TA LB films as electron beam resists⁽³⁾. The material has other advantages; in particular, well ordered films can be deposited at high speeds if the subphase doesn't contain divalent cations⁽⁴⁾.

There have been a number of other materials investigated with structures related to those of the simple fatty acids. These include a range of polymerisable materials, the diacetylenes⁽⁵⁾, and some biologically important materials such as chlorophyll⁽⁶⁾, phospholipids⁽⁷⁾, and cholesterol⁽⁸⁾.

3.2.2 Novel materials from the literature

The current trend in LB film technology is to custom synthesize materials incorporating chemical groups designed to impart specific physical properties to the films. In such materials the 'active' part of the molecule is usually the hydrophilic head group, and the hydrocarbon tail is passive in that it merely serves to render the molecule water-insoluble (except when it contains unsaturated bonds for polymerisation). In many cases it is therefore desirable to reduce the length of the hydrocarbon chain to a minimum, since it effectively dilutes the useful electronic, optical, photoelectrical etc. properties of the head group. This is the origin of the interest in the anthracene derivatives described in Chapter 5 for non-linear optical applications. The parent anthracene derivative, 9-butyl-10-anthrylpropionic acid, can

be made to form high quality multilayers providing the deposition conditions, particularly subphase pH, are very carefully controlled⁽⁹⁾.

Another range of materials which have been studied extensively at Durham are the phthalocyanine dyes. These compounds do not require hydrocarbon chains for insolubility and have exceptional thermal and chemical stabilities, as well as potentially useful electronic structures. Stable LB films of metal free phthalocyanine and tetra-tert-butyl substituted phthalocyanine have been prepared⁽¹⁰⁾ which are of a reproducible quality, but which are not composed of single monolayers. These films are polycrystalline, with no long range order; however, monomolecular or bimolecular layers of an asymmetrically substituted copper phthalocyanine (figure 3.1c) can be produced and have been built up into multilayer assemblies displaying interesting gas-sensitive properties⁽¹¹⁾. A symmetrically substituted silicon phthalocyanine⁽¹²⁾ (figure 3.1d) has shown improved water-surface monolayer characteristics and deposition properties; work is still in progress on this material and a series of closely related phthalocyanines.

Many different substituted dyes have been deposited in LB films, some as homogeneous layers, others as layers in which they are mixed with an inert fatty acid in order to provide a matrix which can confer desirable film-forming properties to the dye. The list of LB film-forming chromophoric materials includes merocyanine⁽¹³⁾, hemicyanine⁽¹⁴⁾, squarylium⁽¹⁵⁾, anthraquinone⁽¹⁶⁾, stilbene^(17,18) and azo⁽¹⁸⁾ dyes. In some cases the molecule contains more than one hydrocarbon chain in order to bring about a particular orientation of the chromophore.

3.2.3 Novel materials used in this project

A wide range of novel materials were investigated in this project. Most of them were designed according to the guidelines discussed in chapter 2 for producing molecules with a high second-order hyperpolarizability (i.e. molecules containing donor and acceptor groups separated by a conjugated system), their water solubility being reduced by the addition of hydrocarbon chains, made as short as possible in order to avoid diluting the non-linear behaviour. The validity of these criteria was tested by studying a series of materials which were closely related to the target molecules but which contained different donor and acceptor combinations, e.g. two acceptors and no donor, one acceptor and no donor; no strong acceptors or donors, etc. Such materials were also of interest for the observation of the effects of subtle molecular changes on LB film properties.

The materials fall into three distinct categories: (i) commercially available chromophores modified by the addition of a hydrophobic tail; (ii) anthracene derivatives based on 9-butyl-10-anthrylpropionic acid⁽⁹⁾; (iii) dipolar chromophores, such as the merocyanine described by Gaines⁽¹⁹⁾. These classes will be discussed in more detail in chapter 5.

3.3 The Conventional Langmuir Trough

There have been many modifications made to the original trough used by Langmuir and Blodgett⁽²⁰⁾, including variations with a single movable barrier⁽²¹⁾ or circular troughs with a radial compression barrier⁽²²⁾. A further variety, employing a constant perimeter barrier⁽²³⁾, is in use at Durham and is described below.

3.3.1 Mechanical construction

A conventional Langmuir trough of the type used at Durham is illustrated schematically in figure 3.2 and a photograph is shown in figure 3.3. The tank itself is made of glass supported by a metal framework, and can be raised or lowered in order to adjust the depth of the water relative to the barriers or to facilitate its removal for cleaning. The barrier employed to enclose an area of the water surface is of the constant perimeter type and consists of a PTFE-coated glass fibre belt, held taut by rollers. One pair of these rollers is attached to a rigid cross-member, whereas the other two pairs are fixed to two cross-members which can be pulled on grooved rollers along steel runners by toothed rubber belts driven by a single motor. The limits of barrier motion are defined by microswitches, and the inset in figure 3.2 illustrates the corresponding extremes of surface area.

The deposition mechanism, or dipping head, consists of a micrometer screw mounted above the water on a movable crossbeam. The screw can be driven by a motor at a constant, but variable, speed in a vertical direction, and the substrates are held in a metal screw clamp affixed to it. The surface pressure is monitored using a Wilhelmy plate consisting of a 1 cm wide strip of filter paper; this is suspended in the water by a thread from a microbalance head above the trough. Changes in surface pressure result in corresponding changes in the effective weight of the plate, which is monitored by the microbalance. The complete structure is housed in a glass-doored cabinet mounted upon a Newport XJ-A pneumatic anti-vibration table. Solvent evaporation is aided by an extractor fan located in the wall of the cabinet and leading to a fume cupboard. Where possible, the structure is made from PTFE, stainless

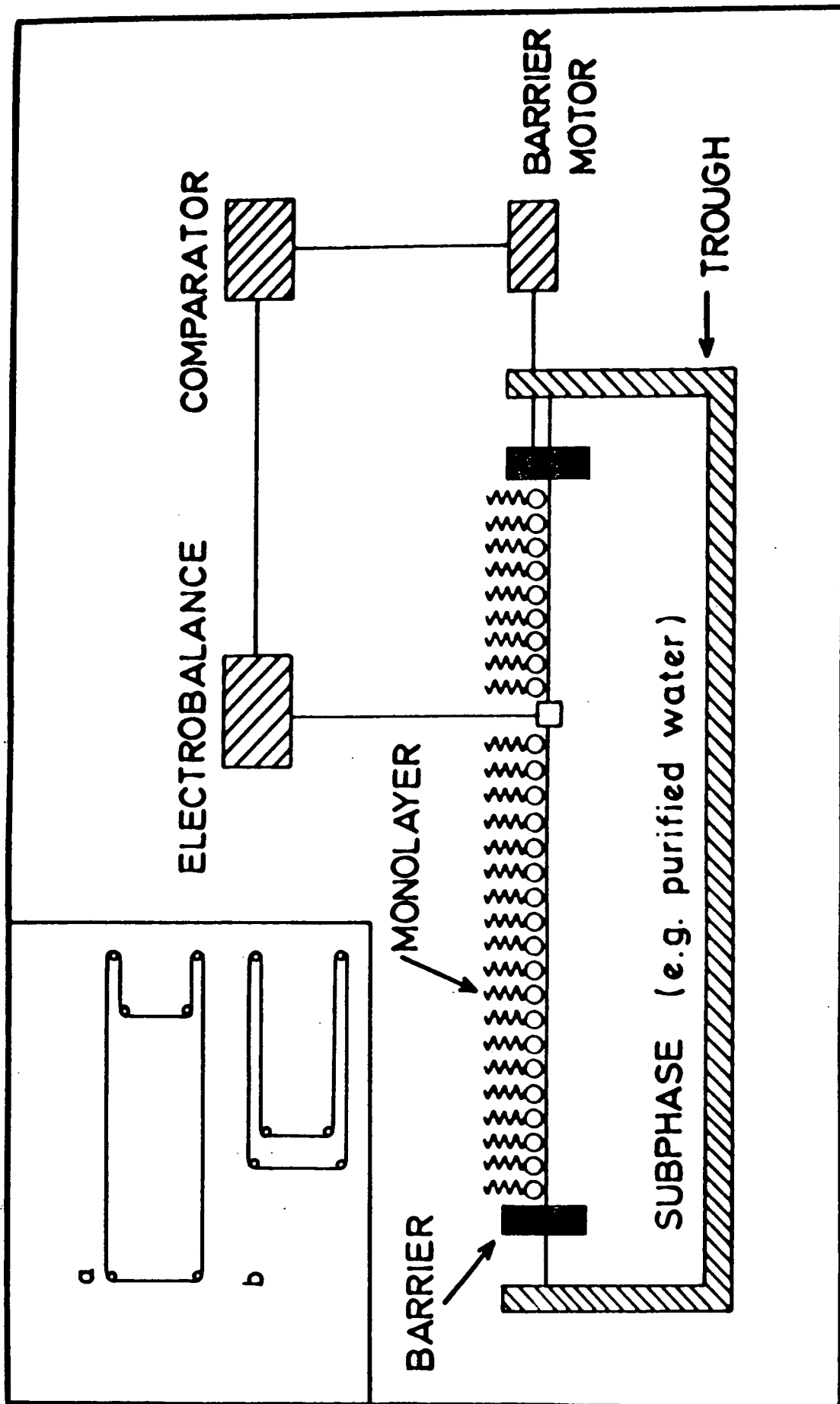


Figure 3.2 Schematic diagram of the constant perimeter barrier Langmuir trough. Inset: plan view of barriers (a) fully open, (b) fully compressed.

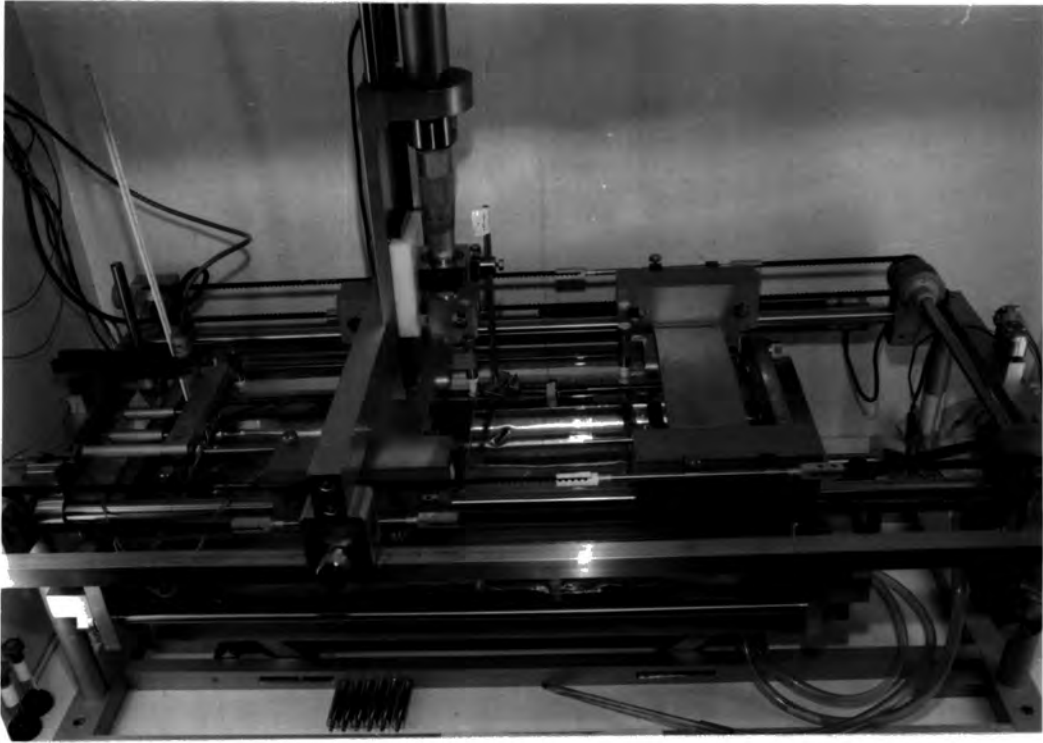


Figure 3.3 Photograph of a conventional Langmuir trough.

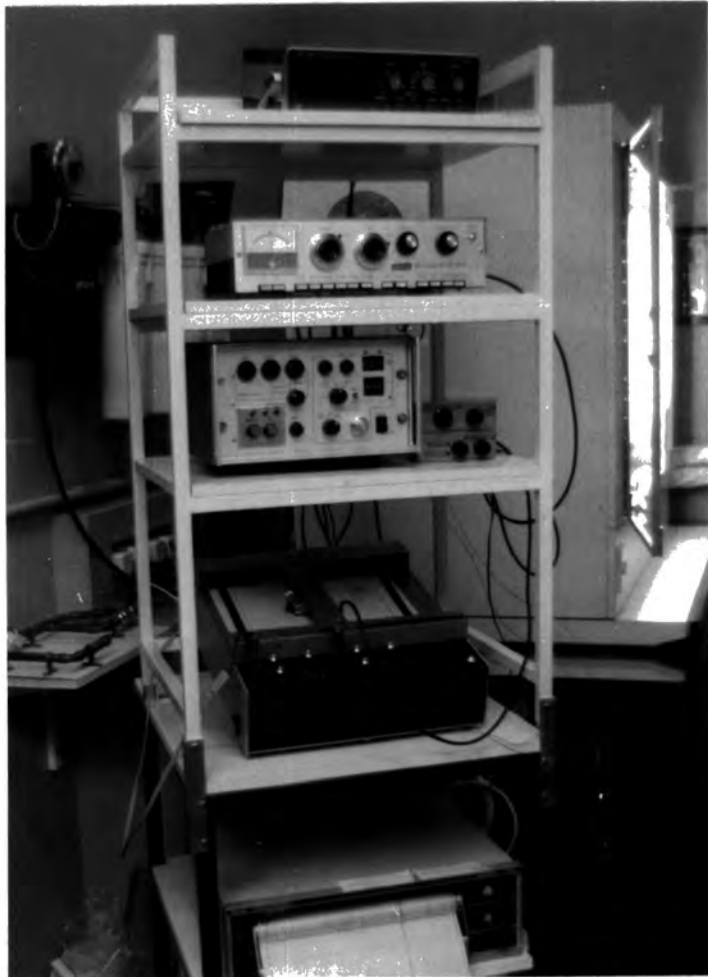


Figure 3.4 Photograph of the instrumentation associated with a conventional Langmuir trough.

steel or anodised aluminium, for both ease of cleaning and reduction of the risk of contamination.

3.3.2 Instrumentation

A photograph of the instrumentation associated with the trough is shown in figure 3.4. The control box enables the user to dictate all of the movements of the barrier and dipping head, and several of the trough functions are automated. There are four possible modes of barrier operation; forward, reverse, control, and auto. In forward and reverse modes the barrier will compress or expand at a speed which can be preselected. In the control mode, which is normally used during deposition, a differential feedback system is used to compress the barrier until the film reaches a preselected surface pressure. A Beckman LM600 microbalance monitors the force acting upon the Wilhelmy plate and an electrical signal representing the difference in pressure from that preset on the microbalance is passed to the control unit via a feedback system with adjustable gain. The auto mode is used exclusively for the deposition of Z-type LB films (see section 3.6). In this mode the substrate is rapidly lowered through the uncompressed monolayer; the monolayer is then compressed and the film allowed to stabilise for a preset time of up to six minutes before deposition commences with the withdrawal of the substrate at prior-selected speed. A further delay of up to thirty minutes may be programmed in order to allow the film to stabilise in air before the next dipping cycle is commenced. The speed and the upper and lower limits of the dipping head movement can be preset, as can be the required number of dipping cycles. High-resolution linear potentiometers attached to the barrier

cross-members and the dipping head allow precise monitoring of film area and substrate position.

Plots of surface pressure (microbalance output) or substrate position (for monitoring film deposition) against surface area can be obtained on the Bryans 29000 X-Y chart recorder. Area and pressure may also be plotted against time on a Bryans 312 two-channel Y-t chart recorder. A Pye-Unicam PW9409 pH-meter is used to continuously monitor the subphase pH, the electrodes for this being mounted at one end of the trough along with a mercury thermometer.

3.3.3 Reduction of contamination

A dust-free environment is essential for the production of good quality LB films, and consequently all the troughs are housed in a class 10000 microelectronics clean room. The water used as a subphase, and in any cleaning operations, undergoes reverse osmosis, double deionisation, activated charcoal organic removal and 0.2 μ m filtration before being delivered to the troughs via high purity polypropylene tubing. High purity subphase water is vital, since impure water can be a major source of ionic and organic contaminants, resulting in excessive monolayer dissolution and poor deposition. The ultrapure water produced has a resistivity which is initially close to its theoretical maximum of 18 M Ω cm, but this value is likely to decrease with the time that the subphase resides in the trough, since ions are likely to be leached out of the glass. In addition, the measurement of resistivity gives no measure of the quantity of unionized organic species present in the water. All of the solvents and other chemicals used in the preparation of spreading solutions, or as additives to the subphase, are of the highest commercially available grade of purity.

A rigorous cleaning procedure is regularly undertaken in which the glass trough is cleaned with chloroform, propan-2-ol, and water. The belt and rollers are cleaned by rinsing in chloroform then refluxing for several hours in propan-2-ol liquid and vapour in a Soxhlet reflux unit. On reassembly, the subphase and Wilhelmy plate are renewed, and the trough instrumentation recalibrated. Before spreading the films, the subphase surface is cleaned by sweeping it with a fine nozzled glass pipe connected to a water driven pump.

3.4 The Alternate Layer Langmuir Trough

The production of alternate layers is important for applications employing non-linear optical, piezoelectrical, or pyroelectrical effects, since such films will have the noncentrosymmetric structures requisite for these phenomena. The alternate layer trough uses a rotating cylinder passing through two independently compressed monolayers to achieve the desired 'ABAB' sequence of layers in a rapid and easy fashion. In order to perform the same function on a conventional trough one would have to clean the subphase surface and spread a fresh monolayer prior to the deposition of each individual layer, a tedious and lengthy task.

3.4.1 Mechanical construction

The mechanical construction of the alternate layer trough is very similar to that of the conventional trough described in section 3.3.1. The barrier assembly is modified so that separate reversible motors drive the barrier elements and allow the independent controlled compression of two different monolayers. Schematic diagrams of the system as a whole and of the barrier assembly are shown in figures 3.5

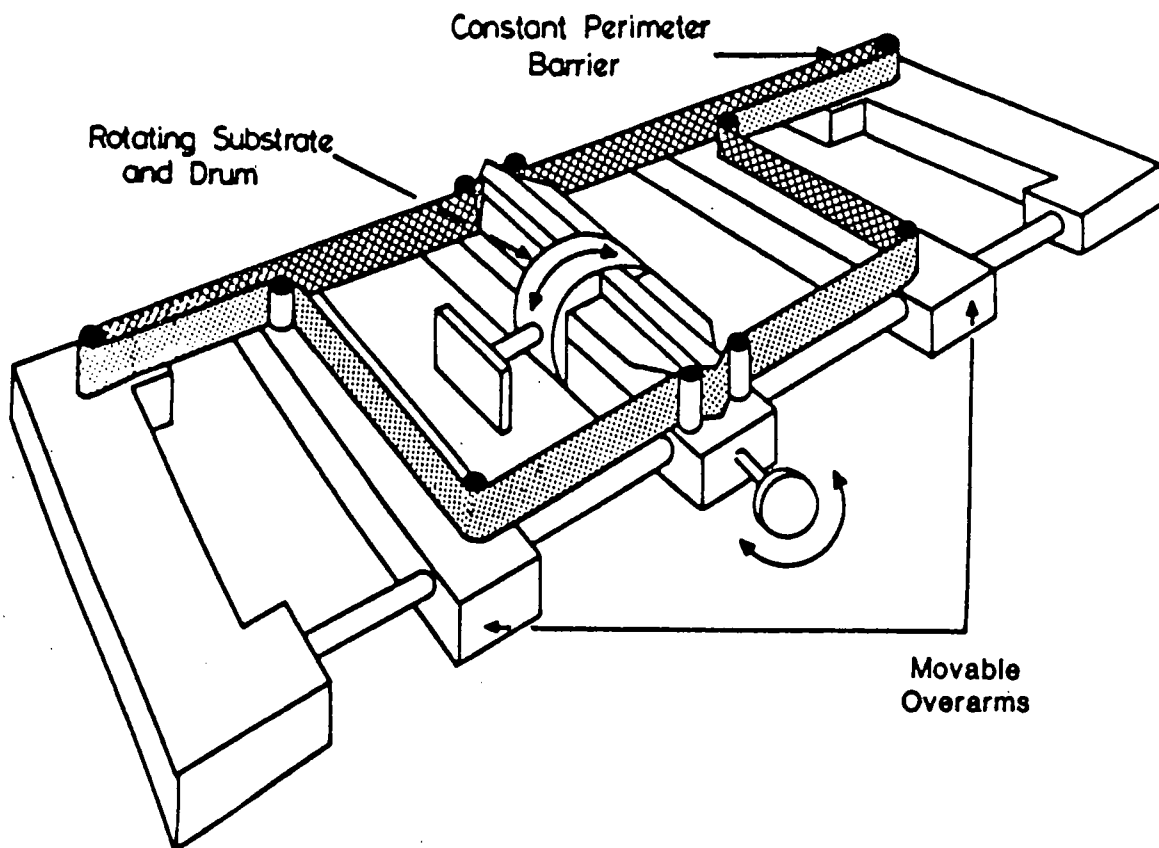


Figure 3.5 Schematic diagram of the alternate layer Langmuir trough.

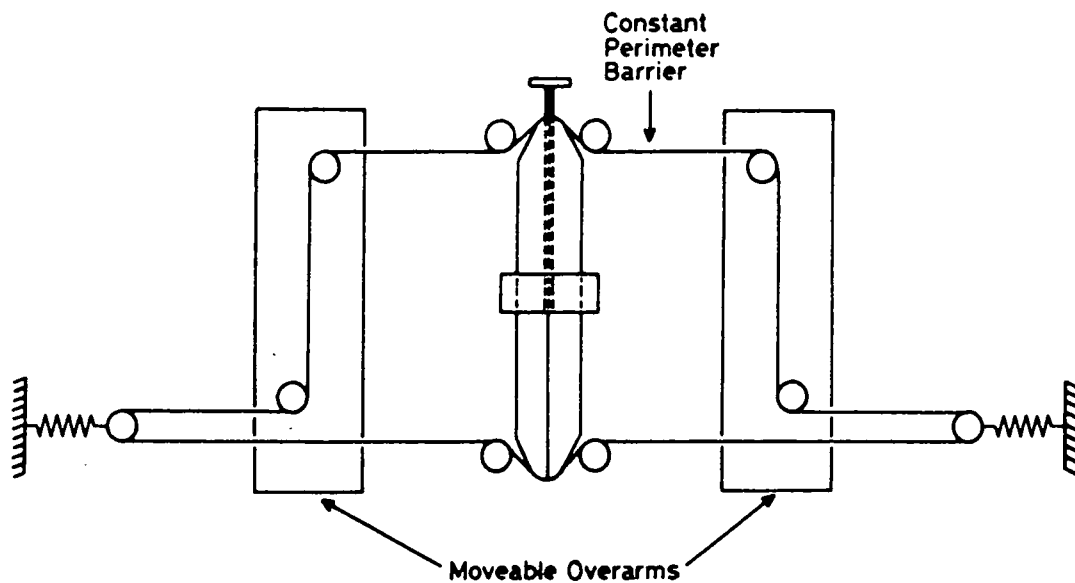


Figure 3.6 Schematic diagram of the barrier assembly for the alternate layer trough (from below).

and 3.6 respectively. There is a separate Wilhelmy plate and microbalance for each arm of the trough, so that the two different materials can be deposited at their optimum surface pressures, even if they are widely differing. The fixed central barrier is divided to accommodate a cylinder which can rotate or oscillate about a central axis, and to which the substrates can be clamped. When the cylinder is rotated the substrate is immersed through a monolayer of the first material and withdrawn through a monolayer of the second; when it is oscillated it merely deposits the same material on insertion and withdrawal, as a conventional trough would do. PTFE inserts extend between the cylinder and the ends of the central barrier in order to prevent leakage of monolayers between the compartments. The oscillatory or rotary motion is transmitted from a motor and gearbox through a detachable coupling to a co-axial spindle on the cylinder. The whole assembly is mounted on a granite slab cushioned with air-filled polyethylene bubbles.

3.4.2 Instrumentation

The control of the barrier movements is exactly the same as with the conventional trough except that now there is a separate set of controls for each compartment. The dipping speed and direction of rotation can be selected by the operator, but the control unit doesn't yet feature a counter for programming a set number of rotations. However, it is envisaged that in the near future this omission will be rectified, and a further modification may be made so that the speed of rotation automatically increases during the period of time that the substrate is not actually traversing an air-water interface. Surface pressure can be plotted against surface area for either compartment

using a Bryans 29000 X-Y chart recorder, whilst two Bryans 27000 Y-t chart recorders can be used to monitor the surface areas as a function of time.

3.4.3 Cross-contamination

There are two possible sources of cross-contamination of the films, arising from the transfer of material from one compartment to another by either (i) the rotating cylinder or (ii) the substrate. This effect has been investigated by Holcroft et al⁽¹⁵⁾, using a highly absorbing squarylium dye and ω -tricosenoic acid. It was found that negligible contamination arose from 20 revolutions of the cylinder. However, when different monolayer combinations were used in which the pick up ratio was poor, contamination was observed.

3.5 Properties of the Water-Surface Monolayer

The most fundamental requirement for a material to be of use in LB film formation is that it should be practically insoluble in the water subphase. However, the conventional concept of bulk solubility is not really meaningful in this context, and figures for such a quantity could only give at best a rough estimate of whether or not a monolayer of the material is likely to be stable at the air-water interface. The two most valuable properties of the water-surface monolayer which can be studied are its pressure-area relationship and the change in surface area with time at constant pressure.

3.5.1 Pressure-area isotherms

If a material forms an insoluble monolayer at the air-water interface, then as the surface area of the trough is reduced the surface pressure will increase. By plotting the calibrated output from the

microbalance against that from the barrier potentiometer, a pressure-area (π -A) curve, or isotherm, can be obtained. The area axis may be converted from trough surface area to surface area per molecule if the number of molecules spread on the surface is known (this can be deduced from the molecular weight of the material and the volume and concentration of the spreading solution). A typical isotherm for stearic acid is shown in figure 3.7. This isotherm represents the 'ideal' situation in which there are three distinct regions, corresponding to two-dimensional "gas", "liquid", and "solid" phases. The steep, linear "solid" portion of the curve can be extrapolated down to the area axis in order to determine the zero pressure limit of the molecular area in the solid phase. This value may then be compared to those obtained from physical representations, such as Ealing CPK molecular models, or computer-generated simulations. Such comparisons can help to indicate the orientation of molecules in the film, along with the possible intermolecular interactions. Indeed, Langmuir⁽²⁴⁾ found that films of long chain fatty acids gave the same cross-sectional area per molecule, irrespective of chain length. He concluded that the films were one molecule thick and that the molecules were oriented nearly vertically on the water surface, the film thickness being the chain length. Few materials display the three distinct "phases" shown by stearic acid, but the shapes of their isotherms help to elucidate the behaviour of the molecules as the film is compressed. Many compounds exhibit "solid" regions, but often only after a series of other phase changes. The curvature of such isotherms, and changes in curvature upon recompression, can be interpreted in terms of molecular rearrangement and interaction.

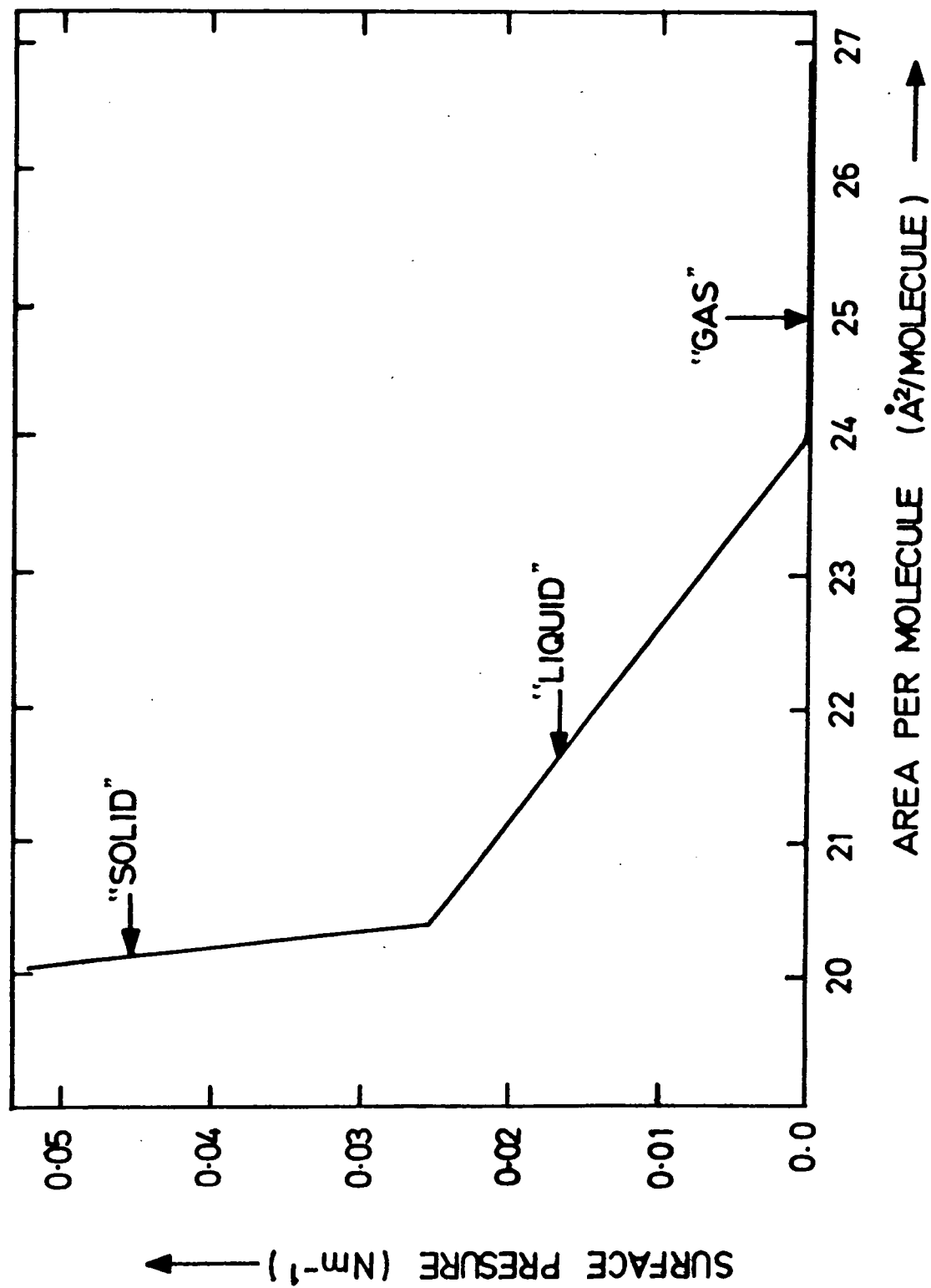


Figure 3.7 Typical stearic acid isotherm

3.5.2 Decay in surface area with time

An ideal Langmuir film would display no decrease in surface area with time when held at a constant surface pressure in its quasi-solid phase. However, in practice all monolayer films show some decay in area with time due to some or all of the following effects: (a) collapse (buckling of the film); (b) rearrangement; (c) dissolution of material into the subphase; (d) evaporation. Normally one can prevent a monolayer from collapsing by keeping the surface pressure below that at which the film becomes unstable; however, in some cases this pressure is too low for efficient transfer to a substrate. The rate of dissolution may depend on several factors, including temperature, pH, and the concentration of various ions in the subphase. With most of the classical fatty acid materials this process can be rendered insignificant by partial salt formation, but dissolution can be quite rapid, and thus a major problem, with many of the more novel materials. The optimum conditions for slowing film collapse must therefore be found. Gaines⁽¹⁾ has studied Langmuir films which dissolve at an appreciable rate and has found that they show an initial rapid desorption, followed by a process obeying equation 3.1:

$$\ln(N) = -kt + C \quad (3.1)$$

where N is the number of molecules remaining on the surface at time t, and k, C are constants. The optimum conditions for reduced solubility can be found by measuring the area of a collapsing film as a function of time for a range of different subphase parameters and noting which gives the smallest value of k.

3.5.3 Monolayer mobility

Although it is desirable that a monolayer should be well-ordered and close-packed, it is important that it should also remain mobile on the water surface if it is to be deposited onto a substrate. If a film is too rigid, then as a substrate is drawn up through it, it will fracture and deposition will take the form of the transfer of film fragments, with large cracks and holes between them.

The 'suction test' provides a simple check on monolayer mobility; the film is held at constant pressure, with the feedback to the barrier drive at maximum gain, and a small amount of material removed using the vacuum nozzle described in section 3.3.3. An adequately mobile film should collapse immediately to maintain the preset surface pressure. Very rigid monolayers can often be made more fluid by mixing the material with a fatty acid or by using a slow-evaporating solvent. In some cases rigidity sets in slowly with time and so the problem can be circumvented by always depositing from a freshly spread monolayer, although this can be rather tedious.

3.6 Experimental Techniques

Having established a material as a viable Langmuir film, the formation of LB films by deposition onto substrates may be investigated. The surface of the subphase is first cleaned by compressing the barriers to minimum area, sweeping the surface with the vacuum nozzle, then expanding back to maximum area. This process is repeated several times. The deposition process then proceeds with monolayer spreading, compression, and finally deposition itself.

3.6.1 Monolayer spreading

The most commonly used solvent for the production of spreading solutions was ARISTAR grade chloroform. Typically, concentrations of approximately 1 gdm^{-3} were used, the mass of material used in forming the solution being accurately determined using an Oertling R52 balance. The solution was dispensed a drop at a time onto the water surface from a height of approximately 2 mm using an Agla microlitre syringe. A micrometer drive on the plunger enabled the volume delivered (typically 0.1 ml) to be measured precisely in order to facilitate molecular area calculations. In most cases the solution was deposited near the centre of the trough to lessen the effect of any residual contamination, but in the situations where very concentrated or slow-spreading solutions had to be used the drops were placed at regular intervals all over the water surface. Complete solvent evaporation was ensured by running the extractor fan for about five minutes after spreading.

3.6.2 Monolayer compression

Pressure-area isotherms were plotted as a matter of course for each new spreading solution and from time to time for older solutions to check that they still gave good quality water-surface monolayers. This was done by compressing the film at a fixed rate in the forward mode. Having established this, fresh monolayers were spread and compressed in control mode to a pressure close to the centre of the solid phase, where the film structure should change very little for relatively large fluctuations in surface pressure. At this stage the decay in surface area with time (section 3.5.2) was studied, or else the film was left for a few minutes to stabilise before commencing deposition.

3.6.3 LB Film deposition

Three possible modes of LB film deposition have been recognized⁽²⁵⁾ and are illustrated in figure 3.8. With most materials deposition is Y-type, with pick up occurring on both insertion and withdrawal of the substrate from the subphase. With this mode the first monolayer is deposited on the first upstroke of a hydrophilic material (giving an odd total number of layers) or on the first downstroke of a hydrophobic material (giving an even total number of layers). Y-type deposition produces a highly symmetrical packing arrangement unless different materials are used for successive layers (as with the alternate layer trough described in section 3.4). At high subphase pH, fatty acids will sometimes deposit only on the downstroke, thus forming X-type films⁽¹⁾. This mode of deposition is generally energetically unfavourable compared to Y-type deposition and there is X-ray evidence for molecular rearrangement during transferral to give films which are essentially Y-type in nature. Z-type deposition, in which pick up occurs only on the upstroke, has been observed in a lightly substituted anthracene derivative⁽⁹⁾ and in asymmetrically substituted copper phthalocyanine⁽¹¹⁾.

An important parameter used to characterize LB film deposition is the deposition (or transfer) ratio. This is defined as the ratio of the area of film removed from the water surface to the area of the substrate moved through the air-water interface, and has a value of unity for ideal deposition.

The success of deposition and the quality of multilayer films depend critically on the structure of the first monolayer, since any faults in it might be propagated into subsequent layers. In addition, the first layer is unique in that it is the only one directly bonded to

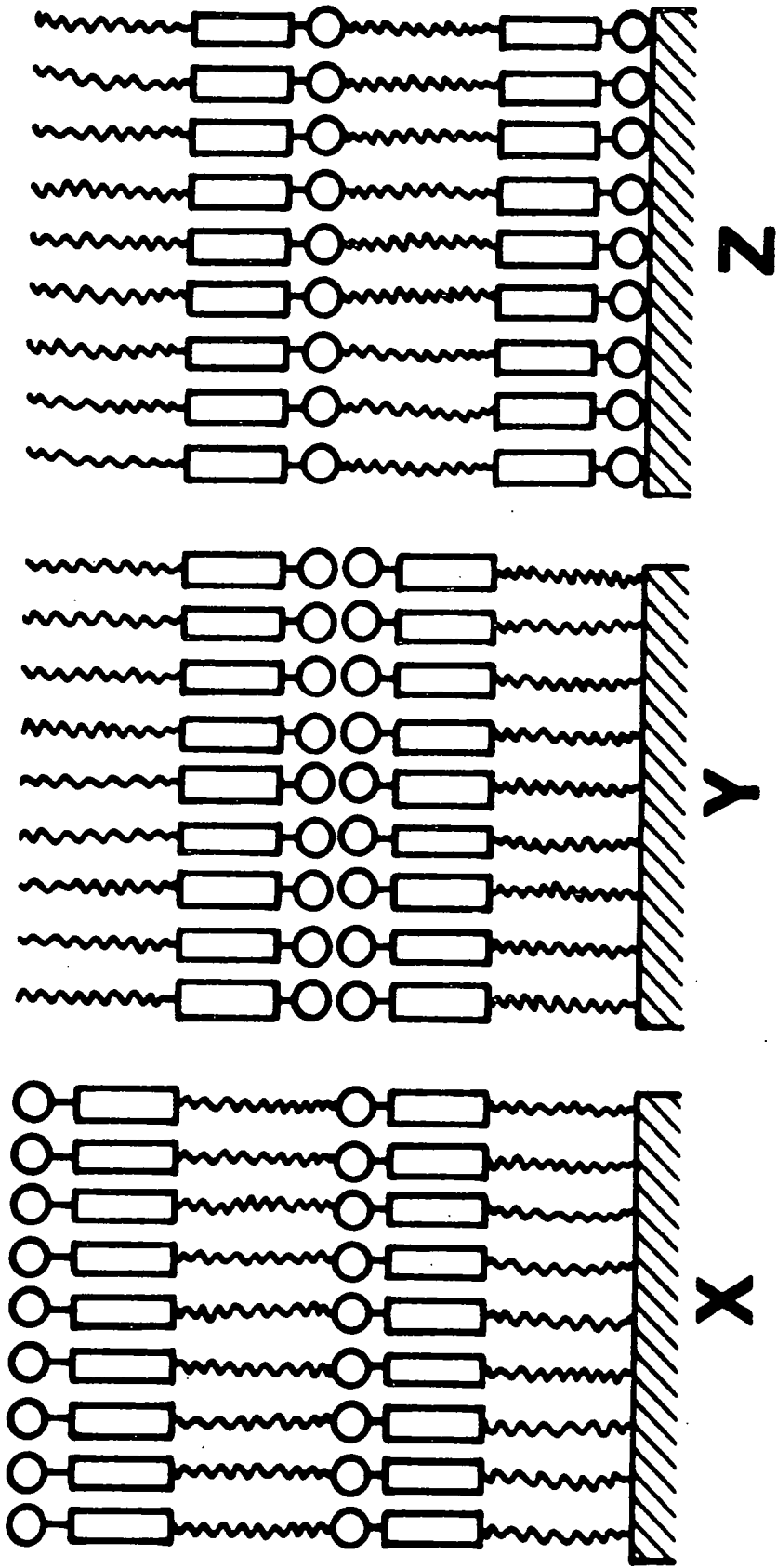


Figure 3.8 LB film deposition modes

the substrate. Thus, there will be a fundamental difference between the forces involved in this process and those involved in bonding succeeding layers to each other. Particular care was therefore taken when depositing the first layer, dipping being commenced immediately after the final surface treatment of the substrate, at low speeds ($\sim 2 \text{ mm min}^{-1}$), and a drainage time of at least 30 minutes was allowed before depositing any further layers.

In the cases where Z-type deposition was attempted, the water-surface monolayer was expanded before the downstroke in order to reduce the risk of any partial pick up during this half of the dipping cycle (in an ideal situation there would be no film on the water surface at all). The trough control unit permits this procedure to be done automatically (section 3.3.2).

3.7 Quality Assessment

At least three major aspects can be identified which pertain to the quality of LB films. Firstly, it is important to know whether the same amount of material is being deposited in each monolayer. Although this information can be deduced from the deposition ratios calculated for each layer from the dipping record (plot of area against time), the accuracy given by this technique is very low (particularly with small samples whose areas are almost insignificant compared to the trough area and/or water-surface monolayers which collapse or dissolve at an appreciable rate). Further problems with this method arise when mixed (heterogeneous) monolayers are being deposited, since the pick ups of the different components cannot be distinguished. The second major point in assessing film quality is the determination of the degree of crystalline

order in the films. A further consideration concerns the nature and number of any defects in the film; for instance, pinholes might occur between crystalline regions and lead to undesirable effects such as the short circuiting of any electrical contacts made to the film.

Most of the molecules investigated in this project had the common structural feature of a polarised conjugated system, designed in order to produce large non-linear optical effects but having the additional property of rendering the materials highly coloured. This strong absorption in the visible gives rise to a useful technique for checking that the pickup is uniform from one layer to the next; the optical absorption can be measured as a function of film thickness (at a fixed wavelength - usually the absorption maximum of the dye) and a linear characteristic should be obtained, provided that interference effects are small. The technique is particularly useful when looking at mixed layers since the absorption maximum of any one of the components at a time can be studied. Analogous linear plots can be made using data from infra-red reflectance spectra⁽²⁶⁾ or from the attenuation of the X-ray photoemission signal⁽²⁷⁾ from a metal substrate onto which the LB film has been deposited. Another technique in this class is to label the molecules of the film with ^{14}C and examine their autoradiographs so that a plot can be made of count rate versus number of monolayers⁽²⁸⁾.

Various diffraction techniques can be used to determine the degree of crystalline order in an LB film. For a complete structural assessment, transmission electron^(29,30), X-ray^(31,32), or neutron diffraction⁽³³⁾ can be employed, but for a rapid identification of the film structure reflection high energy electron diffraction (RHEED) is

adequate⁽³⁴⁾. RHEED is a very convenient technique in that it is non-destructive, and requires minimal sample preparation.

A widely practiced method for checking the consistency of deposition and for finding any major defects is to plot reciprocal capacitance against number of layers in a metal-insulator-metal structure. A linear plot would demonstrate the repeatability of dielectric thickness of each monolayer⁽³⁵⁾ (see section 4.2), but if the film is badly pinholed then all the devices will be short circuited and no meaningful values of capacitance will be obtained. Another method which is useful for observing large defects or particulate contamination is to view the film in reflection between crossed polarizers in an optical microscope; this technique can be extended to the observation of large crystallites in thick (i.e. $\sim 500\text{nm}$) LB films of an epitaxial nature⁽³⁶⁾.

3.8 Possible Applications for LB Films

The original proposed applications for LB films were very simple in nature, such as anti-reflection coatings, step-thickness gauges, and soft X-ray gratings. More recently researchers have been examining the potential of multilayer assemblies for much more subtle and complex uses. The range of such applications has been greatly enlarged by the introduction of the concept of alternate layer systems; such asymmetric structures may be employed as active layers in pyroelectric devices as well as the non-linear optical ones discussed in this thesis.

Passive applications of LB films include the opportunity to form an insulating layer of controllable thickness on semiconductors such as InP which, unlike silicon, do not have a native oxide with good insulating

properties. This is of great interest in the formation of metal-insulator-semiconductor (MIS) structures⁽³⁷⁾ for applications in integrated circuits and planar electronic devices. Similarly, LB films of ω -tricosenoic acid can be used to improve the breakdown strength of silicon-silicon dioxide structures⁽³⁸⁾. The same material has potential as an electron beam resist for microlithography in integrated circuit fabrication, the films being polymerisable and giving a resolution far greater than that of conventional spun photoresists⁽³⁹⁾. LB films can be used as overlays on conventional waveguide structures⁽⁴⁰⁾, the attraction being the precise control over film thickness and refractive index and hence over guided wave velocity.

Electroluminescent and photoconductive properties have been observed from structures incorporating a lightly substituted anthracene⁽⁴¹⁾. Phthalocyanines have interesting semiconducting properties and by making appropriate substitutions it should be possible to obtain films exhibiting p- or n-type conductivity. The electrical conductivities of some phthalocyanines are sensitive to gas ambients⁽¹¹⁾, suggesting applications as gas sensors. Further sensor applications are envisaged in the biological field, where an FET device incorporating an LB film made selective to certain ions or enzymes may be produced and used to monitor the levels of such species, for example potassium ions in the blood. An alternative approach uses the biological species to alter the optical properties of LB films.

LB films may also be used as model systems in fundamental research, such as in the spectroscopy of complex monolayers⁽⁴²⁾, the modelling of biological membranes⁽⁴³⁾, and for the modification of the properties of solid surfaces. A much more detailed account of the possible

applications of LB films can be found in reference 44 and in the next section, which deals with their potential uses in non-linear optical devices.

3.9 Non-Linear Optical Effects in LB Films

In chapter 1 it was stressed that in order for non-linear effects to be utilized in low-power semiconductor laser-driven systems, fully optimized structures are required, such as those employing waveguiding in thin films or fibres. Not only does the LB technique provide a means of depositing organic films of a precisely defined thickness, but it also enables the difficulties encountered in obtaining a noncentrosymmetric crystal containing highly non-linear molecules (section 2.3) to be overcome by using alternate layer systems. As a consequence there has been considerable recent interest in the study of non-linear optical effects in LB films.

One advantage of the use of waveguiding for optical SHG and mixing lies in the fact that phase-matching can be achieved using waveguide dispersion⁽⁴⁵⁾, a phenomenon arising from the dependence of the phase velocity of a given frequency of light on the guiding region dimensions, the refractive index difference between the guiding region and the substrate, and the mode of propagation. In practice the phase matching for the interacting modes can be achieved by tailoring the dimensions of the guiding region (e.g. by lithography) and/or the refractive index difference (e.g. by changing the length of the hydrocarbon tail, or the inclusion of metallic counter ions in the LB film material⁽⁴⁰⁾; alternatively a different substrate material could be used). An additional advantage arises from the dimensions of the guiding region being only of the order of microns for optical wavelengths, so that it

is possible to have the large optical intensities, requisite for non-linear interactions, with modest optical powers. Long interaction lengths are also possible since the optical energy is guided.

It can be shown⁽⁴⁶⁾ that the ratio of second harmonic conversion rates for planar waveguide and bulk samples is of the order of L/λ , where the interaction length, L , is typically 1 cm and the wavelength, λ , is approximately 1 μm . This ratio, in theory $\sim 10^4$, is clearly highly in favour of the waveguide configuration; in practice the ratio is closer to 10^2 due to pump depletion. One further parameter has to be dealt with when optimizing the conversion efficiency in a waveguide structure; the interacting guided modes at the fundamental and harmonic wavelengths may have weakly overlapping transverse energy distributions, and therefore the corresponding overlap integral should be optimized as far as possible⁽⁴⁶⁾. This may be achieved, to a certain extent, by topping a non-linear waveguide by a linear one of high refractive index, or by growing a linear, purely guiding, layer over a non-linear substrate. References 40 and 47-49 provide examples of investigations into the use of LB films as (linear) waveguides or as claddings on prefabricated waveguides.

Third-order non-linear effects do not require a non-centrosymmetric structure and can therefore be observed in conventional Y-type films. The relevant susceptibility, $\chi^{(3)}$, is large in polydiacetylenes and there have been extensive investigations of the non-linear optical properties of multilayers of this material. These include studies of third harmonic generation which has been enhanced, either by varying the fundamental wavelength⁽⁵⁰⁾ to match a resonance in $\chi^{(3)}$, or by exploiting the interference between the radiation generated from

multilayers deposited on the front and back faces of a quartz substrate^(46,51). Furthermore, Carter et al^(52,53) have reported an intensity-dependent refractive index, $n_2 \sim 10^{-6} I$ (where I is the intensity in MW cm^{-2}) for polydiacetylene multilayers in a planar waveguide structure (fabricated by depositing the film onto a metallized grating). This was measured by varying the optical intensity and observing the resultant changes in the coupling angle between the input laser beam and a waveguide mode.

There have been several reports of second harmonic generation from acentric LB film structures; those made by this author may be found in the appendices and will be discussed in later chapters. Girling et al have observed SHG from monolayers of a merocyanine dye⁽⁵⁴⁾ and from layers of the merocyanine⁽⁵⁵⁾ and a hemicyanine⁽¹⁴⁾ dye alternated with a fatty acid material. The first report of this kind was made by Aktsipetrov et al⁽⁵⁶⁾ who used a monolayer of an azo dye; subsequent papers describe the increase in the second harmonic signal strength on increasing the number of layers of the same dye in a non-centrosymmetric LB film structure⁽⁵⁷⁾, and the analysis of reflected second harmonic signals to determine the mutual orientation of neighbouring monolayers in multilayer arrays, the preferred orientation of the microcrystallites, and the molecular alignment in the film⁽⁵⁸⁾. SHG has also been observed from a monolayer of arachidic acid on a silver surface⁽⁵⁹⁾ (as a result of surface plasmon enhancement) and from a water-surface monolayer⁽⁶⁰⁾; in the latter case the data were used to determine the average orientation of the molecules at the air-water interface.

Chollet et al⁽⁶¹⁾ have studied electric field induced second harmonic generation (EFISH) from multilayers of polydiacetylenes. In these experiments the external d.c. field served to break the centrosymmetry of the film; for such a case the observed second harmonic does not arise from $\chi^{(2)}$, but rather its intensity is proportional to $\{\chi^{(3)}(-2\omega; \omega, \omega, 0) E_{\omega}^2 E_e\}^2$, where E_e is the local d.c. field experienced by the polymer and E_{ω} is the field of the laser beam.

The application of large electric fields can produce changes in the optical properties of organic materials. These effects give rise to the technique of electroabsorption, which can be used to measure the orientational order parameter of multilayer films^(62,63). Electroabsorption is a particular branch of the group of experimental methods known as modulation spectroscopy, and involves monitoring the small changes in a sample's optical transmission resulting from the application of an external field. In molecular solids these changes are usually the result of the Stark effect. For a molecule of dipole moment μ and polarizability tensor α , the change in potential energy, ΔU , on placing it in an electric field (which makes an angle θ to μ) is given by:

$$\Delta U = -\mu E \cos\theta + \frac{\alpha}{2} E^2 + \dots \quad (3.2)$$

The term in E in equation 3.2 represents the linear Stark effect, and that in E^2 the quadratic Stark effect. These phenomena could be called "pseudo" non-linear, since they do not involve the molecular hyperpolarizabilities (β , γ , etc.).

Only crystals with polar space groups can exhibit a first-order Stark effect, and in such materials it will generally dominate the second-order effect. In electroabsorption spectra, the first-order Stark effect can usually be recognised as the first derivative of the zero-field absorption curve. Blinov et al^(62,63) have performed an investigation of the linear Stark effect in LB films of an amphiphilic azo compound. This material could be fabricated into X-, Y-, or Z-type multilayers, depending on the deposition conditions employed. As anticipated, the linear Stark spectra exhibited a change in sign on going from X- to Z-type layers, and a radical (by a factor of 50) decrease in amplitude on changing to Y-type deposition. This provides direct evidence for the polar nature of X- and Z-type films.

Crystal structures having non-polar space groups may still exhibit a second-order Stark effect, giving rise to electroabsorption spectra which can be recognised as the second derivative of the zero-field absorption curve. Roberts et al⁽⁴¹⁾ have reported observing this phenomenon in Y-type LB films of a substituted anthracene.

A more detailed discussion of second harmonic generation from LB films may be found in chapter 8.

3.10 Summary

This chapter has reviewed the concepts, technology, and materials associated with the production of LB films. Some methods of analysis of the properties of water-surface monolayers and the deposited multilayer films have been described, along with a selection out of the vast range of possible passive and active applications of LB films.

CHAPTER 4

EXPERIMENTAL TECHNIQUES

4.0 Introduction

This chapter describes the general techniques used to fabricate LB film devices and to characterize these structures and the materials of which they are comprised. The preparation of substrates and the deposition of electrodes is described in section 4.1, whilst in 4.2 the measurement of dielectric thickness for metal-insulator-metal structures is discussed. Section 4.3 deals with spectrophotometric measurements on LB films and solutions, and the optical theme continues in 4.4 with the introduction of the surface plasmon resonance technique for studying multilayer assemblies on silver substrates. The electron diffraction techniques employed for structural characterization of LB films are presented in section 4.5. Finally, techniques for characterizing the non-linear optical properties of bulk powders (4.6) and LB films (4.7) are detailed.

4.1 Device Fabrication

4.1.1 Substrate preparation

(a) Glass

In the cases where the LB films were to be deposited directly onto glass substrates, Corning 7059 glass or Spectrosil B vitreous silica slides were used. The Corning slides were found to be acceptable for optical absorption measurements down to wavelengths of around 340 nm, but below this their transmittance became too small; however, the more

expensive Spectrosil slides could be used as far into the ultra-violet as 180 nm. When the films were to be deposited on a thin layer of metal, this was evaporated onto the surface of an ordinary Chance Select microscope slide.

Identical techniques for surface preparation were employed for all three types of glass. Particulate matter was removed by ultrasonic agitation, firstly in chloroform (followed by rinses in de-ionised water), then in a 20% Decon 90 alkaline soap solution, and subsequently in several batches of fresh de-ionised water as rinses. The slides were then degreased in hot propan-2-ol liquid and vapour for several hours in a Soxhlet reflux unit. This treatment leaves a hydrophilic glass surface, and when this was required the slides were used immediately after cooling. However, in cases where a hydrophobic surface was needed the slides had to be refluxed in a Soxhlet system containing $\sim 0.5\%$ dichlorodimethylsilane in 1,1,1-trichloroethane. Any residue from this treatment was removed by rinsing, firstly in methanol and then in de-ionised water.

(b) Silicon

Two types of silicon wafer were used: (i) p-type, {100} orientation, resistivity 14-21 Ωcm (Wacker-Chemitronic GMBH), and (ii) n-type, {111} orientation, resistivity 10.5-17.5 Ωcm (Dynamit Nobel). Both varieties were cleaned in hot 1,1,1-trichloroethane liquid and vapour in a Soxhlet reflux unit to give hydrophilic surfaces. Hydrophobic surfaces could be obtained by subsequent treatment with dichlorodimethylsilane vapour, as in (a).

(c) Aluminium

Aluminium films were evaporated at a pressure of less than 10^{-5} torr onto Chance Select glass slides which had been previously cleaned

as described in (a). Typically the range of thickness employed, as measured by a quartz crystal oscillator, was 10-100 nm. LB film deposition was commenced immediately after removing the slides from the evaporator; alternatively after refluxing them in propan-2-ol.

(d) Silver

Glass slides were prepared as described in (a). As silver adheres poorly to glass, it was necessary to first evaporate a layer of chromium onto which the silver could be deposited. These evaporations were performed sequentially at a pressure below 10^{-5} torr without letting the sample up to air between stages. As the films were required to be semi-transparent, the layers of silver and chromium were made less than 55 nm and 1 nm thick, respectively. The first monolayer was always deposited immediately after removing the substrates from the evaporator.

(e) Anodized aluminium

To grow an anodic oxide layer, a slide onto which a 300 nm thick aluminium layer had previously been evaporated (as in (c)) was placed in an electrolytic cell containing a solution of diammonium hydrogen citrate (approximately 3% by weight) with a stainless steel counter electrode. A 10V D.C. voltage was then applied across the cell; when the current had fallen nearly to zero (around 5 minutes later) the slide was removed, rinsed in water, and finally refluxed in IPA for several hours prior to LB film deposition.

4.1.2 Electrode deposition

The evaporation of top contacts onto an LB film is a process which requires great care, since conventional LB film materials generally have low melting points and therefore excessive heating has to be avoided. It has been found⁽¹⁾ that the mis-match between the thermal expansion coefficients of the film, electrodes and substrate generates problems if

the substrate is cooled to low temperatures throughout the evaporation, and so this technique was avoided. The procedure adopted was to perform the evaporation very slowly and in stages of approximately 1 nm with a 30 minute time delay between steps, until the desired total thickness had been achieved (typically 15 nm). Between stages a shutter was operated to screen the substrate from thermal radiation from the source. Throughout the evaporation the pressure was maintained below 10^{-5} torr. Two different top contact materials were investigated; gold, and aluminium/gold (formed by evaporating the two metals sequentially, no air being admitted until after the final stage). The latter combination was chosen because the melting point of aluminium is lower than that of gold, thus if this is the first layer then the thermal damage to the film is reduced; the function of the gold overlayer was to prevent problems of oxidation on exposure to the atmosphere.

4.2 Measurement of the Relative Permittivity of LB Films

The concept of the use of plots of reciprocal capacitance against number of monolayers to assess the quality of an LB film was introduced in section 3.7; such plots also readily yield a value for the dielectric thickness of the film at the frequency of measurement. This is an excellent method for evaluating the parameter, since the presence of an interfacial oxide layer of capacitance comparable to that of the LB film precludes the use of many of the techniques used to measure the permittivity of more conventional materials.

4.2.1 Experimental technique

The samples fabricated for these investigations consisted of an LB film of stepped thickness deposited onto an aluminized glass slide. Approximately 20 circular gold or aluminium/gold top contacts were

evaporated onto each step section, the mean value of capacitance being used in the final plots with the standard deviation giving an estimate of the error. Air-drying silver paste was employed to form an electrical contact to the aluminium base electrode, whilst a gold ball, positioned by a micromanipulator probe, made a pressure contact to the gold dots. A Boonton 72BD capacitance meter was used to measure the capacitance at 1 MHz. The samples were desiccated under a low pressure of nitrogen for several hours prior to the measurements, which were performed in a sealable brass sample chamber in order to eliminate light and electrical interference.

4.2.2 Interpretation of results

The total capacitance, C_T , of an LB film MIM structure is expressed in equation 4.1 in terms of a series combination of the LB film capacitance, C_{LB} , and the interfacial aluminium oxide capacitance, C_{OX} .

$$\frac{1}{C_T} = \frac{1}{C_{LB}} + \frac{1}{C_{OX}} \quad (4.1)$$

However, the LB film can be viewed as a parallel plate capacitor of area A , dielectric constant ϵ_r , and thickness Nd , where N is the number of layers and d is the monolayer thickness. Thus 4.1 can be expanded to give

$$\frac{1}{C_T} = \frac{Nd}{\epsilon_o \epsilon_r A} + \frac{1}{C_{OX}} \quad (4.2)$$

Equation 4.2 predicts that a plot of C_T^{-1} versus N will be a straight line of gradient $d(\epsilon_o \epsilon_r A)^{-1}$ and intercept C_{OX}^{-1} . Since ϵ_o and A

are known, the gradient can be used to give a value for the dielectric thickness, d/ϵ_r .

4.3 Measurement of Optical Absorption Spectra

All of the optical characterizations were performed using a Cary 2300 UV-VIS-NIR spectrophotometer. Where solution spectra were required, the solutions were contained in quartz cuvettes. LB film samples were deposited onto either Spectrosil B vitreous silica (for measurements on weakly absorbing films down to 180 nm) or Corning 7059 glass (where measurements below 340 nm were not required, or down as far as 250 nm for films with absorbance > 0.1) slides, as described in 4.1.1. The optical absorption spectra of all of the LB film specimens were recorded in transmission, so that layers on both sides of the glass slides contributed to the absorption.

4.4 Surface Plasmon Resonance

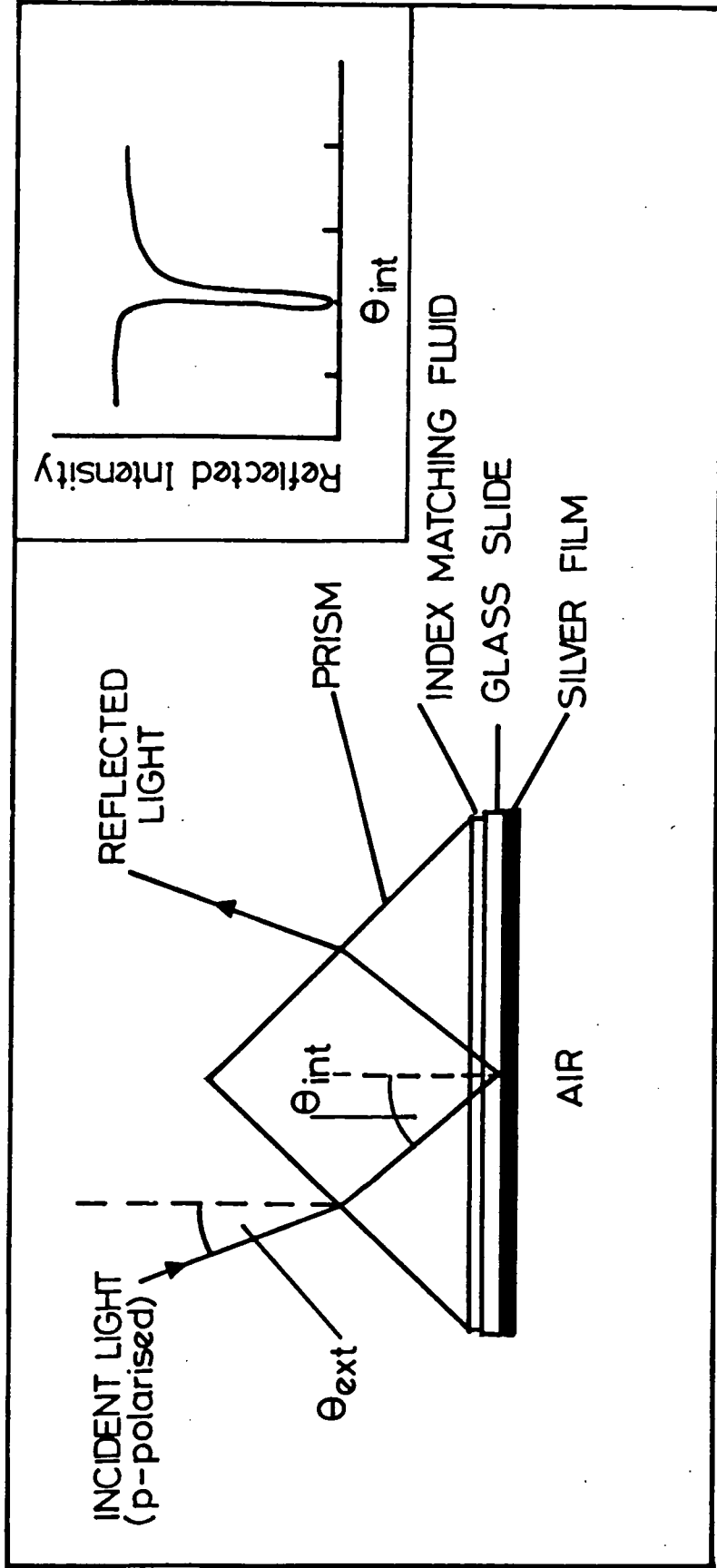
Surface plasma oscillations (SPO's) are collective oscillations of the free charges at a metal boundary which propagate along the interface. The electromagnetic field associated with the motion of the charge is a maximum at the boundary and decays exponentially on both sides, hence SPO's are sensitive to any modification occurring at the interface⁽²⁾. By coating the metal surface with an LB film and observing the effects on the SPO's, the optical constants (thickness and refractive index) of the film can, in principle, be determined^(2,3). An extensive review of SPO's and their applications can be found in reference 4.

The LB film samples used in these investigations were deposited onto silver surfaces prepared by evaporating a thin layer of silver onto

a glass slide (section 4.1.1). SPO's can be excited optically by using evanescent waves in a grating or prism arrangement; prism coupling in the Kretschman configuration (illustrated in figure 4.1 for a silver surface with no LB overlayer) was employed in these experiments. The external angle of incidence, θ_{ext} , of the p-polarised light from a 1mW He Ne laser ($\lambda = 632.8$ nm) could be varied by rotating the laser about an axis centred on the substrate, thus changing the component of the wavevector of the incident light parallel to the prism base. SPO's at the metal surface opposite to the prism were excited by the evanescent field inside the metal when this component matched the real part of the SPO wavevector; this phenomenon was detected by a pronounced minimum in the reflected intensity caused by the strong, resonantly enhanced absorption in the silver film (see inset in figure 4.1). The position and shape of this minimum depends strongly on the optical properties of any overlayer deposited on the silver surface. LB films of transparent materials such as ω -tricosenoic acid display sharp surface plasmon resonance (SPR) minima whose depth is invariant but whose angular position changes progressively with thickness. Highly absorbing or scattering films display broader SPR minima whose angular position also changes progressively but whose depth decreases and width increases with increasing film thickness.

Before commencing each SPR study, the external angle scale of the laser was calibrated by finding the critical angle of a glass slide and adjusting the scale to read the correct value of external angle corresponding to the theoretical internal angle of incidence. A computer program was available to convert between external (θ_{ext}) and internal (θ_{int}) angles of incidence, taking into account the refractive

Figure 4.1



Kretschman arrangement for the observation of surface plasmon resonance by attenuated total reflection. The inset shows the variation of the reflected intensity as a function of angle of incidence.

indices of the prism, index matching fluid, and glass slide. The glass slide was then replaced by the sample and the variation in reflected intensity (measured by a photodiode) observed as a function of θ_{ext} for a region of silver free of LB film. A second computer program was used to plot out a normalised SPR curve of reflectance against θ_{int} from the measured values of θ_{ext} and photodiode voltage. The sample was then translated relative to the prism base in order to bring an LB film-covered region into the beam. Subsequently the process was repeated to generate a new SPR curve for the silver plus LB film, the shift in resonance due to the film being given by $\Delta\theta_{\text{int}} = \theta_{\text{int}}(\text{LB}) - \theta_{\text{int}}(\text{Silver})$. If the LB film structure was stepped in thickness, then a series of resonance curves could be obtained and a plot made of $\Delta\theta_{\text{int}}$ versus number of monolayers. Work is currently underway to develop a computer program to curve-fit the experimental SPR curves to theoretical ones in order to obtain values of thickness and refractive index for the films; such measurements are expected to be comparable in accuracy to ellipsometric techniques, whilst being easier and cheaper to perform. At the moment, however, the results are more qualitative in nature, although a method by which the refractive index may be estimated is described in section 6.3.

4.5 Electron Diffraction

Transmission electron diffraction (TED) and reflection high energy electron diffraction (RHEED) studies were performed in a JEM 120 transmission electron microscope operated at a beam voltage of either 80 kV or 100 kV. For both the TED and RHEED investigations the samples were held in a goniometer positioned below the projector lens; in this position the region of sample contributing to TED was about 200 μm in

diameter. LB films for RHEED investigation were simply deposited on silicon dioxide substrates (silicon wafer fragments possessing a native layer of oxide), whilst the preparation of TED specimens was more complex and is described below.

The most basic requirement for a sample to be suitable for examination by TED is that it must be thin enough to allow transmission of the electron beam; obviously, this is no problem with the LB film itself, but the film must be supported and it is this substrate which creates difficulties. The method used to overcome this problem was the Walkenhorst-Zingsheim technique^(5,6). This involved the deposition of the LB films onto an anodized aluminium slide (section 4.1.1), and the subsequent transfer of the film plus the thin anodic oxide support to an electron microscope copper grid. In order to separate the film and support from the glass slide, the sample was placed in a Petri dish which was then filled with a solution of mercuric chloride and acetic acid to a level slightly higher than the slide surface, but not so high as to completely immerse the slide. The aluminium layer would then be slowly etched away, leaving the LB film with its alumina support floating on the water surface, ready to be lifted from below onto a copper grid and drained on filter paper.

4.6 Kurtz Powder Technique

The Kurtz powder technique^(7,8) is a convenient method for screening large numbers of powdered materials for second-order non-linear optical activity without needing to grow large single crystals or optimize LB film deposition conditions. One major drawback for its use in screening LB film materials is that if the material packs centrosymmetrically (as a lot of long chain dipolar materials will do),

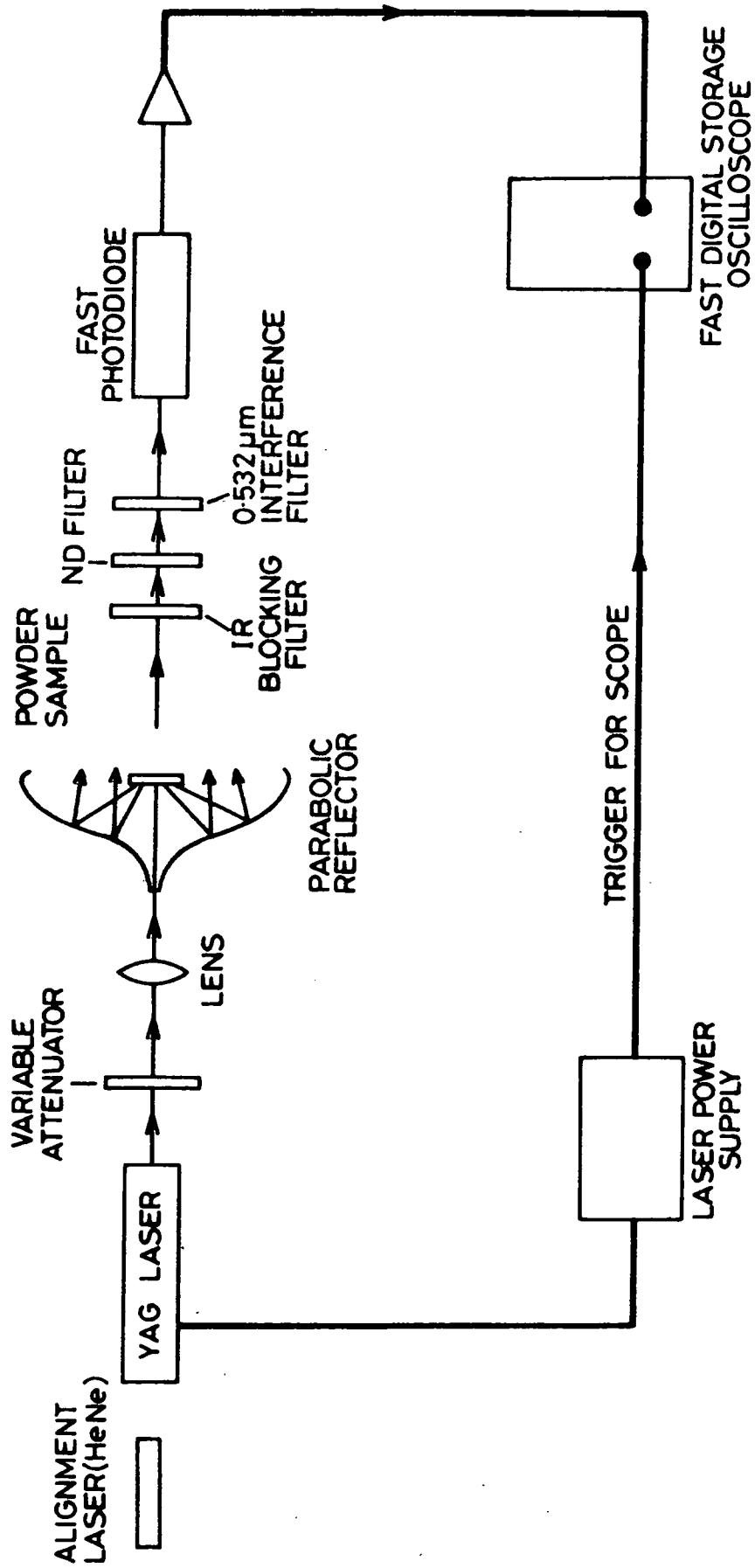


Figure 4.2 Schematic layout of the apparatus used in the Kurtz powder technique.

then even if the molecules do have large β values, no activity will be observed. Thus the technique can only be used as a preliminary check to look for materials with obvious non-linearities so that they can be given immediate attention, and those showing no activity should not be abandoned on this evidence alone (since in acentric LB film form they may be highly non-linear).

In the powder technique a Nd:YAG laser is directed onto a thin layer of powdered material compacted into a cell, and the frequency doubled light emitted from the sample over 4π radians is collected, filtered to remove the fundamental, and detected with a fast photodiode (figure 4.2). The signal produced is then compared with that obtained from a standard powdered sample, such as urea or lithium niobate. The technique is crude in that it detects a convolution of all the tensor components of $\chi^{(2)}$ and makes little attempt to account for the propagation characteristics of the beams. Nevertheless, general trends can be observed and it has been used extensively by workers in the area of single crystals⁽⁹⁾. Great care must be exercised in applying this technique quantitatively, since the results are particle-size dependent (see section 6.4).

4.7 Second Harmonic Generation from LB Films

The measurements described in this section were performed at GEC Hirst Research Laboratories with the collaboration of Drs. I. R. Girling and P. V. Kolinsky. An illustration of the equipment used for the study of second harmonic generation from LB monolayer and multilayer structures is given in figure 4.3; minor variations are detailed in the appropriate results sections (Chapter 3). All of the LB film samples used in this investigation were deposited onto hydrophilic glass slides

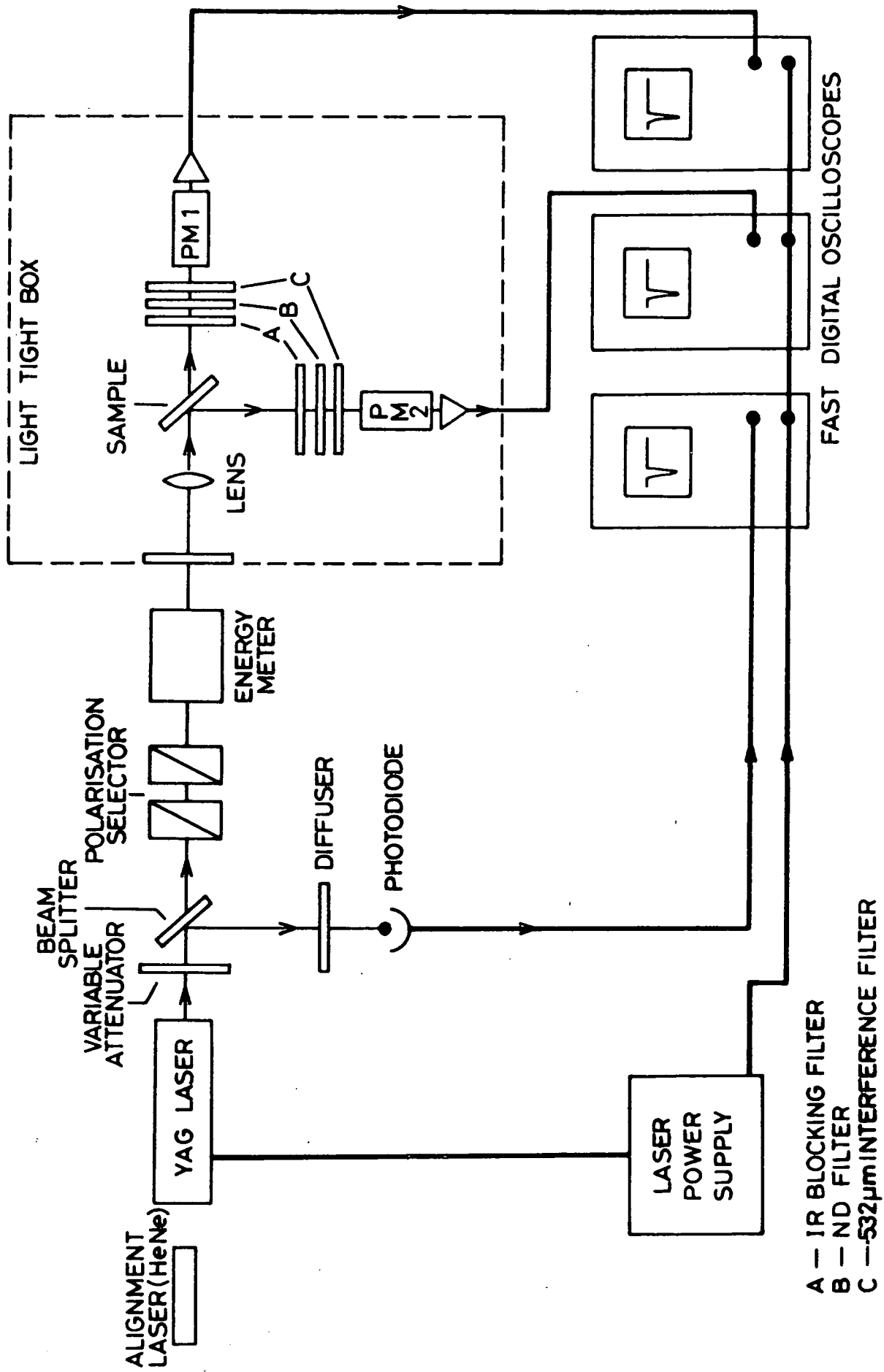


Figure 4.3

Schematic layout of the apparatus used in the study of SHG from LB films.

(sometimes Chance Select, but usually Corning 7059 since the use of the latter seemed to promote better film deposition). Linearly polarized light (Q-switched Nd:YAG, 1.064 μm , 25 ns FWHM), polarized either parallel (p) or perpendicular (s) to the plane of incidence, was directed at a 45° angle of incidence onto the vertically mounted sample. The second harmonic radiation (532 nm) resolved into s- and p-polarized components was detected in both reflection (R) and transmission (T) geometries using photomultiplier tubes at 90° and 180° respectively to the pumping direction. The total energy of each fundamental pulse was measured using a transmission type energy meter (GEC TF series). In addition, the variation in peak power was monitored using a photodiode. The outputs from the photomultiplier tubes and photodiode were all displayed on fast digital oscilloscopes. Infrared blocking filters and 532 nm interference filters were used to ensure that only second harmonic radiation was detected. Pulse energies of up to 2mJ with a beam diameter of approximately 200 μm were used for all the measurements on the LB films.

Results were obtained by averaging over several pulses at a number of different positions on each area of the sample. Absolute values of the electric field at 532 nm ($E(2\omega)$) were obtained by calibrating the system against a y-cut quartz wedge and relating both the second harmonic signals and incident energy to the d_{11} non-linear coefficient of quartz⁽¹⁰⁾ (see section 8.1). Some variations on the basic experiment described above were performed in which the effects of changing the angle of incidence or of rotating the sample about an axis perpendicular to its surface were investigated.

CHAPTER 5

MONOLAYER CHARACTERIZATION

5.0 Introduction

In chapter 3 the three categories of materials which were investigated in this project were introduced; section 5.1 describes the molecules within each class and the reasoning behind their selection. The importance of pressure-area isotherms and monolayer stability studies in the screening of new materials for LB film formation is discussed, and results are presented for each of the new compounds. Finally, the optimum dipping conditions for the most promising materials are given in section 5.4.

5.1 Materials

Since the aim of this project was to develop LB films displaying large optical non-linearities, the emphasis of the work described in this chapter was placed on those materials fulfilling the criteria detailed in chapter 2 for the production of a large second-order molecular hyperpolarizability (β). The basic structure of these molecules therefore comprised of donor and acceptor functionalities separated by a conjugated system, with the addition of hydrophobic groups to improve the stability of the water-surface monolayer. In order to gain an insight into what chemical groups confer good film-forming properties to the molecules, several materials were studied which were subtle variations on the "ideal" ones. It was hoped that a comparison of the non-linear behaviour of LB films of these compounds with those of the target materials could be used to check the validity of the guidelines for obtaining molecules with large values of β .

The three categories of material are discussed in separate sub-sections: modified commercially available materials; anthracene derivatives; and dipolar chromophores.

5.1.1 Modified commercially available materials

This section covers a series of chromophores which were purchased from commercial outlets and subsequently modified in the Department of Chemistry at Durham. The modification usually took the form of the addition of a hydrocarbon tail to the molecule in order to reduce its solubility in water.

2,6-Dichloroindophenol was modified to give M1 and M2 (figure 5.1) which contain the same highly conjugated chromophore, but M1 has a hydrocarbon tail whereas M2 has a shorter fluorocarbon tail. Similarly, compound M3 (figure 5.1) was synthesized from Primulin, a biochemical stain reagent.

5.1.2 Anthracene derivatives

The anthracene derivatives described in this section were all synthesized in the Department of Chemistry at Durham (with the exception of A1, which was purchased from ICI) and are summarised in figure 5.2. Compound A1 is known to form LB films. The very short hydrocarbon chains of A1 ensure that the interesting electronic properties of the delocalized aromatic π -electron system are not greatly diluted; however, their length does give rise to some solubility problems which require careful control of both the subphase pH and the type and concentration of the counterions in order for them to be overcome. A further problem of the molecule is that it is prone to oxidative degradation. Nevertheless, high quality multilayers of A1 have been assembled from which electroluminescence has been observed and which display a marked

Figure 5.1 Modified commercially available materials

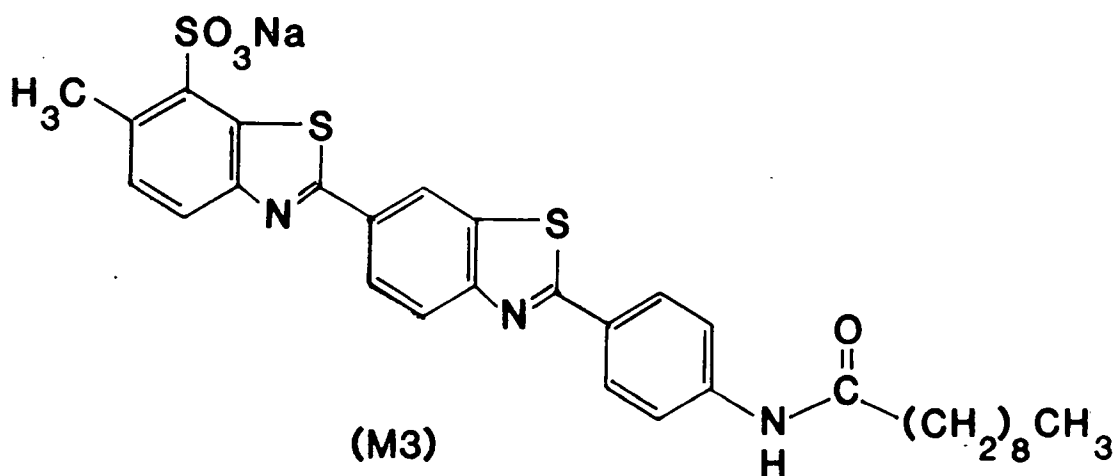
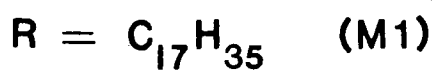
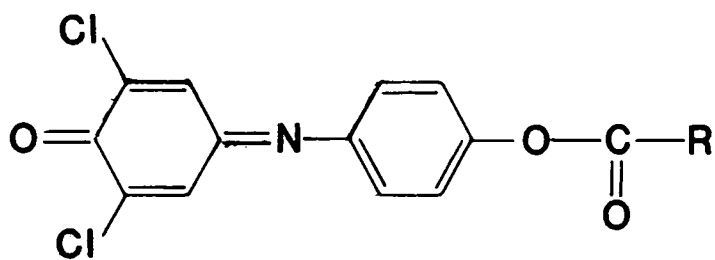
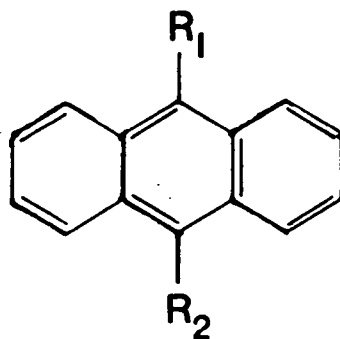


Figure 5.2 Anthracene derivatives



<u>Ref. No.</u>	<u>R₁</u>	<u>R₂</u>
A1	CH ₃ (CH ₂) ₃ —	—(CH ₂) ₂ COOH
A2	F ₃ C—C(=O)—	—(CH ₂) ₂ COOH
A3	CH ₃ (CH ₂) ₃ —	—C(=O)—CF ₃
A4	CH ₃ (CH ₂) ₃ —	—CH(OH)—CF ₃
A5	CH ₃ (CH ₂) ₃ —	—CH=CH—C ₆ H ₄ (N ⁺ CH ₃) ₃ I ⁻
A6	CH ₃ (CH ₂) ₃ —	—CH=CH—COOH
A7	CH ₃ (CH ₂) ₃ —	—CH=CH—C ₆ H ₄ (COOH)
A8	CH ₃ (CH ₂) ₃ —	—CH=CH—C ₆ H ₄ (NO ₂)
A9	CH ₃ (CH ₂) ₃ —	—CH=CH—C ₆ H ₄ (OH)

anisotropy in their conductivity⁽¹⁾, the in-plane value exceeding that in a direction perpendicular to the layers by a factor of 10^8 .

The conjugated system of the anthracene nucleus could prove valuable in enhancing the non-linear effects of any substituent groups attached to it. The other derivatives (A2-9) were synthesized with this in mind, as well as the other advantages of A1 over conventional LB film materials discussed above. In practice, the limitation of most of these materials was found to be solubility (see later sections).

The group R_1 in compounds A1 and A3-9 will be a very weak donor; in A2 it is an acceptor. A much greater range of groups was used for R_2 : in A9 it is a weak donor, whereas in A1, A2, A4, A6 and A7 it is a weak acceptor, and in A3, A5 and A8 it is a much stronger acceptor. Thus there is a range of different types of molecule, falling into the following categories:

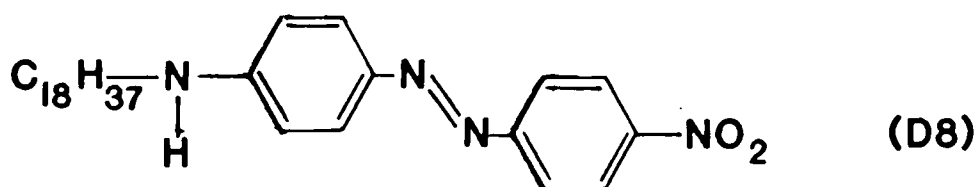
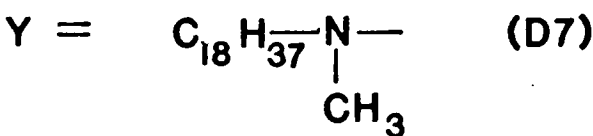
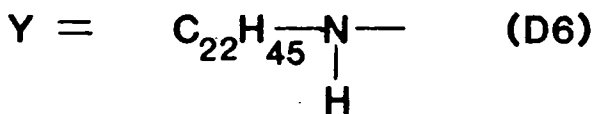
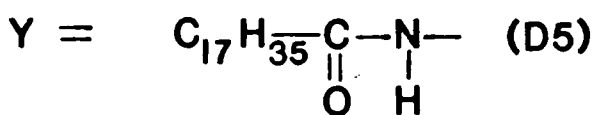
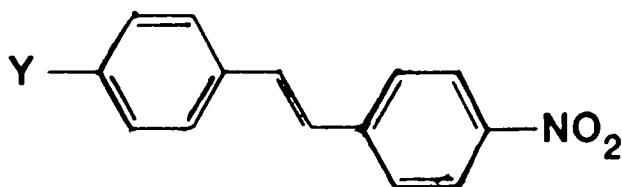
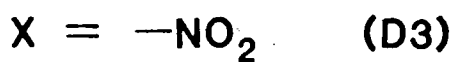
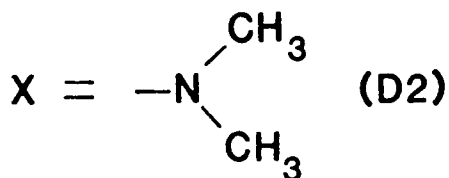
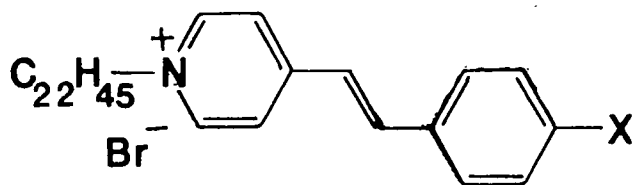
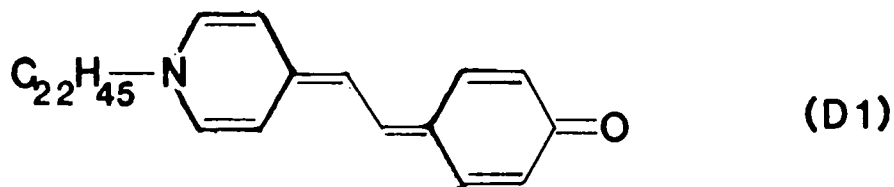
- (i) Weak donor, weak acceptor (A1, A4, A6, A7)
- (ii) Weak donor, strong acceptor (A3, A5, A8)
- (iii) Weak acceptor, strong acceptor (A2)
- (iv) Two weak donors (A9)

5.1.3 Dipolar chromophores

This series of compounds clearly illustrates the use of donor and acceptor groups separated by a conjugated system in order to produce molecules with large β 's. Unlike the anthracene derivatives, all of these molecules possessed long hydrocarbon tails in order to render them water-insoluble.

Samples of the merocyanine dye D1 (figure 5.3) were obtained from two different sources (D1A from G. L. Gaines, Jr., General Electric Corporate Research and Development, and D1B from I. R. Girling, GEC Research), whereas the styrylpyridinium dyes (D2-4) and two of the

Figure 5.3 Dipolar chromophores



stilbene dyes (D5 and D6) were synthesized at Durham. Compound D7 was provided by M. F. Daniel (R.S.R.E., Malvern) and the azo dye D8 was synthesized at Hull University.

In compounds D2-4, the pyridinium group should act as an acceptor; the dimethylamino group of D2 is a donor and therefore D2 has the desired donor/acceptor properties. However, nitro groups are electron acceptors and so D3 has two acceptors and no donor; this should make it a useful compound for demonstrating the need for charge-transfer in the molecule, since D3 should, in theory, exhibit only weak non-linear optical activity. Similarly, a carboxylic acid group is a weak acceptor (although it becomes even poorer on ionization) and so little activity should be expected from D4; however, this functionality might enable the material to form better quality LB films. The stilbene dyes D5-7 all have nitro acceptor groups; the donor in D5 is an amide group, whereas dyes D6 and D7 have the slightly stronger amine donors. Compound D8 represents the azo analogue of D6 and should thus provide a good comparison of the relative merits of stilbene and azobenzene units as conjugated systems.

In summary, D1, D2 and D5-8 are all donor/acceptor chromogens, whereas D3 and D4 have two acceptor groups and no donor.

5.2 The Interpretation of Pressure-Area Isotherms and Monolayer Stability Studies

5.2.1 Pressure-area isotherms

The pressure-area (π -A) isotherm of an "ideal" LB film material, stearic acid, was given in figure 3.7. This isotherm displayed distinct phases in its structure; the presence or absence of any or all of such phases in the isotherms of the novel materials should give clues as to

how their monolayers are behaving as compared to the ideal materials. Materials which register a finite surface pressure at very large molecular areas and whose isotherms have very gentle slopes with increasing pressure are likely to have their molecules lying nearly flat on the water surface when uncompressed⁽²⁾, the act of compression only gradually altering their orientation such that the hydrocarbon chains point vertically. The most promising isotherms display only a small surface pressure prior to the "solid" or condensed phase, which should be quite steep (but not so steep that it becomes impossible to maintain the surface pressure at a constant value within this region, as is the case with some particularly rigid monolayers).

The isotherms are plotted with area per molecule (a_m) as the abscissa; this axis is originally recorded as the area, A, of the water surface enclosed by the trough barriers, and is subsequently converted to the a_m scale using equation 5.1. This relation uses the known concentration of the spreading solution (c) and the volume of solution spread (V) to find the mass of material on the water surface, and hence the number of molecules present (via the molecular weight, M, of the material, and Avogadro's number, N_A).

$$a_m = A \frac{M}{cVN_A} \quad (5.1)$$

The errors in c and V are quite small; in the case of c these inaccuracies arise out of the process of weighing the solid and amount to $\pm 0.5\%$, whereas the error in V depends largely on the method used to dispense the solution. If an Agla precision microsyringe is used, then the error in V should be approximately $\pm 0.3\%$, but if a Hamilton fixed needle microsyringe is used then this figure is likely to be closer to

$\pm 1\%$. There will only be a small error ($\pm 0.5\%$) in the measurement of A for mobile monolayers; however, with rigid monolayers the "arms" of the trough (see figure 3.2 in chapter 3) do not become fully covered with film and this leads to a much larger error in A ($\pm 7\%$ at maximum trough area). The total error in a_m is thus approximately $\pm 1.5\%$ for fluid monolayers but much greater for rigid ones.

It is important to note that the accuracy of the a_m scale is not always as high as one might expect from the precision with which A , c and V are known, since the presence of soluble impurities in the bulk material or any dissolution of the monolayer itself prior to completion of the isotherm will give rise to values of a_m which are too small. It is also important to note that for a_m to be the surface area occupied by one molecule, the spread film must be only one molecule thick; indeed, small values of a_m can often be used as a good indication that monomolecular layers are not being formed. In view of these considerations, a_m is usually referred to as the "apparent" area per molecule.

There are two values of a_m which are particularly useful in characterizing a monolayer. The first of these is a_m^c , the area per molecule at the onset of collapse; the corresponding value of surface pressure, π_c , is also of great interest. Extrapolating the steep, linear, high-pressure region of the isotherm to zero pressure yields the limiting area per molecule in the solid phase, a_m^o (accurate to $\pm 3.5\%$, in view of the errors in extrapolation on top of those of the a_m scale itself).

It is often interesting to compress a monolayer to a surface pressure just below its collapse point, then allow it to relax back to its original area before recompressing it; any changes can be observed

in the form of the isotherm. In cases where a monolayer exhibits significant dissolution, this process will dominate the changes in the isotherm; however, in some situations where solubility is not a problem, changes can be seen in the slope of the π -A curve, due to molecular reorganization, whilst a_m^c remains unchanged.

The onset of collapse of a Langmuir film at high surface pressures can be observed in two different ways. Firstly, the slope of the isotherm reduces markedly at the collapse point, and secondly, striations parallel to the moving edges of the barrier become visible in the film (particularly noticeable with intensely coloured dye materials). The collapse of a Langmuir film is viewed as being the catastrophic failure of the film structure in which the molecules start to pile up on top of each other. With some materials only a small surface pressure can be developed before the onset of collapse, whilst others may form multilayers on the water surface spontaneously upon spreading. Careful observation of the water surface prior to compression can sometimes lead to the identification of materials belonging to the latter category, owing to their tendency to form coloured islands visible to the naked eye. A suitably steep isotherm, but one which displays a low a_m , may occasionally be produced as such a multilayer film is compressed. Such materials are of no use in this form, but frequently they can be diluted to form a mixed monolayer with stearic or arachidic acid in order to produce good quality LB films⁽³⁾. The molar ratio of acid : dye in such mixtures is commonly 3:1, but may be as low as 1:1 or as high as 10:1, depending on how poorly the material behaves. In section 3.5.3 the need for mobility in the monolayer was described; the formation of mixed monolayers, often with relatively low percentages of fatty acid, provides a means of imparting

the desired fluidity. The use of slow-evaporating solvents is another way of circumventing monolayer rigidity, although this approach is highly empirical and is not always successful.

5.2.2 Monolayer stability studies

In order for a material to be of practical use for LB film formation, the rate of dissolution/collapse of the water-surface monolayer at the deposition surface pressure should not be too great (ideally it should be zero). Some representative monolayer area decay curves are included in section 5.3. For some materials this decay can be reduced by the careful optimization of subphase conditions such as temperature, pH, and ionic content, although temperature cannot be conveniently varied with the Langmuir trough used for this work. In this chapter the process of subphase optimization is exemplified by the amidonitrostilbene D5, although its rate of collapse under most conditions was not considered fast enough to be a limiting factor to its usefulness.

The procedures adopted and the conditions used when monitoring the change in film area with time or in plotting an isotherm were standardised as far as possible (constant temperature, compression rate, period of solvent evaporation, etc.) since any of these factors may have a significant effect on the result. Wherever possible, the surface pressure at which the decay in area was studied was selected to be in the centre of the condensed phase in the isotherm.

5.3 Monolayer Characterization : Results

Some typical pressure-area isotherms and monolayer stability studies for the various classes of material investigated are illustrated in figures 5.4 - 5.14. The essential features of these isotherms have

been extracted and appear in table 5.1, together with some general comments. The colours referred to are those of the spreading solutions. Where the films are obviously not monomolecular, the values of a_m^O , a_m^C , and π_c are bracketed as they are not really meaningful. In some cases two figures are given for these quantities; this is where the isotherm possesses two steep regions, either of which could represent a condensed phase (although usually the one at higher molecular area will be the true solid phase, the subsequent shallow region representing collapse and the second steep region arising from the compression of a bilayer). Where "dissolution" is referred to in table 5.1, the term is being used for convenience, since strictly speaking the mechanism by which molecular area decreases with time could be dissolution, collapse, evaporation or rearrangement, or any combination of these phenomena.

Some materials were not sufficiently soluble in chloroform (CHCl_3), or other commonly used volatile organic solvents, to form suitable spreading solutions. In these cases the material was first dissolved in dimethyl formamide (DMF), a very powerful solvent, and then diluted with approximately nine times this volume of chloroform. In view of the miscibility of DMF with water, it was feared that the use of such a solvent would lead to material being taken down into the subphase within droplets of solution during the spreading process, resulting in the measured area per molecule values being too small. However, when a spreading solution of arachidic acid was prepared using an even higher percentage of DMF, it was found to give an isotherm identical in both shape and a_m^O to that obtained when pure chloroform was used as a solvent.

TABLE 5.1 Summary of Langmuir film properties of materials investigated

Material	Solubility	Colour	a_m^o /nm ²	a_m^c /nm ²	π_c /mN m ⁻¹	Comments
M1	-	-	-	-	-	Water-soluble
M2	Readily in DMF/CHCl ₃	Red/Brown	0.21	0.13	40	Slow rate of dissolution at 32 mN m ⁻¹
M3	Fairly in DMF. Deposited in 1:9 DMF/CHCl ₃ mixture	Yellow	0.23	<0.19	>40	Negligible dissolution at 25 mN m ⁻¹
A1	Readily in CHCl ₃	Colourless	0.43	0.39	25	Rapid dissolution at 15 mN m ⁻¹ - only of practical use at pH < 4.5
A2	Readily in CHCl ₃	Red	0.18	0.13	>40	Very slow dissolution at 40 mN m ⁻¹
A3	Readily in CHCl ₃	Golden	-	-	-	Highly soluble in subphase
A4	Readily in CHCl ₃	Pale Yellow/Green	0.38	0.32	7	Rapid dissolution at 7 mN m ⁻¹
A5	Readily in CHCl ₃	Orange/Red	-	-	-	High soluble in subphase
A6	Readily in CHCl ₃	Yellow	(0.10)	(0.07)	(12)	Moderately soluble at 11 mN m ⁻¹
A7	Readily in CHCl ₃	Pale Yellow	-	-	-	Highly soluble in subphase
A8	Readily in CHCl ₃	Yellow	0.38/ (0.18)	0.35/ (<0.13)	5/ (>40)	Very slow dissolution at 5 mN m ⁻¹ Fairly slow dissolution at 36 mN m ⁻¹

TABLE 5.1 (Cont)

Material	Solubility	Colour	a_m^0/nm^2	a_m^c/nm^2	$\pi_c/\text{mN m}^{-1}$	Comments
A9	Readily in CHCl_3	Yellow	0.29/ (0.17)	0.26/ (<0.12)	9/ (>40)	Slow dissolution at 7 mN m^{-1} and 40 mN m^{-1}
D1	Readily in CHCl_3	Turquoise (dilute) Red/Purple (concentrated)	0.67 /0.32	0.41 /0.19	28 /47	Negligible dissolution at 28 mN m^{-1} . Rapid dissolution at 41 mN m^{-1} , reduced if $\text{pH} > 8$
D2	Readily in CHCl_3	Red	0.34	<0.26	>40	Distinct phase change at $\pi \sim 10 \text{ mN m}^{-1}$, $a \sim 0.9 \text{ nm}^2$. Fairly slow dissolution at 40 mN m^{-1}
D3	Readily in CHCl_3	Orange/Brown	0.60	<0.39	>40	Shallow isotherm
D4	Moderately in DMF. Deposited in 1:9 DMF/ CHCl_3 mixture	Colourless	(0.12)	(<0.11)	(>40)	Negligible dissolution at 30 mN m^{-1}
D5	Readily in CHCl_3	Yellow	0.30	<0.26	>40	Fairly slow dissolution at 32 mN m^{-1}
D6	Readily in CHCl_3	Amber/Orange	0.33	<0.29	>40	Slow dissolution at 30 mN m^{-1}
D7	Readily in CHCl_3	Orange	(0.08)	(<0.06)	(>40)	Very slow dissolution at 25 mN m^{-1} . However, spreads as islands (i.e. not a monolayer)
D8	Readily in CHCl_3	Orange	(0.28)	(<0.21)	(>40)	Rapid dissolution at 30 mN m^{-1} . Spreads as islands (i.e. not a monolayer)

5.3.1 Modified commercially available materials

Compound M1, a long hydrocarbon chain derivative of 2,6-dichloroindophenol, proved to be water-soluble, whereas M2, the analogue with a shorter fluorocarbon tail, was much more insoluble. Isotherms of M2 were found to be almost identical throughout the pH range 4.5 - 9.0, and a typical one is shown in figure 5.4. Although this does not display the distinct phase changes of stearic acid, it is sufficiently steep at high surface pressures to be of interest for further study. The inset to figure 5.4 illustrates the high stability of a water-surface monolayer of M2.

It seems highly probable that the Langmuir films of M2 are not truly monomolecular, since the a_m^0 value of 0.21 nm^2 is much closer to the cross-sectional area of a hydrocarbon chain than to that of the more bulky fluorocarbon chain or the chromophore. This problem arises again with the Primulin derivative M3, whose suitably steep isotherm is also shown in figure 5.4 and whose a_m^0 of 0.23 nm^2 seems very small for such a bulky chromophore. Since the films exhibit no sign of dissolution, the only possible explanation for the low values of area per molecule, other than bilayer formation, is that the bulk solid contained a high percentage of soluble impurities.

5.3.2 Anthracene derivatives

The preparation of LB films of compound A1, 9-butyl-10-anthrylpropionic acid (or C4 anthracene) has been extensively discussed by Vincett et al⁽⁴⁾, but since it forms the basis of this group of materials it warrants a brief description here. Figure 5.5 shows the pressure-area isotherms for A1 at three different values of subphase pH; it can easily be seen that lowering the pH increases the collapse surface pressure and renders the material less water-soluble,

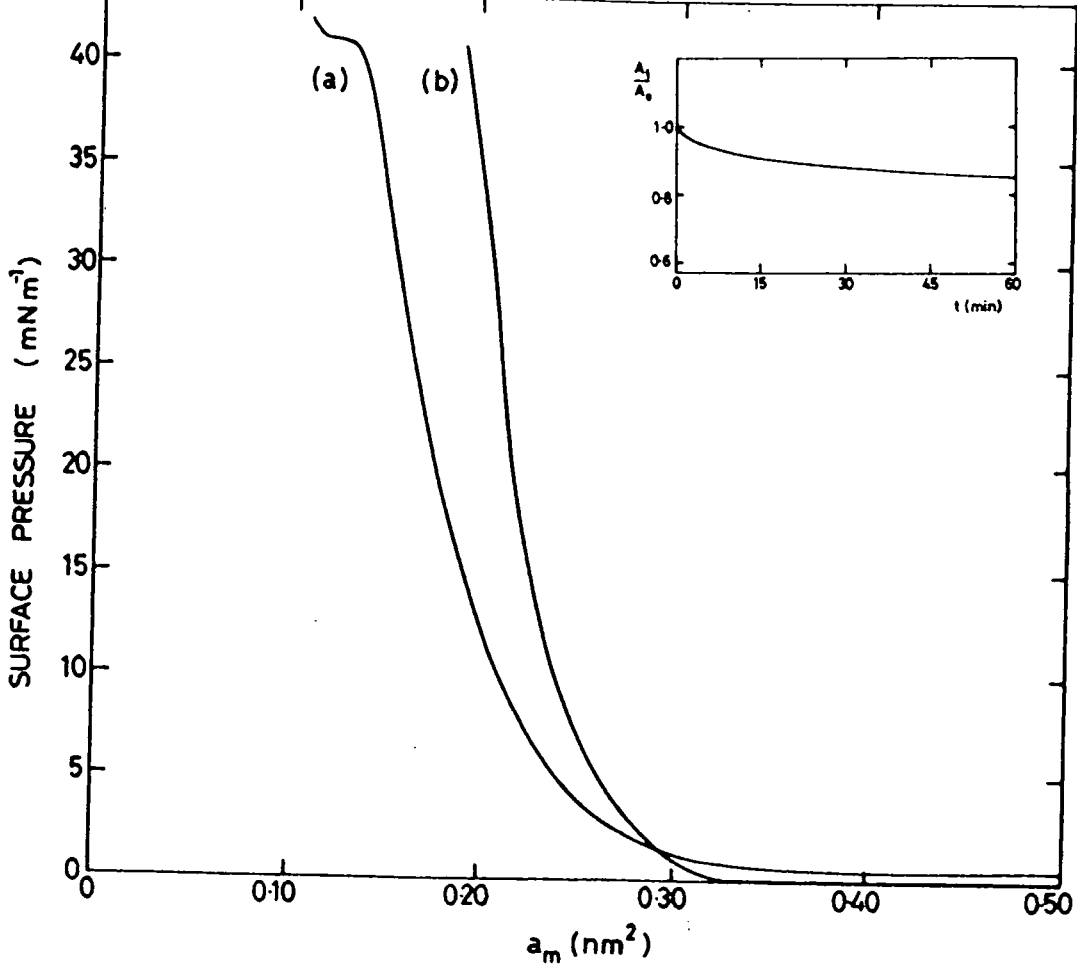


Figure 5.4 Pressure-area isotherms for (a) M2, pH=5.5 (2×10^{-4} M CdCl₂); (b) M3, pH=5.8 (2×10^{-4} M CdCl₂). Inset: Change in fractional area of M2 monolayer with time ($\pi = 32 \text{ mN m}^{-1}$, pH=5.4, 2×10^{-4} M CdCl₂).

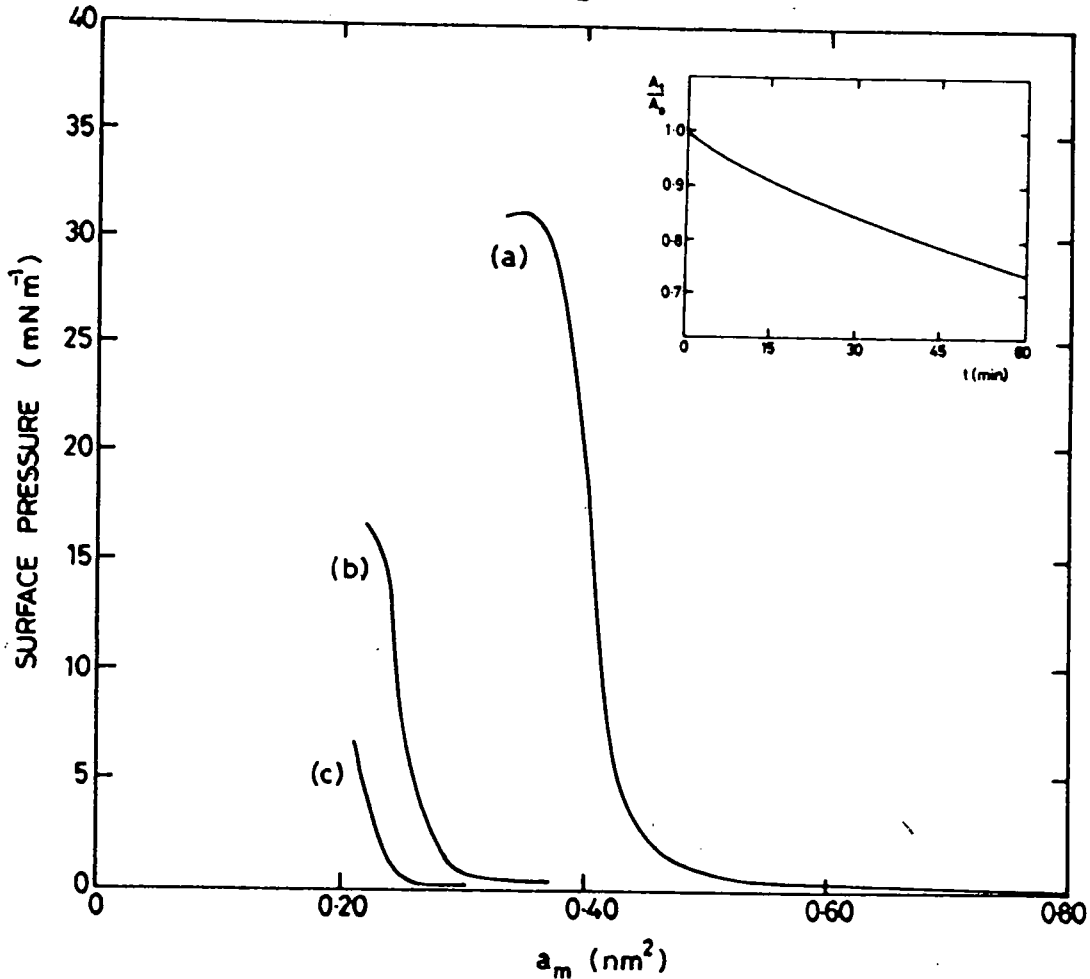


Figure 5.5 Pressure-area isotherms for Al on a 2×10^{-4} M CdCl₂ subphase (a) pH=4.4, (b) pH=6.2, (c) pH=8.0. Inset: Change in fractional area of Al monolayer with time ($\pi = 15 \text{ mN m}^{-1}$, pH=4.5, 2×10^{-4} M CdCl₂).

thereby giving rise to a value of a_m^0 not inconsistent with the dimensions of the molecule (at high pH rapid dissolution gives rise to very small values of the apparent a_m^0). The inset to figure 5.5 reveals that even at a pH of 4.5 there is a considerable solubility problem, although the material is still useful if a large area of monolayer is spread initially. It is not beneficial to have a pH of less than 4.5, since below this figure most of the carboxylic acid groups will remain unionized whereas film cohesion is improved by salt formation.

Compound A2 represents the first variation on C4 anthracene, with the butyl group being replaced by the even shorter COCF_3 . Although the resultant isotherm appears to have a steep region and a very high collapse surface pressure (figure 5.6a), the value of a_m^0 of 0.18 nm^2 is far too small for the film to be monomolecular; this figure cannot be accounted for by dissolution, since this is slow even at 40 mN m^{-1} (table 5.1). However, it was found that by making a mixed monolayer of A2 with arachidic acid in a ratio of one A2 molecule to 2.65 molecules of arachidic acid (present as cadmium arachidate under the subphase conditions employed) an isotherm could be obtained which displayed three distinct phase changes and a steep condensed phase line. The abscissa for this curve is calibrated in terms of the area per "average" molecule in the mixture; thus $a_m^0 (\text{mixture}) = \frac{a_m^0 (\text{A2}) + 2.65 a_m^0 (\text{arach.acid})}{3.65}$.

Rearranging this equation and substituting in the known value, $a_m^0 (\text{arach.acid}) = 0.20 \text{ nm}^2$, and the value measured from figure 5.6b, $a_m^0 (\text{mixture}) = 0.26 \text{ nm}^2$, gives $a_m^0 (\text{A2}) = 0.42 \text{ nm}^2$. This is remarkably close to the value of a_m^0 for C4 anthracene (0.43 nm^2), suggesting that the A2 molecules are not aggregated within the film, i.e. that the mixing process has been successful in preventing spontaneous collapse.

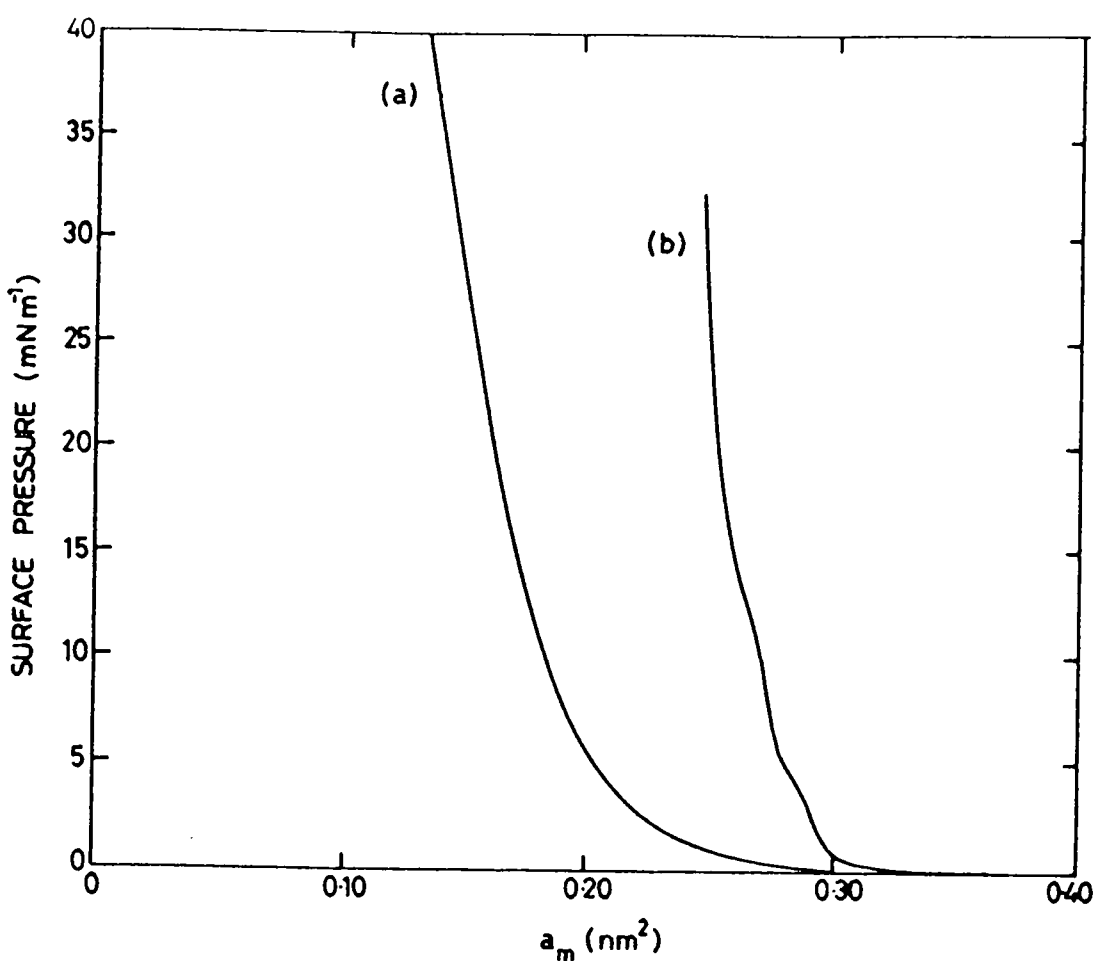


Figure 5.6 Pressure-area isotherms for (a) A2 and (b) mixture of 1 mole A2 to 2.65 mole arachidic acid, on a 2×10^{-4} M CdCl_2 subphase, pH=5.6.

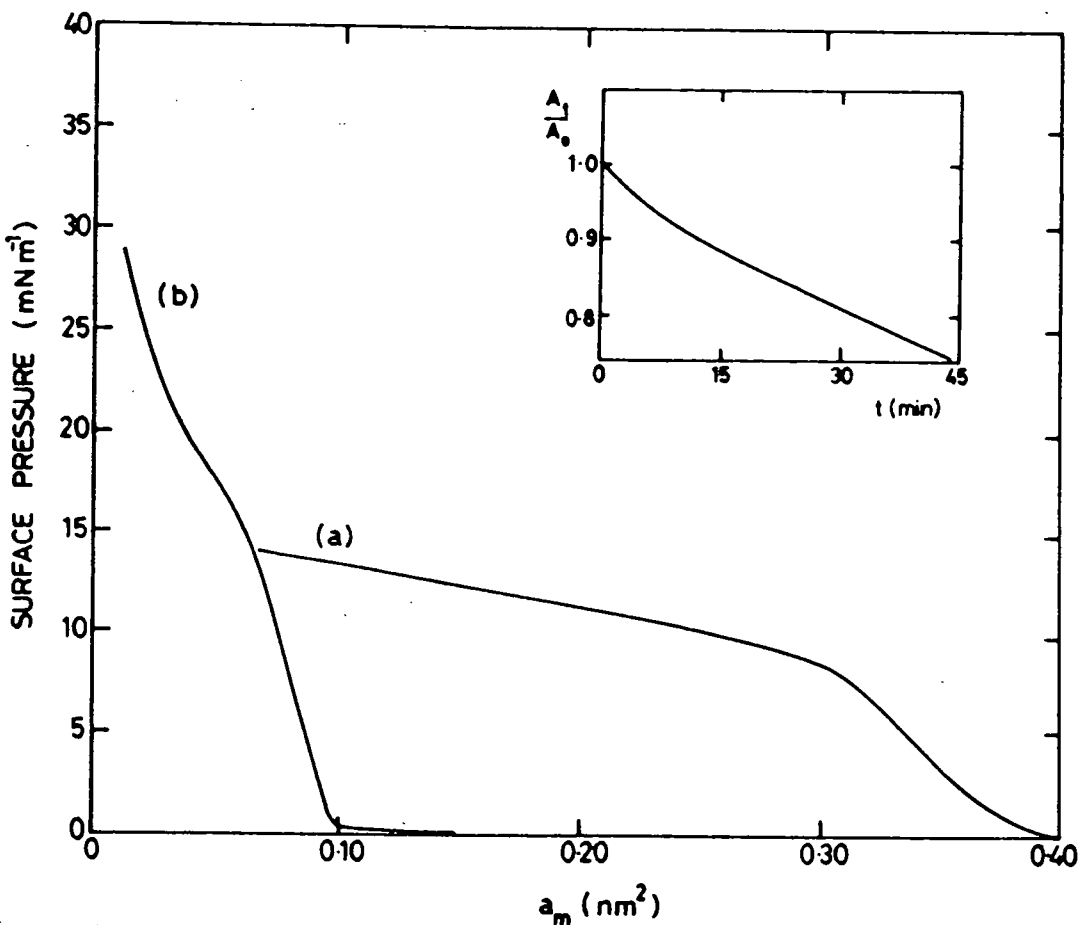


Figure 5.7 Pressure-area isotherms for (a) A4, pH=5.8 (no ions), and (b) A6, pH=5.7 (2×10^{-4} M CdCl_2). Inset: Change in fractional area of A4 monolayer with time ($\pi = 7$ mN m $^{-1}$, pH=5.8, no ions).

Compound A3 is complementary to A2 in that in this material the COCF_3 group replaces the propionic acid group of A1 instead of the butyl group. Since A3 was found to be highly soluble in the subphase this implies that the COCF_3 group of A3 is more hydrophilic than the propionic acid group of A1, and hence that A2 possesses two hydrophilic groups and no hydrophobic group. If this is the case, then A2 would be expected to be the most soluble of the three materials, which it clearly is not. One possible explanation for this behaviour is that the potentially high solubility of A2 is reduced by the formation of multilayers or aggregates of molecules in films of pure A2, and by the cadmium arachidate matrix in the case of mixed monolayers. An alternative explanation is that compound A3 has been oxidised to the more soluble anthraquinone, giving rise to misleading results.

Although the isotherms of A4 and A6 are quite similar in their form (figure 5.7), the values of a_m^0 (0.38 nm^2 for the former and 0.10 nm^2 for the latter - see table 5.1) indicate that they represent totally different processes. The portion of the π -A curve of A4 for $a_m = 0.36 - 0.32 \text{ nm}^2$ probably corresponds to a monolayer solid phase; the true a_m values are likely to be somewhat larger than these measured ones, the discrepancy arising from the rapid dissolution of the layer (see inset, figure 5.7). Conversely, the portion of curve of corresponding shape for A6 is bounded by $a_m = 0.09 \text{ nm}^2$ and $a_m = 0.07 \text{ nm}^2$, and since the film is only moderately soluble in the subphase, these values are not consistent with the film being monomolecular. Unfortunately, even A4 is unlikely to be of use as an LB film material due to its low collapse pressure and high solubility.

The problem of excessive water-solubility arose again with compound A5, which showed no sign of forming an insoluble monolayer throughout

the pH range 4.5-9.0. This material possesses an extended conjugated system and a powerful pyridinium acceptor group, which could have given rise to interesting non-linear optical effects. Similarly, compound A7 was found to be highly soluble in the subphase. It is rather surprising that A7 should be even more soluble than A6, since their molecular formulae are identical apart from the presence of an extra benzene ring in the former.

The π -A curves of compounds A8 and A9 are very similar (figure 5.8), both displaying two steep regions separated by one which is more shallow. Similar isotherms were obtained throughout the pH range 4.0 to 9.5. The a_m^0 values obtained by extrapolating the two steep regions down to zero pressure (table 5.1) indicate that for both materials the first region (high a_m^0) arises from monolayer compression whereas the second region (low a_m^0) arises from multilayer compression, the intermediate stage being monolayer collapse. Monolayer dissolution cannot be used as an explanation for the low a_m^0 values in the second region, since film area was found to decay only very slowly with time when the pressure was held constant within any of the steep regions. The low values of π_c for the true monolayers implies that these materials are unlikely to form good quality LB films.

The molecular formulae of A7, A8 and A9 are very similar, all three materials having the same conjugated system and hydrophobic butyl group; in fact this series was designed to illustrate the effect on the non-linear behaviour of changing just the polar head group portion of R_2 (see molecular formulae in figure 5.2). The COOH, NO₂, and OH groups were selected for their widely differing electronic properties (see section 5.1.2). However, the poor behaviour of these materials as Langmuir films has rendered such a study impossible.

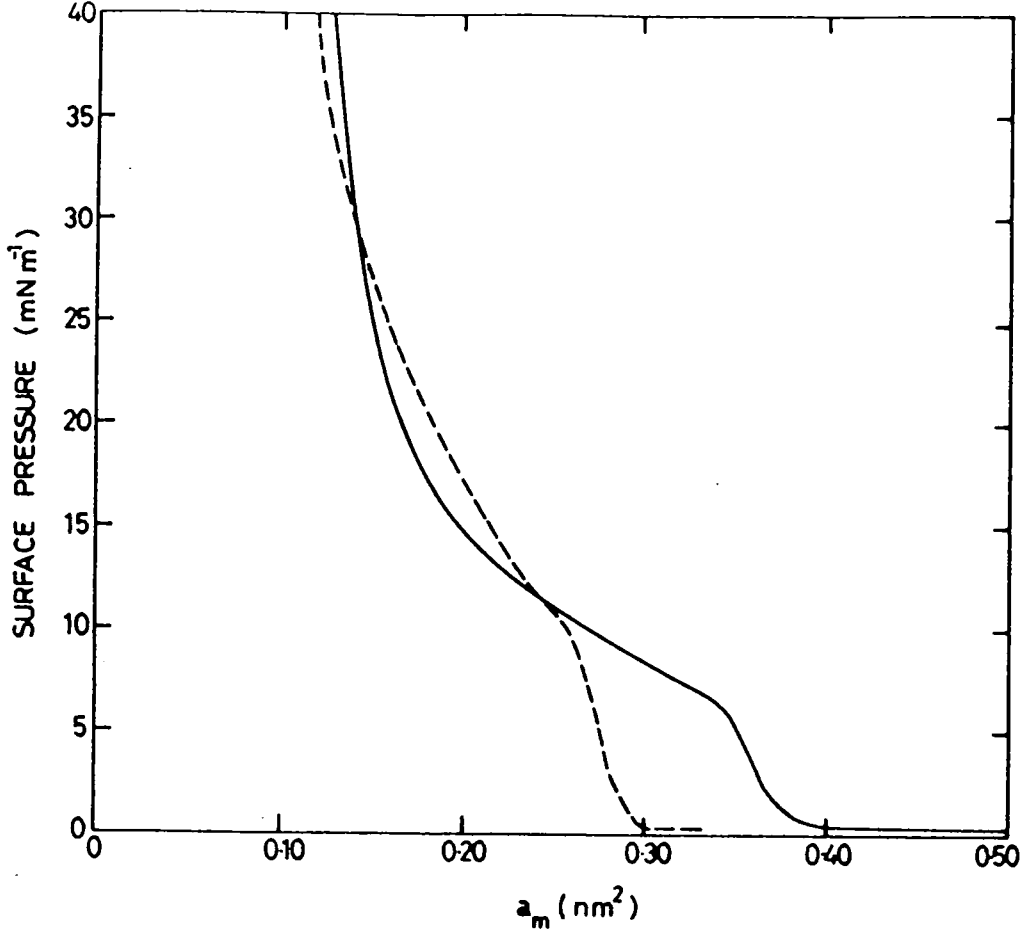


Figure 5.8 Pressure-area isotherms for A8 (—) and A9 (----), on a 2×10^{-4} M CdCl_2 subphase, pH=5.5.

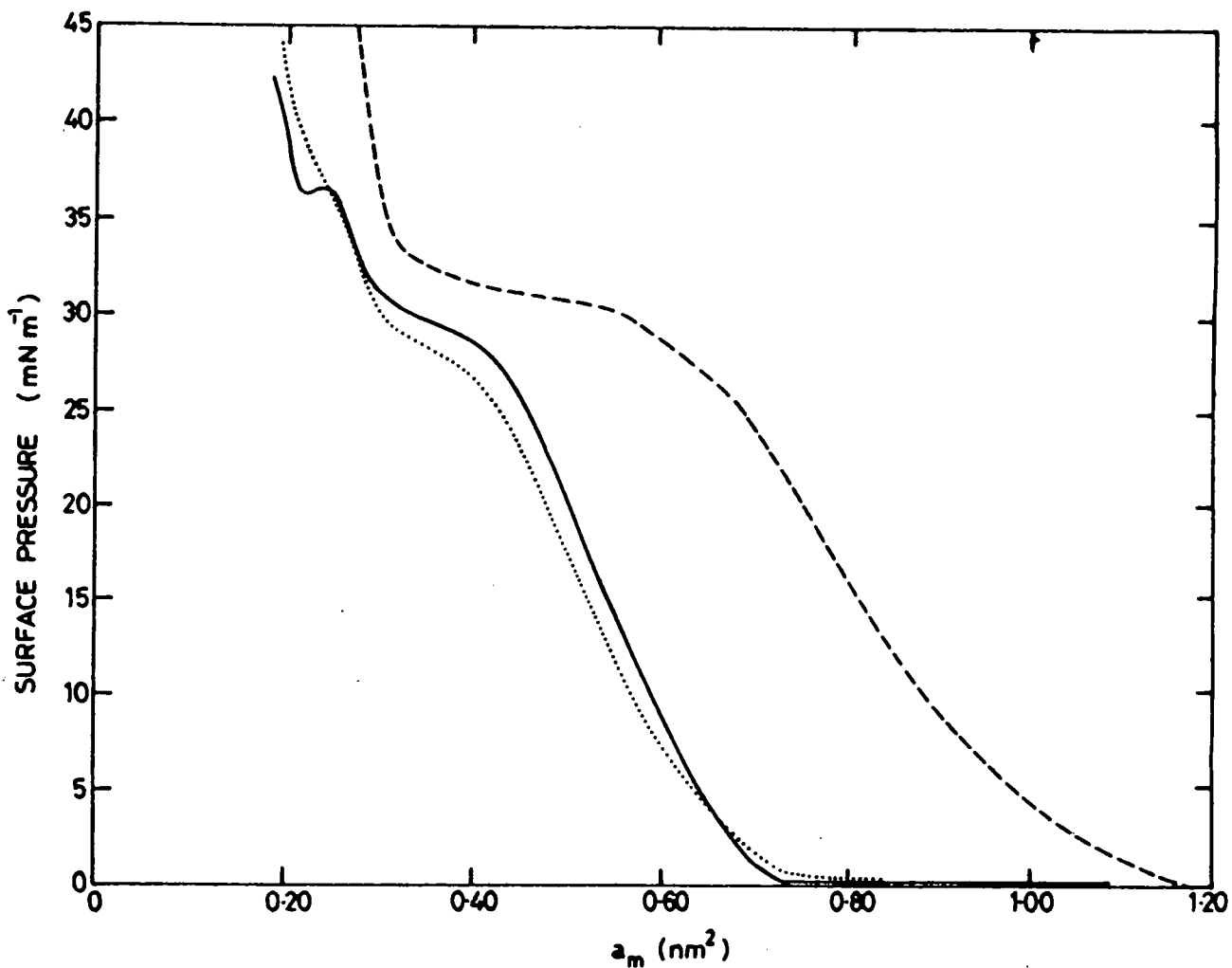


Figure 5.9 Pressure-area isotherms for D1 (i) D1A (pH=7.6, 10^{-3} M $(\text{NH}_4)_2\text{SO}_4$) (----), (ii) D1B (pH=7.4, no ions) under slow (—) and rapid (....) compression.

5.3.3 Dipolar chromophores

The two different samples of the merocyanine D1 were found to give similar isotherms (figure 5.9). This dye was of great interest in view of its particularly large second-order hyperpolarizability in low polarity solvents, as determined by electric field induced second harmonic generation^(5,6), and its ability to form insoluble monolayers⁽⁷⁾ and alternate layer LB films⁽⁸⁾. This material provides a good illustration of the importance of controlling as many factors as possible when obtaining an isotherm: there are distinct changes in the π -A curve of D1B in figure 5.9 when the rate of compression is altered. There are two steep regions in the isotherm (three in the case of very slow compression); initially it was assumed that the one at lower surface pressure corresponded to a monomolecular condensed phase, whilst that at high pressure was the result of the compression of a multilayer film. However, the a_m^0 measurements were not inconsistent with the high pressure region being the solid monolayer phase and the lower pressure region being due to some other phase. In the event, both regions were investigated for monolayer stability.

The subphase conditions selected depended on the ultimate goal : (i) initial experiments were aimed at producing low pressure merocyanine monolayers, and alternating layers with a long chain amine; since the amine required the presence of sulphate ions, the subphase used was $10^{-3} \text{ M } (\text{NH}_4)_2 \text{ SO}_4$ (aq), pH \sim 7.5; (ii) subsequent investigations were made of high pressure merocyanine monolayers, and alternating layers with ω -tricosenoic acid; the subphase employed here had pH $>$ 7.0 with no added ions. It was found that monolayers of D1 exhibited negligible dissolution at a surface pressure of 28 mN m^{-1} (table 5.1), but at 41 mN m^{-1} dissolution was rapid, only 10% of the initial monolayer area

remaining after a period of one hour at a pH of 7.5, although increasing the pH to 8.5 greatly improved stability (70% remaining after an hour). The reasonably high pressures to which the monolayers can be taken, and the lack of major solubility problems, makes the production of LB films from either "solid" regime of D1 worthwhile pursuing.

The hemicyanine dye, D2, provides another example of the extreme caution needed when interpreting isotherms. The three curves shown in figure 5.10 were all performed under identical subphase conditions and compression rates, and indeed they do coincide over the small pressure range $36-42 \text{ mN m}^{-1}$, yet at lower pressures there are vast differences in their slopes. Only one factor was changed from one isotherm to the next - the period of time for which the solvent was evaporated. Better (steeper) isotherms were obtained with short evaporation times, suggesting that perhaps the retention of some solvent in the monolayer is improving its physical characteristics, or else that the molecules undergo some kind of rearrangement on the water surface prior to compression. There appears to be some kind of phase change in monolayers of D2 at $\pi \sim 10 \text{ mN m}^{-1}$, $a_m \sim 0.9 \text{ nm}^2$. Variations in subphase pH or ion content had very little effect on the isotherms. The $\text{C}_{16}\text{H}_{33}$ and $\text{C}_7\text{F}_{15}\text{CO}$ analogues of D2 gave rise to very expanded isotherms, with no steep region prior to collapse at $\sim 35 \text{ mN m}^{-1}$, whilst the iodide salt of the $\text{C}_6\text{F}_{13}\text{C}_2\text{H}_4$ analogue barely registered a surface pressure at all before it collapsed. However, with respect to monolayers of D2 itself, their high collapse surface pressure and low rate of dissolution (inset, figure 5.10), coupled with a measured limiting area per molecule (table 5.1) which is consistent with the film being monomolecular, render D2 a suitable candidate for the formation of LB multilayers.

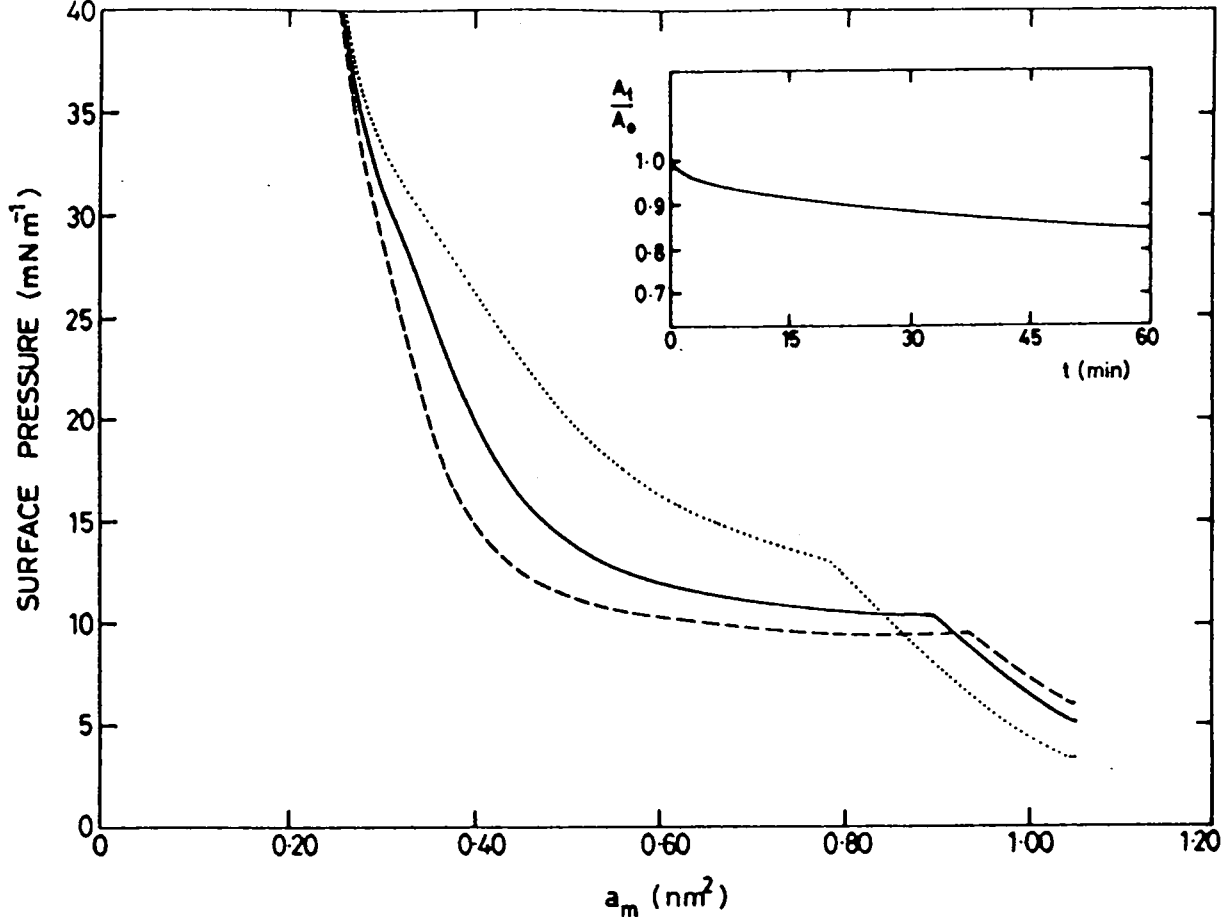


Figure 5.10 Pressure-area isotherms for D2, $2 \times 10^{-4} \text{ M CdCl}_2$ subphase, $\text{pH}=5.7$, for different periods, t , of solvent evaporation. (i) $t=2$ mins (----), (ii) $t=4$ mins (—), (iii) $t=10$ mins (....). Inset: Change in fractional area of D2 monolayer with time ($\pi=40 \text{ mN m}^{-1}$, $\text{pH}=5.8$, $2 \times 10^{-4} \text{ M CdCl}_2$).

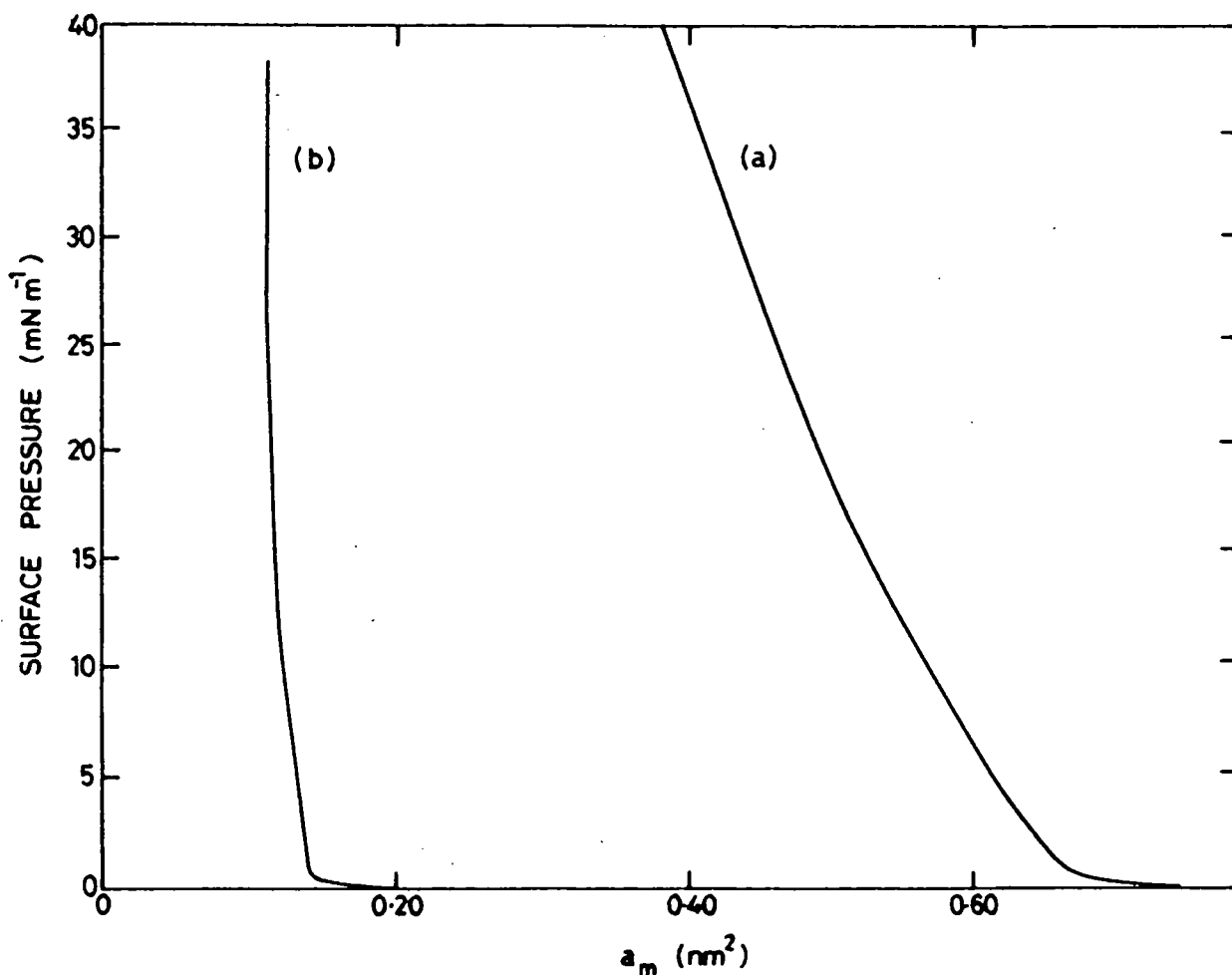


Figure 5.11 Pressure-area isotherms for (a) D3, $\text{pH}=9.1$ (no ions), and (b) D4, $\text{pH}=5.8$ (no ions).

Compounds D3 and D4 were closely related to D2, the only differences being in the head group. Of this set, D2 should be the most promising from the non-linear optical point of view (as discussed in section 5.1.3), and was therefore studied in the greatest depth, but D3 and D4 do serve to illustrate how subtle changes to a molecule can greatly affect monolayer behaviour. The isotherm of D3 was shallow but not expanded (figure 5.11), with a high collapse surface pressure and area per molecule values consistent with a true monolayer; the $C_{16}H_{33}$ analogue of D3 gave a very expanded isotherm exhibiting collapse at ~ 30 $mN m^{-1}$. In contrast, D4 gave a very steep isotherm which was unaffected by the presence or absence of $CdCl_2$ in the subphase and which displayed sharp phase changes (figure 5.11). These films exhibited negligible dissolution at $30 mN m^{-1}$ (table 5.1). In spite of these observations, the area per molecule values were less than half those expected for a true monolayer. Interestingly, the $C_{18}H_{37}$ analogue of D4 gave an isotherm more closely resembling that of D3 and with area per molecule values consistent with a monolayer; this might indicate that the sample of D4 itself contained a high percentage of soluble impurities, giving rise to erroneous a_m values.

Of all the materials studied, D5 gave probably the most promising isotherm, it being steep, with a high collapse pressure and an area per molecule scale consistent with a monomolecular layer (figure 5.12a). The π -A curve was found to be largely independent of pH, being only slightly shallower at $pH > 8$ and unchanged at $pH = 4.4$. Monolayers of D5 exhibited a fairly slow decay in area with time at $32 mN m^{-1}$ (inset, figure 5.12), but the onset of rigidity in the layer (as revealed by the suction test of section 3.5.3) limited their useful lifetime to approximately 100 minutes. The yellow colour of a spreading solution

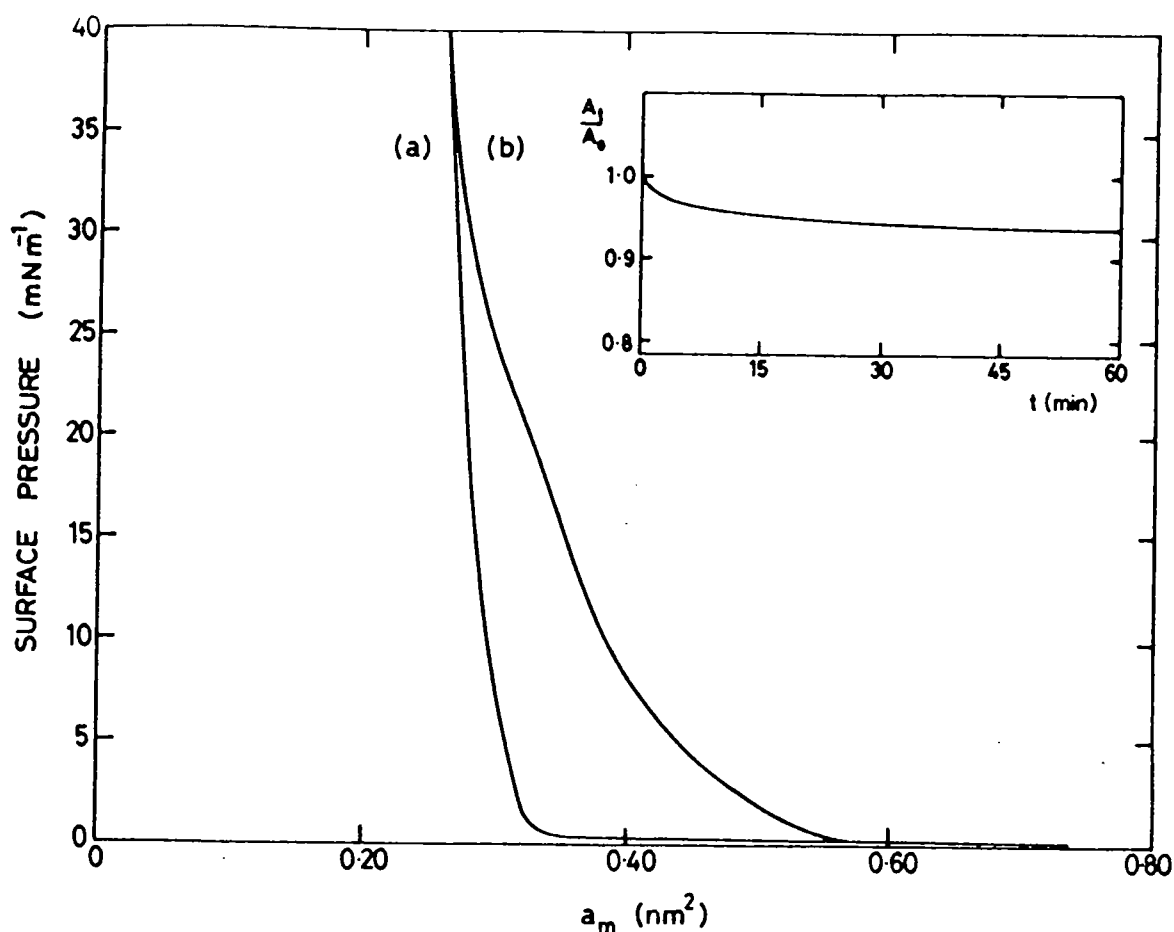


Figure 5.12 Pressure-area isotherms for D5, pH=5.8 (no ions), (a) fresh spreading solution, (b) 2 month old spreading solution. Inset: Change in fractional area of D5 monolayer with time ($\pi = 32 \text{ mN m}^{-1}$, pH=5.7, $2 \times 10^{-4} \text{ M CdCl}_2$).

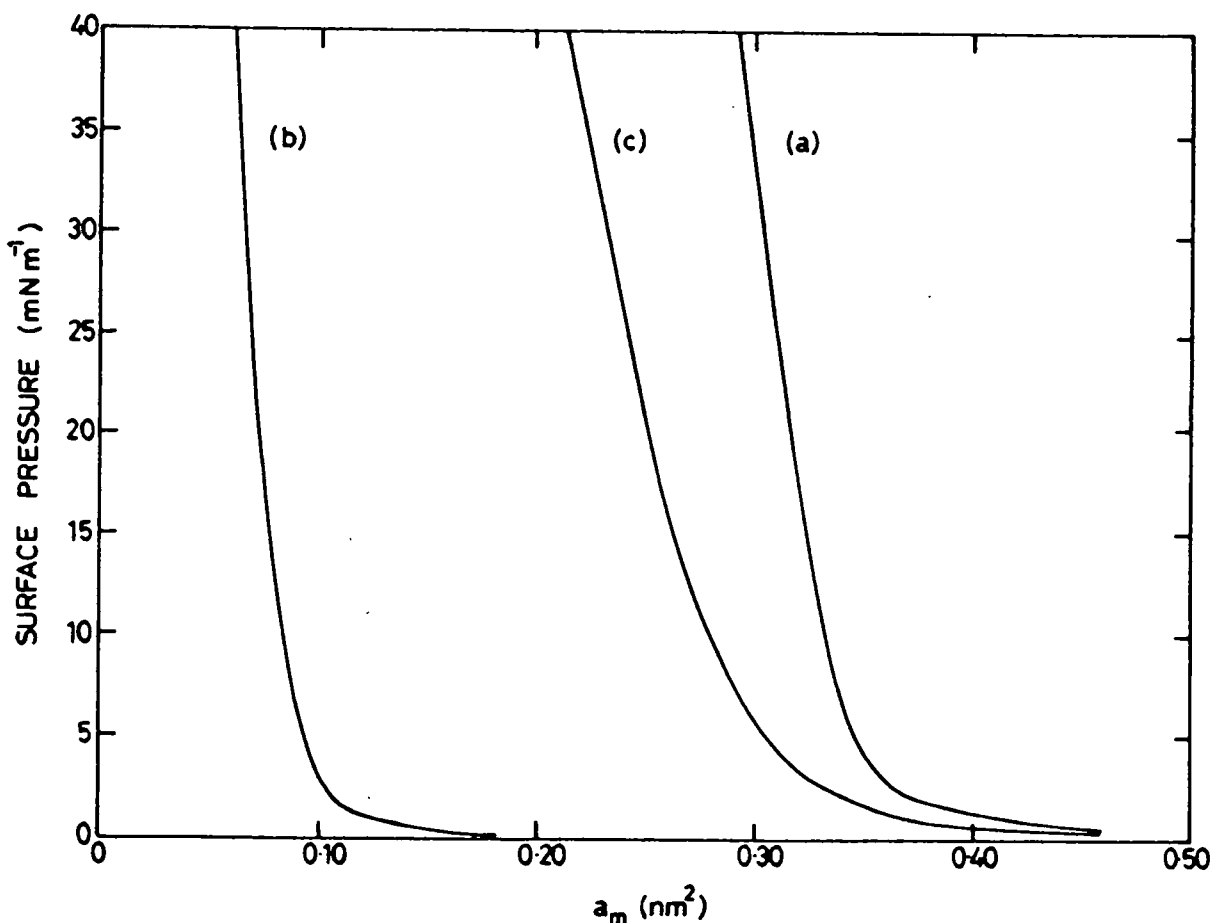


Figure 5.13 Pressure-area isotherms for (a) D6, pH=5.7 ($2 \times 10^{-4} \text{ M CdCl}_2$); (b) D7, pH=5.7 (no ions); (c) D8, pH=9.0 ($2 \times 10^{-4} \text{ M CdCl}_2$).

of D5 was noticeably bleached over a period of several weeks, and a two month old solution gave rise to a much shallower isotherm (figure 5.12b) than does a fresh solution, although the area per molecule is approximately the same at very high surface pressure. Care was therefore taken to ensure that all future studies were performed using solutions less than two weeks old. Molecules of D5 possess a nitro acceptor and an amide donor separated by a stilbene conjugated system of bonds, and should therefore display a significant non-linearity.

The rate of decay of the surface area of D5 monolayers with time was studied as a function of subphase conditions (figure 5.14). The decay process in each case can be seen to commence with relatively rapid dissolution, followed by a process obeying equation 3.1, i.e. $\ln(N) = -kt + C$. Since the initial area of film spread was not identical in each case, and since the $t=0$ position was difficult to define, the most important aspect of this study was to find the optimum conditions for reducing the slope of the \ln (film area) versus time plot (i.e. for reducing k), rather than trying to reduce the initial dissolution. It can be seen from figure 5.14 that with no ions added to the subphase a pH of 4.0 or 5.6 gives approximately the same value of k , whilst that for pH = 9.3 is slightly larger. Surprisingly, the addition of CdCl_2 to the subphase seems to reduce k , especially at pH \sim 5.7.

Another particularly interesting compound is D6, in which the slightly stronger amine donor replaces the amide group of D5. Once again the isotherm is steep, the collapse surface pressure high, and the measured area per molecule consistent with monolayer formation (figure 5.13). At 30 mN m^{-1} the area was found to decay only very slowly with time, but rigidity set in quite rapidly and to a much greater extent

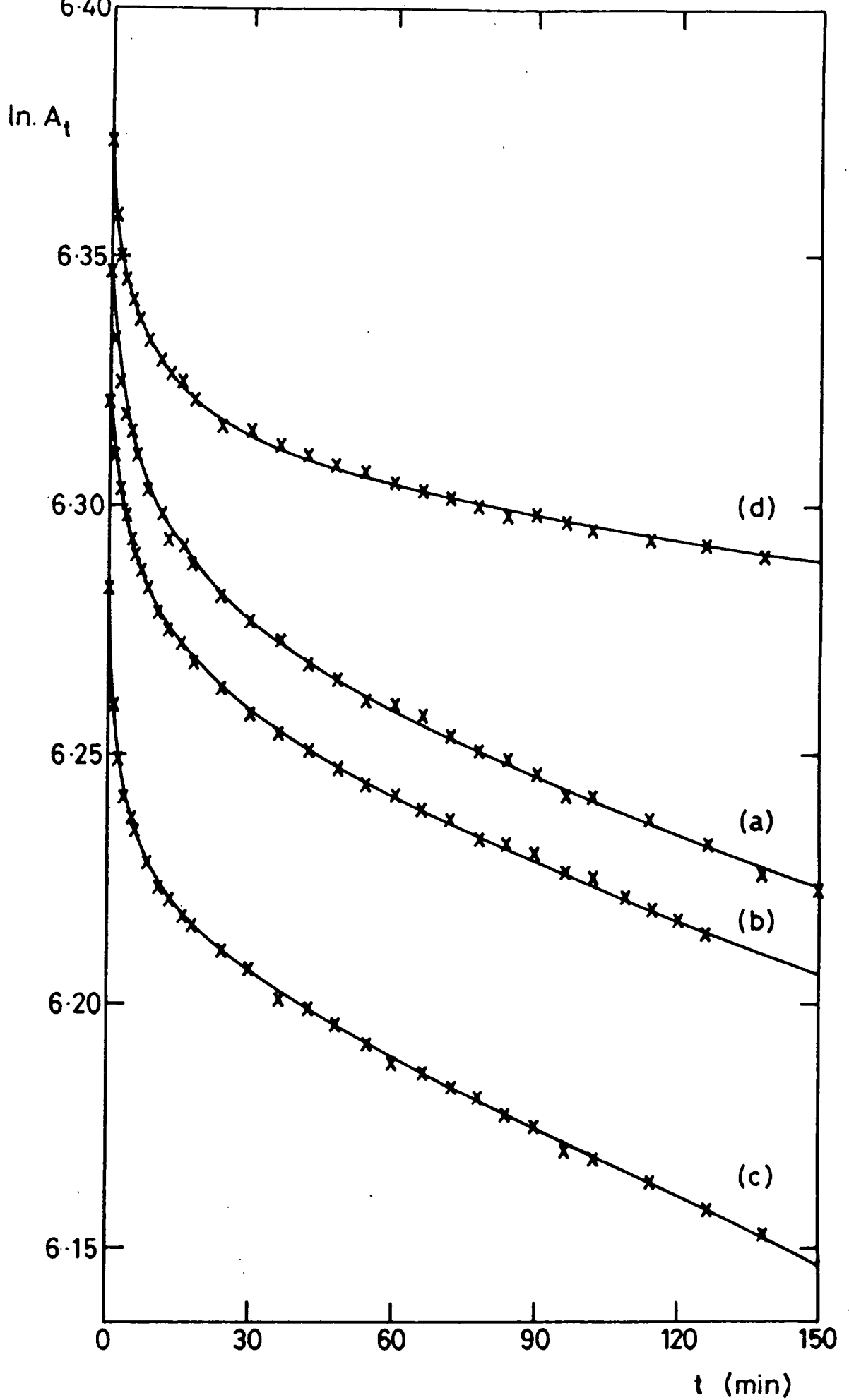


Figure 5.14

Decay in area of a Langmuir film of D5 with time for different subphase conditions. (a) pH=5.6 (no ions), (b) pH=4.0, (no ions), (c) pH=9.3 (no ions), (d) pH=5.7 (2×10^{-4} M CdCl_2).

than with D5, rendering the monolayer unsuitable for LB film deposition less than one hour after spreading.

The next material in the series, D7, has a tertiary amine replacing the secondary amine donor group of D6. Although this material has a steep isotherm (figure 5.13) and exhibits little dissolution, the a_m^0 value of 0.08 nm^2 clearly indicates that the film is not monomolecular. Indeed, careful observation of the water surface immediately after spreading revealed the presence of oily patches approximately 0.5 cm in diameter, arising from a strong tendency for the dye molecules to aggregate in an antiparallel fashion. However, satisfactory isotherms were obtained for a mixed monolayer containing five molecules of arachidic acid to one of D7. Similarly D8, the azo analogue of D6, formed islands of material prior to compression, and although steep isotherms were obtained at pH values of 4.7 (figure 5.13) and 9.0, the films collapsed rapidly when held at a surface pressure of 30 mN m^{-1} . Once again a mixture of 5 moles of arachidic acid to one of dye was found to give a good isotherm and stable monolayer.

5.4 Film Transfer

Having studied the properties of the water-surface monolayers of each compound, the next stage was to attempt to transfer these layers to solid substrates and build up multilayer structures. The techniques described in this section for the assessment of the quality of deposited films are very simple; more sophisticated methods can be found in chapter 6. In section 3.6.3 the concept of deposition ratio was introduced; this quantity was estimated from the plots of film area against time obtained for each dip, and was the primary indication of whether the same amount of material was being deposited in each

monolayer. Where deposition was particularly poor, visual observation of the substrate would often reveal regions where islands of collapsed film had been picked up; in cases where the deposition was of a better quality, the same technique could be used to check that the colour of reasonably thick (~ 20 layers) films was uniform over the whole sample. A final test which could be employed was to breathe on the film, which would take up the moisture; the resultant clouding of the layer then helped to show up any regions in which the deposition was non-uniform.

In view of the results of earlier sections, not all of the materials were deemed to be suitable for deposition. Compounds M1, A3, A5 and A7 were all too soluble in the subphase, whilst A4 rapidly collapsed and layers of A6 were not monomolecular. A2, D7 and D8 were only studied as mixtures with arachidic acid. Shortage of time precluded further investigation of D3 and D4, which seemed unlikely to show interesting non-linear optical effects.

Table 5.2 summarises the dipping conditions employed for materials which were found to give LB films of poor or moderate quality, whilst table 5.3 details the same quantities for those compounds giving high quality (Y-type) films. In the situations where a material gave rather patchy coverage, variations in subphase conditions, deposition surface pressure, dipping speed, and substrate preparation were investigated, and only the most successful combination is given in the tables.

Several materials would deposit as monolayers on hydrophilic substrates, but these layers would come off again on subsequent immersions of the substrate in the subphase, being replaced by a fresh monolayer on withdrawal. Z-type deposition was attempted with all these materials, but without success. Unusual materials in this respect were M3 and D2, which would transfer a layer to a substrate on each

TABLE 5.2 Dipping conditions for materials forming poor/moderate quality LB films

Material	Subphase	Surface Pressure (mN m^{-1})	Substrates Investigated	Comments
M2	2×10^{-4} M CdCl_2 pH = 5.6	32	Hydrophilic glass	Multilayers not attempted. Monolayer extremely patchy (if a true monolayer at all).
M3	10^{-3} M NaCl pH = 4.2	30	Hydrophilic glass, Al_2O_3 , indium tin oxide	Monolayer looked uniform, but gave unusual result when exposed to moisture: did not mist up at all. Multilayers (up to 4 layers thick) were patchy, with deposition only on withdrawal
A8	2×10^{-4} M CdCl_2 pH = 5.5	5	Hydrophilic glass	Multilayers not attempted. Uniform monolayer.
		35	Hydrophilic glass	Multilayers not attempted. Moderately uniform monolayer.
A9	2×10^{-4} M CdCl_2 pH = 5.5	7.5	Hydrophilic glass	Multilayers not attempted. Rather patchy monolayer.
		40	Hydrophilic glass	Multilayers not attempted. Rather patchy monolayer.
D2	No ions or 2×10^{-4} M CdCl_2 pH 9.0	35	Hydrophilic glass	Multilayers are of moderate quality. Deposition mainly on withdrawal. Surface pressures up to 47 mN m^{-1} with wide ranges of subphase conditions produce little change in behaviour.

TABLE 5.3 Dipping conditions for materials forming high quality LB films

Material	Subphase	Surface Pressure (mN m ⁻¹)	Substrates Investigated	Comments
A1	2x10 ⁻⁴ M CdCl ₂ pH=4.5 - 4.8	15	Al ₂ O ₃ , Si	Good quality multilayers up to 500 layers thick. Occasionally gives apparently Z-type deposition. Prone to oxidative degradation.
A2/A.A. (1:2.65)	2x10 ⁻⁴ M CdCl ₂ pH = 5.7	30	Ag with overlayers of cadmium arachidate	Uniform orange film (over 20 layers successfully deposited).
	10 ⁻³ M (NH ₄) ₂ SO ₄ pH = 7.5	28	Hydrophilic glass, Al ₂ O ₃ with overlayers of ω-TA, Si	Fairly good quality red/orange film, turning yellow in air due to protonation (over 30 layers successfully deposited).
D1	No ions pH > 8	41.5	Si	Very slow monolayer compression required; tendency towards spontaneous collapse. Moderate quality red/orange film, turning yellow in air (over 10 layers successfully deposited).
D5	No ions, or 2x10 ⁻⁴ M CdCl ₂ pH = 5.6	32	Hydrophilic/hydrophobic glass or Si, Al ₂ O ₃ , indium tin oxide, Ag with overlayers of ω-TA	Generally gives excellent quality films (over 30 layers successfully deposited). Monolayer needs replenishing after ~ 100 mins, due to onset of rigidity.
D6	No ions, or 2x10 ⁻⁴ M CdCl ₂ pH = 5.6	30	Hydrophilic glass or Si	Good quality films (over 10 layers successfully deposited). Monolayer needs replenishing after ~50 mins, due to onset of rigidity.
D7/A.A. (1:5)	2x10 ⁻⁴ M CdCl ₂ pH = 5.5	30	Glass with cadmium arachidate overlayers	Good quality films (over 40 layers successfully deposited).
D8/A.A. (1:5)	2x10 ⁻⁴ M CdCl ₂ pH = 5.7	30	Hydrophilic glass	Multilayers not attempted. Good quality monolayer.

withdrawal but not on insertion, whilst pre-deposited layers would remain firmly bonded. Although this might appear to constitute Z-type deposition, when this was attempted using the automated feature of the trough, the film quality was much poorer than usual. This might suggest that M3 and D2 do in fact deposit in a Y-type mode, with the molecules undergoing some form of reorientation immediately prior to transfer to the substrate.

Conventional Y-type LB films are of no interest for second-order non-linear optical processes, owing to their inherent centrosymmetry; however, this limitation can be overcome by the use of alternate layer systems, as discussed elsewhere in this thesis. Since the subphase is common to both of the components of such a system, its contents cannot be optimized for each of them simultaneously. Frequently one of the materials will be more tolerant to non-ideal dipping conditions than the other, in which case they can be suited to the most "demanding" compound. Table 5.4 summarises the deposition features of the several different alternate layer systems investigated; the surface pressures employed for each material were the same as for single component Y-type films.

5.5 Summary

This chapter has reviewed the techniques available for characterizing water-surface monolayers in order to find the optimum conditions for LB film deposition. The novel materials investigated in this project have been introduced, and the reasoning behind their selection discussed. Results have been presented for 20 different compounds, out of which four (A1, D1, D5 and D6) gave rise to highly uniform Y-type multilayers, a fifth (D2) formed moderately good films,

TABLE 5.4 Dipping conditions for alternate layer systems

Material deposited (withdrawal)	Material deposited (insertion)	Subphase	Substrates Investigated	Comments
D1	ω -TA	10^{-3} M (NH_4) ₂ SO ₄ pH = 7.5	Si	D1 deposited at 28 mN m ⁻¹ . 120 bilayers deposited, rather poor quality.
	C ₂₂ H ₄₅ NH ₂	10^{-3} M (NH_4) ₂ SO ₄ pH = 7.5	Al ₂ O ₃ with ω -TA overlayers	D1 deposited at 28 mN m ⁻¹ . 6 bilayers deposited, containing visible defects.
A.A.	D5	2×10^{-4} M CdCl ₂ pH = 5.8	Glass with cadmium arachidate overlayers	Good quality films (up to 10 bilayers deposited successfully).
D2	D5	2×10^{-4} M CdCl ₂ pH = 9.0	Hydrophilic glass	Excellent quality films (up to 10 bilayers deposited successfully).
D2	D6	2×10^{-4} M CdCl ₂ pH = 9.0	Hydrophilic glass	Good quality films (2 bilayers deposited successfully).

and three others (A2, D7 and D8) could be deposited as mixed monolayers. The optimum dipping conditions for these materials have been given, along with those for several alternate layer systems of interest for their potentially large optical non-linearities.

Considering a generalised molecule, $R-G_1-C-G_2$, where R is the hydrocarbon tail, C is the conjugated system, and G_1 , G_2 are donor (D) or acceptor (A) groups, then these results can be summarized as follows:

	Material	R	G_1	G_2
Highly uniform multilayers	A1	C_4H_9	D (weak)	A (weak)
	D1	$C_{22}H_{45}$	D	A
	D5	$C_{17}H_{35}$	D	A
	D6	$C_{22}H_{45}$	D	A
Moderately good films	D2	$C_{22}H_{45}$	A	D
Mixed monolayers	A2	CF_3CO	A	A (weak)
	D7	$C_{18}H_{37}$	D	A
	D8	$C_{18}H_{37}$	D	A

In the next chapter some physical characteristics of these films are described, whilst chapter 7 is concerned with their structural assessment. Finally, chapter 8 deals with studies of second harmonic generation from LB monolayers and multilayers of these novel materials.

CHAPTER 6

SOME TECHNIQUES FOR THE CHARACTERIZATION OF LB FILMS

AND MATERIALS : RESULTS AND DISCUSSIONS

6.0 Introduction

Although the primary objective of this project was to produce LB films displaying large optical non-linearities, the linear optical properties of the films are also very important in determining which applications they may be appropriate to. The real component of the linear susceptibility is responsible for the refraction of light, whilst the imaginary part accounts for absorption (see Chapter 2). Optical absorption measurements performed on solutions and LB films of the various dyes described in Chapter 5 as forming good quality multilayers are described in section 6.1. Such data is useful for determining the range of fundamental wavelength over which radiation can be frequency-doubled by the film; in addition, studies of absorbance (at a fixed frequency) as a function of film thickness can be employed to assess the uniformity of deposition from one layer to the next (see section 3.7). The results of surface plasmon resonance studies are presented in section 6.3; these can be used to estimate the refractive index of the film, and the shape of the resonance curves can yield qualitative information concerning the film quality (i.e. if it scatters the incident radiation very badly).

Many potential applications for LB films in non-linear optics (e.g. electro-optic modulation) require the application of an electric field across the device; it is therefore important to be able to make electrical contacts to the films. In section 6.2 the measurement of capacitance as a function of film thickness is described; such

experiments are useful for assessing the quality of multilayers (see Chapter 3) as well as in determining the success of top contact deposition.

The Kurtz powder technique is a widely practiced simple method for screening large numbers of compounds for second-order non-linear optical activity^(1,2). It is normally used to identify suitable candidates for single-crystal studies, but in section 6.4 the advantages and disadvantages of its application to powdered samples of LB film material are discussed and some results presented. One way of assessing the potential of a new material at the earliest possible stage is to calculate a theoretical value for its second-order molecular hyperpolarizability. The results of a few such computations are given in section 6.5.

6.1 Optical Absorption

6.1.0 Background

The optical absorption spectrum is an important characteristic for any LB film destined for an application in the field of optics, since it determines what wavelengths of light can propagate through the film without being heavily attenuated by absorption losses. In particular, efficient frequency doubling requires the careful matching of the non-linear material to the fundamental wavelength; ideally the absorption edge should be near to the second harmonic wavelength but must not include it (see section 2.3.2).

Studies of absorbance (at a fixed wavelength, usually an absorption maximum) as a function of film thickness can be used to check that the deposition of material is uniform from one monolayer to the next (see section 3.7). The Beer-Lambert law for dye solutions is: $A = \epsilon cd$,

where A is the absorbance, ϵ the molar extinction coefficient, c the concentration, and d the path length. For an LB film, cd is equivalent to $N\sigma$, where N is the number of monolayers and σ is the surface density of dye molecules. Assuming that the material obeys this law, and that interference effects can be neglected, a linear plot of absorbance versus number of monolayers would be indicative of consistent monolayer pick-up. This technique is also used in section 6.1.4 to demonstrate that the same proportion of dye is picked up in successive layers deposited from a mixed water-surface monolayer.

In section 6.1.1 the differences in the optical absorption characteristics of two resonance forms of a merocyanine dye are used to monitor the progress of its protonation reaction. This is an important process, since the second-order hyperpolarizability of one resonance form is much larger than that of the other.

Contrasting the absorption spectra obtained for solutions of a given material in different solvents with that given by an LB film can often yield interesting information concerning the local environment of the molecules in the film. Changes in solvent polarity can produce large spectral shifts, a phenomenon frequently referred to as solvatochromism. Such effects can be particularly large for chromophores exhibiting extensive intramolecular charge transfer, as in the case of the conjugated donor-acceptor systems studied in this project. Solvatochromic effects depend largely on there being a change in the dipolar characteristics of a molecule when it is promoted to the excited state.

The arguments used to explain the observed spectral shifts of solutions and LB films will be very similar for each material. Therefore, in order to avoid subsequent repetition, a general discussion

will now be given in which the merocyanine-type compounds are taken as an example. Merocyanines (defined as chromogens based on a donor-usually an amino group - and a carbonyl acceptor) fall into three distinct classes, according to the polarity of the ground state⁽³⁾:

- (i) Weakly polar compounds. In the ground state these materials have a low degree of charge separation (usually because of the inclusion of weak electron donors and acceptors) and show a high degree of bond alternation (i.e. the bonds in the conjugated system are alternately double and single in their order). The excited state of such compounds generally exhibits a high degree of charge transfer from donor to acceptor, and thus has a large dipole moment. This will be accompanied by a significant tendency towards bond equalisation (i.e. to successive bonds having the same strength). Polar solvents will stabilise the excited state more than the ground state, and thus such materials display a bathochromic (towards longer wavelength) shift of the first absorption band when the solvent polarity is increased.
- (ii) Highly polar compounds. These arise from the combination of a powerful donor and acceptor, resulting in a ground state of high polarity. The ground state also shows strong bond alternation, due to the unequal contributions of the neutral and charge separated resonance forms. In the excited state, the polarity is reduced, due to charge migration from the negative end of the dipole to the positive end. Bond equalisation thus occurs. Polar solvents will stabilise the ground state of such dyes more than the excited state, and will thus produce a hypsochromic (towards shorter wavelength) shift of the absorption band.

(iii) Moderately polar compounds. In these dyes there is a strong tendency towards bond equalisation in the ground state, implying that the contributions of the neutral and charge separated forms are almost equal. There is little change in polarity in the first excited state, and thus such compounds show only small solvent shifts.

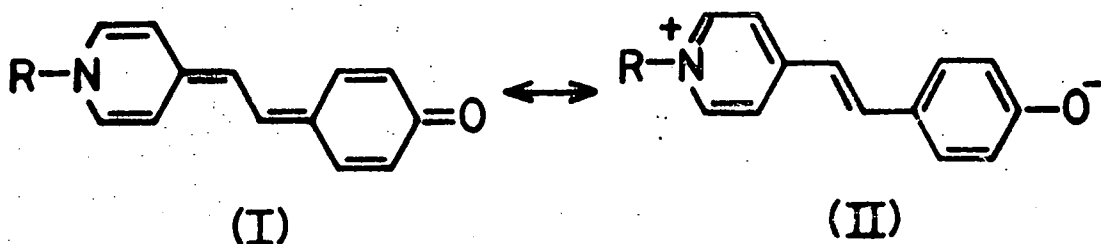
The spectral shifts displayed by charge-transfer dyes in LB film form can largely be attributed to the closely related phenomenon of dipole-dipole interactions. Parallel alignment of dipoles within the film will result in the relative stabilisation of the electronic state of lowest polarity, whereas antiparallel alignment will favour the state of highest polarity; the orientation of dipoles at angles to each other will result in the splitting of the band, one half being blue shifted, the other red shifted with respect to the original band⁽⁴⁾. In addition to dipole-dipole interactions, there are crystal field effects which give rise to a further spectral shift coupled with a broadening of the absorption bands relative to those exhibited by solutions. The vibrational fine structure associated with electronic transitions and often observed in the absorption spectra of solutions is usually lost in the spectra of LB films.

A phenomenon which sometimes arises in LB films of dye materials is the formation of what are commonly termed J aggregates (after Jelley). These aggregates exhibit intense narrow-band absorption spectra, bathochromically shifted from the molecular absorption⁽⁵⁾; such features were not observed in any of the LB film spectra reported in this section, and therefore aggregate formation is not referred to in subsequent discussions.

In sections 6.1.1-6.1.7, the optical absorption characteristics of the most promising materials described in Chapter 5 will be presented.

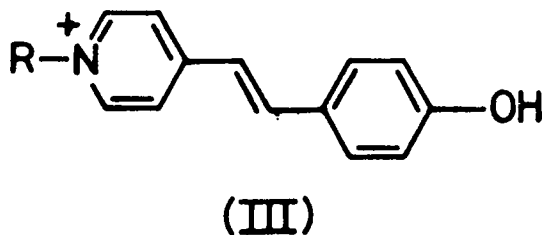
6.1.1 Merocyanine (compound D1)

Having stated in section 6.1.0 that a merocyanine dye can be placed into one of three categories according to the polarity of the ground state, compound D1 represents a curiosity in that the polarity of the solvent can change it from a moderately polar dye into a highly polar one by strong stabilisation of the charge separated form in the ground state⁽³⁾. The resultant solvatochromism has been reported by Gaines⁽⁶⁾ for the n-hexadecyl analogue of D1, whose solutions range in colour from blue in chlorinated hydrocarbons to red in ethanol, according to the relative contributions made in the ground state by the resonance forms I and II (below).



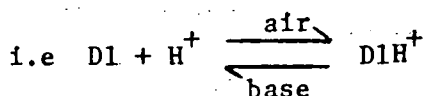
The second-order hyperpolarizability, β , is sensitive to charge transfer structural changes; thus the value of β , as determined by electric field induced second harmonic generation, would be expected to vary with solvent polarity, and this has, in fact, been verified by Levine et al⁽⁷⁾. Dulčić⁽⁸⁾ reports the value of β ($\sim 4 \times 10^{-48} \text{ C}^3 \text{ m}^3 \text{ J}^{-2}$) for the methyl homologue of D1 (in dimethyl sulphoxide) as being the largest measured for molecules of the same length.

The enolic oxygen of compound D1 reacts readily with acid (protonation) to form III (below), which is yellow⁽⁶⁾. This reaction is



highly undesirable from the non-linear optical viewpoint, since the donor in molecule III is the OH group, which performs the function only very weakly. This is in contrast to the much stronger donor and acceptor groups in I; thus the second-order hyperpolarizability of I is much superior to that of III.

The main disadvantage of D1 as an LB film material for potential non-linear optical applications lies in its reactivity towards acids. LB films of D1, as deposited from an alkaline subphase, were red-orange in colour; however, if allowed to stand in air they turned yellow within an hour, due to protonation. It was found to be possible to effect partial deprotonation of the films by exposing them to ammonia vapour or 10^{-3} M sodium hydroxide solution; however, the films quickly reverted to the protonated form when removed from the basic environment. The progress of the protonation reaction could be monitored by recording the optical absorption spectrum of a film at regular time intervals after deprotonation (figure 6.1). An isosbestic point was observed at 442nm; the presence of such a point is consistent with a simple protolytic equilibrium involving only two forms, D1 (red) and D1 H⁺ (yellow).



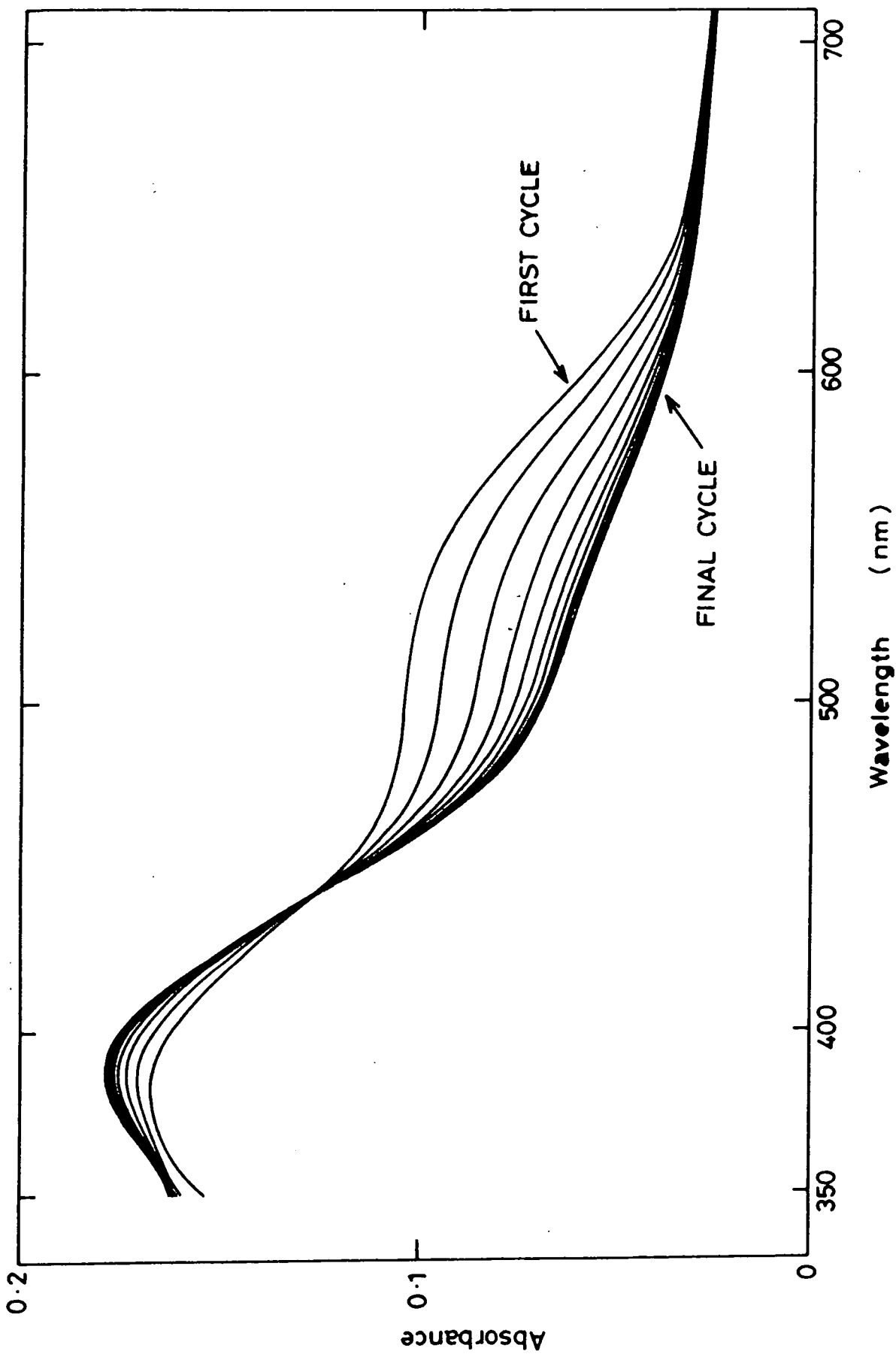


Figure 6.1 Optical absorption spectra of a 78-layer merocyanine LB film after deprotonation (scan rate = 1 nm s^{-1} ; cycle time = 30 mins.).

Repeated cycling of the multilayers between the yellow and red forms did not produce any visible degradation of the film quality. The wavelengths of the absorption peaks due to D1 and $D1H^+$ are difficult to determine precisely: the former is taken to be 522 nm, but since it only appears as a shoulder on the $D1H^+$ peak, this figure is only approximate; the latter lies between 380 nm and 392 nm, there being some very slight spectral shift as a function of the molar ratio of one species to the other in the film.

In view of the finite scan rate used to obtain the spectra, the ~ 390 nm peak in figure 6.1 will have been recorded some two minutes after the 522 nm one; thus, in order to get a more accurate estimate of the absorbance values at the two peaks simultaneously, figure 6.2 was produced. This plot was obtained by monitoring the absorbance at 392 nm for a period of one minute, then that at 522 nm for a further one minute, before returning to 392 nm and repeating the cycle again, many times over. The graph clearly demonstrates the growth of the $D1H^+$ peak at the expense of the D1 peak, and could in turn be used to construct figure 6.3, in which the change in absorbance at 392 nm is plotted against the change in absorbance at 522 nm (relative to the absorbance figures immediately after treatment with alkali). The slight deviation of figure 6.3 from the expected linear characteristic⁽⁹⁾ could probably be explained by inaccuracies in defining the wavelength of the absorption maxima, especially in view of the slight spectral shifts (noted above) which seem to occur during the conversion process. Davidson and Jencks⁽⁹⁾ have obtained an analogous plot for solutions of the methyl homologue of D1 ($D1'$), in which one peak is due to $D1'$ and the other to a complex of $D1'$ with a component of a salt added to the solution; the changes in molar ratio of complex to $D1'$ (and hence in the

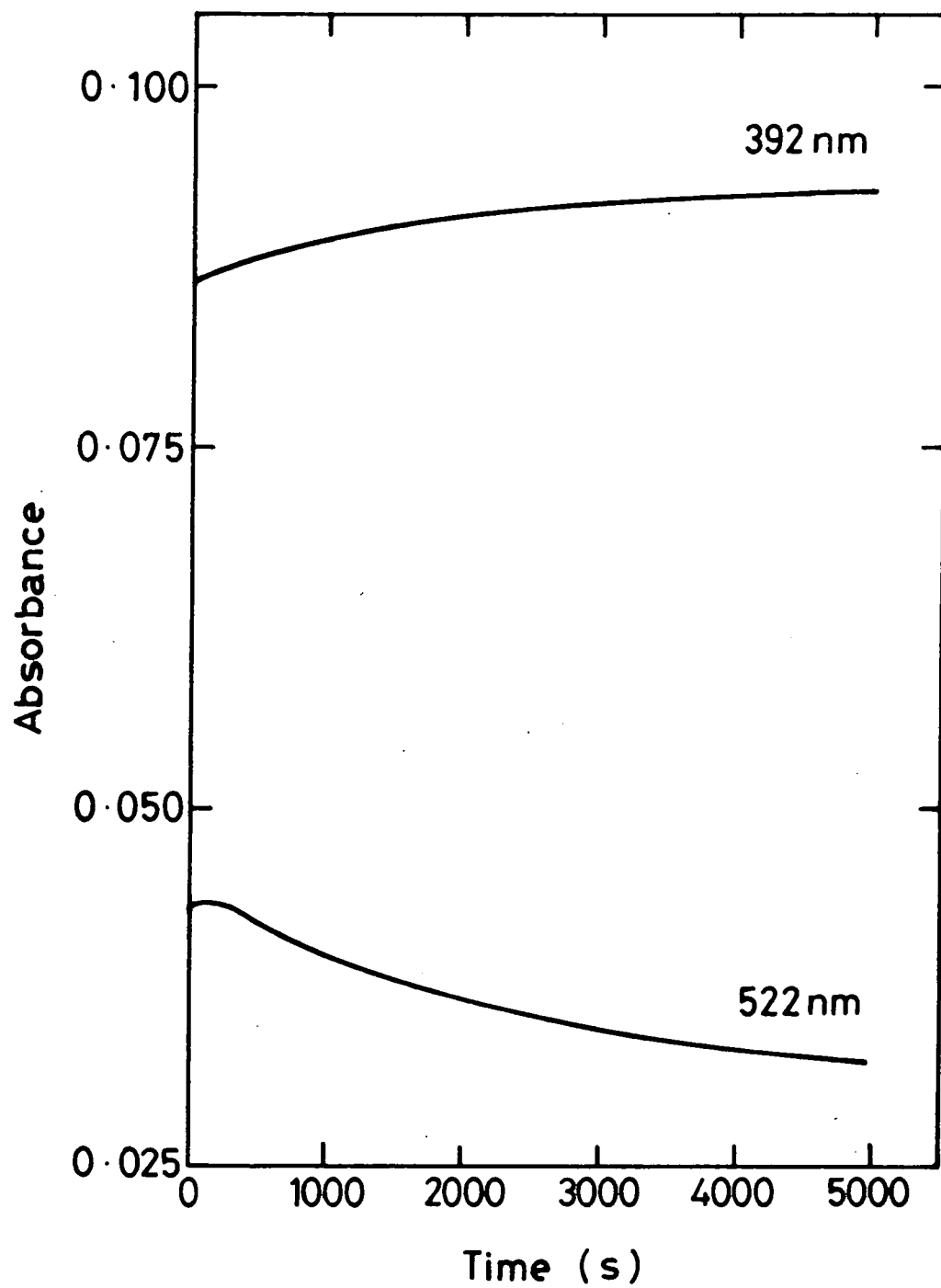


Figure 6.2

Plots of absorbance at 392 nm and 522 nm versus time for an LB film of merocyanine after deprotonation.

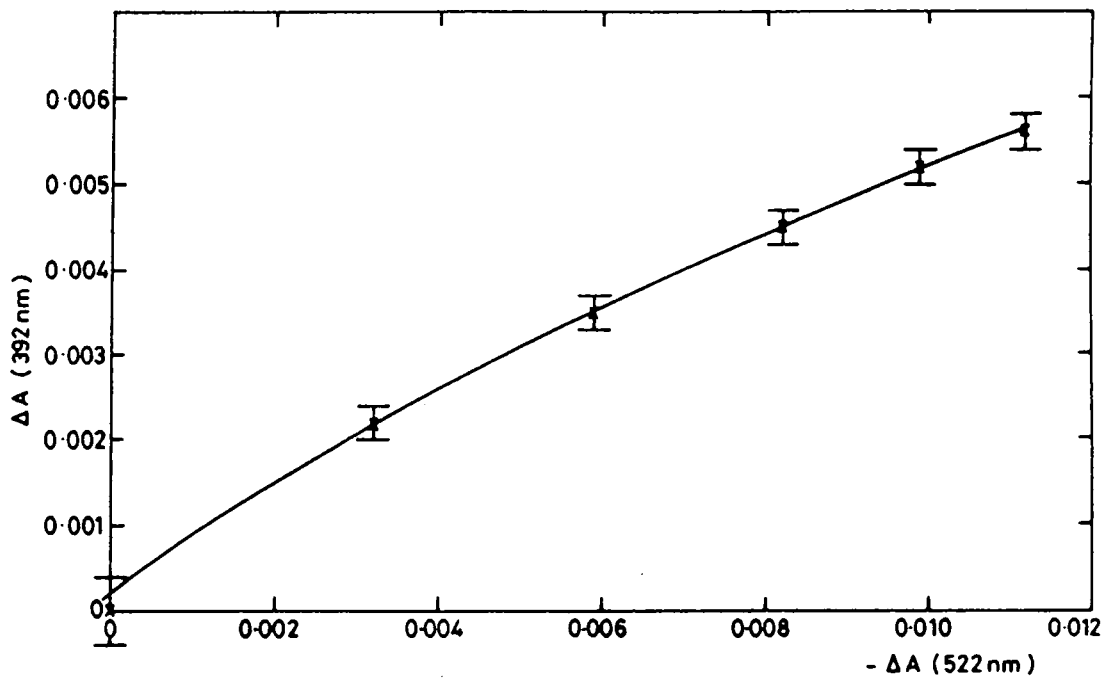


Figure 6.3

Plot of change in absorbance at 392 nm versus change in absorbance at 522 nm for an LB film of merocyanine at various time intervals after deprotonation.

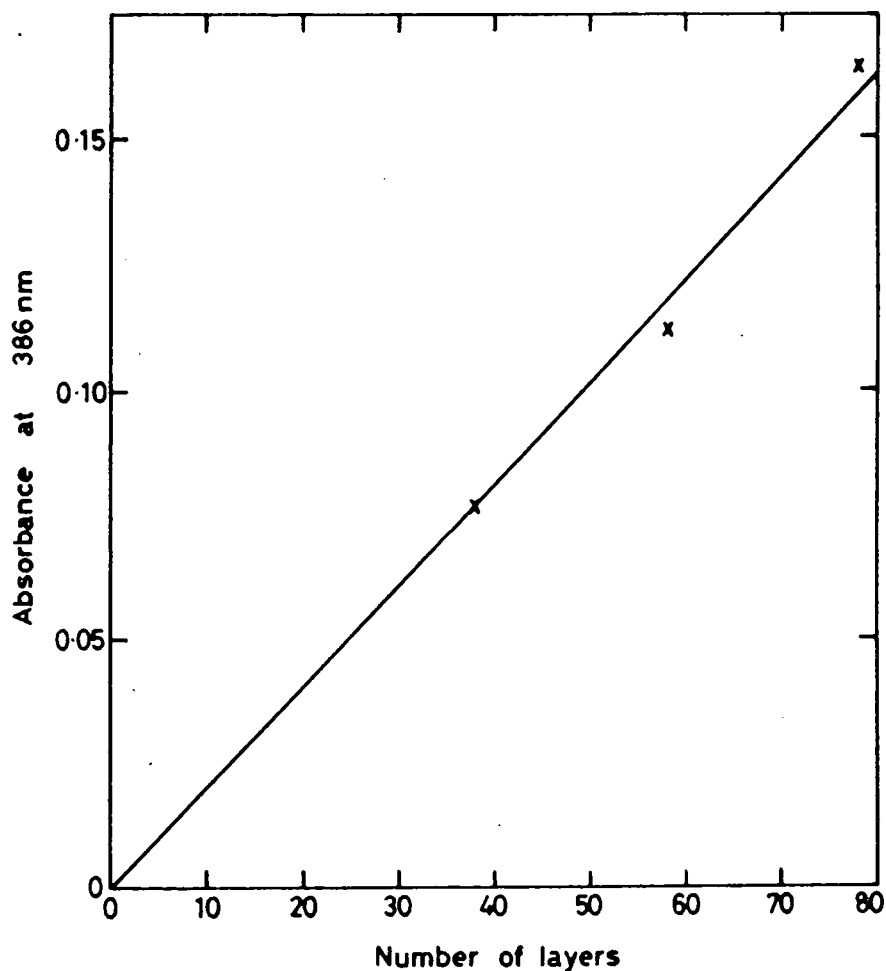


Figure 6.4

Plot of absorbance (at 386 nm) versus number of layers for a merocyanine LB film of stepped thickness.

ratio of the absorption peaks) were achieved by varying the concentration of the salt in the solution.

Studies by Daniel and Smith⁽¹⁰⁾ of the relative intensities of the phenolic O-H in-plane deformation mode ($D1H^+$) and the quinoidal C=O stretching vibration (D1) in the infrared spectrum of an LB film of D1, before and after exposure to ammonia vapour, have confirmed the existence of the protolytic equilibrium.

A plot of absorbance versus number of monolayers is shown in figure 6.4 for a merocyanine LB film of stepped thickness; it reveals that the material obeys the Beer-Lambert law quite well, confirming the deposition to be uniform. The dye was left in its protonated form in order to prevent changes in the profile of the spectra occurring during the measurements.

6.1.2 Amidonitrostilbene (compound D5)

The optical absorption spectra of solutions of amidonitrostilbene (compound D5) in chloroform and in cyclohexane, and of a 60-layer LB film of the material, are shown in figure 6.5. It is interesting to note that in chloroform there is a slight bathochromic shift of the first absorption band (i.e. of the lowest energy electronic transition) relative to its position when nonpolar cyclohexane is the solvent. This is indicative of a higher degree of charge transfer in the first excited state than in the ground state. Another effect which can readily be seen on examination of figure 6.5 is that in cyclohexane solution the peak absorbance of the second absorption band (i.e. the one at shorter wavelength) is much greater than that of the first absorption band, whereas the reverse is true in chloroform solution. It should be noted that the vibrational fine structure was only observed for the case of the second absorption band of the cyclohexane solution. The spectrum of

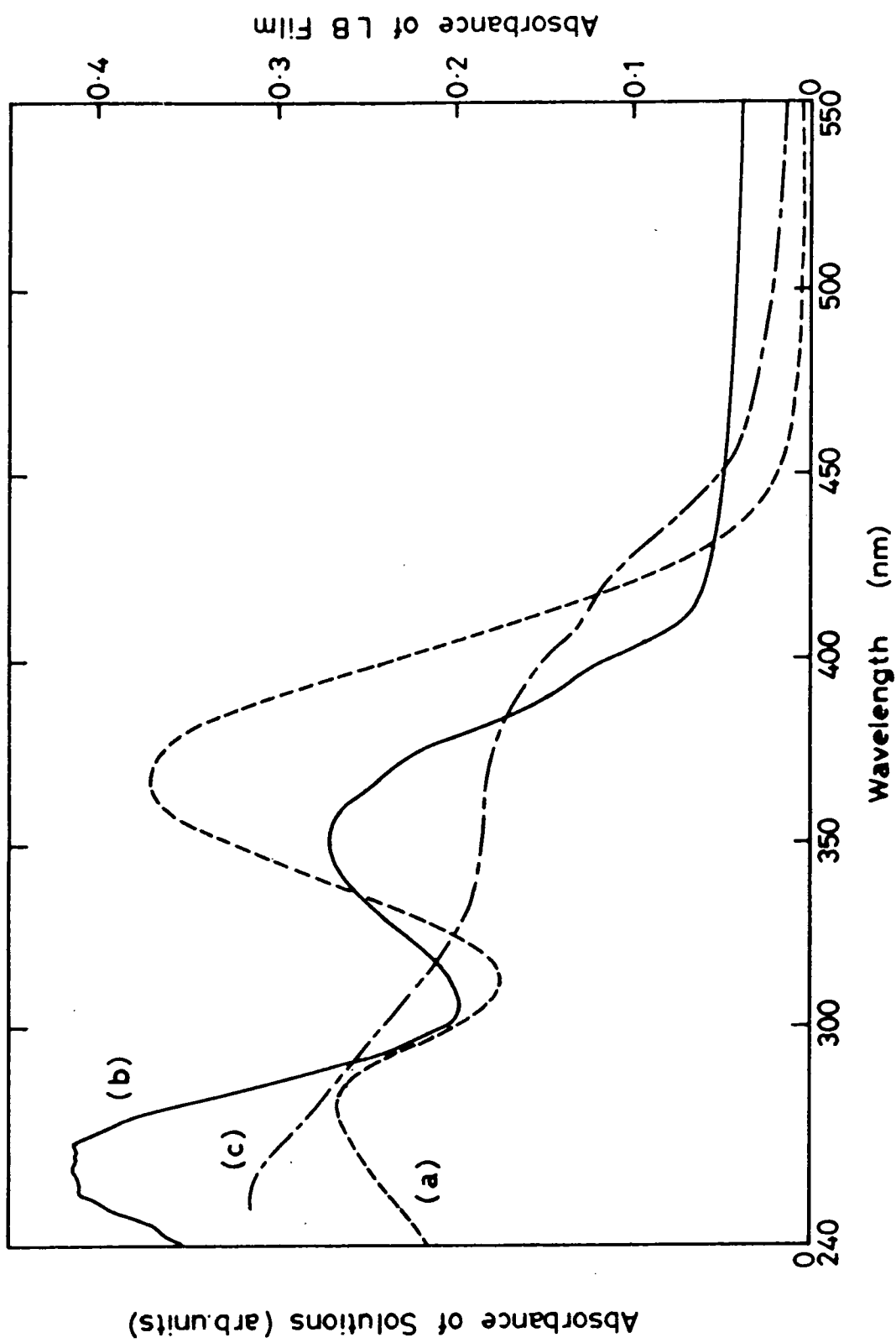


Figure 6.5 Optical absorption spectra of amidonitrostilbene: (a) solution in chloroform; (b) solution in cyclohexane; (c) 60-layer LB film.

the LB film exhibits a splitting of the first absorption band, indicative of an angular distribution of dipoles within the layers; in addition, this band is significantly broadened and shifted in wavelength by crystal field effects.

A plot of absorbance at 370 nm against number of monolayers gave an excellent straight line fit (figure 6.6), indicative of highly uniform LB multilayer deposition. The fact that the points derived from films deposited on hydrophilic and hydrophobic substrates lie on the same line indicates that the material has wide applicability. A solution of D5 in chloroform becomes bleached within a period of a few weeks; in contrast, the absorption spectrum of a sample containing 60-layers of D5 decreased in intensity by only $\sim 20\%$ and was unchanged in profile over a period of several months. This increased stability of the multilayers relative to solutions is complementary to the observations of Mooney et al⁽¹¹⁾, who found a significantly lower photoisomerization yield in LB films of a long chain trans-stilbene compared to that in most organic solvents. Monolayers containing D5 mixed with cadmium arachidate were found to give absorption spectra of identical profile to those of the undiluted material, the intensities of the absorptions simply being reduced in proportion to the fractional area of the layer occupied by cadmium arachidate.

6.1.3 Aminonitrostilbene (compound D6)

Aminonitrostilbene (compound D6) is a closely related material to D5, the essential difference lying in the replacement of the amide functionality in the latter with an amine group, which should be a rather stronger donor. Figure 6.7 shows the optical absorption spectra of D6 in chloroform solution, cyclohexane solution, and LB film form.

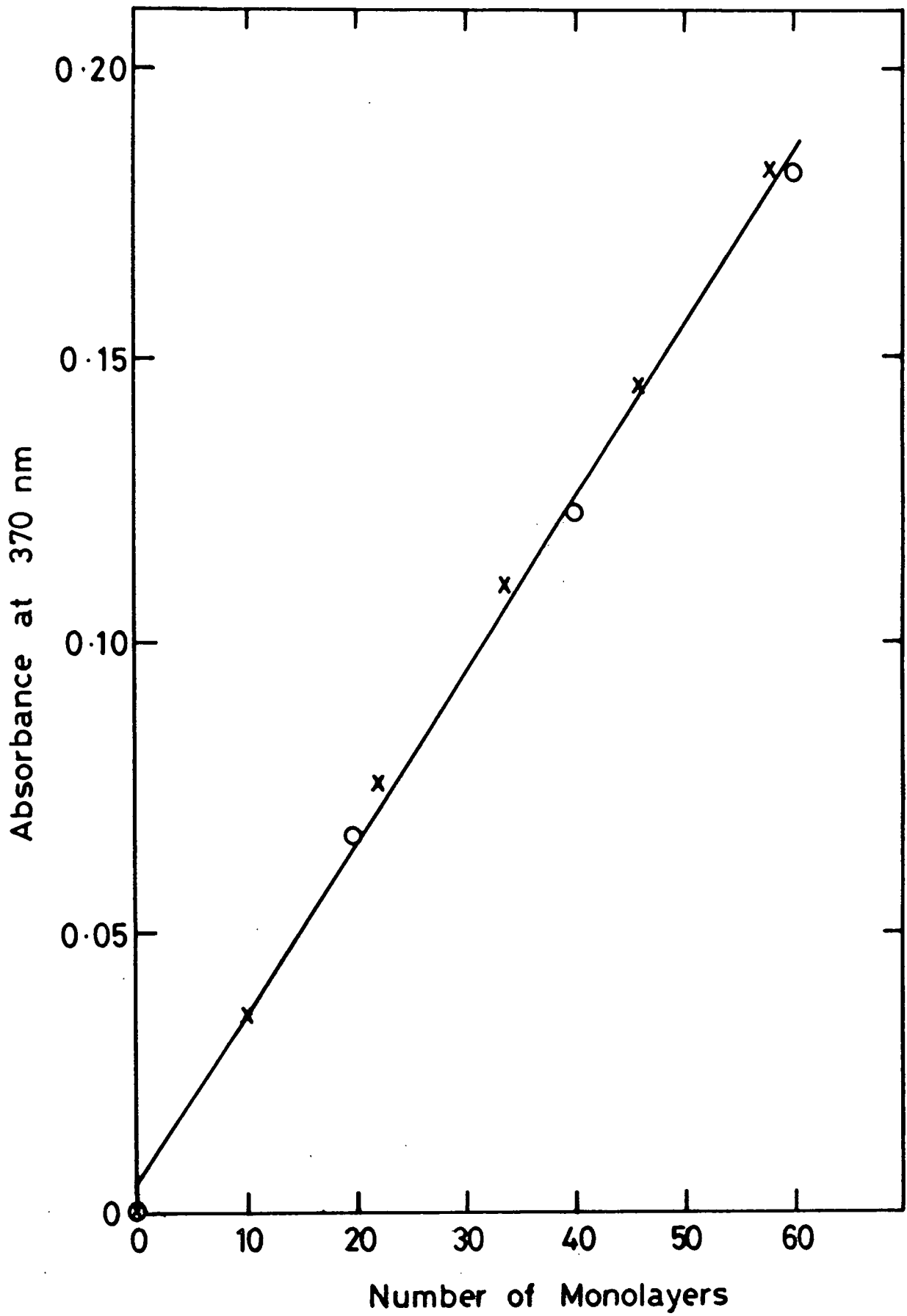


Figure 6.6

Absorbance at 370 nm versus number of monolayers for LB films of amidonitrostilbene on glass substrates; x-hydrophilic glass, O-hydrophobic glass.

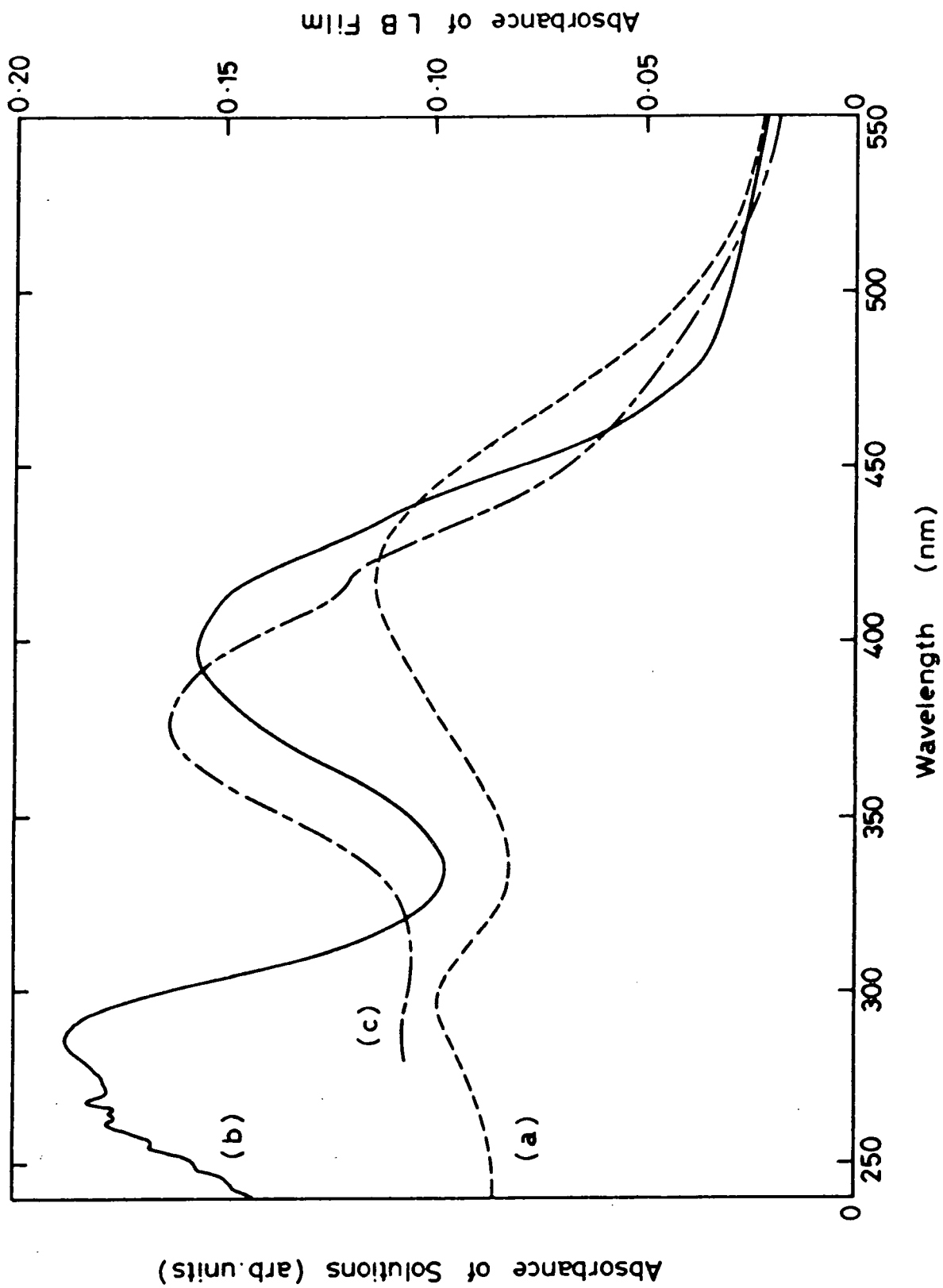


Figure 6.7 Optical absorption spectra of aminonitrostilbene: (a) solution in chloroform; (b) solution in cyclohexane; (c) 30-layer LB film.

These spectra display the same features as were observed with D5, namely:

- (i) a slight bathochromic shift of the first absorption band in chloroform relative to cyclohexane;
- (ii) in cyclohexane solution the peak absorbance of the second absorption band is greater than that of the first absorption band, whereas the reverse is true in chloroform solution;
- (iii) the spectrum of the LB film exhibits a splitting and broadening of the first absorption band (although the lower wavelength half exhibits a clear maximum in the case of D6 but not with D5).

In addition, the solution absorption peaks are both at longer wavelength in D6 compared to D5 (for a given solvent); for the first absorption band, this difference is approximately 50 nm in either solvent. Such a change is probably due to the greater donor strength in D6 bringing about a higher degree of charge transfer in the ground state and thereby reducing the difference in energy between that and the first excited state.

A plot of peak (376 nm) absorbance against thickness for an LB film of D6 yielded a good straight line, indicating a uniform pick-up of material from one monolayer to the next. (figure 6.8).

6.1.4 Tertiary aminonitrostilbene (compound D7)

Unlike D5 and D6, the tertiary aminostilbene (compound D7) could not be deposited in single component multilayers; however, good film quality could be obtained by diluting the individual monolayers with arachidic acid (1 mole of dye to 5 moles of acid), present as cadmium arachidate under the subphase conditions used. Figure 6.9 shows the optical absorption spectra obtained for three different multilayer

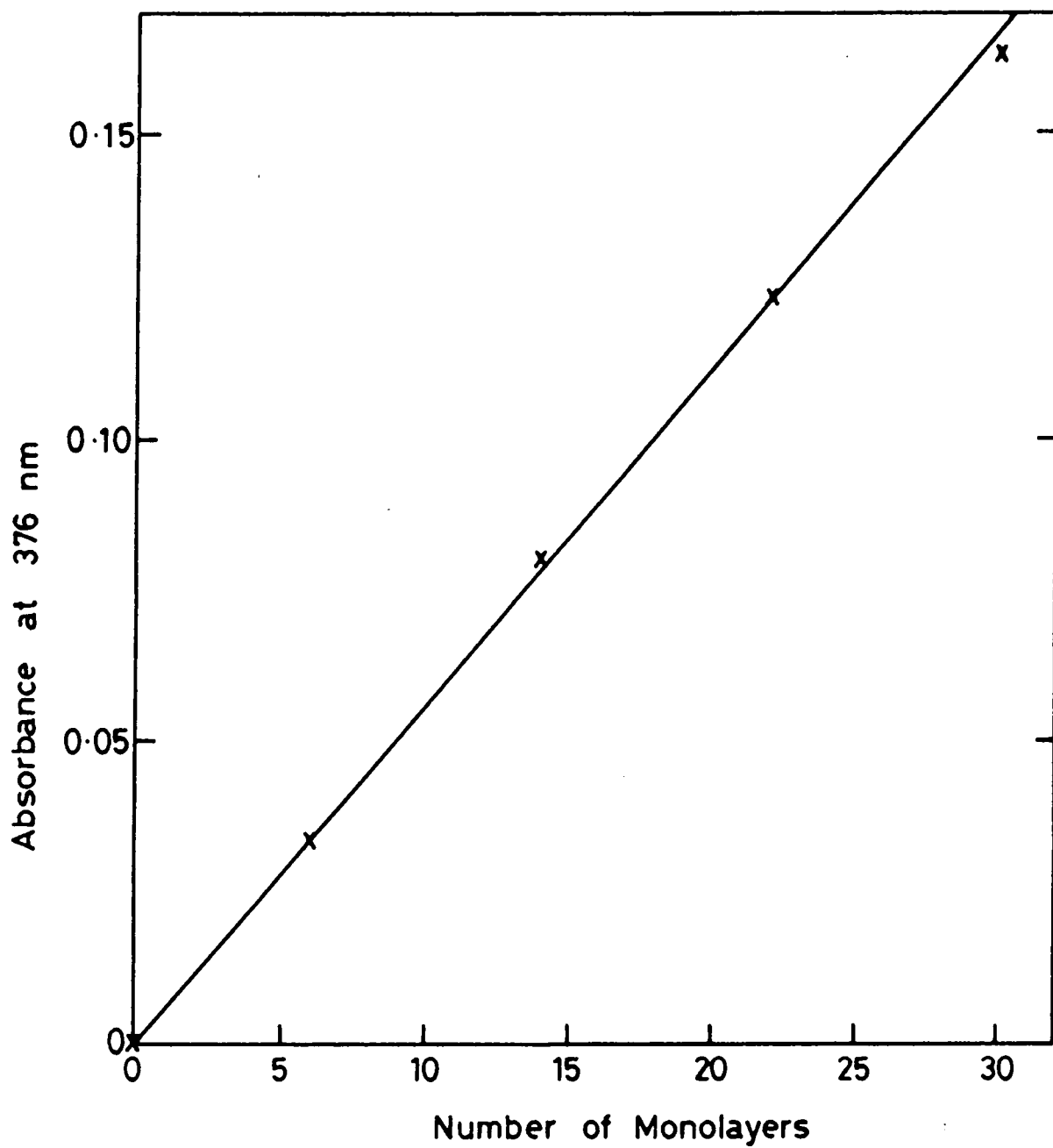


Figure 6.8

Plot of absorbance at 376 nm versus number of monolayers for an aminonitrostilbene LB film of stepped thickness.

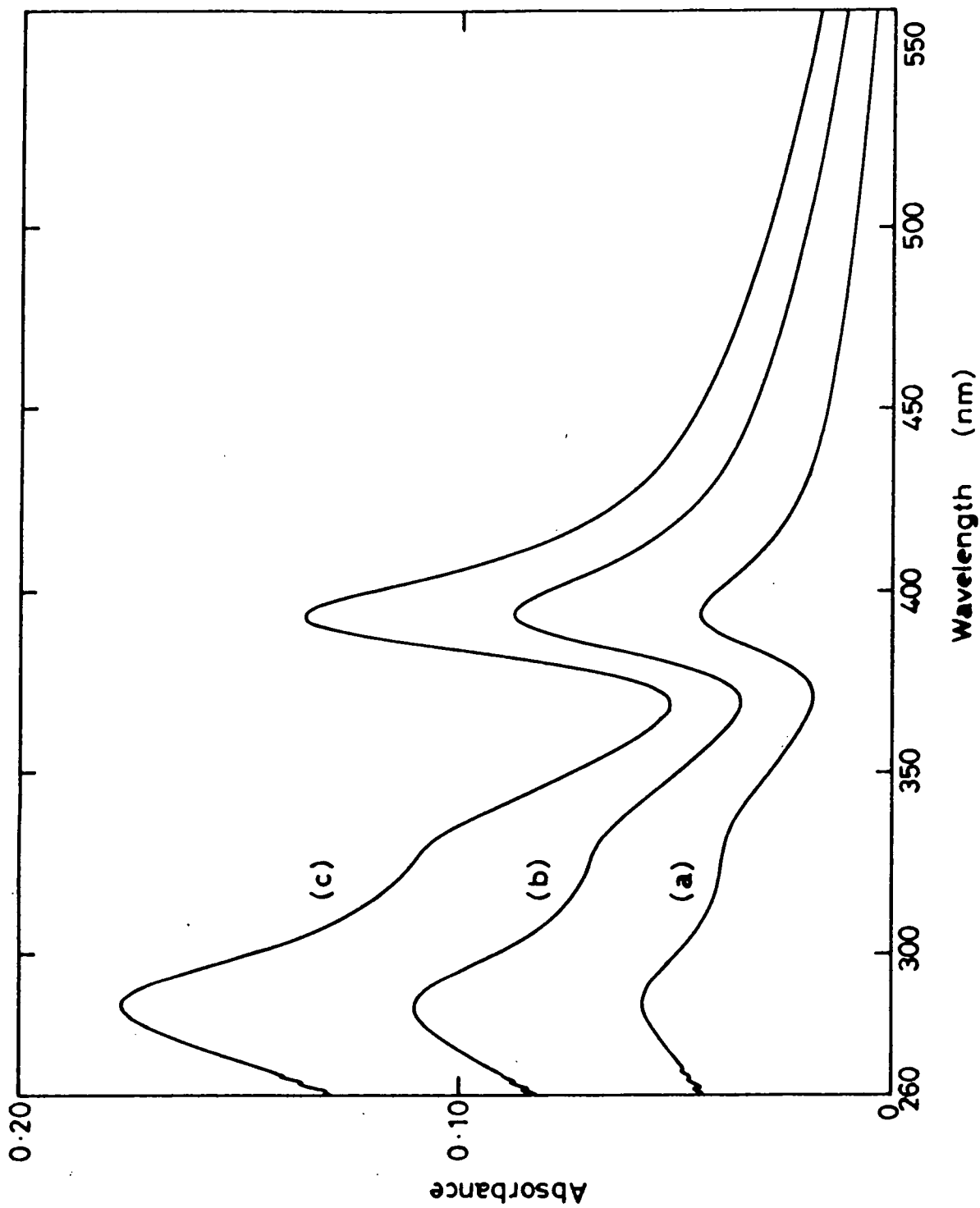


Figure 6.9 Absorption spectra for 3 different thicknesses of an LB film of D7 mixed with cadmium arachidate deposited onto 12 layers of cadmium arachidate: (a) 28 mixed layers; (b) 56 mixed layers; (c) 84 mixed layers.

thicknesses, deposited onto a substrate consisting of a Corning 7059 glass slide with cadmium arachidate overlayers. The peaks in these spectra are particularly sharp for an LB film, probably as a consequence of the dye molecules being dispersed in an "inert" fatty acid matrix and therefore behaving more like "free" molecules. The contrast in this behaviour compared to that reported in section 6.1.2 for D5, where the production of a mixed layer did not increase the sharpness of the peaks, is probably due to the smaller molar ratio of acid to dye in the latter case. As expected, the peak of the first absorption band (394 nm) lies close to that observed for the secondary aminonitrostilbene (D6) in cyclohexane (397 nm), since the molecules are very similar in nature and their environments are effectively nonpolar in both cases.

The spectra given in figure 6.9 were used to construct plots of peak absorbance, for the first and second absorption bands, against the number of mixed layers deposited (figure 6.10). Both of these graphs were linear, indicating that the same amount of absorbing material was being picked up in each monolayer; the fact that these lines passed through the origin confirmed that D7 was indeed the absorbing species responsible for each peak in the spectrum (see note below).

NB. If either peak had been due to cadmium arachidate, then the absorbance, A , would have been given by $A = ka$, where k is a constant and a is the effective number of cadmium arachidate layers. Now, if F is the fractional area of D7 present in each mixed layer, and there are m mixed layers (deposited on top of 12 layers of pure cadmium arachidate) in the region of film being considered, then $a = 12 + m(1-F)$. Thus $A = 12k + mk(1-F)$, and the intercept on the m -axis (i.e. when $A=0$) would be at $m = -12/(1-F)$; since $0 < 1-F < 1$, this gives $m < -12$. However, if the peak under consideration is due to D7, then $A \propto m$ and the line will pass through the origin.

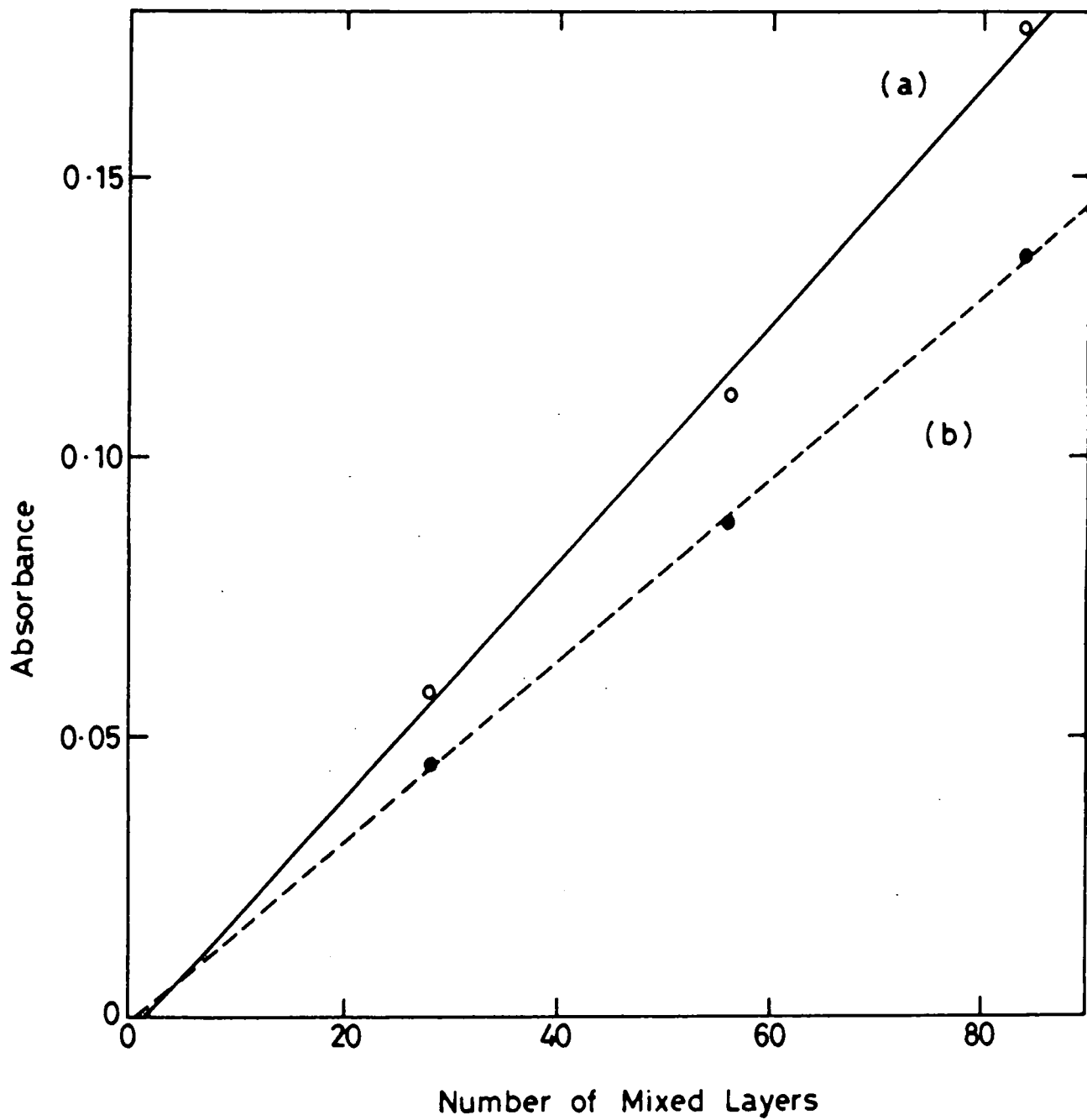


Figure 6.10

Absorbance at (a) 285 nm and (b) 394 nm versus the number of mixed layers for an LB film of D7/cadmium arachidate of stepped thickness.

6.1.5 Hemicyanine (compound D2)

A comparison of the optical absorption spectra of an LB film of hemicyanine (compound D2) and its solution in chloroform is shown in figure 6.11. The first absorption band is broadened and hypsochromically shifted in the LB film relative to the solution. If the dipoles are assumed to have a parallel alignment within the film, then the electronic state of lowest polarity will be energetically favoured (due to dipole - dipole repulsions); a blue shift of the first absorption band implies that the ground state has been stabilized relative to the first excited state, and thus that the first electronic transition is accompanied by an increase in the degree of charge transfer. Vibrational fine structure was observed in the second absorption band of the solution, but not in any other regions of the spectra. Accurately linear plots of absorbance at 264 nm and 376 nm versus number of monolayers were obtained (figure 6.12), characteristic of uniform deposition.

The second-order non-linear optical properties of a mixed monolayer system incorporating hemicyanine and cadmium arachidate have been investigated (see Chapter 8), and the complementary optical characterization is given in section 6.1.7.

6.1.6 The alternate layer hemicyanine/amidonitrostilbene system

Alternate layers of hemicyanine (D2) and amidonitrostilbene (D5) constitute a donor-acceptor: inverted donor-acceptor system, and are therefore likely to display large non-linear optical effects (see Chapter 8). It was thus of interest to characterize the optical absorption properties of such arrays. The optical absorption spectrum of a sample consisting of 11-layers of hemicyanine alternated with 10-layers of amidonitrostilbene is given in figure 6.13. A plot of peak

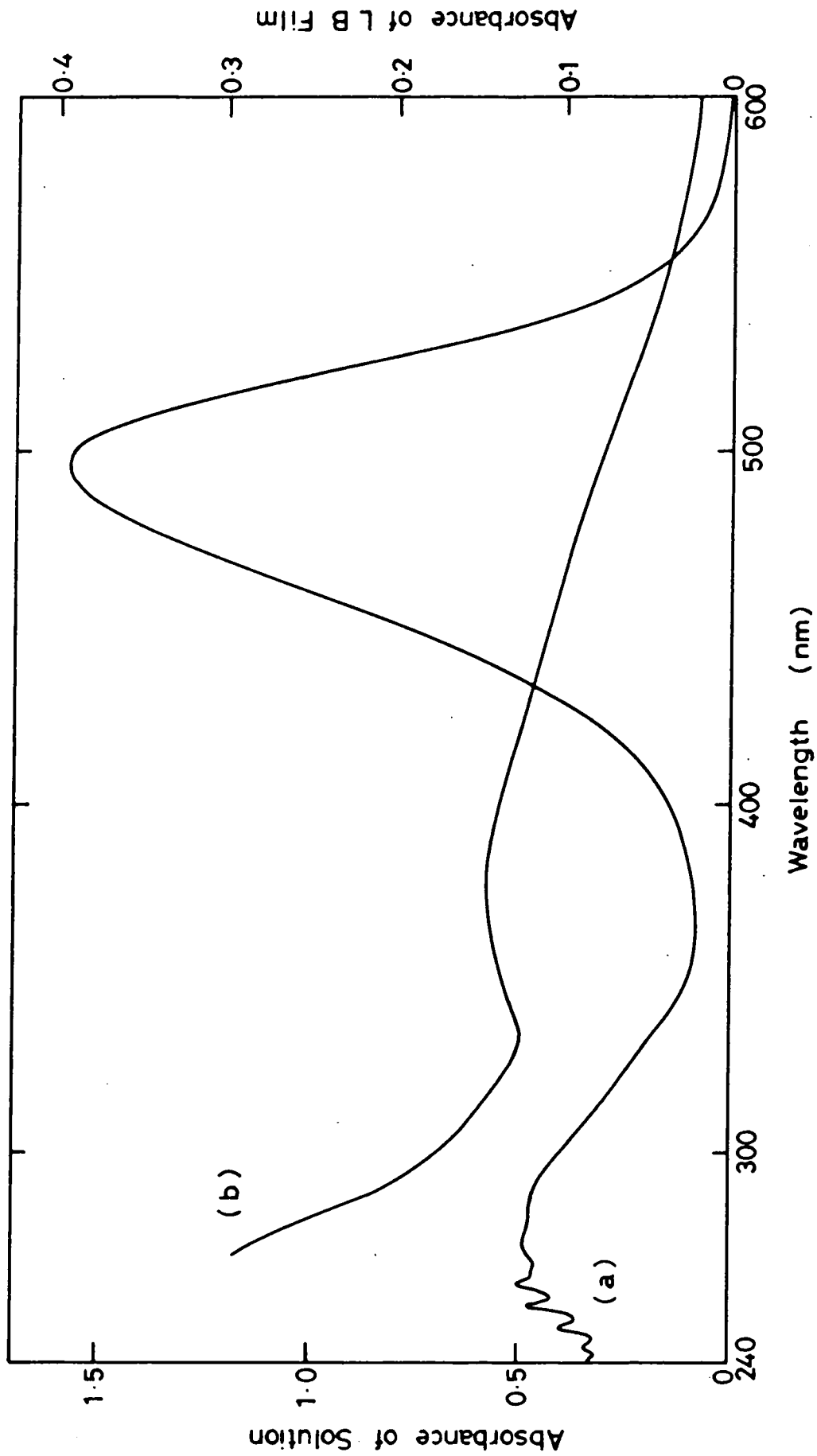


Figure 6.11 Optical absorption spectra of hemicyanine: (a) $4.5 \times 10^{-5} M$ solution in chloroform; (b) 36-layer LB film.

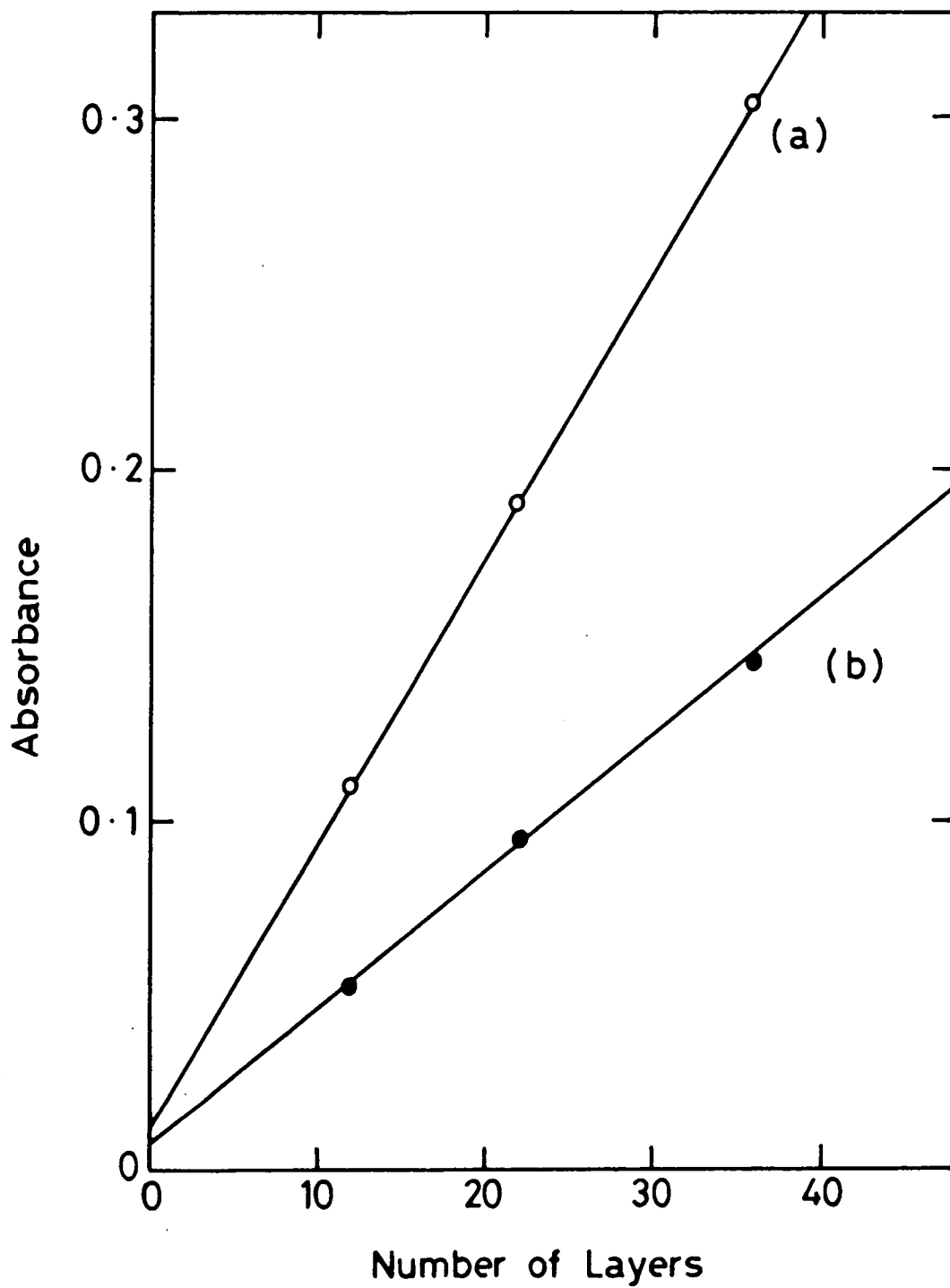


Figure 6.12

Absorbance at (a) 264 nm and (b) 376 nm versus the number of monolayers for a hemicyanine LB film of stepped thickness.

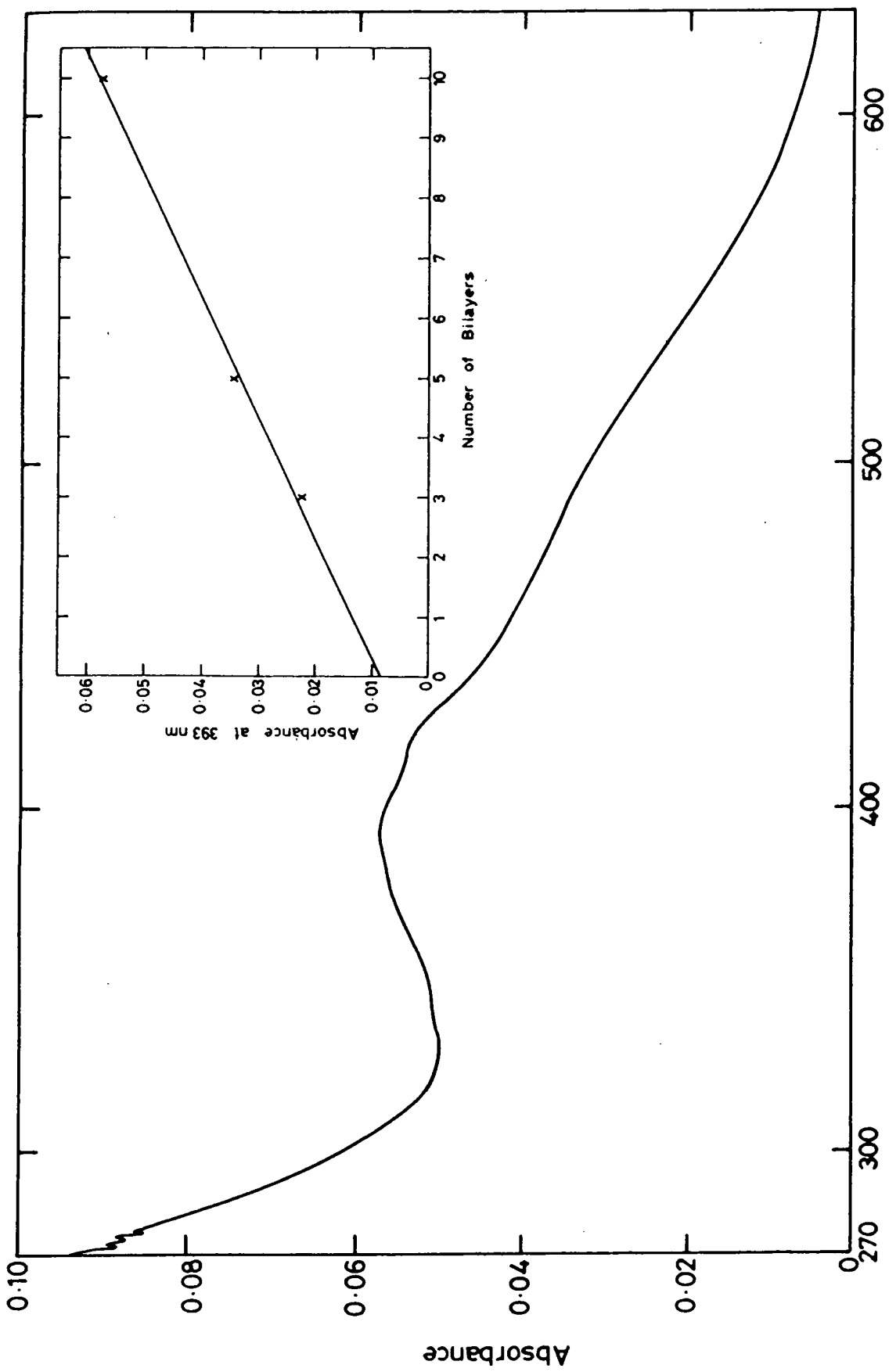


Figure 6.13 Optical absorption spectrum of an alternating layer LB film containing 11-layers of hemicyanine and 10-layers of amidonitrostilbene. Inset: Plot of absorbance at 393 nm versus the number of bilayers for a hemicyanine/amidonitrostilbene alternating layer LB film of stepped thickness.

(393 nm) absorbance against the number of bilayers deposited is shown in the inset, and gives a reasonable fit to a straight line. As expected, this line does not pass through the origin, due to the additional first layer of hemicyanine.

The spectrum shown in figure 6.13 is clearly not the result of a simple weighted addition of the spectra of Y-type multilayers of hemicyanine (figure 6.11) and amidonitrostilbene (figure 6.5). This can be seen from the fact that the first absorption band of hemicyanine gives an absorbance peak at 376nm, whilst the broad first and second absorption bands of amidonitrostilbene give rise to an absorbance which increases with decreasing wavelength over the entire range 250-500 nm; thus any linear combination of the two will give a first absorption peak below 376 nm, whereas the alternate layer system displays a distinct peak at 393 nm. A possible explanation for this phenomenon may lay in the opposite direction of the first excited state dipoles, with respect to the hydrocarbon tails, of D2 compared to D5. Although the direction of charge transfer is unchanged in going from the ground to the first excited state in either molecule, the degree of this transfer is much greater in the excited state. Now, when the molecules are placed head to head in the multilayer structure, the positive end of the hemicyanine dipole will be adjacent to the negative end of the amidonitrostilbene dipole and in this situation the excited state of either molecule will be more stable than in conventional Y-type multilayers (where the ends of adjacent dipoles have the same sign). This stabilization of the excited states is likely to produce a bathochromic shift in the first absorption bands of both molecules, in accordance with the observed peak at 393 nm for the alternate layer system.

6.1.7 The hemicyanine/cadmium arachidate system of mixed monolayers

Mixed monolayers are frequently used to improve the deposition characteristics of dye materials⁽¹²⁾, and in Chapter 8 the hemicyanine/cadmium arachidate system is used as a model to investigate the effects of dilution on the non-linear optical properties of LB films. This section describes the optical absorption characteristics of such monolayers.

Optical absorption spectra for a pure hemicyanine monolayer and a mixed monolayer of hemicyanine and cadmium arachidate (containing 56% dye, by area) are shown in figure 6.14. There are significant differences in the spectra of hemicyanine monolayers (figure 6.14) and multilayers (figure 6.11); these will be discussed later in this section. The signal-to-noise ratios encountered in this part of the study were rather low, as a result of the extremely small absorbances of such thin films, and slight baseline shifts were observed between samples, due to small differences in the absorbance of different substrates (Spectrosil B vitreous silica slides); accurately quantitative measurements of peak absorbance as a function of dye concentration were therefore not possible. However, over the range of concentrations studied (15-100% dye, by area), there was a definite trend towards increasing peak absorbance in the first absorption band (normalized by dividing the measured absorbance by the fractional area of dye in the film) with decreasing dye concentration. This pattern was not reflected in the second absorption band, whose intensity was simply proportional to the hemicyanine concentration. Similarly, the first absorption band exhibited a bathochromic shift on dilution (from ~ 419 nm for 100% dye to ~ 470 nm for 15% dye) whereas the shift in the second absorption band was negligible.

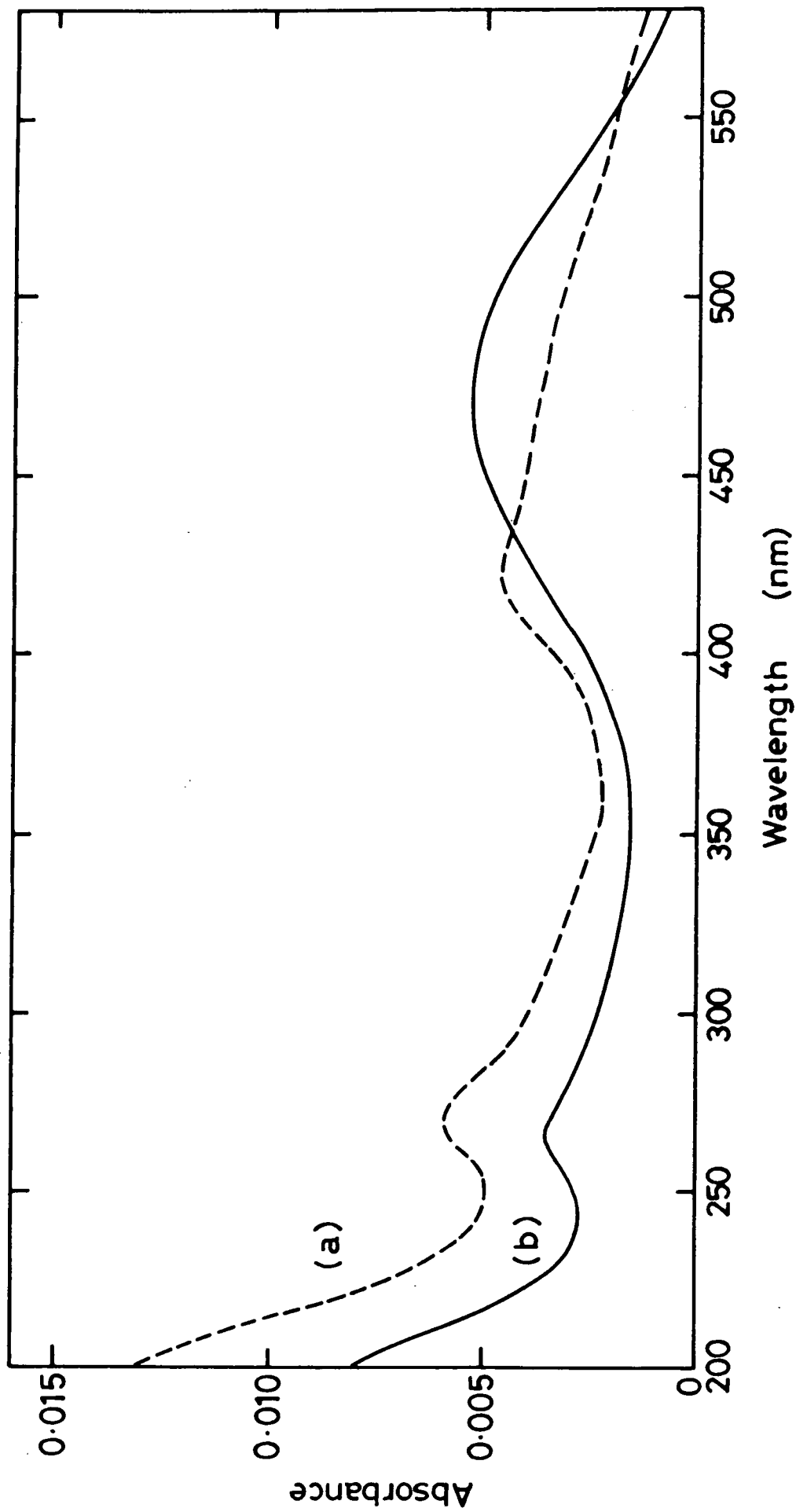


Figure 6.14 Optical absorption spectra of : (a) pure hemicyanine monolayer; (b) mixed hemicyanine/cadmium arachidate monolayer (containing 56% hemicyanine by area).

The general observations of the effects of dilution are typified by the spectra shown in figure 6.14; the first absorption band of the dye is shifted from ~ 419 nm in the pure monolayer to ~ 467 nm in the mixed layer, and this change is accompanied by an increase in peak absorbance (even before normalization to allow for the lower dye concentration). In contrast, the second absorption band of the dye in the mixed layer is barely shifted (265 nm cf. 269 nm in the homogeneous layer), and the peak absorbance is very close to 56% of that of the pure dye monolayer. A possible explanation for these results lies in the effects of dipole - dipole interactions on the stability of the first excited state. In section 6.1.5 the hypsochromic shift of the first absorption band of a multilayer LB film of hemicyanine relative to a solution was interpreted as being due to the influence of parallel dipole alignment on the stability of the highly polar first excited state. By forming a mixed monolayer the dye molecules are being placed in an environment more closely resembling that of the solution, hence the shift of absorption back towards longer wavelengths; in addition, the more favourable conditions for charge transfer are likely to give rise to an increase in the intensity of the peak. A similar argument may hold in order to explain the difference in behaviour between hemicyanine monolayer and multilayer structures. In Y-type films, the dipoles are oriented with their positive ends adjacent, which is unfavourable for the increased degree of charge transfer which accompanies the first electronic transition. A monolayer doesn't have an opposing layer of dipoles next to it, and hence is likely to display a bathochromic shift of the first absorption band relative to the multilayers, as was observed (the absorption maximum of the 36-layer film in figure 6.11 was at ~ 376 nm cf. 419 nm in the monolayer). Presumably the second electronic

transition does not involve such a great change in the polarity of the molecules as the first, since it was largely unaffected by monolayer dilution or multilayer formation.

The shift of the first absorption peak towards 470 nm in the mixed monolayers brings it closer to the second harmonic of the 1.064 μm radiation used in the non-linear optical characterization described in Chapter 8, without significantly increasing the absorbance of the film at that wavelength. In view of the desirability of an absorption edge close to the second harmonic (section 2.3.2), as well as the sensitivity of β to charge transfer structural changes, this phenomenon is likely to be manifested again in the studies of second harmonic generation.

6.2 Determination of the Relative Permittivity

Plots of reciprocal capacitance against the number of layers in a metal-LB film-metal structure can be used to demonstrate the repeatability of dielectric thickness of each monolayer (see sections 3.7 and 4.2). Figure 6.15 shows such a graph for an LB film of the amidonitrostilbene D5 of stepped thickness 9-33 layers sandwiched between an aluminized glass substrate and gold top electrodes. Although this graph gives a very good fit to a straight line, the intercept on the $1/C$ axis is negative; however, equation 4.2 predicts a positive intercept related to the capacitance of the interfacial oxide layer. This feature can be explained by assuming that, when the top contacts are deposited, they penetrate a small number of layers due to the thermal energy of the atoms in the metal vapour. Thus, if N' layers of film were deposited and a small number, E , were penetrated, then the real number of layers (N) which should be used in equation 4.2 is



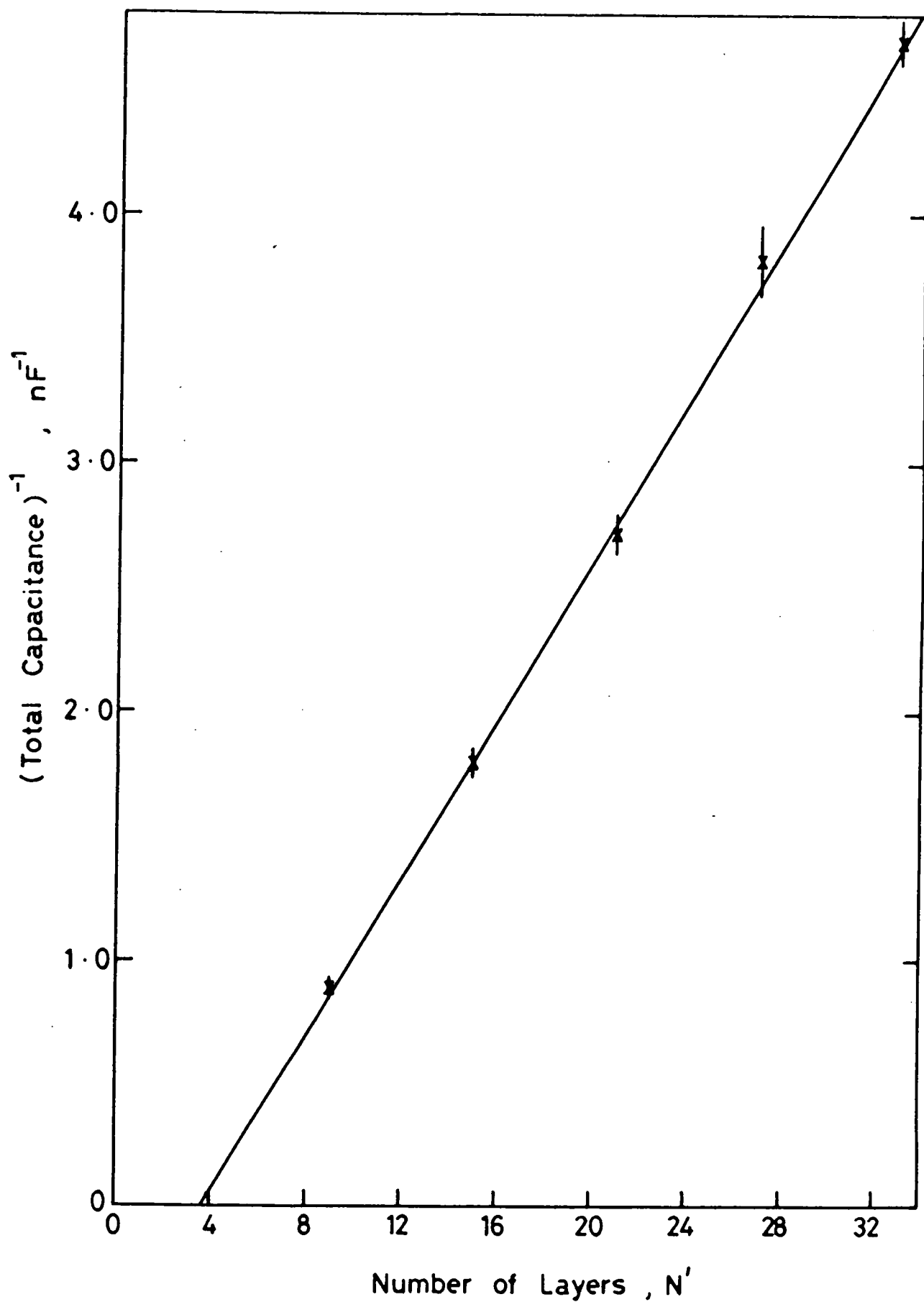


Figure 6.15

Inverse capacitance versus number of layers for a step structure of amidonitrostilbene (D5).

$N = N' - B$. The equation can then be rewritten as:

$$\frac{1}{C_T} = \frac{1}{C_{ox}} - \frac{Bd}{\epsilon_o \epsilon_r A} + \frac{N'd}{\epsilon_o \epsilon_r A} \quad (6.1)$$

Thus, if $\frac{Bd}{\epsilon_o \epsilon_r A} > \frac{1}{C_{ox}}$ then the intercept will be negative. Now, the capacitance of a gold- Al_2O_3 - aluminium device was measured directly (by making contact to a gold dot on a region of the sample free of film). This gave $1/C_{ox} = 0.49 \pm 0.02 \text{ nF}^{-1}$, which can now be used to estimate the value of B. The point on the graph in figure 6.15 where

$\frac{1}{C_T} = \frac{1}{C_{ox}}$ will correspond to $N' = B$; in this manner B was found by interpolation to be approximately 7 layers.

Attempts to reduce the effects of the burning through of top contacts by using different top contact materials (see section 4.1.2) proved to be unsuccessful. When aluminium/gold electrodes were deposited onto an otherwise identical sample to that used above, the capacitance values obtained were extremely low, which is consistent with the formation of additional layers of oxide on the top contacts.

The gradient of the graph in figure 6.15 gives $d/(\epsilon_o \epsilon_r A) = 0.159 \text{ nF}^{-1}$; the diameter of the dots was measured to be $0.9 \pm 0.1 \text{ mm}$, and taking the dominant error to be in this figure, a value for the dielectric thickness of $d/\epsilon_r = 0.90 \pm 0.20 \text{ nm}$ is obtained. The length of an amidonitrostilbene molecule was estimated to be 3.8 nm from measurements performed on an Ealing CPK molecular model. On the assumption that the molecules have an average tilt of $54 \pm 1^\circ$ with respect to the substrate normal (see section 7.3.5), a monolayer thickness of 2.2 nm is obtained; thus $\epsilon_r = 2.4 \pm 0.5$.

The problem of penetration of the top electrode metal through the surface of the LB film might be accounted for by the wide spacings between adjacent hydrocarbon tails within each monolayer, arising from the mismatch between the cross-sectional areas of the tails and the chromophores in the molecules (see section 7.3). A similar phenomenon was observed with many of the other materials studied in this project; for example, LB films of the merocyanine D1 always gave rise to MIM structures which were short-circuited. One possible way of avoiding such difficulties might be to deposit a few layers of a material such as arachidic acid (in which the entire length of the molecules can pack closely together) on top of the dye layers.

6.3 Surface Plasmon Resonance Studies of Amidonitrostilbene Multilayers

The techniques and applications of surface plasmon resonance (SPR) spectroscopy were briefly reviewed in Chapter 4. In this section some results are described for multilayers of the amidonitrostilbene (compound D5).

Amidonitrostilbene formed poor quality multilayers when deposited directly onto a silver coated glass slide; however, uniform films could be obtained by first depositing five layers of ω -tricosenoic acid (ω -TA) onto the silver, and then building up the dye layers on top of the acid. A structure was produced consisting of the following steps: bare silver; silver plus 5-layers of ω -TA; silver, 5-layers of ω -TA, plus 2, 4, 6, 8, 10 layers of dye. SPR curves were obtained for each of these regions, and figure 6.16 shows the results for areas whose uppermost coatings are silver, ω -TA, and 2, 6, 10 dye layers. The constant depth of the resonance and reasonably minor increase in its width on increasing the film thickness provide evidence that the film is not highly scattering or absorbing at the wavelength of the laser (632.8 nm); this was to be

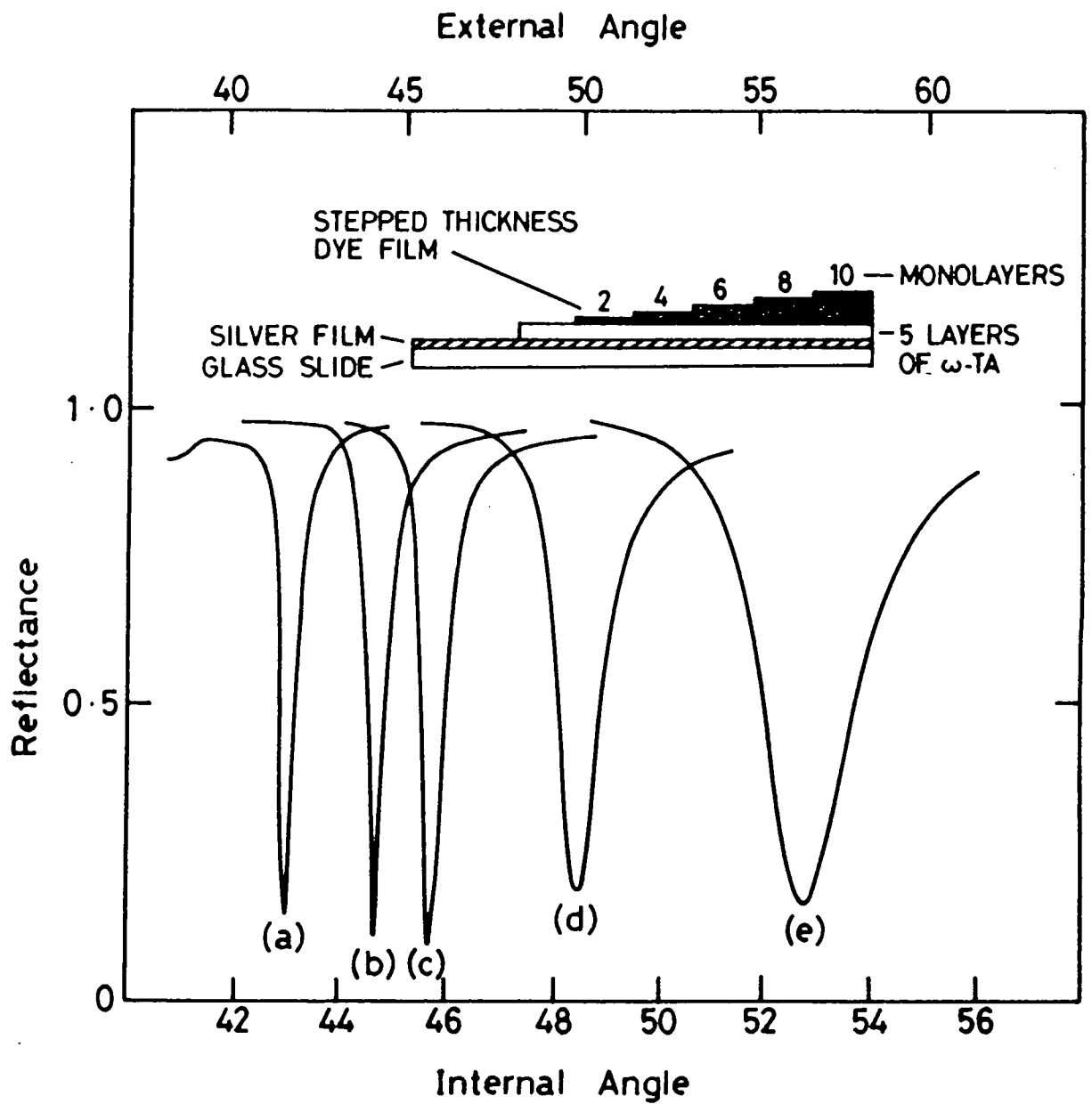


Figure 6.16

SPR curves for (a) silver; (b) silver plus 5-layers of ω -TA. Other curves are as for (b) but with an additional covering of N layers of D5, where N=2 (c), 6 (d), 10(e). Inset: structure of sample.

expected in view of the absorption cut-off displayed by the films above ~ 500 nm (figure 6.5).

A computer program was available to calculate theoretical SPR curves from input data comprised of the thickness and the refractive indices of the metal and dielectric layers. The values of the silver film thickness, $t(\text{Ag})$, and refractive index, $n(\text{Ag})$, were adjusted to give a curve which closely fitted the experimental one (in terms of resonance angle and depth of the reflectance minimum). These parameters were fixed in subsequent calculations at the optimum values thus determined of $t(\text{Ag}) = 61.7$ nm and $n(\text{Ag}) = 0.068 + 63.096 i$. Next, the SPR curve from the 5 layers of ω -TA was treated in a similar manner, each monolayer being assumed to have a thickness of 2.8 nm (giving $t(\omega\text{-TA})=14$ nm) whilst the refractive index was varied to obtain the best fit (assuming negligible absorption i.e. no imaginary terms), which was found to be for $n(\omega\text{-TA}) = 1.626 + 0 i$. Unfortunately, the SPR curves obtained from the dye regions of the film could not be fitted so precisely, since the computer program was written for a metal film with a single component overlayer and therefore only one value of the LB film refractive index could be used, not different ones for the dye and the ω -TA.

Using refractive indices of 1.626 (i.e. that obtained for ω -TA, which should be less than that of the dye) and 2.000 (which should be greater than that of the dye) two theoretical SPR curves were generated for each of the different film thicknesses. The shift in the resonance angle relative to that for the silver layer was then plotted as a function of the total film thickness (calculated by assuming a dye monolayer thickness of 2.2 nm, as used in section 6.2) for the two sets of theoretical data and for the experimental results (see figure 6.17).

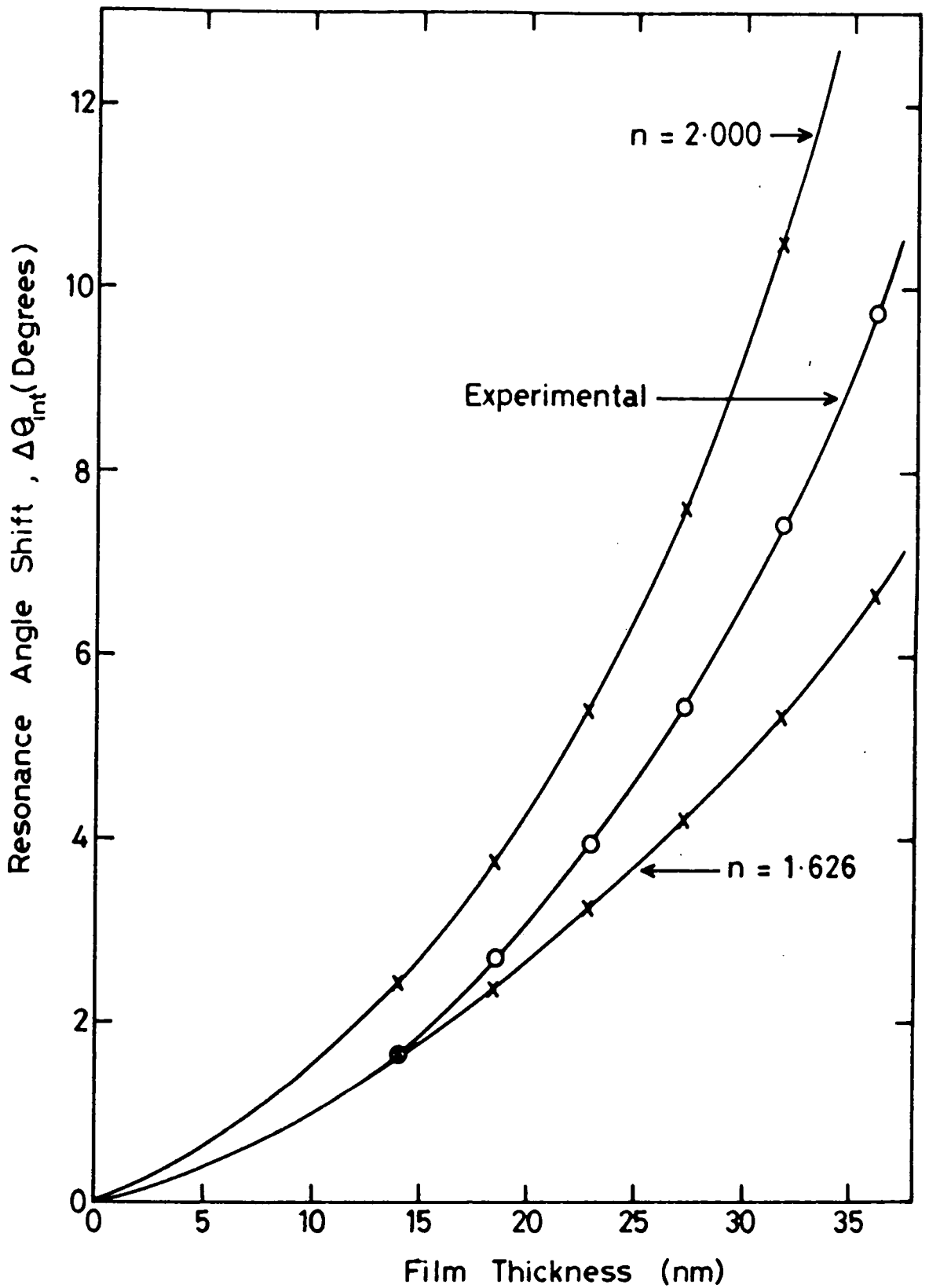


Figure 6.17

Surface plasmon resonance shifts as a function of film thickness for the experimental results described in section 6.3.1 and for theoretical data obtained by assuming values of the refractive index.

These three curves are clearly diverging, and since the experimental results lie between the two theoretical curves this would imply that the refractive index of the dye layers is intermediate between 1.626 and 2.000, as expected. Thus $n(D5) = 1.8 \pm 0.1$ at a wavelength of 632.8 nm, giving a corresponding value for $\epsilon_r(D5)$ of 3.2 ± 0.4 , which is not inconsistent with the value obtained in section 6.2 from capacitance measurements at 1 MHz ($\epsilon_r = 2.4 \pm 0.5$).

SPR studies were also performed on the hemicyanine (compound D2)/amidonitrostilbene alternate layer system. The results of this investigation are presented in Chapter 9, in which a Pockels effect electro-optic modulator utilising SPR is described.

6.4 The Kurtz Powder Technique

The Kurtz powder technique was introduced in section 4.6 as a convenient method for screening large numbers of powdered materials for second-order non-linear optical activity without needing to grow large single crystals or optimize LB film deposition conditions. By studying the second harmonic intensity as a function of particle size it is also possible to ascertain whether the non-linearity could be phase matched in a single crystal^(1,13). Although this knowledge is less important for materials which are to be used in LB film form, since the desired effect can be achieved in such structures by making use of waveguide dispersion (see Chapter 3), the particle-size dependence means that great care must be used if the technique is to be applied quantitatively.

The origin of the effect of particle size on SHG intensity is illustrated in figure 6.18. For very small particles, of radius (r) less than the average coherence length ($l_{coh} = \pi c / \{\omega[n(2\omega) - n(\omega)]\}$), no serious phase error can occur and so the total integrated SHG intensity

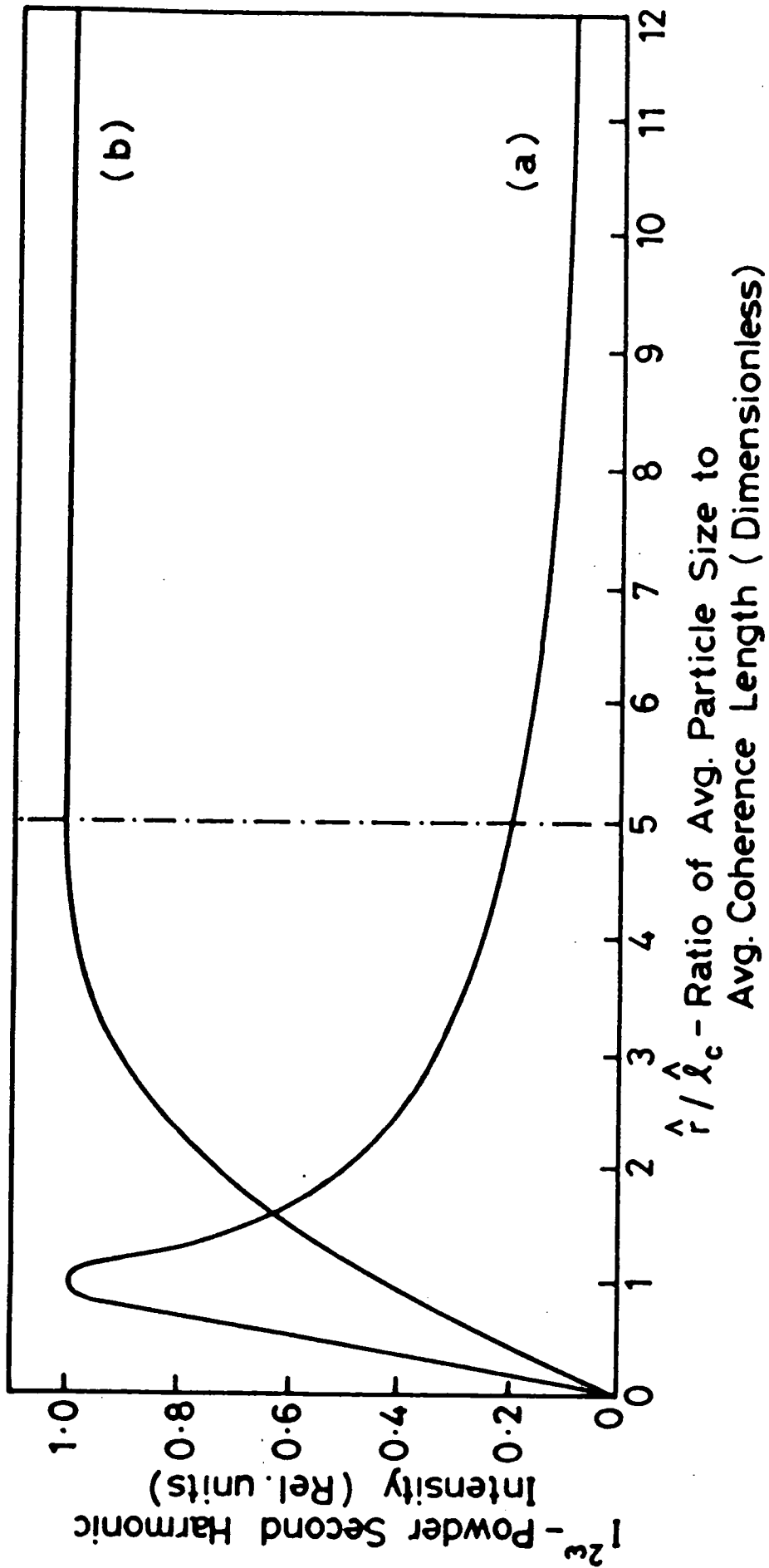


Figure 6.18 Typical results for powders of (a) non-phase-matchable and (b) phase-matchable crystals in the Kurtz powder technique (after reference 13).

increases with r as the result of a trade-off between increasing interaction efficiency and decreasing number of particles. With non-phase-matchable materials, once $r > l_{coh}$ (so that for most or all orientations phase-mismatch effects become apparent), the SHG intensity varies inversely with r because the amount of SHG obtained from each particle does not increase as rapidly as the number of particles decreases. Curve (a) in figure 6.18 therefore exhibits a pronounced maximum. However, for a material which is phase matchable, once the particle size reaches the average coherence length, the gain in SHG from the particles that are correctly oriented approximately balances the loss due to the decrease in the number of particles. Thus the overall SHG intensity remains essentially constant, as illustrated by curve (b) in figure 6.18.

In collaboration with Dr. M. Goodwin of Plessey (Caswell) Ltd., powder efficiencies were measured (relative to lithium niobate) for a selection of the materials which appear elsewhere in this thesis. The results of this survey are presented in table 6.1; in view of the disappointingly small signals obtained, no detailed analysis of SHG as a function of particle size was performed.

It will be seen in Chapter 8 that the low powder efficiencies observed from compound D5 and the two analogues of D2 in this section are in stark contrast to the results of studies of second harmonic generation from LB films. This reflects the fact that dipolar chromophores with long hydrocarbon chains will tend to pack centrosymmetrically in the bulk phase (due to dipolar interactions between the chromophores and inter-chain van der Waal's bonding), thereby giving negligible powder efficiencies, despite the inherently large second-order hyperpolarizabilities of the molecules, which could

TABLE 6.1

Summary of Kerr powder test results (relative to lithium niobate)

Material	SHG observed	$\frac{I_{2\omega} \text{ (sample)}}{I_{2\omega} \text{ (LiNbO}_3\text{)}}$
M2	No	-
A2	No	-
A5	Yes	10^{-2}
A6	Yes	10^{-2}
D2 (C ₁₈ H ₃₇ analogue)	No	-
D2 (C ₆ F ₁₃ C ₂ H ₄ analogue)	Yes	10^{-1}
D5	Yes	10^{-2}

be exploited in LB films. It is therefore concluded that although the Kurtz powder technique has proved invaluable in assessing the potential of new compounds for use as single crystal second-order non-linear media, its application to materials intended for incorporation into LB films is of very limited importance.

6.5 Theoretical Values for β

One way of determining an order of priority for the study of new materials is to calculate theoretical values for the second-order molecular hyperpolarizabilities, β . Since such a procedure does not require a specimen of the compound, it can be used at an early stage to identify materials with low β and thus save the time and expense of chemical synthesis as well as that involved in optimizing and characterizing LB film deposition.

The calculations are rather complex and are only feasible when performed by computer. Since the programs have only recently been sufficiently refined, they were applied to the materials in this project after LB film characterization had been completed; however, it is envisaged that in the future such theoretical modelling of the molecules will play an increasingly important role in the screening of new materials at a much earlier stage. The values of β reported in this section were obtained by J. Hill of British Telecom Research Laboratories.

The calculation of β coefficients was performed in two stages. Firstly the position and strength of the first electronic absorption band was determined, together with the changes in the dipole moment of the molecule which accompanies this transition. These predictions were made by a version of a PPP-SCF-CI molecular orbital calculation program,

which was adapted by Hill for implementation on a Hewlett Packard 9000. In the second stage these data were inserted into a program to calculate the molecular hyperpolarizability of the test molecule. This program was written by Hill utilising equation A3 in reference 14.

Table 6.2 gives the dipole moment, position of the first electronic absorption band (in cyclohexane), and β (vect), calculated for several of the molecules investigated in this project. The column ' β (vect)' is the value of β at a particular frequency vectored onto the ground state dipole moment direction.

The predictions of the absorption band maxima are in reasonable agreement with those obtained experimentally in section 6.1. For example, the theoretical λ_{\max} for the amidonitrostilbene (D5) was 376 nm (cyclohexane solution); the observed values were 368 nm (in chloroform), 351 nm (in cyclohexane), and \sim 370 nm (in LB multilayers). Similarly, for compound D7 theory gave $\lambda_{\max} = 427$ nm (in cyclohexane) and a value of 394 nm was obtained for LB films containing the dye mixed with cadmium arachidate.

It can be seen on examination of table 6.2 that the closer the second harmonic wavelength gets to λ_{\max} , the greater is the value of β (cf. section 2.3.2). As anticipated in the discussions in Chapter 5, the theoretical values of β for compounds D1 and D2 are very high; although the corresponding figures for D5, D7 and D8 are somewhat smaller, they still represent a significant improvement on many of the materials reported in the literature (see table 2.3). The larger β for D7 compared to D5 is in accordance with the stronger donor nature of the tertiary amine group in the former compared to the amide functionality in the latter. Compound A2 has a strong acceptor but only a weak donor; nevertheless, the values of β predicted by the model are much smaller

TABLE 6.2

Theoretical values of dipole moment, position of the first electronic absorption band (cyclohexane solution), and β (vect) for several different molecules

Material	λ_{max} (nm)	Dipole moment (10^{-30} Cm)	β (vect) ($10^{-50} \text{ C}^3 \text{ m}^3 \text{ J}^{-2}$)			
			1.05 μm	1.30 μm	1.55 μm	1.90 μm
A2	391	12	0.3	0.2	0.1	0.1
D1	550	72.4	-	- 416.7	- 224	- 160
D2	554	25	-	- 400.8	- 211	- 149
D3	392	78.7	- 49.0	- 32	- 27	- 23
D4	406	72.1	- 85.7	- 53.4	- 43.4	- 37.5
D5	376	16	66.1	48.6	41.9	37.9
D7	427	34.7	158	88.0	69.4	58.6
D8	416	32	138	81.6	65.3	56.0

than those expected from the qualitative arguments put forward in Chapter 5. This implies that the anthracene nucleus may perhaps be unsuitable for forming the conjugated system, and had this data been available at the outset of the project such derivatives would have been given a lower priority. It is also very interesting to note that the theoretical values of β for D3 and D4 are comparable with those of D5. Since D3 and D4 both contain two acceptor groups and no donor, yet D5 has the classic donor-acceptor system, this was rather surprising. The origin of this effect may well lie in the conjugated system, the stilbene bridge perhaps being less efficient in this role than the phenyl pyridinium ethene functionality.

The theoretical data given in this section will be referred to again in Chapter 8, in which the results of some investigations of second harmonic generation from LB films are reported.

6.6 Summary

The optical absorption spectra of a number of LB film materials with potentially large optical non-linearities have been obtained; such characteristics are important in determining the wavelength ranges over which the films may be usefully applied. Comparisons of the spectra obtained for a given material in solvents of differing polarity have been used to assess the degree of charge transfer in the first excited state relative to the ground state, and the differences between solution and LB film spectra have been interpreted in terms of the effect of dipole-dipole interactions on the level of charge separation in the molecules. Studies of absorbance (at two fixed wavelengths) against time have been used to follow the protonation reaction of a merocyanine dye. Estimates of deposition uniformity have been obtained for several

different LB film materials by measuring absorbance as a function of multilayer thickness and examining the closeness of fit of the results to the Beer-Lambert law.

An alternating layer structure incorporating hemicyanine and amidonitrostilbene dyes was found to have an absorbance peak bathochromically shifted relative to the position expected by the simple addition of the spectra of equivalent numbers of layers of the two materials taken separately in conventional Y-type films. Mixed monolayers of hemicyanine with cadmium arachidate were found to display an enhanced and bathochromically shifted first absorption band relative to that seen for a homogeneous monolayer.

Amidonitrostilbene LB film MIM structures were found to give a linear plot of reciprocal capacitance against film thickness, indicating that the dielectric thickness of each monolayer (measured as 0.90 ± 0.20 nm) was highly reproducible. The intercept of this plot was consistent with seven layers of film being penetrated on fabricating the top electrical contacts; the situation with other dye films was considerably worse, with most of the samples being short-circuited.

Surface plasmon resonance curves were obtained for Y-type LB films of amidonitrostilbene and were used to estimate the relative permittivity of the layers. The similarity of the depth of resonance to that obtained with bare silver, and the sharpness of the minima, provided evidence that the films were not highly absorbing or scattering at the frequency of measurement.

The Kurtz powder technique for assessing second-order optical non-linearity was applied to several of the materials studied elsewhere in this project. However, no activity was observed in any of the compounds. It was concluded that although valuable for screening single

crystal materials, there was little point in using the technique on the compounds used for LB film formation, since they will tend to adopt centrosymmetric crystal structures in the bulk phase, even though their molecules may still possess large β 's which could be exploited in multilayer arrays. A more promising approach for identifying molecules with potentially large optical non-linearities, involving the calculation of theoretical β values, was introduced and results were presented for several of the materials used in this project. It is likely that this technique will find more extensive use in the future, since it can be applied prior to chemical synthesis and thus save a lot of wasted time and effort by identifying materials with small β 's at the earliest possible stage.

CHAPTER 7

ELECTRON DIFFRACTION STUDIES OF LB FILMS : RESULTS

AND DISCUSSION

7.0 Introduction

This chapter is concerned with the structural characterization of LB films of several of the novel materials described elsewhere in this thesis. The structure of the first monolayer is critical in determining the success of deposition and the quality of LB multilayer assemblies⁽¹⁾; particular emphasis has therefore been placed on the study of such thin films. However, despite the fact that relatively thick (0.1-1.0 μ m) LB films can be investigated by a variety of techniques, such as optical birefringence⁽²⁾, shallow angle X-ray diffraction⁽³⁾, and infrared spectroscopy⁽⁴⁾, there are few methods available with sufficient sensitivity for the characterization of monolayers (although high resolution infrared spectroscopy can sometimes be used⁽⁵⁾). One set of techniques which is suitable for probing the structure of such ultra-thin layers utilises the effect of the strong interaction of a beam of high energy electrons with matter. This has lead to the application of electron microscopy⁽⁶⁾, transmission electron diffraction⁽⁵⁾ (TED), and reflection high energy electron diffraction⁽⁵⁾ (RHEED). Although TED allows a complete identification of the molecular packing, it involves complicated and delicate sample preparation (see chapter 4), which could affect the LB film. In contrast, RHEED can be used to study the structure of LB films, in situ, on a semiconductor substrate. The RHEED technique has frequently been applied to multilayer films^(1,7,8), but to date its use with monolayers has been limited.

Figure 7.1 shows an 80kV RHEED pattern obtained from a monolayer of cadmium arachidate deposited on a {111} silicon substrate. It is interesting to note that this pattern possesses all the features exhibited by that of the 11-layer sample of cadmium stearate shown in reference 7 (stearic acid being identical to arachidic acid apart from the slightly shorter hydrocarbon chain). This provides good evidence for the propagation of the structural order of the first monolayer through to subsequently deposited layers. Similar investigations are reported for other materials in later sections, as are the effects of changes in deposition conditions on the crystalline order of amidonitrostilbene (compound D5) LB films and a detailed structural characterization of multilayers of C4 anthracene (compound A1).

7.1 Calibration of Electron Diffraction Patterns

In order to convert measured distances in transmission or reflection electron diffraction patterns into lengths in real space, the patterns must first be calibrated against the diffraction pattern obtained under the same operating conditions (accelerating voltage, lens current, etc.) from a sample whose interplanar spacings are already accurately known. If the distance R from the centre spot of a diffraction pattern represents the length d in real space in the specimen, then for TED:

$$Rd = \lambda L \quad (7.1)$$

and for RHEED:

$$Rd = \frac{\lambda L}{2} \quad (7.2)$$

where λ is the wavelength of the electron beam, and L is the camera length⁽⁹⁾. Clearly, λL and $\lambda L/2$ are constants if the operating conditions remain unchanged, and both these equations can be simplified to give:

$$Rd = K \quad (7.3)$$

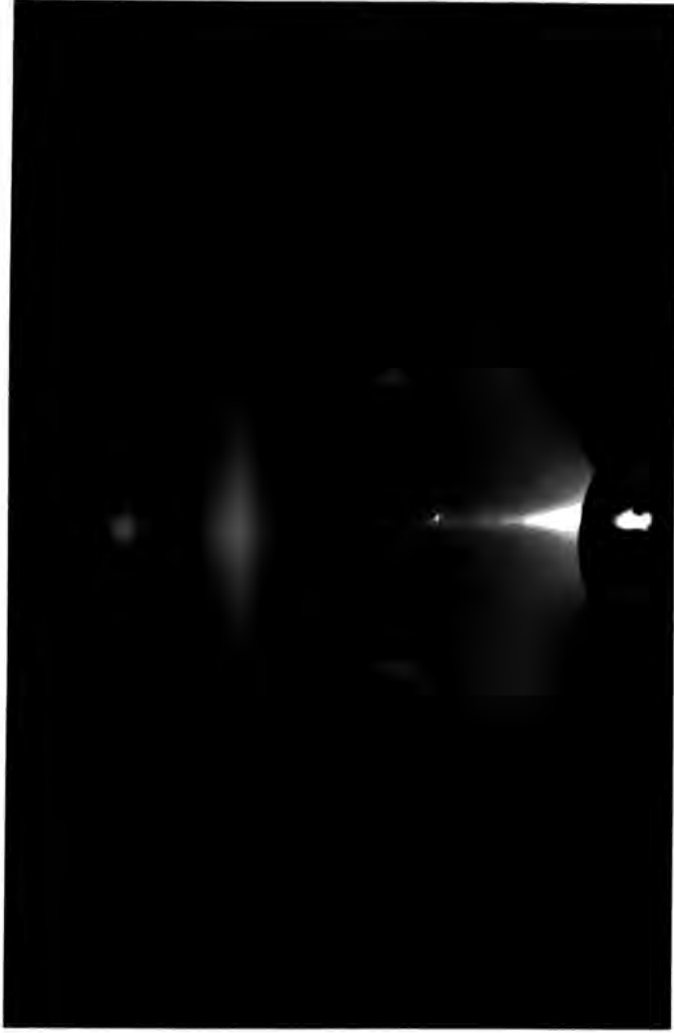


Figure 7.1 80kV RHEED pattern of a cadmium arachidate monolayer deposited on a {111} silicon substrate.

where K is a new constant (which will have twice the value for TED compared to RHEED performed at the same wavelength).

Typical calibration materials used in this study were aluminium foil (TED) and evaporated aluminium on glass (RHEED); both of these specimens gave rise to the characteristic rings of aluminium. Aluminium has a face-centred cubic structure; structure factor considerations therefore dictate that only those planes whose Miller indices (hkl) are all even or all odd will give rise to finite diffracted intensity^(9,10). Now, the interplanar spacing, d, is given by equation 7.4.

$$d = \frac{a_0}{\sqrt{N}} \quad (7.4)$$

where $N = h^2 + k^2 + l^2$, and a_0 is the lattice parameter ($a_0 = 0.40497$ nm for aluminium⁽¹⁰⁾).

Combining equations 7.3 and 7.4 for two different interplanar spacings, d_1 and d_2 , of the reference material, gives:

$$\frac{d_1}{d_2} = \frac{\sqrt{N_2}}{\sqrt{N_1}} = \frac{R_2}{R_1}$$

For aluminium, the smallest allowed value of N is 3, and this will be the ring closest to the centre spot. This ring can therefore be used to assign values of N to all the other rings in the reference diffraction pattern (equation 7.5).

$$N_2 = 3 \left(\frac{R_2}{R(111)} \right)^2 \quad (7.5)$$

The outermost ring was selected, since it could be measured to the greatest precision, and the calculated value of N substituted into equation 7.4 to give the value of d . This was then inserted, along with the quantity R obtained directly from the diffraction pattern, into equation 7.3, enabling K to be determined. It is then a simple matter to use this value of K to convert measured values of R for a test sample into interplanar spacings.

7.2 C4 Anthracene (compound A1)

7.2.1 Background

The range of LB film materials available which do not require large saturated moieties to render them stable at the air-water interface is not restricted to anthracene derivatives alone; there has been great interest shown recently in LB films of lightly substituted porphyrins and phthalocyanines. However, C4 anthracene (compound A1) is known to retain its as-deposited layer structure, whereas structural studies of thick films of porphyrins have revealed that recrystallization takes place rapidly after deposition of these materials, leaving little trace of the required organized anisotropic layer structure⁽¹¹⁾.

Although a study of some aspects of the LB film structure of C4 anthracene has already been performed by Vincett and Barlow⁽³⁾, the techniques which they employed (optical absorption and X-ray diffraction) were not capable of determining the molecular orientation within the film to a high degree of precision or of distinguishing between different possible space groups. In the model proposed by Vincett and Barlow, the unit cell contained two molecules located in adjacent monolayers and the long axis of the anthracene nucleus was tilted at 55-65° to the substrate normal. TED and RHEED can be employed

to provide further information about the film structure; they enable the crystalline symmetry to be determined, and can be used to establish the orientation of the rigid moieties with respect to the crystalline axes⁽¹²⁾ (see Appendix 1). In this section, RHEED and TED patterns of C4 anthracene LB films are presented and the unit cell parameters, including the number of molecules it contains, are deduced.

7.2.2 Results

Figure 7.2(a) shows the 100 kV TED pattern recorded from a 25-layer LB film of C4 anthracene on a thin alumina substrate, prepared as described in section 4.5. This displays well-defined spots which, in view of their rectangular in-plane symmetry, may be ascribed to a single crystalline grain. The pattern can be indexed as arising from an orthorhombic structure with the beam incident along the [100] axis, and figure 7.2(b) illustrates how Miller indices can be assigned to the spots accordingly. There appear to be systematic absences along both of the main axes, and the positions of two of these are indicated by open circles labelled "S".

The RHEED pattern of an 11-layer film of C4 anthracene on a silicon substrate is shown in figure 7.3. The diffraction spots on the central normal to the substrate lie on rings of lower intensity. Parallel to this central row of spots and symmetrically displaced to either side of it is a series of diffracted streaks of intensity. Figure 7.3 differs from RHEED patterns of other LB film materials^(5,8) in that the spots are unusually well defined and the central row of spots displays the fine splitting expected from the bilayer periodicity.

7.2.3 Discussion and conclusions

On the assumption that the diffraction streaks seen in the RHEED pattern extend to the shadow edge of the sample, the distance of each



Figure 7.2a 100kV TED pattern of a 25-layer LB film of C4 anthracene deposited on alumina.

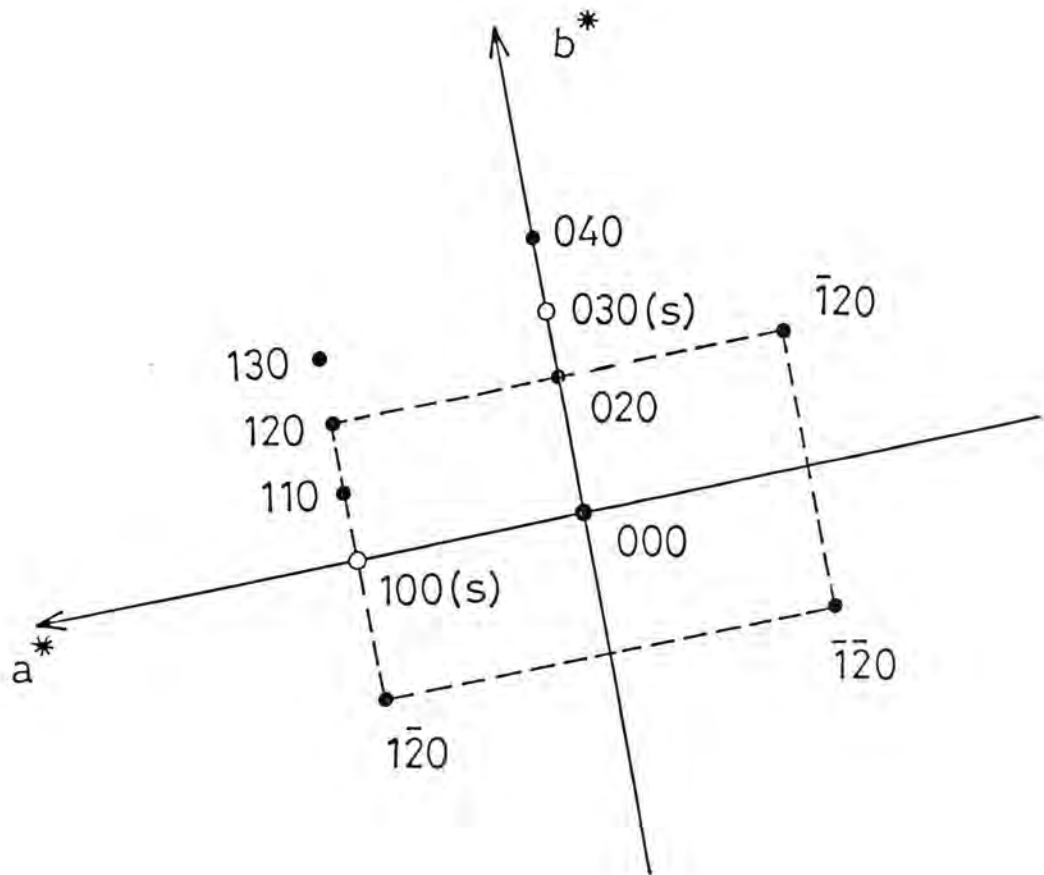


Figure 7.2b Assignment of Miller indices to the TED pattern shown in (a).

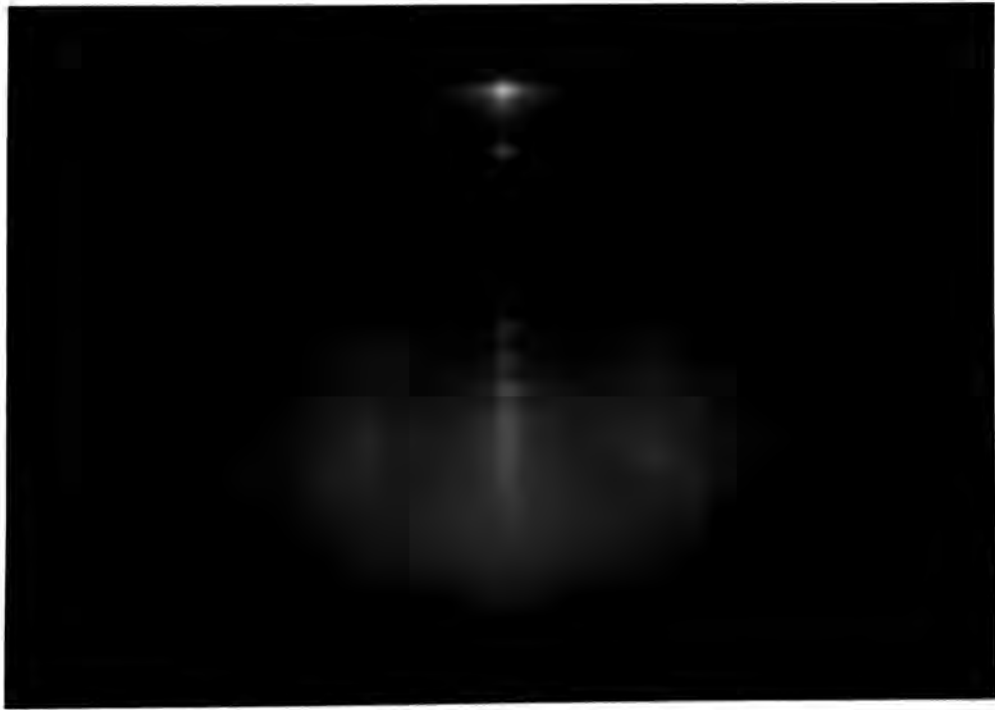


Figure 7.3 80kV RHEED pattern of an 11-layer LB film of C4 anthracene deposited on {100} silicon.

TABLE 7.1

Comparison of TED and RHEED data for (hk0) d-spacings in LB films of C4 anthracene.

Miller Indices	d-spacings (nm) (TED pattern)	d-spacings (nm) (RHEED pattern)
(020)	0.775	-
(100)	0.500 ⁺	0.505
(110)	0.490	0.485
(120)	0.430	0.420
(040)	0.385	0.390
(130)	0.365	0.360
(140)	0.295 [#]	0.295
(200)	0.250 [#]	0.245

+ Systematic absence - inferred value.

Value deduced from extrapolation.

streak from the centre of the pattern should correspond to the radius of one of the spots in the TED pattern. This comparison is given in table 7.1, in which the Miller indices have been assigned on the basis of the rectangular symmetry exhibited by the TED pattern and where the lattice parameters (a,b,c) are such that $a < b < c$. The table includes d-spacings from the TED pattern which have been inferred for a systematic absence or deduced by trigonometry from existing spacings. Inspection of this table confirms the very good agreement between the results obtained using the two different modes of diffraction, and that the film structure is the same on both Al_2O_3 and SiO_2 substrates.

The unit cell lattice parameters a and b can be deduced from the data given in table 7.1, whilst the value of c can be found from the additional d-spacings corresponding to the diffraction spots lying on the central normal in the RHEED pattern (figure 7.3). As a result it was deduced that the unit cell is orthorhombic, with the following lattice parameters:

$$a = 0.51 \text{ nm}$$

$$b = 1.54 \text{ nm} \quad \alpha = \beta = \gamma = 90^\circ$$

$$c = 2.45 \text{ nm}$$

From these figures it can be seen that the area per unit cell in the substrate plane (ab) is 0.79 nm^2 . Comparison with the area per molecule of $0.39\text{--}0.43 \text{ nm}^2$ in the "solid" phase of the water-surface monolayer (chapter 5) indicates that the unit cell contains two molecules in any cross-section and, since it extends over two layers, it consists of a total of four molecules.

In appendix 1 it is shown that a comparison of the RHEED pattern of figure 7.3 with a computer-generated intensity distribution of the diffraction pattern of a single moiety can be used to deduce the tilt angle ψ of the anthracene long axis to the substrate normal. The value obtained, $\psi = 60 \pm 1^\circ$, represents a narrowing of the range (55 - 65°) reported by Vincett and Barlow⁽³⁾, and is shown to be consistent with stereochemical considerations. Furthermore, consideration of such factors as the close packing of molecular crystals, and of symmetry features such as systematic absences in the TED pattern of figure 7.2, are shown to lead to the identification of the space group as Pba 2.

7.3 Amidonitrostilbene (compound D5)

7.3.1 Background

It was reported in chapter 5 that water-surface monolayers of the amidonitrostilbene D5 displayed excellent pressure-area isotherms and could be readily transferred to a variety of different substrates by the LB technique (also see Appendix 2). Since the molecules might also be expected to display a large second-order hyperpolarizability, it was important to know whether they were in an ordered state within the deposited layers. Such a structure is required in order to promote a macroscopic non-linear response which could approach the effect that the molecules would give if optimally aligned.

In this section, an investigation of the ordering within LB films of amidonitrostilbene on different substrates and as a function of film thickness and deposition conditions (including pH, age of the water-surface monolayer, and orientation of the substrate with respect to the moving barriers of the trough) is reported. The main technique

employed was RHEED, due to its convenience (see section 7.0) and the difficulties involved in preparing TED specimens less than 11-layers thick.

7.3.2 Effect of film thickness

RHEED studies were performed on LB films of amidonitrostilbene with thickness varying from one to fifteen monolayers, deposited on silicon substrates. A typical 80 kV RHEED pattern obtained from an LB monolayer of amidonitrostilbene, deposited with the chromophore adjacent to the silicon substrate, is shown in figure 7.4. The high degree of structural order is remarkable for an LB film and significantly better than has been observed for simple fatty-acid assemblies^(5,7,8). It is important to note that the pattern obtained was independent of the direction of the incident electron beam in the plane of the film. The latter observation indicates that the layer is comprised of a mosaic structure of grains in which the long axes of all the chromophores have a common tilt angle away from the substrate normal, but in which the tilt azimuth varies from grain to grain.

The pattern of figure 7.4 contains a rectangular matrix of reflections in which the diffraction spots located along the substrate normal and parallel to the shadow edge of the substrate correspond to interplanar spacings of 1.24 nm and 1.28 nm, and sub-multiples of these, respectively. However, due to systematic absences, it should be noted that the largest d-spacing measured in the direction along the substrate normal is 0.62 nm. The d-spacings for planes lying parallel to the substrate should correspond to some intramolecular periodicity, whereas the spacing for planes perpendicular to it should correspond to intermolecular distances. It seems likely that the monolayer structure will be stabilized by hydrogen bonding between the hydrogens and carbonyl oxygens of amide groups in adjacent molecules.

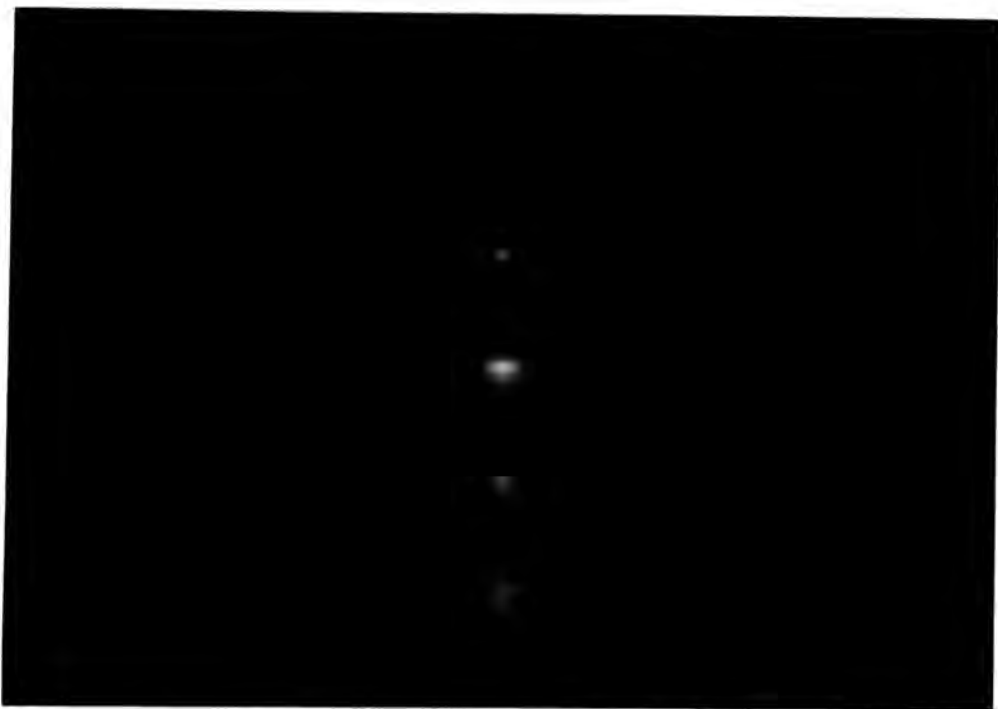


Figure 7.4 80kV RHEED pattern of an amidonitrostilbene monolayer deposited on a {111} silicon substrate.

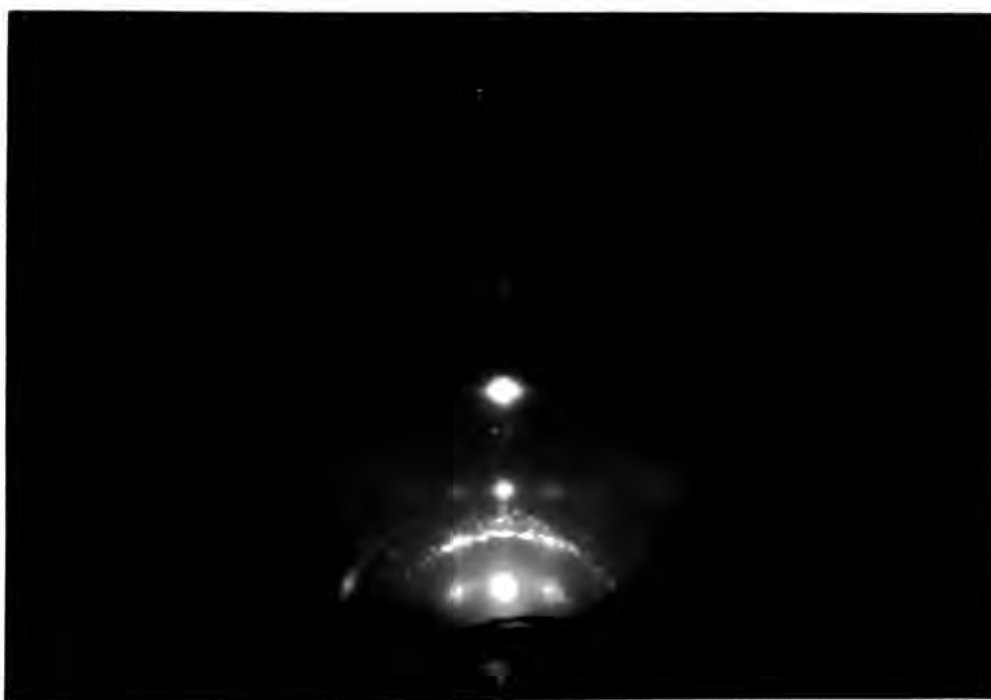


Figure 7.5 100kV RHEED pattern of a 3-layer LB film of amidonitrostilbene deposited on a {111} silicon substrate.

The diffraction pattern in figure 7.4 indicates that the chromophores are extremely well-ordered; however, the reverse is true of the hydrocarbon tails. RHEED patterns from LB films of fatty acids display clear arcs due to the ordering of the hydrocarbon chains⁽⁷⁾ (see figure 7.1); in corresponding positions, diffraction patterns of amidonitrostilbene show at best only faint diffuse rings. This is to be expected when considering the difference in cross-section between the chromophore and the tail; even when the chromophores are close-packed, there is still room for motion of the tails, thereby reducing their order.

From previous work on the epitaxial deposition of LB layers⁽¹⁾, it might be expected that the exceptional degree of order in the first monolayer of amidonitrostilbene would give rise to a very high quality multilayer structure. However, RHEED studies on different numbers of layers were indicative of progressively poorer crystalline order with increasing thickness. Figure 7.5 shows a typical 100kV RHEED pattern obtained from a 3-layer film; although it still displays sharp spots, there is now evidence of arcs passing through a number of them, and some complete rings are also present. When the thickness is taken as high as 12-layers, the RHEED patterns (figure 7.6) consist entirely of spotty rings, with no sharp individual spots at all; this is indicative of a totally polycrystalline structure. When the relatively poor order of the hydrocarbon tails in the amidonitrostilbene monolayer is considered, it is perhaps not surprising that in multilayer structures this disorder extends to the chromophore itself.

7.3.3 Effect of different substrates

Identical RHEED patterns were recorded from monolayers of amidonitrostilbene deposited on {111} or {100} silicon. This is not

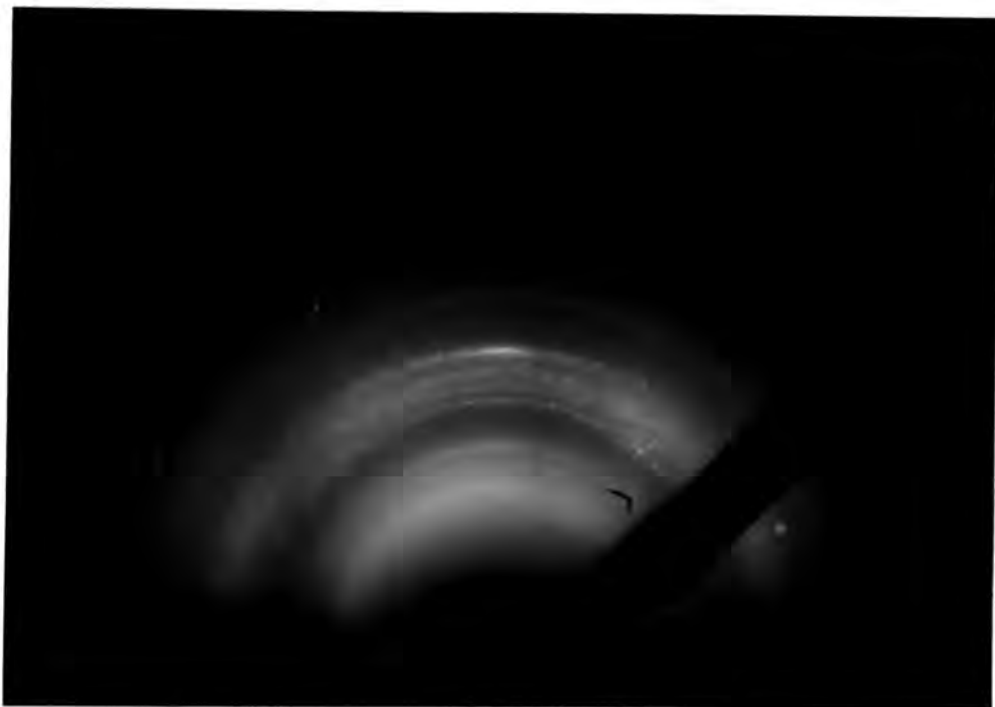


Figure 7.6 100kV RHEED pattern of a 12-layer LB film of amidonitrostilbene deposited on a {100} silicon substrate.

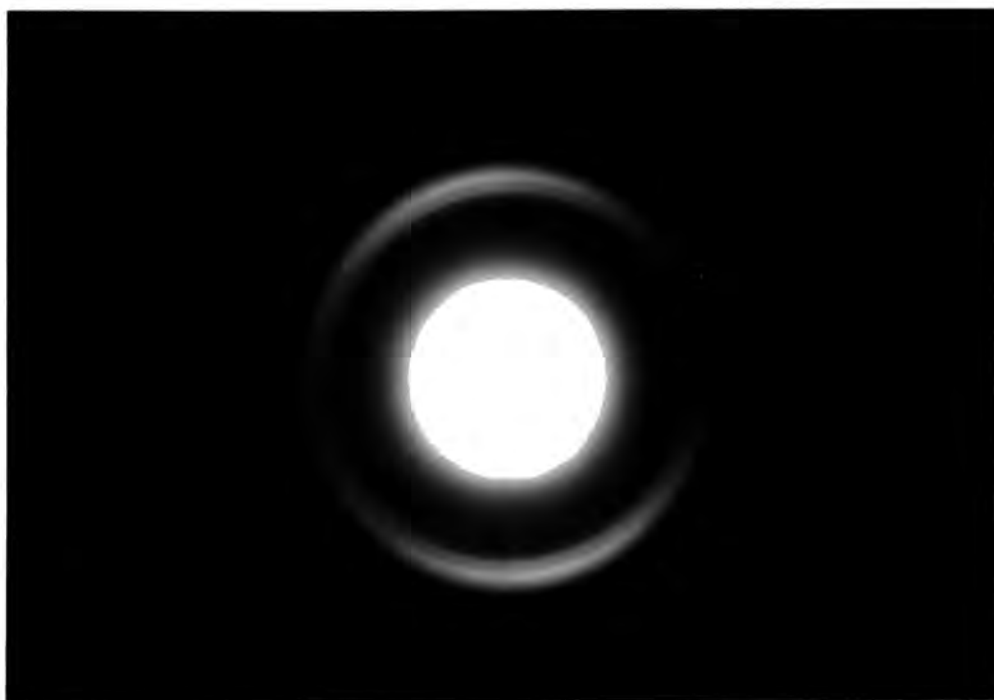


Figure 7.7 80kV TED pattern of an 11-layer LB film of amidonitrostilbene deposited on alumina.

surprising when the technique used for substrate preparation is considered; the silicon was not etched, it was merely degreased - thus, in both cases, the LB films will have been deposited on a native layer of oxide.

The second type of material used as a substrate was alumina; this was selected because of its suitability for forming TED specimens (chapter 4). An 80kV TED pattern of an 11-layer film is shown in figure 7.7. The only important feature in this pattern is the close doublet of rings, corresponding to interplanar spacings of 0.446 nm and 0.420 nm; longer exposure of the photographic plate to the diffracted electron beams resulted in patterns displaying a number of additional rings of smaller d-values, but these could be ascribed to mercurous chloride deposits resulting from the sample preparation technique⁽¹²⁾. The absence of spots in figure 7.7 implies that the structure is polycrystalline with a characteristic grain size of much less than the ~ 200µm diameter of the electron beam. The d-values measured from figure 7.7 do not correlate very well with sub-multiples of the 1.28 nm spacing (measured parallel to the shadow edge of the silicon substrate) in the RHEED patterns of monolayers of amidonitrostilbene. This could be due to the change in crystalline order with film thickness (as observed in section 7.3.2) or to a difference in structure arising from the new substrate material. In order to differentiate between these two possibilities, a RHEED investigation was made of an 11-layer film deposited on an alumina substrate (see figure 7.8). This pattern displays broad rings with significant arcing, and is largely indicative of a lower degree of order than that observed for a comparable film on a silicon substrate (figure 7.6), although some of the difference could be due to the Al₂O₃ substrate charging up under the influence of the

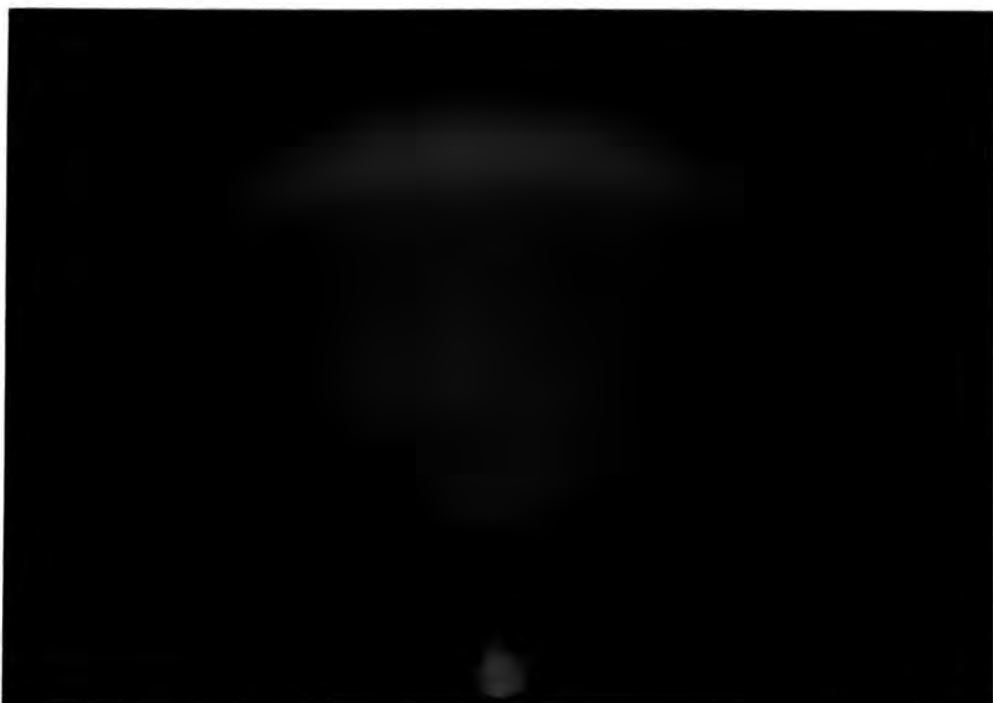


Figure 7.8 80kV RHEED pattern of an 11-layer LB film of amidonitrostilbene deposited on an alumina substrate.

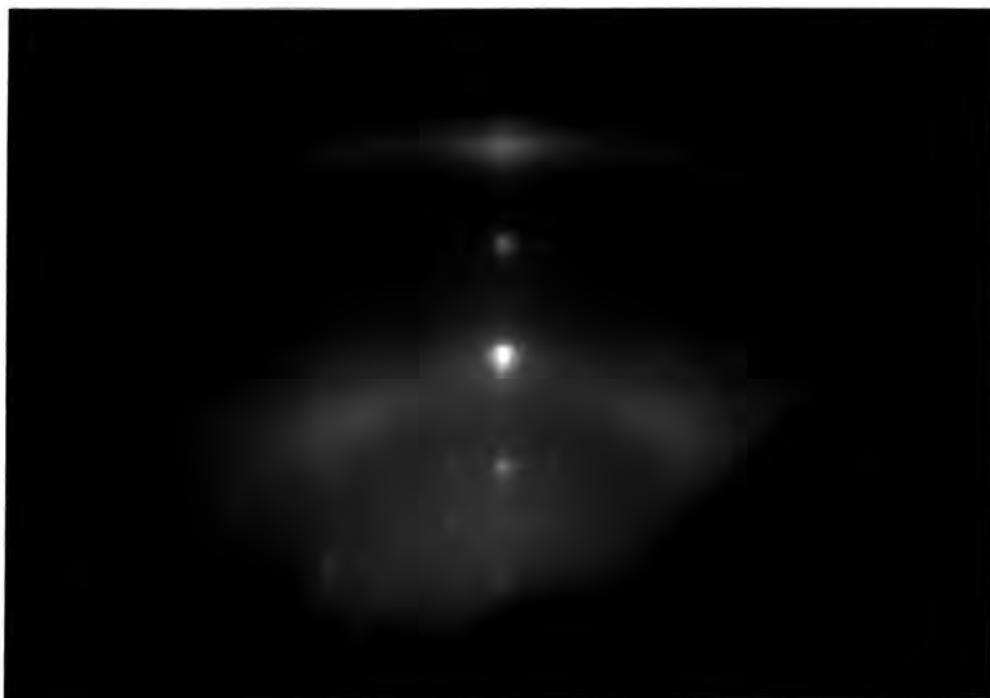


Figure 7.9 80kV RHEED pattern of a monolayer of amidonitrostilbene deposited onto a {111} silicon substrate from an aged Langmuir film on a water subphase at pH=9.0.

electron beam. The study by TED of a monolayer deposited on an alumina substrate would have been the ideal way to distinguish between charging effects and changes in structure as a result of using a different substrate material; however, the preparation of a specimen for such a study could not be accomplished successfully.

7.3.4 Effect of deposition conditions

An extensive RHEED investigation has been performed into the effects of various changes in the deposition conditions on the order displayed by monolayer and multilayer films of amidonitrostilbene assembled on silicon substrates. In addition to film thickness, the following three parameters were varied:

- (i) Subphase pH. The values employed were ~ 5.5 and ~ 9.0 ; these were the optimum values (determined in Chapter 5) for Y-type multilayers of D5 and for alternating layers of D5 with D2, respectively. This part of the study was to check that the layers of amidonitrostilbene within any alternate layer system would still be highly ordered when deposited at the higher pH required for D2.
- (ii) Age of the water-surface monolayer. In chapter 5, monolayers of amidonitrostilbene were observed to become more rigid the longer the period of time that they remained compressed on the surface of the subphase. It was postulated that this rigidity might be responsible for the poor order displayed by multilayer films, since the last few layers would be deposited from a monolayer which had been compressed for over an hour. In order to test this theory, a monolayer was deposited from an aged Langmuir film (A), i.e. one which had been compressed for a very long period of time, and a multilayer film was

assembled from a fresh water-surface monolayer (F), i.e. one which was renewed every dipping cycle (\sim 15 minutes).

(iii) Orientation of substrate with respect to the trough barriers.

The importance of this parameter arises from the flow patterns of material within the water-surface monolayer during the deposition process⁽¹³⁾. Three different orientations were employed: perpendicular to the moving barriers (P); facing the shorter moving barrier (S); and facing the longer moving barrier (L).

The RHEED patterns given by a monolayer and a 9-layer LB film deposited from aged water-surface monolayers are shown in figures 7.9 and 7.10, respectively. The former displays the rectangular matrix of spots seen with a fresh monolayer and associated with excellent crystalline order, but in addition there are some strong arcs, indicating a small degree of imperfection. In figure 7.10 the matrix of spots has been replaced by a single central column of spots, and the arcs have extended to become rings; this implies a much greater level of disorder, although it is still superior to that seen in figure 7.6 for a 12-layer film. The patterns obtained from all of the samples in this study closely resembled one of those shown in figures 7.4, 7.5, 7.6, 7.9 or 7.10, and this match is given in table 7.2, which provides a complete summary of the survey.

Comparison of sample numbers 1, 5 and 6 in table 7.2 reveals that the orientation of the substrate with respect to the trough barriers has had little effect on the crystalline order of an amidonitrostilbene monolayer deposited from the fresh regime. However, the slightly better order for 9 and 15 layer films (Nos. 10 and 12) compared to a 12 layer

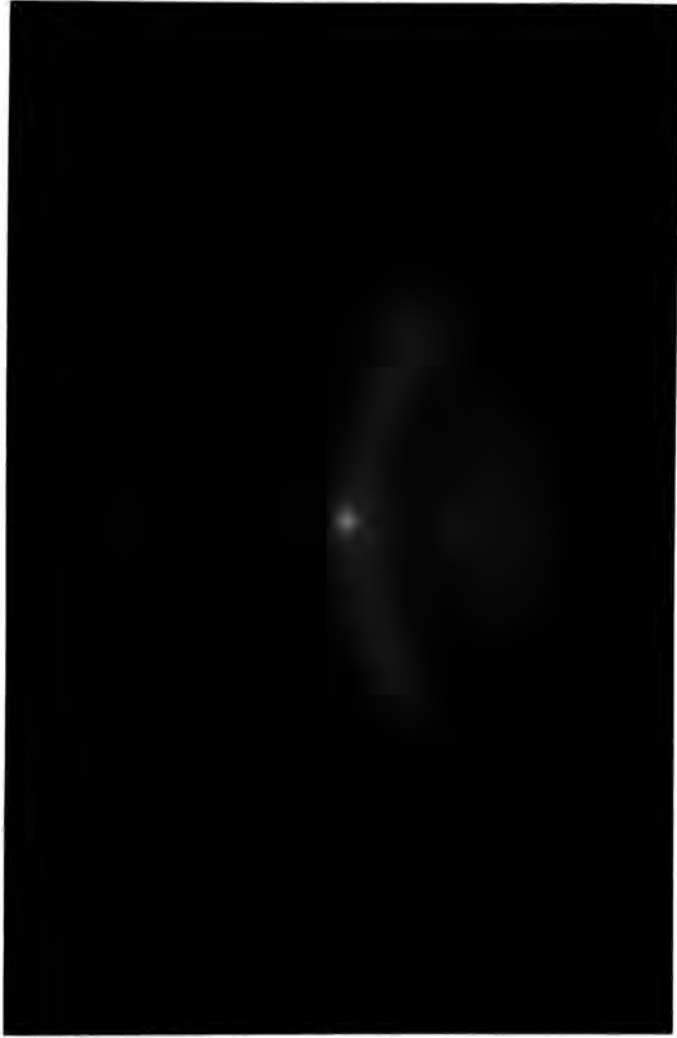


Figure 7.10 80kV RHEED pattern of a 9-layer LB film of amidonitrostilbene deposited onto a {111} silicon substrate from an aged Langmuir film on a water subphase at pH=5.6.

TABLE 7.2 Summary of the effect of deposition conditions on the order displayed by LB films of amidonitrostilbene (see text for definition of symbols)

No. of layers	Subphase pH	Age of water-surface monolayer	Orientation of substrate wrt barriers	RHEED pattern giving closest match	Comments	Ref. No.
1	5.5	F	L	7.4	Rectangular matrix of sharp spots.	1
1	9.2-	F	P	7.9	Rectangular matrix of spots; some strong arcs. Some patches visible when sample breathed on.	2
1	5.6	A	P	7.9	Rectangular matrix of spots; some strong arcs. Visible regions of collapsed film on sample.	3
1	9.0	A	P	7.9	Rectangular matrix of spots; some strong arcs.	4
1	5.5	F	P	7.4	Rectangular matrix of sharp spots.	5
1	5.5	F	S	7.4	Rectangular matrix of sharp spots.	6
9	5.6	F	P	7.10	Central column of spots; arced rings. Film looked highly uniform.	7
9	5.6	A	P	7.10	Central column of spots; arced rings. Visible regions of collapsed film on sample.	8
3	5.5	F	L	7.5	Matrix of sharp spots, some arced; a few rings.	9
9	5.5	F + A	L	7.10	Central column of spots; arced rings.	10
12	5.4	F + A	S	7.6	Spotty rings; no sharp spots. Film looked slightly streaky.	11
15	5.5	F + A	L	7.10	Central column of spots; arced rings.	12

film (No. 11), all deposited from an initially fresh Langmuir film which was not renewed (and will therefore have been ~ 100 minutes old by the end of the last layer), might imply that this factor becomes more significant in older, less mobile, films. Further experiments involving 9-15 layer films deposited under similar conditions, but with the substrate perpendicular to the barriers, are clearly required. Examination of the results for samples 2 and 5 indicates that although highly ordered monolayers can be obtained at the higher subphase pH, the optimum value of ~ 5.5 gives slightly better results. The superior order observed with sample 5 relative to 3 shows the importance of having a mobile water-surface monolayer in the transfer of even a single monolayer to a substrate; similarly, when thicker structures are built up (Nos. 7 and 8), the use of non-rigid monolayers promotes the deposition of a more uniform film (see "comments" column in table 7.2), even if this effect is not observed in the RHEED pattern, due to other disruptive influences within the multilayers.

7.3.5 Chromophore orientation in monolayers

Earls et al⁽¹²⁾ have deduced the orientation of the chromophores in LB films of hemicyanine by the comparison of an experimentally determined RHEED pattern with a computer-generated intensity distribution of the diffraction pattern of a single moiety. A similar approach has been used with C4 anthracene (see appendix 1), and in this section it is applied to amidonitrostilbene.

Reasonable values for bond lengths, angles and atomic scattering factors for the chromophore, and also for the hydrocarbon tail, were chosen and used by Dr. I. R. Peterson (GEC Research) to compute the intensity distributions shown in figures 7.11a and b. Note that

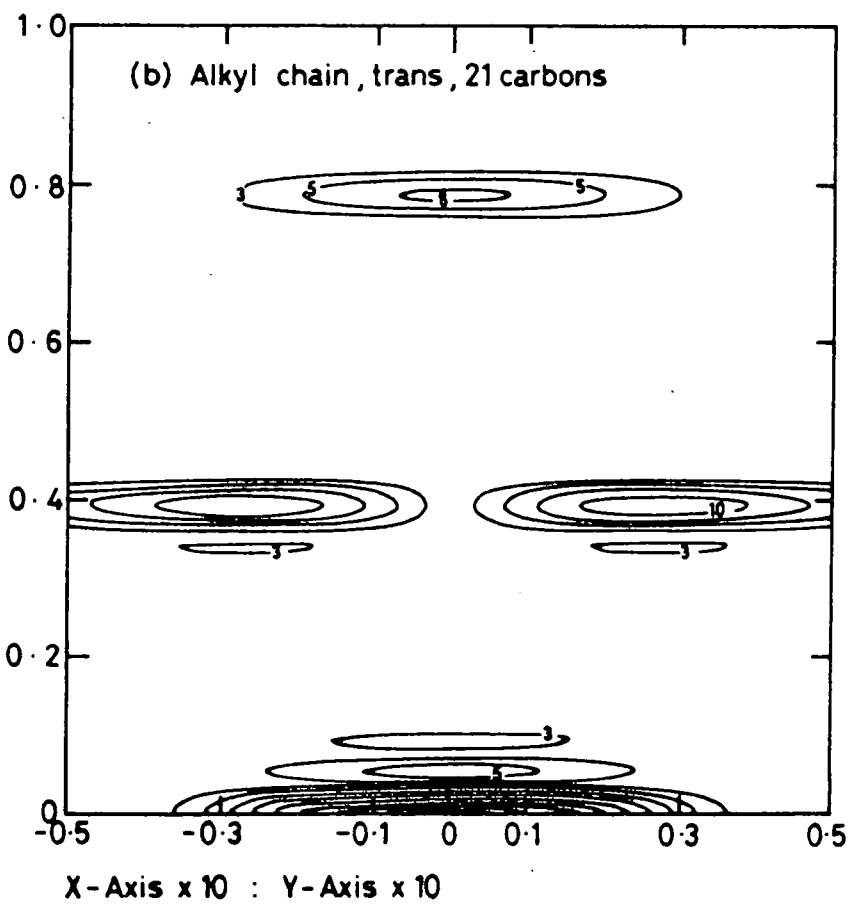
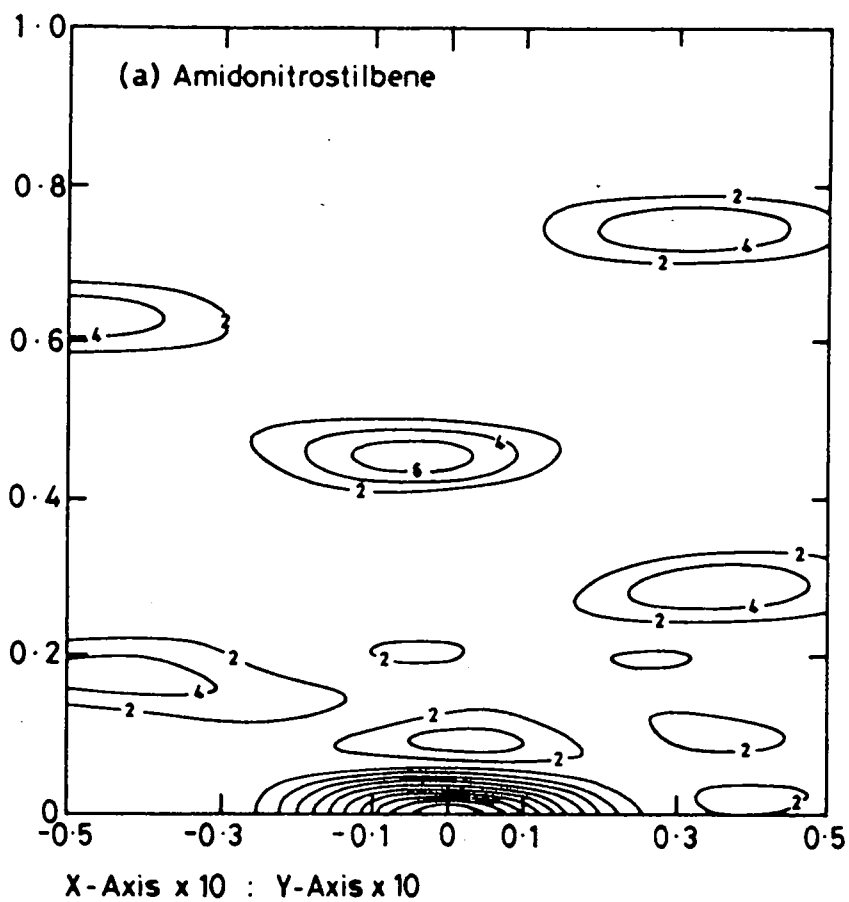


Figure 7.11

Computer-generated diffracted intensity distributions for the beam incident normal to : (a) the amidonitrostilbene nucleus; (b) the hydrocarbon tail, with their long axes vertical.

although figure 7.11b is really for a chain containing 21 carbons, the distribution given by a 17 carbon tail should be very similar. The RHEED pattern obtained from a monolayer of amidonitrostilbene (figure 7.4) was replotted to the same scale as figure 7.11 to facilitate comparison. There is only one good match between the experimental pattern and the computed distribution; this is consistent with both the chromophore and the hydrocarbon tail long axes having a tilt angle ψ to the substrate normal of $54 \pm 1^\circ$; such a value is very large compared to other LB arrays.

7.3.6 Conclusions

LB monolayers of amidonitrostilbene exhibit excellent crystallinity, and it is likely that their structure is highly stabilized by hydrogen bonding. Unfortunately, this property is not propagated through to multilayer films, the structural order becoming progressively poorer with increasing thickness. Although monolayer quality was found to be quite acceptable when a subphase pH of ~ 9.0 was employed, slightly better results were obtained at the lower value of ~ 5.5 . The importance of mobility in the water-surface monolayer was reflected by the superior crystalline order and film uniformity displayed by monolayer and multilayer LB films deposited from freshly spread Langmuir films compared to the results given by aged layers. The orientation of the substrate in the trough during deposition was found to be unimportant if the water-surface monolayer is sufficiently fluid.

Alumina substrates were found to be unsuitable for RHEED studies, owing to their tendency to become charged by the electron beam. The difficulties involved in preparing a sample less than ~ 3 layers thick for TED (films of this thickness and less gave rise to RHEED patterns indicative of good structural order) from which a spot pattern could be

expected, has made it impossible to correlate RHEED and TED observations as was done in the structural analysis of C4 anthracene in section 7.2. This, coupled with the invariance of the RHEED pattern of an amidonitrostilbene monolayer to rotation of the substrate about an axis normal to its surface (indicating no preferred orientation of the crystallites), means that although interplanar spacings can be calculated from the RHEED data, in the absence of any independent structural data the spots cannot be indexed or the lattice parameters deduced. An analysis involving the matching of the RHEED patterns to a computer generated intensity distribution of the diffraction pattern of a single moiety gave a value of the tilt angle, ψ , of the molecule, with respect to the substrate normal, of $54 \pm 1^\circ$.

7.4 Other Materials

7.4.1 Aminonitrostilbene (compound D6)

A typical 80kV RHEED pattern obtained from an LB monolayer of aminonitrostilbene (compound D6) deposited on a {111} silicon substrate is shown in figure 7.12. Although this pattern is similar to that of the amidonitrostilbene (D5) given in figure 7.4 (indicating the same basic packing arrangement), most of the diffraction spots are of a significantly lower intensity than are the corresponding reflections obtained from monolayers of D5. The essential difference in the molecular structure of D5 and D6 is that the amide group in the former material has been replaced by a simple amine. Thus the possibility of hydrogen bonding between the adjacent chromophores in the monolayer is substantially reduced. It is therefore concluded that such interactions play a dominant role in the in-plane ordering of the molecules in monolayers of D5.



Figure 7.12 80kV RHEED pattern of a monolayer of aminonitrostilbene (D6) deposited onto a {111} silicon substrate.

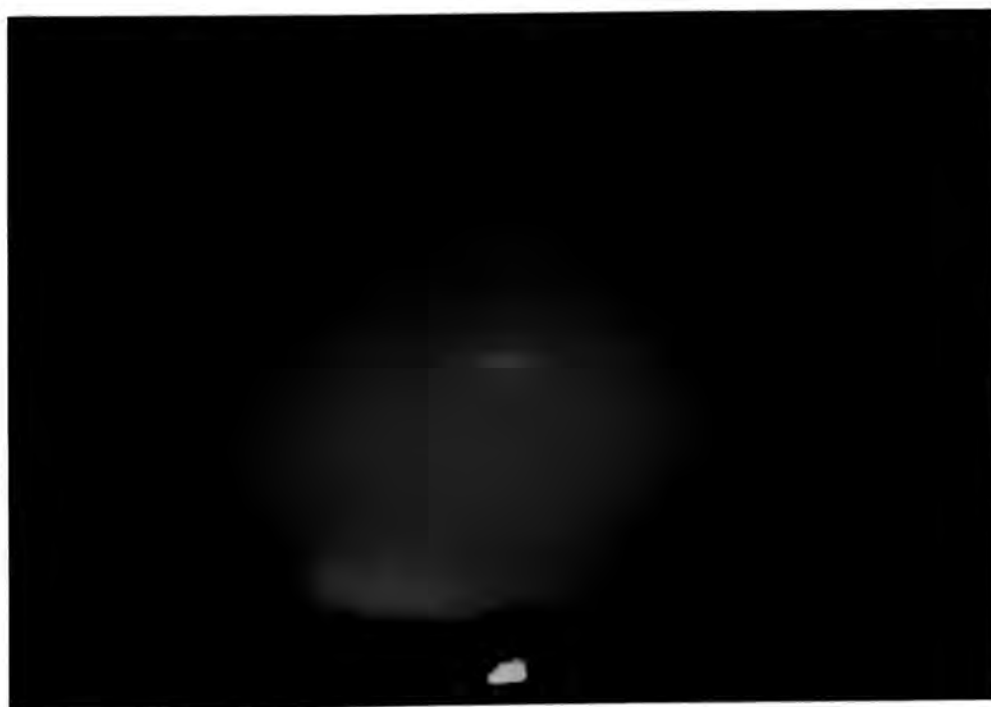


Figure 7.13 80kV RHEED pattern of a monolayer of hemicyanine (D2) deposited onto a {111} silicon substrate.

RHEED patterns from monolayers of D6 display clear arcs (as at A in figure 7.12) corresponding to ordering of the hydrocarbon tails; this is in contrast to the behaviour observed for D5 (section 7.3.2), which showed only very faint diffuse rings in the equivalent positions. This suggests that the removal of the carbonyl group reduces the effective size of the chromophore and enables the closer approach of the tails.

In summary, although the molecules may be slightly closer packed in monolayers of D6, in D5 the order of the chromophore section of the molecule is more regular due to the stabilizing influence of intermolecular hydrogen bonding.

7.4.2 Merocyanine (compound D1)

RHEED investigations were performed on 7 and 11-layer LB films of the merocyanine (compound D1) deposited onto silicon substrates. Films from both the high and low surface pressure dipping regimes detailed in Chapter 5 were studied, before and after performing the deprotonation procedure (immersion in 10^{-3} M NaOH solution) described in Chapter 6. In each case the patterns obtained were identical, displaying only a few very broad, diffuse rings. It was concluded that the merocyanine LB films were completely amorphous.

7.4.3 Hemicyanine (compound D2)

Figure 7.13 shows the 80kV RHEED pattern obtained from a monolayer of the hemicyanine dye (compound D2) deposited onto a {111} silicon substrate. The original pattern observed on the phosphor screen displayed a row of three spots parallel to the substrate shadow edge, and a column of spots perpendicular to it; although not unlike the pattern given by amidonitrostilbene monolayers, fewer spots were present, indicating that the structural order was not quite as good. Unfortunately, the hemicyanine film rapidly became charged in the

electron beam, and the recorded pattern of figure 7.13 is somewhat poorer than seen in the first place.

The RHEED pattern of an 11-layer LB film of hemicyanine exhibited only a single broad arc, implying that the high degree of crystalline order displayed by a monolayer of the material does not extend to thicker films.

Earls et al⁽¹²⁾ have performed a detailed structural investigation of hemicyanine, employing both TED and RHEED techniques. They conclude that in addition to crystalline multilayer regions (in which the chromophore and alkyl tail are essentially parallel to each other and tilted at 40° to the substrate normal), the films appear to contain at least two other phases. In the first of these phases the molecules lie parallel to the substrate, and in the second the alkyl chains are loosely packed and translationally disordered.

7.4.4 The hemicyanine/amidonitrostilbene alternate layer system

Multilayer LB films containing hemicyanine (D2) alternating with amidonitrostilbene (D5) display large optical non-linearities (see Chapter 8) and in this section their structure is investigated by RHEED. In view of the excellent degree of crystalline order exhibited by monolayers of the individual materials and the poorer order observed in Y-type multilayers, it was of interest to see into which category the alternate layers fell.

A typical 80kV RHEED pattern obtained from an alternating layer LB film containing three layers of hemicyanine and two layers of amidonitrostilbene is shown in figure 7.14. The pattern contains a strong and a weak arc on the central axis, and a pair of arcs symmetrically displaced off-axis corresponding to large d-spacing; there is also evidence of a polycrystalline ring close to the centre spot.



Figure 7.14 80kV RHEED pattern of 3 layers of hemicyanine (D2) alternated with 2 layers of amidonitrostilbene (D5) deposited onto a {111} silicon substrate.

This represents about the same level of structural order which would be expected from conventional Y-type films of the same thickness of either material; thus it seems that the two compounds are sufficiently compatible to form high quality supermolecular arrays. The RHEED pattern obtained from two layers of hemicyanine and one of amidonitrostilbene was similar to that obtained from a monolayer of hemicyanine (section 7.4.3), except that the spots were a little more obvious in the case of the alternate layer system. This was to be expected, in view of the exceptional degree of ordering shown by very thin amidonitrostilbene layers.

7.5 Summary

High energy electron diffraction studies (mainly in reflection, but with some transmission data to support them) have been performed on a variety of LB films of materials used elsewhere in this project. C4 anthracene, the molecule on which the whole series of anthracene derivatives was based, was found to form LB films with an orthorhombic unit cell containing four molecules, and the lattice parameters of this cell were determined.

Monolayers of the amidonitrostilbene, D5, were found to exhibit excellent crystallinity; however, in the case of multilayers the structural order was found to become progressively poorer with increasing film thickness. The effects of subphase pH, substrate orientation during the deposition process, and age of the water-surface monolayer on the quality of LB films of D5 were investigated, and the most important factor was found to be the need for a mobile (therefore freshly spread) Langmuir film from which to deposit the layers. It was postulated that the monolayer structure of D5 is significantly stabilized by hydrogen bonding, in view of the rather poorer order shown

by monolayers of D6, a material which has essentially the same molecular structure as D5, only with the amide functionality replaced by an amine group. The molecules in monolayers of D5 were found to have an average tilt angle of $54 \pm 1^\circ$ with respect to the substrate normal.

LB films of the merocyanine, D1, were found to be amorphous, whilst hemicyanine (D2) monolayers displayed significantly better order, although not as good as D5. Finally, the hemicyanine/amidonitrostilbene alternate layer system was investigated and the structure found to be well-ordered.

Studies of second harmonic generation from several monolayer and multilayer systems, including the ones described in sections 7.3 and 7.4, are presented in the next Chapter.

CHAPTER 8

SECOND HARMONIC GENERATION FROM LB FILMS : RESULTS

AND DISCUSSION

8.0 Introduction

This chapter is concerned with the observation of second harmonic generation (SHG) from Langmuir-Blodgett monomolecular and multilayer arrays. Following an explanation of how absolute values for the electric fields at 2ω were obtained, the discussion is split into sections according to the type of LB film under investigation. Sections 8.2 and 8.5 deal with SHG from homogeneous and heterogeneous monolayers, respectively. In section 8.3 multilayers are studied in which the active layers are alternated with an inert spacer material in order to produce the desired noncentrosymmetric structure. Similarly, section 8.4 describes the use of two different active materials, giving rise to a supermolecular array in which the non-linearities of the individual layers should be additive.

With all the samples studied in this work, regions of the substrates free of film gave no detectable signal, confirming that any radiation observed during the subsequent investigations was a property of the organic layer. In addition, the radiation was clearly identified as second harmonic by its narrow bandwidth (using interference filters at 520 nm and 540 nm) and its narrow temporal profile. The second harmonic signals, being quadratic in incident laser energy, were normalised by dividing by the square of the incident laser energy; this process is described in greater detail in the next section.

8.1 Calibration of Experimental System

The experimental system used in these investigations was described in section 4.7. Three different techniques were employed in order to obtain absolute values of the electric field at 532 nm ($E_{2\omega}$), although all of them involved calibrating the system against a y-cut quartz wedge and relating both the second harmonic signals and incident energy to the d_{11} non-linear coefficient of quartz. These methods are described separately in sections 8.1.1 - 8.1.3.

The calibration procedure consisted of translating a 2° wedge of y-cut quartz in a direction perpendicular to the laser beam and determining the positions of the minima of second harmonic signal in the resultant pattern of Maker fringes. These results were used to estimate (to a greater degree of accuracy than was possible by direct observation) the wedge positions for maximum signal intensity. A series of readings of incident energy and second harmonic signal (and peak incident power, in the case of the experimental configuration shown in figure 4.3) were then taken for each of four maxima, and the results averaged. The manner in which these calibration figures were used was dependent on the method of normalisation to be employed.

8.1.1 Signals normalised with respect to photodiode response

With the experimental system arranged as shown in figure 4.3, there were two methods available for normalising the second harmonic signals obtained from the test samples and the quartz calibration specimen; either with respect to the peak power measured by the photodiode (as described in this section), or with respect to the total pulse energy recorded by the transmission type energy meter (as detailed in section 8.1.2). The methods have many common elements, and give very similar results.

In order to be able to interpret the calibration data, the power of the incident light, I_ω , must first be calculated. Assuming the incident beam has a Gaussian temporal profile with a peak power I_0 , then $I_\omega = I_0 \exp(-t^2/\sigma^2)$, where σ is a constant. If the incident power is at half its peak value at time τ , then

$$\sigma = \tau (-\ln 0.5)^{-1/2} \quad (8.1)$$

and hence σ can be calculated from the value of 2τ , the measured full width at half maximum (FWHM). The total energy of the pulse, E , is given by

$$E = \int_{-\infty}^{+\infty} I_\omega dt = \sigma I_0 \sqrt{\pi}$$

However, the true energy reaching the sample was really $E'F$, where E' is the recorded incident energy but where a filter transmitting a fraction F of the light is located between the energy meter and the sample. The peak incident power is then given by:

$$I_0 = E'F/\sigma\sqrt{\pi} \quad (8.2)$$

The periodic oscillations in second harmonic power as a function of thickness (referred to earlier as "Maker fringes") arise from dispersion in the quartz. If the wavevector mismatch between the bound and free harmonic waves in the crystal is Δk (where $\Delta k = 2k_\omega - k_{2\omega}$), then the period of these oscillations is $l_{\text{coh}} = \pi/\Delta k$. The quantity l_{coh} is known

as the "coherence length" and for normal incidence it is given by⁽¹⁾:

$$l_{\text{coh}} = \lambda_1 / 4 (n_{2\omega} - n_\omega) \quad (8.3)$$

where λ_1 is the free-space wavelength of the fundamental wave (1.064 μm for the laser used in this investigation). Since, in an anisotropic medium, n_ω and $n_{2\omega}$ depend upon the electric polarization direction of the fundamental and second harmonic waves respectively, it follows from equation 8.3 that each non-linear optical coefficient has a coherence length associated with it. For p-polarized incident and signal radiation with a y-cut quartz wedge the pertinent quantities are⁽¹⁾: $d_{11} = (0.364 \pm 0.040) \times 10^{-12} \text{ mV}^{-1}$; $n_\omega = 1.5341$; $n_{2\omega} = 1.5468$.

Rewriting equation 8.3 in terms of the wavevector mismatch:

$$\Delta k = 4\pi (n_{2\omega} - n_\omega) / \lambda_1 \quad (8.4)$$

The theoretical second harmonic power, $I_{2\omega}$, generated by a single mode Gaussian beam of angular frequency ω , incident along a principal axis of a plane parallel slab of thickness L of a nonabsorbing non-linear crystal is given by⁽¹⁾:

$$I_{2\omega} = \frac{2 (\mu_0)^{3/2} (\epsilon_0)^{1/2} \omega^2 d_{11}^2 (I_\omega)^2 L^2}{\pi W_0^2 n_{2\omega} (n_\omega)^2} \left[\frac{\sin (L\Delta k/2)}{(L\Delta k/2)} \right]^2 \quad (8.5)$$

where W_0 is the spot radius of the fundamental beam ($2W_0 = 207 \mu\text{m}$ in these investigations), d_{11} is the relevant SHG coefficient, and μ_0, ϵ_0 are the permeability and permittivity of free space, respectively.

At the maxima in the Maker fringe pattern, $\sin(L\Delta k/2)=1$, and with the experimental conditions employed, equation 8.5 reduces to:

$$I_{2\omega} = \frac{8 (\mu_o)^{3/2} (\epsilon_o)^{1/2} \omega^2 d_{11}^2 (I_o)^2}{\pi W_o^2 n_{2\omega} (n_\omega)^2 (\Delta k)^2} \quad (8.6)$$

Substituting the appropriate values of I_o and Δk (obtained from equations 8.2 and 8.4) into equation 8.6 gives the peak second harmonic power emerging from the wedge. If this signal gives rise to a voltage V_s (quartz) from the photomultiplier detector, and the relationship between the detector voltage and signal power is

$$I_{2\omega} = a V_s \quad (8.7)$$

then the value of the constant, a , can be calculated using

$$a = I_{2\omega} \text{ (quartz)} / V_s \text{ (quartz)} \quad (8.8)$$

Corresponding relationships hold for the incident power and photodiode detector voltage (V_L):

$$I_\omega = b V_L \quad (8.9)$$

where the value of b is given by

$$b = I_o \text{ (quartz)} / V_L \text{ (quartz)} \quad (8.10)$$

V_L (quartz) is the measured value of V_L corresponding to the value of I_o (quartz) calculated from equation 8.2.

Having established the relationships between the detector voltages and the incident and signal powers, the voltages (or powers) measured in the investigation of LB film structures must be converted into the electric field ratios of the fundamental and second harmonic. The second harmonic signals, being quadratic in incident laser energy, have to be normalised by dividing by the square of incident power (or energy). If E_ω and $E_{2\omega}$ are the incident and signal field strengths, respectively, then the desired normalised signal, S , is

$$S = |E_{2\omega}|^2 / |E_\omega|^4 \quad (8.11)$$

In later sections this notation is modified to take into account the polarizations of the beams (s or p) and the detection geometry (reflection, R, or transmission, T). Thus $T^{s \rightarrow p} = |E_{2\omega}^p|^2 / |E_\omega^s|^4$ represents p-polarised signal intensity from s-polarised incident radiation in the transmission geometry; a corresponding notation is used for the other polarisations and geometry.

In general, the power (I) of a beam of radiation can be written in terms of its average Poynting vector (N) and the area of the beam (A):

$$I = A N \quad (8.12)$$

where N is given by⁽²⁾

$$N = n |E|^2 (2 \mu_0 c)^{-1}$$

Hence

$$I = n A |E|^2 (2 \mu_o c)^{-1} \quad (8.13)$$

Applying equation 8.13 to the fundamental and second harmonic waves gives:

$$\frac{I_{2\omega}}{(I_\omega)^2} = 2 \mu_o c \cdot \frac{n_{2\omega}}{(n_\omega)^2} \cdot \frac{A_{2\omega}}{(A_\omega)^2} \cdot \frac{|E_{2\omega}|^2}{|E_\omega|^4} \quad (8.14)$$

If the beams have a Gaussian spatial profile of the form $N(r) = N_o \exp(-r^2/\rho^2)$ then

$$I = \int_0^\rho N(r) \cdot d^2r = N_o \pi \rho^2 \quad (8.15)$$

and comparison of equations 8.12 and 8.15 yields:

$$A_\omega = \pi \rho^2 \quad (8.16)$$

For the fundamental beam, $\rho_\omega = W_o/\sqrt{2}$ and therefore

$$A_\omega = \pi W_o^2/2 \quad (8.17)$$

The second harmonic has a narrower spatial (and temporal) profile than the fundamental, and $\rho_{2\omega} = \rho_\omega/\sqrt{2}$. Hence:

$$A_{2\omega} = \pi W_o^2/4 \quad (8.18)$$

Assuming that $n_{2\omega} \sim n_{\omega} \sim 1$ for radiation in air, substitution of 8.17 and 8.18 into equation 8.14 gives:

$$S = \frac{|E_{2\omega}|^2}{|E_{\omega}|^4} = \frac{\pi W_o^2}{2 \mu_o c} \cdot \frac{I_{2\omega}}{(I_{\omega})^2} \quad (8.19)$$

Further substitution from equations 8.7 and 8.9 leads to an expression involving the experimentally determined quantities:

$$S = \frac{|E_{2\omega}|^2}{|E_{\omega}|^4} = \frac{\pi W_o^2 a}{2 \mu_o c b^2} \cdot \frac{V_s}{V_L^2} \quad (8.20)$$

Equation 8.20 enables absolute values of the electric field of the second harmonic to be calculated from a value of the signal voltage from the photomultiplier (normalised by the square of the output voltage from the photodiode monitoring the incident beam) obtained by averaging over several pulses and different areas of the sample.

8.1.2 Signals normalised with respect to total incident energy

It is possible to obtain absolute values of $E_{2\omega}$ by using an experimental arrangement without a photodiode to monitor the peak energy of each pulse, but otherwise identical to the one shown in figure 4.3. In this case the measured signal voltages have to be normalised with respect to the total energy of each pulse.

Taking equation (8.19) and substituting for $I_{2\omega}$ from 8.7 and for I_{ω} from 8.2 gives:

$$S = \frac{|E_{2\omega}|^2}{|E_{\omega}|^4} = \frac{\pi^2 W_o^2 a \sigma^2}{2 \mu_o c F^2} \cdot \frac{V_s}{(E')^2} \quad (8.21)$$

The value of a in this expression can be calculated from a quartz calibration experiment exactly as described in section 8.1.1.

8.1.3 Signals normalised with respect to quartz

A third type of normalisation procedure was employed for some of the studies; this involved the use of a variation on the experimental set-up shown in figure 4.3. In this new configuration the diffuser and photodiode were replaced with a second (reference) quartz wedge, a system of filters, and a photomultiplier. The wedge was positioned to correspond to a maximum in the Maker fringe pattern, and for each shot of the laser the second harmonic signals obtained from both this reference and the sample were fed to a boxcar averager.

Denoting the power incident on the reference quartz as I_{ω} (ref), and the resultant signal power as $I_{2\omega}$ (ref), with corresponding detector voltage V (ref), it follows from equation 8.6 that I_{ω} (ref) \propto $[I_{2\omega}$ (ref)]^{1/2}. Now, as the power incident on the sample, I_{ω} , is proportional to that incident on the reference quartz, and since V (ref) \propto $I_{2\omega}$ (ref), it can be seen that:

$$I_{\omega} = z[V(\text{ref})]^{1/2} \quad (8.22)$$

where z is a constant. Using equation 8.19 and substituting for $I_{2\omega}$ from 8.7 and for I_{ω} from 8.22 gives:

$$S = \frac{|E_{2\omega}|^2}{|E_{\omega}|^4} = \frac{\pi W_0^2 a}{2 \mu_0 c z^2} \cdot \frac{V_s}{V(\text{ref})} \quad (8.23a)$$

Quartz calibration experiments (one each for s- and p-polarized incident radiation) can be employed in order to calculate the value of a/z^2 . If the power incident on the quartz wedge in the sample arm of the system is I_ω (cal.), and it produces a signal voltage V_s (quartz) related to a second harmonic power $I_{2\omega}$ (quartz), whilst the corresponding detector voltage in the reference arm is V (ref, cal.), then equations 8.8 and 8.22 yield:

$$\frac{a}{z^2} = \frac{I_{2\omega} \text{ (quartz)} V \text{ (ref, cal.)}}{V_s \text{ (quartz)} I_\omega^2 \text{ (cal.)}}$$

Substitution for $I_{2\omega}$ (quartz) from equation 8.6 then gives:

$$\frac{a}{z^2} = \frac{8 (\mu_o)^{3/2} (\epsilon_o)^{1/2} \omega^2 d_{11}^2}{\pi W_o^2 n_{2\omega} (n_\omega)^2 (\Delta k)^2} \cdot \frac{V \text{ (ref, cal.)}}{V_s \text{ (quartz)}} \quad (8.23b)$$

Equations 8.23 can then be used together in order to compute calibrated signal strengths from measured signal voltages normalised by the signal obtained from a reference sample.

In practice the methods detailed in sections 8.1.1 and 8.1.2 gave very similar results, whereas the technique described in this section was subject to drift of the boxcar averager. Most of the measurements were therefore performed using either of the first two approaches.

8.2 Second Harmonic Generation from Homogeneous Monolayers

8.2.1 A comparison of materials

A comparison of the calibrated second harmonic signal strengths, for different polarizations and detection geometries, obtained from

homogeneous (i.e. single component) monolayers of various materials is given in table 8.1. In each case the angle of incidence was 45° . Compounds A8 and A9 (deposited under both the high and low surface pressure conditions detailed in table 5.2) were also investigated in this manner, but gave no measurable signals at all. In view of the low theoretical value of β predicted for A2 (a closely related material) in chapter 6, this observation provides further evidence that the anthracene nucleus is a poorer conjugated system than, say, a stilbene bridge.

The merocyanine, D1, was not studied since it had already been extensively characterized by Girling et al⁽³⁾, and their results have simply been quoted in the table. It is interesting to note that they found, as expected, that the addition of a second layer to form a symmetrical bilayer resulted in the SHG being extinguished. Furthermore, protonation of the dye was found to suppress SHG (as anticipated from the discussion in section 6.1.1) and the experiments had to be performed in an enclosed cell containing ammonia vapour. Girling et al deposited monolayers from both the high and low pressure regimes described in chapter 5, and the signal strength was significantly greater from the former. This was due to its higher surface density of molecules and a probably smaller spread of the distribution of ψ , the angle of inclination of the molecular axes of the dye to the substrate normal. For the high surface density monolayers, the average value of ψ was calculated to be 13.4° and β was found to be $(350 \pm 100) \times 10^{-50} \text{ C}^3 \text{ m}^3 \text{ J}^{-2}$ (in reasonable agreement with the theoretical value given in table 6.2). The 532 nm wavelength of the second harmonic is close to an excitation peak in the deprotonated form of the dye, and this resonantly enhances β . However, there is a

TABLE 8.1 Calibrated signal strengths ($10^{-27} \text{ m}^2 \text{ V}^{-2}$) obtained for monolayers of various materials (\dagger values for D1 are taken from reference 3)

Material	$T^{P \rightarrow P}$	$R^{P \rightarrow P}$	$T^{S \rightarrow P}$	$R^{S \rightarrow P}$	$T^{S \rightarrow S}$	$R^{S \rightarrow S}$	$T^{P \rightarrow S}$	$R^{P \rightarrow S}$
M3	0.11 ± 0.03	0	0.02 ± 0.01	0	0	0	0	0
D2	9.7 ± 0.4	1.5 ± 0.2	0.68 ± 0.06	0.76 ± 0.06	0.15 ± 0.01	0.06 ± 0.02	0.06 ± 0.01	0.12 ± 0.03
D5	0.69 ± 0.05	0.070 ± 0.017	0.078 ± 0.024	0.080 ± 0.016	-	-	0.012 ± 0.012	0
D6	0.42 ± 0.03	0.015 ± 0.010	0.11 ± 0.01	0.049 ± 0.006	-	-	-	-

D1 [†] (High surface density)	-	0.104 ± 0.020	-	0.092 ± 0.014	-	Weak	-	Weak
D1 [†] (Low surface density)	-	0.045 ± 0.009	-	0.026 ± 0.007	-	Weak	-	Weak

corresponding enhancement in the dielectric constant, which results in a reduced coupling of the near 'vertical' polarisation field to the near 'horizontal' field of the second harmonic radiation.

The amidonitrostilbene, D5, gave second harmonic signal strengths which were comparable with those obtained from the merocyanine under the same conditions of polarisation and detection geometry; however, by far the largest signals were given by the hemicyanine, D2. Although the value of β for the hemicyanine (calculated⁽⁴⁾ as $(116 \pm 20) \times 10^{-50} \text{ C}^3 \text{ m}^3 \text{ J}^{-2}$, which is somewhat smaller than the theoretical value given in table 6.2) is less than that for the merocyanine, it also has a much smaller dielectric constant, and since the SHG efficiency depends on the ratio β/ϵ , the overall efficiency of the hemicyanine is the greater of the two materials. Furthermore, the better average alignment of the hemicyanine dye with respect to the incident field ($\psi = 24^\circ$)⁽⁴⁾ results in a stronger signal than that given by the merocyanine.

It was rather surprising that the aminonitrostilbene, D6, gave slightly smaller signals than those obtained from D5. The amine group in D6 should be a rather stronger donor than the amide functionality in D5; however, the better film quality observed for monolayers of D5 (see chapter 7) might have had a stronger influence on the overall SHG efficiency than did a small change in the degree of intramolecular charge-transfer. Inspection of table 6.2 reveals that the ratio of the second harmonic signals obtained from D2 and D5 monolayers is approximately as expected from a comparison of the theoretical β values for the constituent molecules.

The signals observed from a monolayer of the Primulin derivative, M3, were very weak, the only measurable ones being for the p-polarised second harmonic. These signals were smaller than those observed from

symmetrical bilayers of merocyanine⁽³⁾ or hemicyanine⁽⁵⁾, and their low values could be due to either the material having a relatively small β , or else to the films actually being bilayers rather than true monolayers. In fact the latter possibility was postulated in section 5.3.1 to account for the rather low values of the area per molecule observed in the pressure-area isotherms of M3.

8.2.2 Effect of in-plane anisotropy on SHG from amidonitrostilbene monolayers

This section is concerned with the investigation of any in-plane anisotropy of a film, such as a partial alignment of the molecules with dipping direction. A glass substrate, onto which a monolayer of amidonitrostilbene had been deposited, was mounted in the vertical plane with the laser beam incident at 45° in the horizontal plane; the sample was then rotated about an axis perpendicular to the substrate, and the effect on the $T^{P \rightarrow P}$ signal studied. Although a large range of values were observed ($0.3-0.9 \times 10^{-27} \text{ m}^2 \text{ V}^{-2}$), there was no obvious correlation with the angle through which the substrate was turned. Since the centre of rotation of the specimen was not coincident with the point of incidence of the laser beam, this scatter of the signal strength was assumed to be caused predominantly by variations in SHG efficiency from one area of the sample to the next (the values used in table 8.1 represent an average taken over several different regions of the sample but with the longest dimension of the substrate always vertical). The effects of any in-plane anisotropy are thus considerably smaller than those arising from translational non-uniformity in the film.

8.3 SHG From Alternating Layer Structures Containing Active and Passive Components

The importance of having a non-centrosymmetric crystalline structure to the observation of second-order optical non-linearity in the solid state was discussed in chapter 2. Conventional, single component, Y-type LB films are centrosymmetrical; however, by depositing two different materials in successive layers, alternating multilayer systems can be built up (as described in chapter 3) which are acentric. The investigation of one such array is detailed in this section. The first of the materials (amidonitrostilbene) was chosen in view of the SHG efficiency it displayed in monolayer form, whilst the second compound was a relatively inactive material (cadmium arachidate), which served simply as a "spacer" for the active layers. Girling et al have demonstrated SHG from similar structures involving the merocyanine, D1⁽⁶⁾, or the hemicyanine, D2⁽⁵⁾, alternated with ω -tricosenoic acid.

8.3.1 Effect of thickness

Alternating layers of amidonitrostilbene and cadmium arachidate were deposited onto one side of a glass substrate (the dye on the upstroke), and the second harmonic signal studied as a function of the film thickness for a fixed (45°) angle of incidence. The transmitted p-polarised signal resulting from a p-polarised incident beam was considerably larger than any of the other signals, and its variation with the number of bilayers is illustrated in figure 8.1. Ideally the $T^{P \rightarrow P}$ signal should increase quadratically with the number of bilayers, since the films are thin compared to the wavelength of the incident light and therefore coherent addition is expected. Figure 8.1 does reveal an apparently superlinear response, although the optimum 1:4:9:100 ratio was not achieved; the observed ratio was in fact 1:1.5:2.9:15. The deviation of the ratios from those theoretically

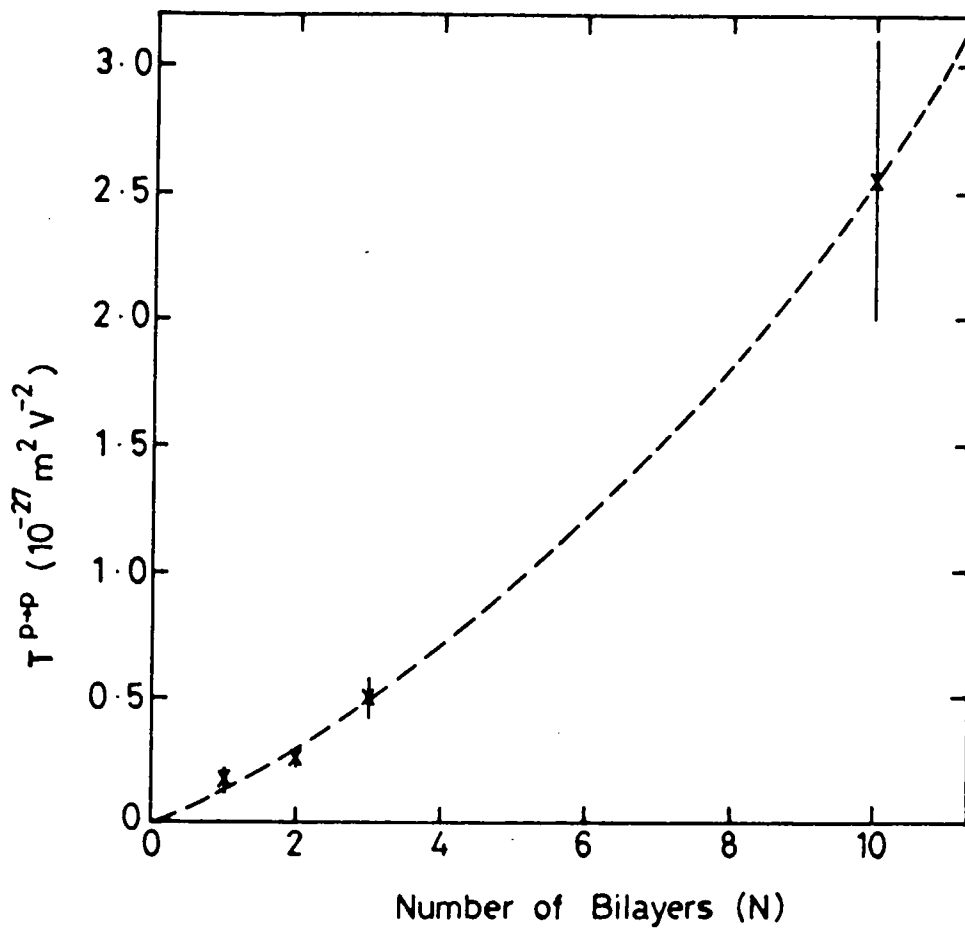


Figure 8.1 $T^{P \to P}$ second harmonic signal strength as a function of the number of bilayers in an amidonitrostilbene/cadmium arachidate alternate layer structure.

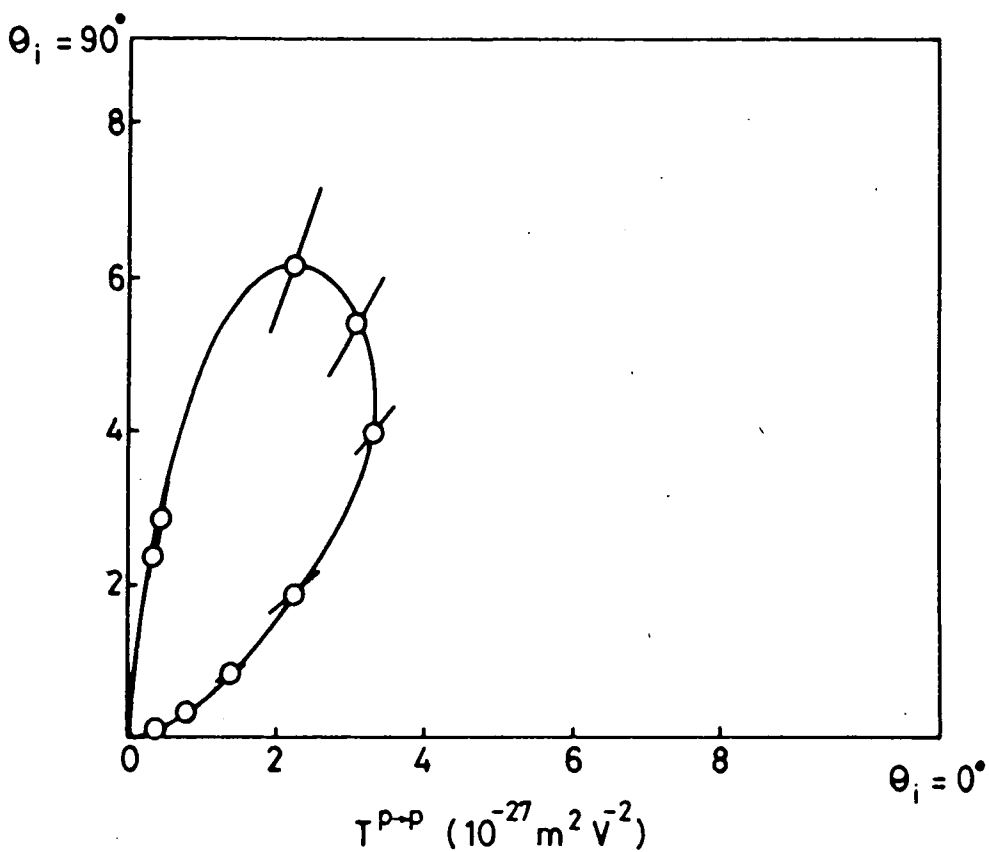


Figure 8.2 $T^{P \to P}$ second harmonic signal strength as a function of angle of incidence (θ_i , measured relative to the substrate normal), for an LB film containing 10 layers of amidonitrostilbene alternated with cadmium arachidate.

predicted may be due to a degradation in film quality with increasing thickness, or to the figure for the first "bilayer" being anomalous since it was really due to a monolayer of the dye with the chromophore adjacent to the substrate (instead of being next to a layer of carboxylate groups as in all the other bilayers).

The $T^{P \rightarrow P}$ signal obtained from the monolayer of D5 (equivalent to a single bilayer) in this investigation was significantly smaller than that reported for a similar structure in section 8.2. This phenomenon was attributed to the samples studied in this section being at least two months old, and indeed a two week old monolayer was found to give a very similar signal to that given in table 8.1 when placed in the experimental system immediately after the characterization of the alternate layers had been completed. No such degradation was observed in the case of hemicyanine monolayers or the hemicyanine/amidonitrostilbene alternate layers discussed in section 8.4; this is an important consideration, since it will determine the lifetime of any future device incorporating these films.

8.3.2 Effect of angle of incidence

An alternating layer system of amidonitrostilbene and cadmium arachidate, containing ten layers of the dye, was deposited onto one side of a glass substrate. The sample was mounted in a vertical plane, and could be rotated about a vertical axis (parallel to the dipping direction) in order to study the variation in the $T^{P \rightarrow P}$ signal as a function of θ_1 , the angle of incidence of the fundamental beam (relative to the substrate normal). Since the laser beam did not exactly intersect the axis of rotation of the specimen, it was impossible to avoid tracking across the sample as it was rotated. However, the observed variations in the signal (see figure 8.2) were so large that any minor variations in SHG efficiency at different points in the film were almost insignificant.

The $T^{P \rightarrow P}$ signal strength shows a distinct peak at $\theta_i = 70^\circ \pm 5^\circ$. Such a peak might be expected if the dye molecules are not aligned precisely along a normal to the substrate, but rather subtend an average angle ψ to it (if ψ was zero then $T^{P \rightarrow P}$ would be a maximum at grazing incidence). At the first inspection this might suggest a method for calculating ψ from the value of θ_i for which the $T^{P \rightarrow P}$ signal is a maximum; however, in reality the situation is much more complex.

The quadratic polarization, $\underline{P}^{(2)}$, of a film comprised of molecules with third-rank second-order molecular hyperpolarizability tensor β , under the influence of an electric field \underline{E} , is

$$\underline{P}^{(2)} = \beta \cdot \underline{E} \cdot \underline{E}$$

and will be most effective when it is parallel to the transmitted electric field vector, \underline{E}_t . The second harmonic signal, I , should thus be proportional to the dot product of $\underline{P}^{(2)}$ and \underline{E}_t

$$\text{i.e. } I \propto \underline{E}_t \cdot \underline{P}^{(2)}$$

$$\therefore I \propto \beta \cdot \underline{E} \cdot \underline{E} \cdot \underline{E}_t$$

Now, the relevant electric field in the film, \underline{E} , is really the sum of the incident (\underline{E}_i) and reflected (\underline{E}_r) fields

$$\text{i.e. } \underline{E} = \underline{E}_i + \underline{E}_r$$

so that the calculations cannot be performed simply using the incident field only. A further complication arises in that the measured second

harmonic signal will have been decreased by reflection off the back face of the glass slide (and in fact this would result in zero $T^{P \rightarrow P}$ signal at 90° incidence even if the molecules were aligned perfectly normal to the substrate).

In conclusion, the effect of varying the angle of incidence on the $T^{P \rightarrow P}$ signal will be dominated by reflectance effects and not by the orientation of the chromophores with respect to the substrate. It is therefore not possible to simply extract the molecular tilt, ψ , from the angle of incidence for which the second harmonic signal is a maximum. However, a more detailed fitting of the data, using formulae analogous to those used by Girling et al⁽⁵⁾ for 45° incidence, might enable a more accurate value of ψ to be determined than is possible from measurements made at a single angle of incidence.

8.3.3 Interference effects

An alternating layer structure of amidonitrostilbene and cadmium arachidate, containing ten layers of the dye, was deposited onto each side of a glass substrate. The effect on the $T^{P \rightarrow P}$ signal of varying the angle of incidence was investigated as in section 8.3.2. Whereas the sample with one face coated with LB film gave rise to only one peak in $T^{P \rightarrow P}$, a series of maxima and minima were observed for the one with both faces covered. Over the range of angle of incidence 0° - 45° , the $T^{P \rightarrow P}$ signal varied between zero and $22 \times 10^{-27} \text{ m}^2 \text{ V}^{-2}$ (the largest peak in this series); between the same angular limits the greatest signal given by the single-sided sample was $2.9 \times 10^{-27} \text{ m}^2 \text{ V}^{-2}$ (although at $\theta_i = 70^\circ$ a signal of $6.6 \times 10^{-27} \text{ m}^2 \text{ V}^{-2}$ was obtained). This contrast in the behaviour provides evidence that the origin of the fringe pattern from the double-sided sample lies in the interference between front and back layer generated harmonic beams. A similar phenomenon has been observed

by Zyss⁽⁷⁾ for third harmonic generation from LB films of polydiacetylene.

8.4 SHG From Alternating Layer Structures Containing Two Different Active Components

8.4.0 Background

The construction of a noncentrosymmetric multilayer array by alternating layers of an "active" non-linear material with an "inert" spacer, such as the salt of a fatty acid, was discussed in section 8.3. Likewise it should be possible to produce alternating multilayers in which both components are active and in which their contributions are constructive. This could be achieved by using materials in which the β tensors are directed in opposite senses with respect to the hydrophobic tails; such molecules could be obtained by attaching the hydrocarbon chains to the donor end of the chromophore in one case and to the acceptor end in the other. The resulting bimolecular hyperpolarizability should be of the order of the algebraic sum⁽⁷⁾, $\beta_1 + \beta_2$. Figure 8.3 illustrates the contrast in the contributions made to the optical non-linearities of LB films constructed in three different ways: (i) conventional Y-type mode; (ii) active material alternated with an inert spacer; (iii) alternation of two different active materials.

Two different doubly active alternate layer systems were investigated: hemicyanine (D2) and amidonitrostilbene (D5); and hemicyanine (D2) and aminonitrostilbene (D6). In the case of the hemicyanine molecule the hydrocarbon tail is attached to the acceptor, whereas in the nitrostilbenes it forms part of the donor. However, since the donor and acceptor groups are different in the two components of the arrays, there is still no guarantee that the β vectors of the

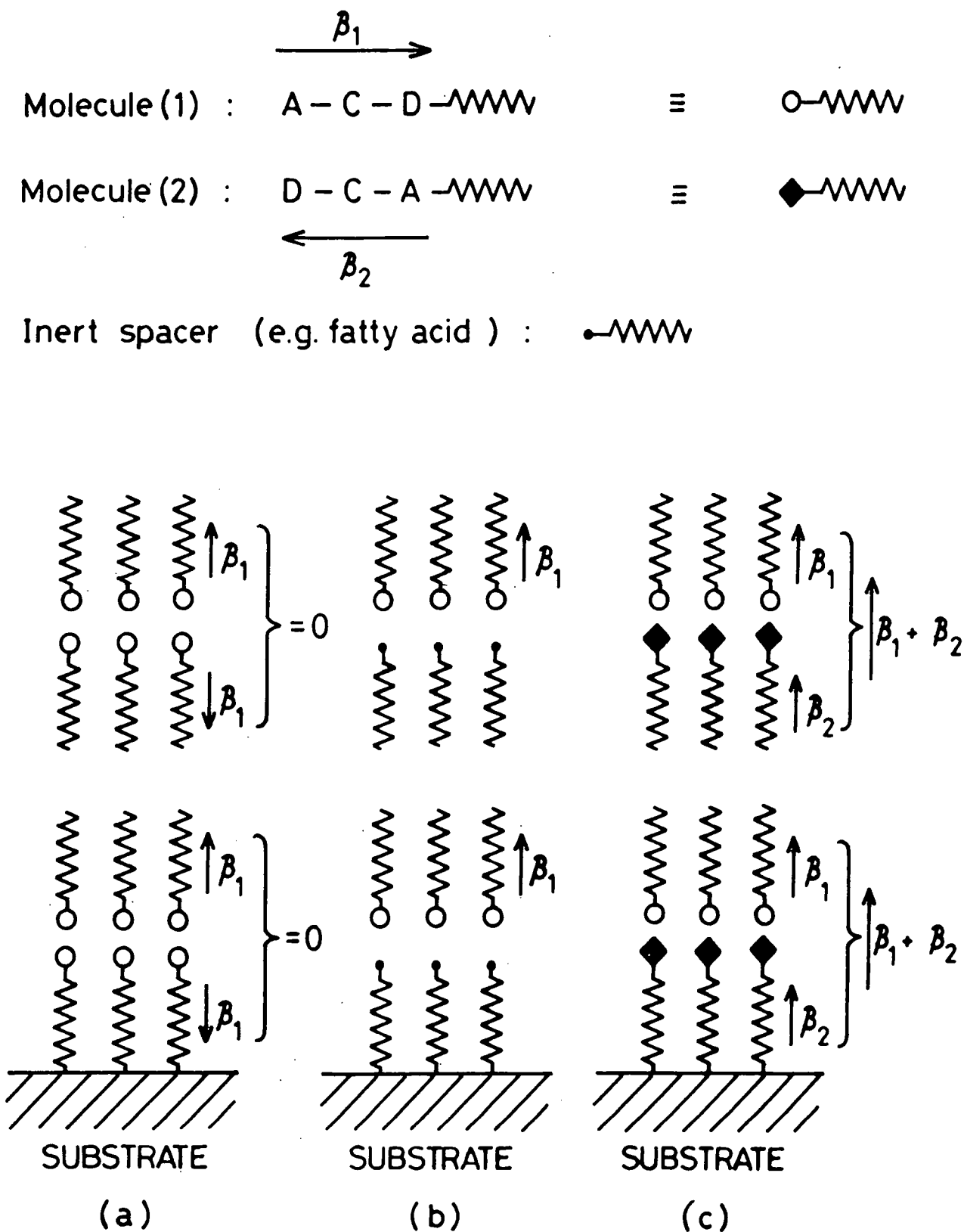


Figure 8.3

The effects on the overall second-order optical non-linearity of an LB film resulting from the construction of different types of multilayer array :

- (a) cancellation of β 's in a conventional Y-type film;
- (b) production of a noncentrosymmetric structure by alternating an active dye with an inert spacer material;
- (c) use of two different non-linear materials, with donor and acceptor groups in opposite senses with respect to the hydrophobic tails, to give a structure in which all the layers are active and their contributions are constructive.

molecules will be oppositely oriented with respect to the hydrocarbon tails.

The theoretical calculations described in section 6.5 gave the sign of $\beta(\text{vect})$ for D2 as being opposite to that for D5 and D7 (the closest analogue of D6 to be modelled). Now, $\beta(\text{vect})$ represents $\underline{\beta}$ vectored onto the ground state dipole moment direction, $\underline{\mu}_g$, and if $\underline{\mu}_g$ has opposite directions, with respect to the hydrocarbon chain, in the hemicyanine relative to the nitrostilbenes, then this would imply that $\underline{\beta}$ has the same direction (again relative to the hydrophobic tails) in all three molecules. However, if $\underline{\mu}_g$ has the same direction for all the molecules, then $\underline{\beta}$ must be oppositely directed (with respect to the tails) in D2 compared to D5 and D6. There is no doubt over the direction of $\underline{\mu}_g$ in the nitrostilbenes: the nitro group will be at the negative end of the dipole. The situation is not so clear for hemicyanine, in which the dimethyl amino group will acquire a slightly positive charge but in which the pyridinium acceptor already has a full positive charge to start with. Essentially the problem lies in the location of the negative counterion to the pyridinium group; if it close to the acceptor group then the dimethylamino group will be at the positive end of the dipole, but if it has migrated some distance away then the dimethylamino group may be at the negative end of the ground state dipole. Thus the doubt over the direction of $\underline{\mu}_g$ in hemicyanine gives rise to a complex situation in which it is difficult to predict whether or not the two components in the alternating layer systems will complement each other.

8.4.1 Comparison of the D2/D5 and D2/D6 systems

A summary of the second harmonic signals obtained from alternating multilayers containing three layers of hemicyanine and two of either

amidonitrostilbene or aminonitrostilbene is given in table 8.2. It can be seen that the two systems show very similar SHG efficiencies, the one containing amidonitrostilbene being perhaps the slightly superior. In theory D6 should have a slightly larger β than D5 (see section 6.5) due to the removal of the electron withdrawing carbonyl group from the donor functionality. This might suggest that the β 's for hemicyanine and the nitrostilbenes all have the same direction, the larger second harmonic signals for the D2/D5 system resulting from a lesser cancellation of the β of D2 by that of D5 compared to that caused by D6. However, the larger second harmonic signals obtained for monolayers of D5 relative to D6 (section 8.2.1, table 8.1) controverts this argument, instead implying that the β of D5 is greater than that of D6, in which case the β 's of the nitrostilbenes and the hemicyanine must be complementary (i.e. oppositely directed relative to the hydrocarbon chains).

The situation is clearly not a simple one; there are many inter-related factors operating, many of which are extremely difficult to quantify. Two such potentially important influences which have not been considered are (i) the difference in crystalline structure (both the degree of order and the orientation of the chromophores) between the two systems; and (ii) the effect on the charge transfer band (and hence on β) of the molecules in one layer resulting from having a layer of different polarized molecules adjacent to them.

8.4.2 A detailed study of the D2/D5 system

The structures investigated in this part of the study contained N layers of D5 and N+1 layers of D2, where N=0-10. In order to evaluate the non-linearity of the bilayer system, the effects of the extra layer of hemicyanine (the layer with the chromophore adjacent to the substrate) had to be eliminated. If there is coherent addition of the

TABLE 8.2 Calibrated signal strengths ($10^{-27} \text{ m}^2 \text{ V}^{-2}$) obtained for alternate multilayer structures containing three layers of hemicyanine and two of a nitrostilbene dye.

System	$T^{p \rightarrow p}$	$R^{p \rightarrow p}$	$T^{s \rightarrow p}$	$R^{s \rightarrow p}$
D2/D5	209±14	14.1±0.8	7.7±0.5	7.2±0.6
D2/D6	173±11	8.2±0.7	7.6±0.8	5.9±0.5

signals produced by each bilayer, then for a given polarization and detection geometry the total signal field strength, $E_{2\omega}$, can be written as:

$$E_{2\omega} = E_{2\omega} (L1) + N E_{2\omega} (BL) \quad (8.24)$$

where $E_{2\omega} (L1)$, $E_{2\omega} (BL)$ are the signals produced by the first layer and by a bilayer, respectively. The experimentally determined quantity is S , where $S = |E_{2\omega}|^2 / |E_{\omega}|^4$. Substituting for $E_{2\omega}$ in the expression for S by using equation 8.24:

$$S = \left[\frac{|E_{2\omega} (L1)|^2}{|E_{\omega}|^4} + \frac{N |E_{2\omega} (BL)|^2}{|E_{\omega}|^4} \right] \quad (8.25)$$

$$\therefore S^{\frac{1}{2}} = S(L1)^{\frac{1}{2}} + N \cdot S (BL)^{\frac{1}{2}}$$

A plot of $S^{\frac{1}{2}}$ versus N should therefore yield a straight line whose gradient is equal to the average value of $S^{\frac{1}{2}}$ for a bilayer.

The arguments of the preceding paragraph could also be applied to alternate layer systems containing only one active component, in order to remove the effects of the first (unpaired) layer, which arise from the use of hydrophilic substrates. Figure 8.4 shows a plot of $S^{\frac{1}{2}}$ against N for the $T^{P \rightarrow P}$ signal obtained from the amidonitrostilbene/cadmium arachidate system discussed in section 8.3.1. The data (extracted from figure 8.1) give a good fit to a straight line, and the gradient yields a value of $T^{P \rightarrow P} (BL)$ of $(0.019 \pm 0.004) \times 10^{-27} \text{ m}^2 \text{ V}^{-2}$. This figure is more than an order of magnitude less than that given for a monolayer of amidonitrostilbene in section 8.2; this change

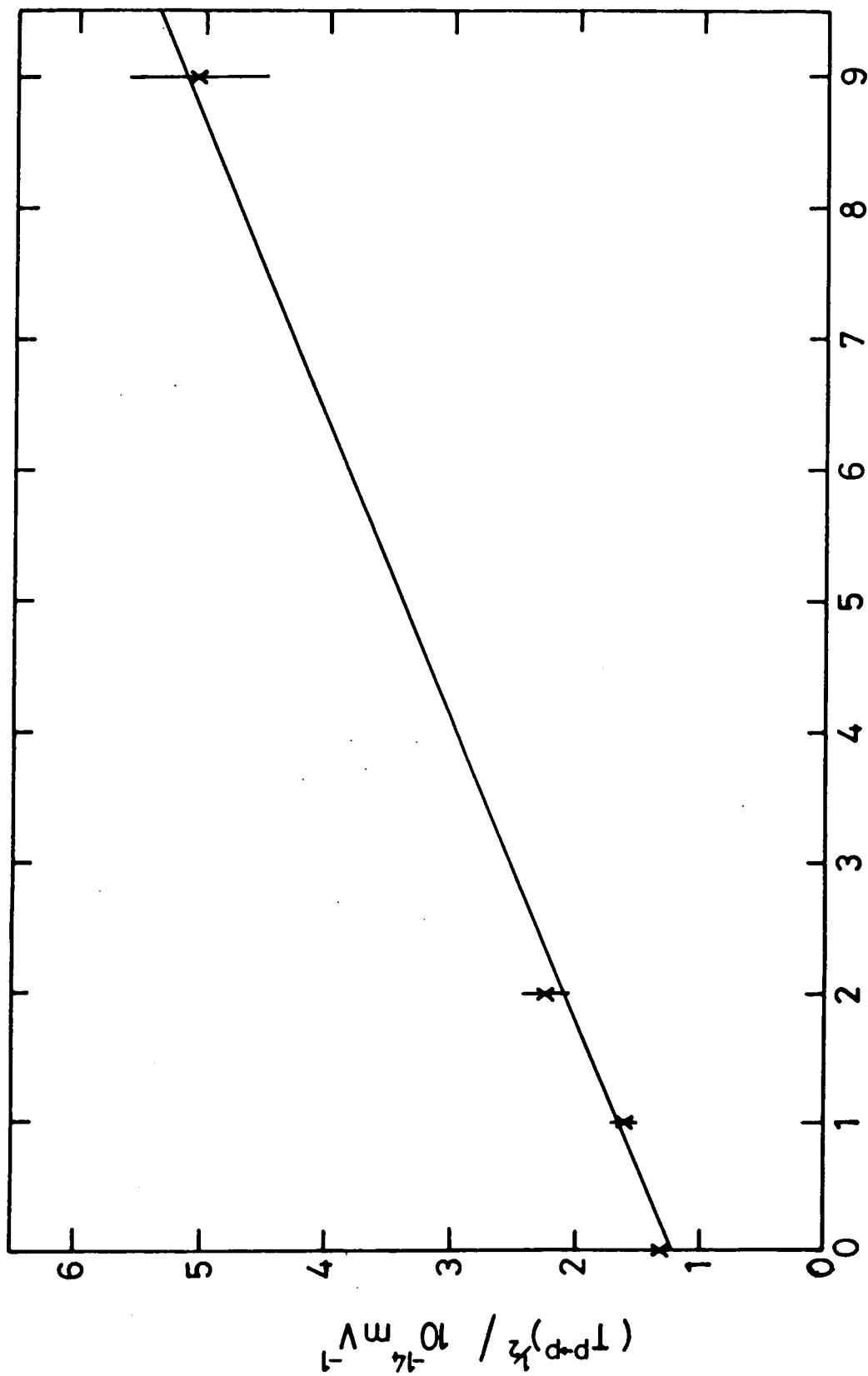


Figure 8.4 Plot of the square root of the I_{P+P} second harmonic signal strength versus the number of amidonitrostilbene/cadmium arachidate bilayers in an alternating layer structure.

in efficiency may partly be accounted for by the age of the sample (as discussed in section 8.3.1), with a further reduction arising from the film quality degrading with increasing thickness.

The $T^{P \rightarrow P}$ signals obtained from the amidonitrostilbene/hemicyanine alternate layer system gave rise to a graph of $S^{\frac{1}{2}}$ versus N (figure 8.5) which could be fitted moderately well to a straight line, whose gradient yielded the value $T^{P \rightarrow P} (BL) = (13 \pm 3) \times 10^{-27} \text{ m}^2 \text{ V}^{-2}$. Once again the problem of thicker films suffering from poorer quality has apparently arisen, since the first few points in figure 8.5 could be fitted to a much steeper line than that enforced by the points at higher values of N . Even at $N=10$, the films are still very thin ($< 100\text{nm}$) and therefore problems of phase mis-match between the second harmonic radiation generated at various points in the multilayers are unlikely to account for this behaviour.

Data for a system in which hemicyanine was alternated with an inert material (ω -TA) could have been obtained from reference 5; however, since data were only available for $N=1-3$, any reduction in efficiency at higher values of N would not be seen. An alternative approach which could have been taken is to simply take the difference in $S^{\frac{1}{2}}$ values between regions of say $N=1$ and $N=2$, or between $N=2$ and $N=3$, to calculate values of $S(BL)$ for each system. Comparisons could then have been drawn between the data obtained for a given thickness range. However, in the case of the $D2/\omega$ -TA system the errors involved in taking such a difference would have been prohibitively large, whilst the values of $R^{P \rightarrow P}$, $T^{S \rightarrow P}$ and $R^{S \rightarrow P}$ for the $D5/\text{cadmium arachidate}$ system described in section 8.3.1 were so small that they could not be measured accurately. Further calculations were therefore based on the data given in section 8.2.1 for monolayers of $D2$ and of $D5$. The corresponding data for the

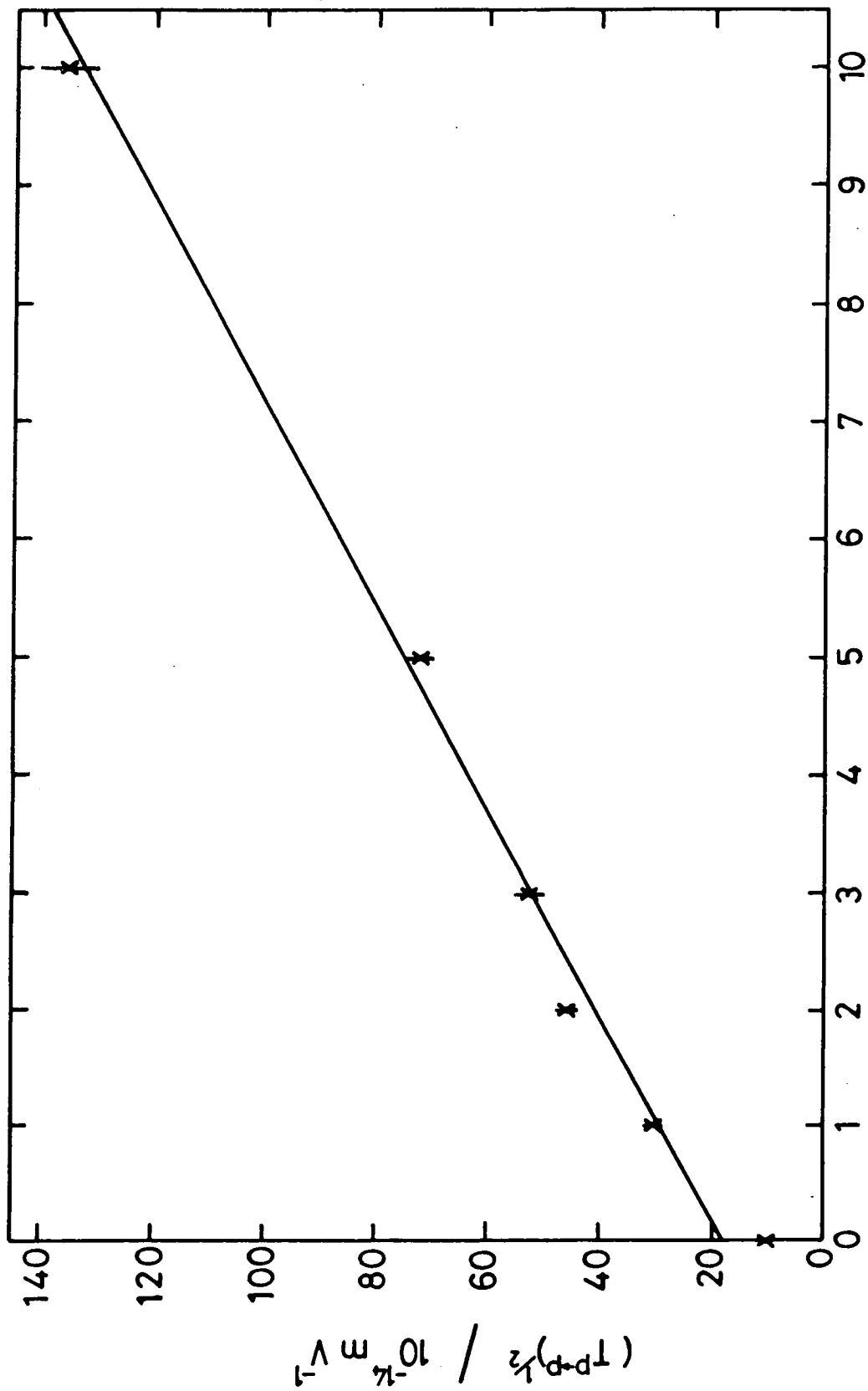


Figure 8.5 Plot of the square root of the $T^{P \rightarrow P}$ second harmonic signal strength versus the number of hemicyanine/amidodinitrostilbene bilayers in an alternating layer structure.

D2/D5 system were obtained by taking the difference in $S^{\frac{1}{2}}$ values between regions of $N=0$ and $N=1$ (for which the error was significantly less than that in the case of $D2/\omega$ -TA) and squaring the result.

Average values of $R^{P \rightarrow P}$, $T^{S \rightarrow P}$, and $R^{S \rightarrow P}$ for a single bilayer over the range $N=0-10$ were obtained by making $S^{\frac{1}{2}}$ versus N plots (figure 8.6) analogous to that given in figure 8.5 for $T^{P \rightarrow P}$. The $R^{P \rightarrow P}$ curve deviated markedly from linearity for $N > 3$, whilst the $T^{S \rightarrow P}$ plot displayed some curvature for $N > 5$; in these cases the average signal strength was calculated from the linear portion. A good straight line fit was obtained for the $R^{S \rightarrow P}$ data. This average set of data for the first ten bilayers was used alongside the figures obtained for the $N=0-1$ interval for comparison with the monolayer values (table 8.3). However, greater emphasis was placed on the $N=0-1$ information since it was obtained from a film whose thickness resembled that of the layers with which it was being compared.

The signal strengths given in the first few columns of table 8.3 were analysed in terms of the second harmonic surface susceptibilities ($\chi^{(2)}$) for the thin organic layers using the approach of Girling et al⁽⁵⁾. This required the linear dielectric constant components normal to the substrate to be known for each of the films at frequencies of both $\omega(\epsilon_1)$ and $2\omega(\epsilon_2)$. Since the values of ϵ_1 and ϵ_2 were not accurately known, they were substituted into the equations at the latest possible stage.

Girling et al⁽⁵⁾ solved Maxwell's equations in the vicinity of the film by assuming that the second harmonic polarization, generated in the dye by the fundamental incident radiation, was confined to an infinitesimal surface layer. The expressions obtained for the $T^{P \rightarrow P}$, $R^{P \rightarrow P}$, $T^{S \rightarrow P}$ and $R^{S \rightarrow P}$ signal strengths are given as equations 8.26 below,

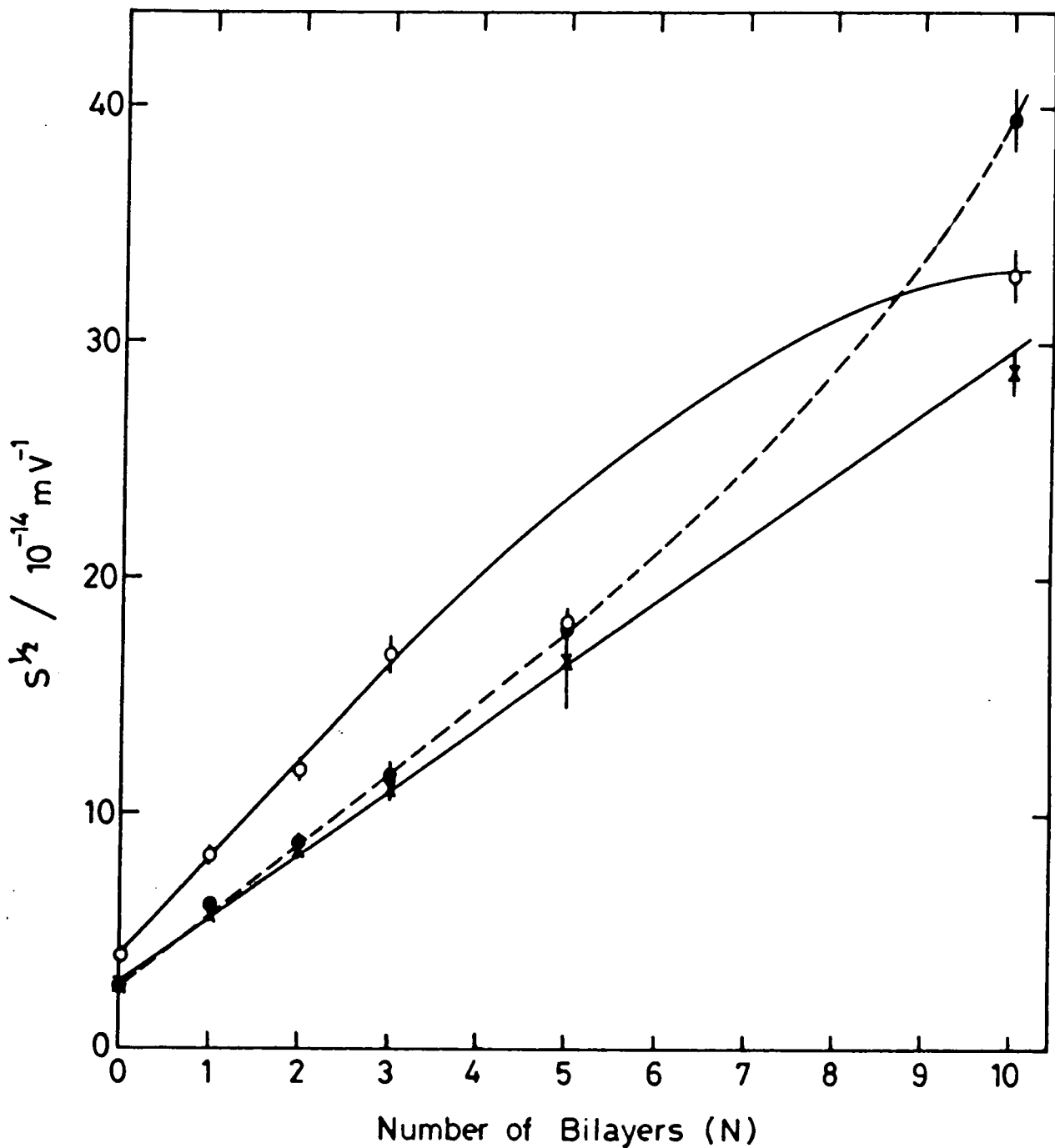


Figure 8.6

Plot of the square root of the $R^{P \rightarrow P}$ (o), $T^{S \rightarrow P}$ (●), and $R^{S \rightarrow P}$ (x) second harmonic signal strengths versus the number of hemicyanine/amidonitrostilbene bilayers in an alternating layer structure.

TABLE 8.3 Calibrated signal strengths ($10^{-27} \text{ m}^2 \text{ V}^{-2}$) and derived second harmonic surface susceptibilities ($10^{-32} \text{ C m V}^{-2}$), including the dielectric constants normal to the film, for alternate layer systems of D5/cadmium arachidate, D2/ ω -TA and D2/D5

System	T ^{p+p}	R ^{p+p}	T ^{s+p}	R ^{s+p}	$\frac{\nu^{(2)}}{X} \frac{zyy}{\epsilon_2}$	$\frac{\nu^{(2)}}{X} \frac{yyz}{\epsilon_1}$	$\frac{\nu^{(2)}}{X} \frac{zzz}{\epsilon_2 \epsilon_1^2}$
D5 (Monolayer)	0.69 ± 0.05	0.070 ± 0.017	0.078 ± 0.024	0.080 ± 0.016	2.7 ± 0.4	5.2 ± 0.3	5.4 ± 0.7
D2 (Monolayer)	9.7 ± 0.4	1.5 ± 0.2	0.68 ± 0.06	0.76 ± 0.06	8.0 ± 0.3	20.6 ± 0.7	17.5 ± 1.1
D2/D5 bilayer (N=0-i)	43.3 ± 4.2	1.9 ± 0.4	1.2 ± 0.2	0.84 ± 0.17	9.5 ± 0.9	37.8 ± 2.2	39.6 ± 3.6
D2/D5 bilayer (average over N=0-10)	13 ± 3	1.7 ± 1.0	0.9 ± 0.4	0.73 ± 0.10	8.6 ± 1.1	23.3 ± 3.8	20.4 ± 5.8

in which the film normal is taken to be the z-axis, and the x-axis is defined as the direction of the s-polarized radiation. The s→s and p→s signals were extremely small for either detection geometry.

$$T^{p \rightarrow p} = \left| \frac{\omega \sigma}{2\epsilon_0 c} \cdot t_{pp}(T) \cos \theta \left[\frac{-\sin \theta}{\epsilon_2} \cdot P_z + \frac{(\epsilon_g - \sin^2 \theta)^{1/2}}{\epsilon_g} \cdot P_y \right] \right|^2 \quad (8.26a)$$

$$R^{p \rightarrow p} = \left| \frac{\omega \sigma}{2\epsilon_0 c} \cdot t_{pp}(R) \cos \theta \left[\frac{\sin \theta}{\epsilon_2} \cdot P_z + \frac{(\epsilon_g - \sin^2 \theta)^{1/2}}{\epsilon_g} \cdot P_y \right] \right|^2 \quad (8.26b)$$

$$T^{s \rightarrow p} = \left| \frac{\omega \sigma}{2\epsilon_0 c} \cdot \frac{t_{sp}(T)}{\cos \theta} \left[\frac{-\sin \theta}{\epsilon_2} \cdot \beta_{zxx} + \frac{(\epsilon_g - \sin^2 \theta)^{1/2}}{\epsilon_g} \cdot \beta_{yxx} \right] \right|^2 \quad (8.26c)$$

$$R^{s \rightarrow p} = \left| \frac{\omega \sigma}{2\epsilon_0 c} \cdot \frac{t_{sp}(R)}{\cos \theta} \left[\frac{\sin \theta}{\epsilon_2} \cdot \beta_{zxx} + \frac{(\epsilon_g - \sin^2 \theta)^{1/2}}{\epsilon_g} \cdot \beta_{yxx} \right] \right|^2 \quad (8.26d)$$

In all equations 8.26, θ is the angle of incidence, ϵ_g is the dielectric constant of the glass substrate, and the transmission coefficients (t) correct for reflection of both ω and 2ω radiation at the air-film-glass interface. In terms of the surface density, σ , of the dye, the second order surface susceptibility is:

$$\chi_{ijk}^{(2)} = \sigma \beta_{ijk} \quad (8.27)$$

where β_{ijk} are the components of the molecular hyperpolarizability, inclusive of any in-plane local field corrections.

The polarizations, P_y and P_z , are given by

$$P_i = \beta_{iyy} - 2\beta_{iyz} \frac{\epsilon_g \sin\theta}{\epsilon_1 (\epsilon_g - \sin^2\theta)^{1/2}} + \beta_{izz} \frac{\epsilon_g^2 \sin^2\theta}{\epsilon_1^2 (\epsilon_g - \sin^2\theta)} \quad (8.28)$$

Assuming that $\beta_{zxx} \sim \beta_{zyy}$ (i.e. films are isotropic within the plane, as described in section 8.2.2), and that $\beta_{yxx} \sim 0$ (negligible s→s signal), substitution of equation 8.27 into equations 8.26c and 8.26d accompanied by rearrangement gives:

$$\frac{\chi_{zyy}^{(2)}}{\epsilon_2} = \frac{2\epsilon_0 c \cos\theta (T^{s \rightarrow p})^{1/2}}{\omega \sin\theta t_{sp}(T)} \quad (8.29a)$$

$$\frac{\chi_{zyy}^{(2)}}{\epsilon_2} = \frac{2\epsilon_0 c \cos\theta (R^{s \rightarrow p})^{1/2}}{\omega \sin\theta t_{sp}(R)} \quad (8.29b)$$

Similarly, assuming that β_{zyz} , β_{yyy} , and $\beta_{yzz} \sim 0$ (isotropic film with negligible s→s and p→s signals), equation 8.28 yields

$$P_y = -2\beta_{yyz} \frac{\epsilon_g \sin\theta}{\epsilon_1 (\epsilon_g - \sin^2\theta)^{1/2}} \quad \text{and}$$

$$P_z = \beta_{zyy} + \beta_{zzz} \frac{\epsilon_g^2 \sin^2\theta}{\epsilon_1^2 (\epsilon_g - \sin^2\theta)}$$

which, when substituted into equations 8.26a and 8.26b, give:

$$\frac{2\epsilon_0 c (T^{P \rightarrow P})^{\frac{1}{2}}}{\omega \cos \theta t_{pp}(T)} = \frac{-\sin \theta}{\epsilon_2} \chi_{zyy}^{(2)} - \frac{\epsilon_g^2 \sin^3 \theta}{\epsilon_2 \epsilon_1^2 (\epsilon_g - \sin^2 \theta)} \chi_{zzz}^{(2)} - \frac{2\sin \theta}{\epsilon_1} \chi_{yyz}^{(2)} \quad (8.30a)$$

$$\frac{2\epsilon_0 c (R^{P \rightarrow P})^{\frac{1}{2}}}{\omega \cos \theta t_{pp}(R)} = \frac{\sin \theta}{\epsilon_2} \chi_{zyy}^{(2)} + \frac{\epsilon_g^2 \sin^3 \theta}{\epsilon_2 \epsilon_1^2 (\epsilon_g - \sin^2 \theta)} \chi_{zzz}^{(2)} - \frac{2\sin \theta}{\epsilon_1} \chi_{yyz}^{(2)} \quad (8.30b)$$

where use has been made of equation 8.27. Addition of equations 8.30a and 8.30b followed by rearrangement gives:

$$\frac{\chi_{yyz}^{(2)}}{\epsilon_1} = \frac{\epsilon_0 c}{2\omega \sin \theta \cos \theta} \left[\frac{(T^{P \rightarrow P})^{\frac{1}{2}}}{t_{pp}(T)} + \frac{(R^{P \rightarrow P})^{\frac{1}{2}}}{t_{pp}(R)} \right] \quad (8.31)$$

The corresponding relation for $\chi_{zzz}^{(2)}$ can be obtained by subtracting equation 8.30a from 8.30b, and is :

$$\frac{\chi_{zzz}^{(2)}}{\epsilon_2 \epsilon_1^2} = \frac{\epsilon_0 c (\epsilon_g - \sin^2 \theta)}{\omega \epsilon_g^2 \cos \theta \sin^3 \theta} \left[\frac{(R^{P \rightarrow P})^{\frac{1}{2}}}{t_{pp}(R)} - \frac{(T^{P \rightarrow P})^{\frac{1}{2}}}{t_{pp}(T)} \right] - \frac{(\epsilon_g - \sin^2 \theta)}{\epsilon_g^2 \sin^2 \theta} \cdot \frac{\chi_{zyy}^{(2)}}{\epsilon_2} \quad (8.32)$$

where the value of $\chi_{zyy}^{(2)}/\epsilon_2$ can be taken from equation 8.29a or b.

For Corning 7059 glass, the refractive index is 1.530 (at 589.3 nm, although it will be assumed to be this value at ω and 2ω as well), therefore $\epsilon_g = 2.341$. Contributions to the transmission coefficients arise from reflection of both ω and 2ω radiation at each interface; care has to be taken in selecting the appropriate factors, bearing in mind that the LB film is extremely thin and therefore the air-film-glass interface effectively behaves as a single boundary, across which the tangential components of the electric fields at ω and 2ω must be continuous. The individual component transmission coefficients contained within each overall coefficient, t , can be calculated for the appropriate polarizations using the Fresnel formulae⁽⁸⁾. However, these factors only deviate slightly from unity, and do not represent a significant contribution when the errors in the experimentally determined signal strengths (and in the values of the dielectric constants used in subsequent calculations) are considered. This is exemplified by the s+p signals in table 8.3; according to equations 8.29, $(T^{s+p})^{1/2}/(R^{s+p})^{1/2} = t_{sp}(T)/t_{sp}(R)$, and thus the ratio of the two signals should be constant from one row of the table to the next, which in practice is clearly not the case (for instance, $T^{s+p} < R^{s+p}$ for D2 whereas $T^{s+p} > R^{s+p}$ for the D2/D5 system). In the calculations which follow it has therefore been assumed that $t \approx 1$.

Values of $\chi_{zyy}^{(2)}/\epsilon_2$ were calculated (see table 8.3) for monolayers of D2 and D5, and for D2/D5 bilayers (for both the first bilayer and the average over ten bilayers). This was achieved by using the s+p signal strength data in equations 8.29 and averaging the results obtained for the transmission and reflection geometries. Similarly, the p+p data were substituted into equation 8.31 to generate values of $\chi_{yyz}^{(2)}/\epsilon_1$, and

the same information was used again in conjunction with the $\chi_{zyy}^{(2)}/\epsilon_2$ data already calculated, in order to obtain the figures for $\chi_{zzz}^{(2)}/\epsilon_2\epsilon_1^2$ from equation 8.32.

On the assumption that the underlying molecular hyperpolarizabilities are dominated by single components (β) along the long molecular axis, β_{ijk} can be rewritten as:

$$\beta_{ijk} = \beta r_i r_j r_k \quad (8.33)$$

where $\underline{\hat{r}} = (\sin\bar{\psi} \cos\phi, \sin\bar{\psi} \sin\phi, \cos\bar{\psi})$ and $\bar{\psi}, \phi$, are the average polar angle and azimuthal angle, respectively, of the dye relative to the film normal (z-axis).

The absence of any anisotropy in the films indicates that any degree of local molecular orientation has been averaged out over the area of the incident beam (diameter $\sim 200 \mu\text{m}$). An isotropic ϕ average may therefore be used in the analysis of the results. Furthermore, if any local orientation is over areas smaller than the $\sim 1 \mu\text{m}$ wavelength then the electric fields themselves must be averaged, resulting in the replacement of β_{ijk} by its ϕ average in equations 8.26. This averaging over the field strengths leaves only two distinct β_{ijk} components⁽⁵⁾ (equations 8.34 and 8.35), the rest being zero; it also results in zero s-polarized second harmonic signal.

$$\beta_{zzz} = \beta \cos^3 \bar{\psi} \quad (8.34)$$

$$\beta_{zyy} = \beta_{zxx} = \frac{1}{2} \beta \cos \bar{\psi} \sin^2 \bar{\psi} \quad (8.35)$$

Note that equation 8.35 applies for all sequences of the zyy and zxx subscripts, and hence the β_{ijk} (and therefore $\chi_{ijk}^{(2)}$) coefficients should be symmetric to such permutations. A comparison of the $\chi_{zyy}^{(2)}/\epsilon_2$ and $\chi_{yyz}^{(2)}/\epsilon_1$ columns of table 8.3 therefore leads to $\epsilon_2 \geq 2\epsilon_1$. This is not inconsistent with the second harmonic energy being close to the lowest electronic molecular excitation, since under such circumstances ϵ_2 would be resonantly enhanced. Taking a reasonable, non resonant value $\epsilon_1=2$ for all three systems, the above symmetry condition yields the values of ϵ_2 shown in table 8.4. Note that the value of ϵ_2 for D5 (3.9 ± 0.8) is approximately what would be expected from a consideration of the corresponding quantity at a wavelength of 632.8 nm ($\epsilon = 3.2 \pm 0.4$), as determined by surface plasmon resonance (section 6.3).

Returning to equation 8.35, substituting for β from 8.34 gives a relation from which the average polar angle can be found:

$$\tan \bar{\psi} = \left[\frac{2\beta_{zyy}}{\beta_{zzz}} \right]^{\frac{1}{2}} = \frac{1}{\epsilon_1} \left[\frac{2(\chi_{zyy}^{(2)}/\epsilon_2)}{(\chi_{zzz}^{(2)}/\epsilon_2\epsilon_1^2)} \right]^{\frac{1}{2}} \quad (8.36)$$

Similarly, substituting for $\cos \bar{\psi}$ in equation 8.35 using 8.34 gives:

$$\beta = \left[\frac{(2\beta_{zyy} + \beta_{zzz})^3}{\beta_{zzz}} \right]^{\frac{1}{2}}$$

Replacing the β_{ijk} terms with surface susceptibilities:

$$\beta = \left[\frac{\chi_{zyy}^{(2)}}{\epsilon_2} + \frac{\chi_{zzz}^{(2)}}{\epsilon_2 \epsilon_1} \epsilon_1^2 \right]^{3/2} \left[\frac{\chi_{zzz}^{(2)}}{\epsilon_2 \epsilon_1} \epsilon_1^2 \right]^{-1/2} \frac{\epsilon_2}{\sigma} \quad (8.37)$$

The values of $\bar{\psi}$ and β shown in table 8.4 were calculated for each system by applying equations 8.36 and 8.37 to the data given in table 8.3 (assuming $\epsilon_1=2$). In view of the similar areas occupied by molecules of D2 and D5 (0.28 nm² and 0.27 nm², respectively) at the deposition surface pressures, the surface density was taken to be the same for both dyes ($\sigma = 3.64 \times 10^{18} \text{ m}^{-2}$).

A good agreement can be seen between these figures and the results of preliminary calculations⁽⁴⁾, and also with the data given by Girling et al⁽⁵⁾ for an alternate bilayer of D2/ ω -TA (which required a more complex analysis due to the observation of a significant s-polarized signal). The measured hyperpolarizabilities of D2 and D5 are somewhat smaller than the theoretical values given in chapter 6, although they are both of the expected order of magnitude. It is interesting to note that the value of $\bar{\psi}$ (26.4°) obtained for the monolayer of D5 is considerably less than that obtained by RHEED in chapter 7 (54° \pm 1°), and may be due to differences in the structure of the films on glass and silicon substrates.

It is evident that the bilayer is a much superior second harmonic material than is predicted by a simple addition of the β coefficients of the separate layers. Even if the bilayer data averaged over N=0-10 are used, the value of β obtained is as good as for the sum of the β 's for the D2 and D5 monolayers (assuming that the β 's are in complementary

TABLE 8.4 Derived hyperpolarizabilities (β), average polar angles ($\bar{\psi}$), and dielectric constant components normal to the substrate at a frequency of 2ω (ϵ_2), for LB monolayers of D2 and D5, and for a D2/D5² bilayer.

System	ϵ_2	β ($10^{-50} \text{ C}^3 \text{ m}^3 \text{ J}^{-2}$)	$\bar{\psi}$
D5 (monolayer)	3.9 ± 0.8	32 ± 15	26.4°
D2 (monolayer)	5.1 ± 0.4	134 ± 26	25.6°
D2/D5 bilayer (N=0-1)	7.9 ± 1.2	410 ± 140	19.2°
D2/D5 bilayer (average over N=0-10)	5.4 ± 1.6	160 ± 130	24.6°

directions). Since the "effective β " is likely to be much greater in thinner layers (as was observed for the first bilayer), the monolayer data will be the optimum achievable for the individual materials and hence the superadditivity in the bilayers is clear.

Although the chromophores in the bilayer are in close proximity and might be expected to interact strongly, the active groups in the separate bilayers and in the initial hemicyanine monolayer are separated by "passive" alkyl chains. Thus the second harmonic intensity is expected to increase quadratically with the number of bilayers, and figures 8.4 and 8.5 reveal that this is approximately the case. However, comparison of the value of β for a "typical" bilayer (obtained by using these plots to produce figures averaged over the first ten bilayers) with the one for the first bilayer alone illustrate the deviations from ideality which can occur with increasing thickness. Such behaviour may be due to a progressive degradation of film quality as the number of layers is increased. Girling et al⁽⁵⁾ attributed a similar phenomenon in D2/ ω -TA alternate layers to changes in the in-plane order, but the relatively small s-polarized signals obtained for even a single D2/D5 bilayer renders such an explanation unlikely in the present case.

The major source of errors in the measurements of β and $\bar{\psi}$ arise from uncertainties in the values of the dielectric constants. Perhaps a more accurate result would be obtained if this parameter could be determined for each material at both ω and 2ω in an independent experiment. Such an investigation might involve ellipsometry or depositing the dyes onto a silver substrate and observing the resultant shifts in the SPR curves, using sources of the appropriate wavelength.

8.4.3. Conclusions

Optical non-linearity in an alternating donor-acceptor : inverted donor-acceptor dye multilayer has been demonstrated. The second-order hyperpolarizability for a hemicyanine/amidonitrostilbene bilayer was found to be much greater than that expected by simply adding the hyperpolarizabilities for the individual dye monolayers. When the amidonitrostilbene dye was substituted by an aminonitrostilbene, there was a slight decrease in the SHG efficiency of the bilayer.

8.5 SHG From Heterogeneous Monolayers

8.5.1 The D2/cadmium arachidate system

Not all substituted dye materials will form homogeneous LB films; some have to be diluted with a fatty acid by up to a factor of ten in order to render them suitable for deposition by the LB technique. It was therefore of interest to use the hemicyanine dye (D2), which could be deposited in homogeneous films and which also had a particularly high value of β (see sections 8.2 and 8.4), as a model system to study the effects of dilution on non-linear behaviour.

SHG investigations of mixed monolayers of hemicyanine and cadmium arachidate with mole fractions of hemicyanine ranging from $\sim 0.1 - 1.0$ were undertaken. For each monolayer, the fractional film area, F , constituted by hemicyanine was calculated from the mole fraction of hemicyanine present in the spreading solution. It was assumed that a hemicyanine molecule occupies a surface area of approximately 0.35 nm^2 and an ionized arachidic acid molecule an area of 0.20 nm^2 (values measured from surface pressure-area isotherms of the materials) at the deposition surface pressure of 30 mN m^{-1} . If it is assumed that the dielectric constants of the film at ω and 2ω , and the values of β_{ijk} for the hemicyanine molecules, are unaltered as a result of the dilution,

then replacing σ with $\sigma_H F$ (where σ_H is the surface density of a pure hemicyanine monolayer) in equations 8.26 predicts a linear increase in $S^{\frac{1}{2}}$ (for p→p and s→p polarizations) with F, reaching a maximum for a 100% hemicyanine monolayer. This is also true for the s→s and p→s signals, since they too are quadratic in σ ⁽⁵⁾. Figures 8.7 and 8.8 show plots of $S^{\frac{1}{2}}$ versus F for the T^{P→P} and T^{S→P} signals; the dashed lines represent the theoretical linear response described above. It is very interesting to note that, for example, the T^{P→P} second harmonic signal is a factor of four times greater for a mixture containing equimolar quantities of hemicyanine and arachidic acid than for a pure hemicyanine monolayer. All of the other possible combinations of polarization and detection geometry gave signals which were also a maximum (out of the range of concentrations studied) for the equimolar mixture, although the ratio of these signals to that for the pure hemicyanine were not always as great as with the T^{P→P} signal.

Examination of figures 8.7 and 8.8 reveals that $S^{\frac{1}{2}}$ does indeed increase linearly with F for mixtures containing rather less than an equimolar quantity of dye, although the gradient of this line is much greater than that of the hypothetical one. The same was found to be true for the other polarizations and detection geometries, although the scatter of the points was much worse for s-polarized second harmonic signals. Table 8.5 summarises the values obtained for the ratio of the slope of the initial linear regions of the $S^{\frac{1}{2}}$ against F plots to the theoretical gradients.

One possible explanation for the enhanced signals might lie in the lower dielectric constant for cadmium arachidate compared to hemicyanine at a frequency of 2ω . This would be in accordance with the observation that the linear region of the $S^{\frac{1}{2}}$ versus F plots does not extend beyond

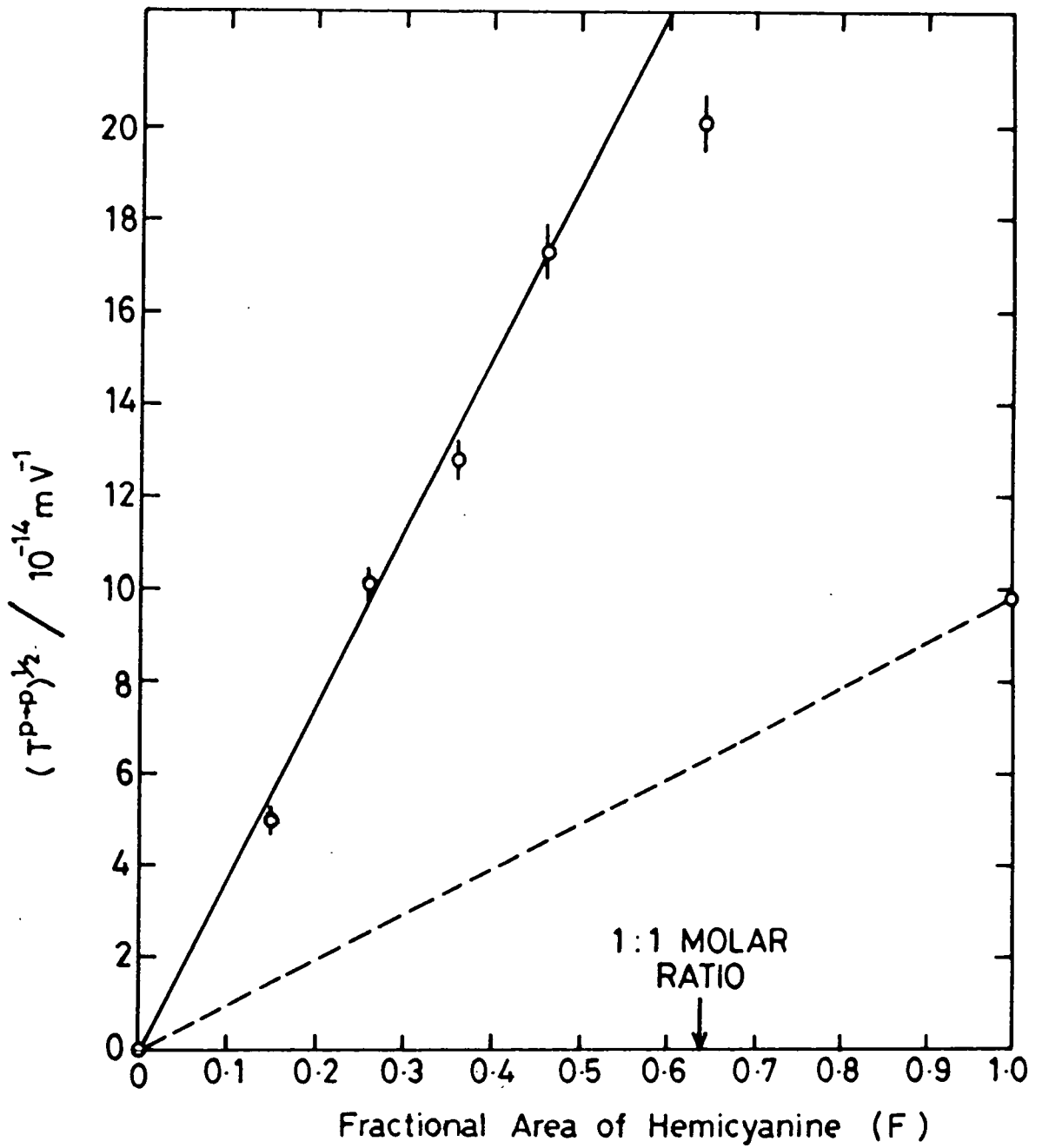


Figure 8.7

Plot of the square root of the $T^{P \rightarrow P}$ second harmonic signal strength versus the fractional area constituted by the dye in hemicyanine/cadmium arachidate mixed monolayers.

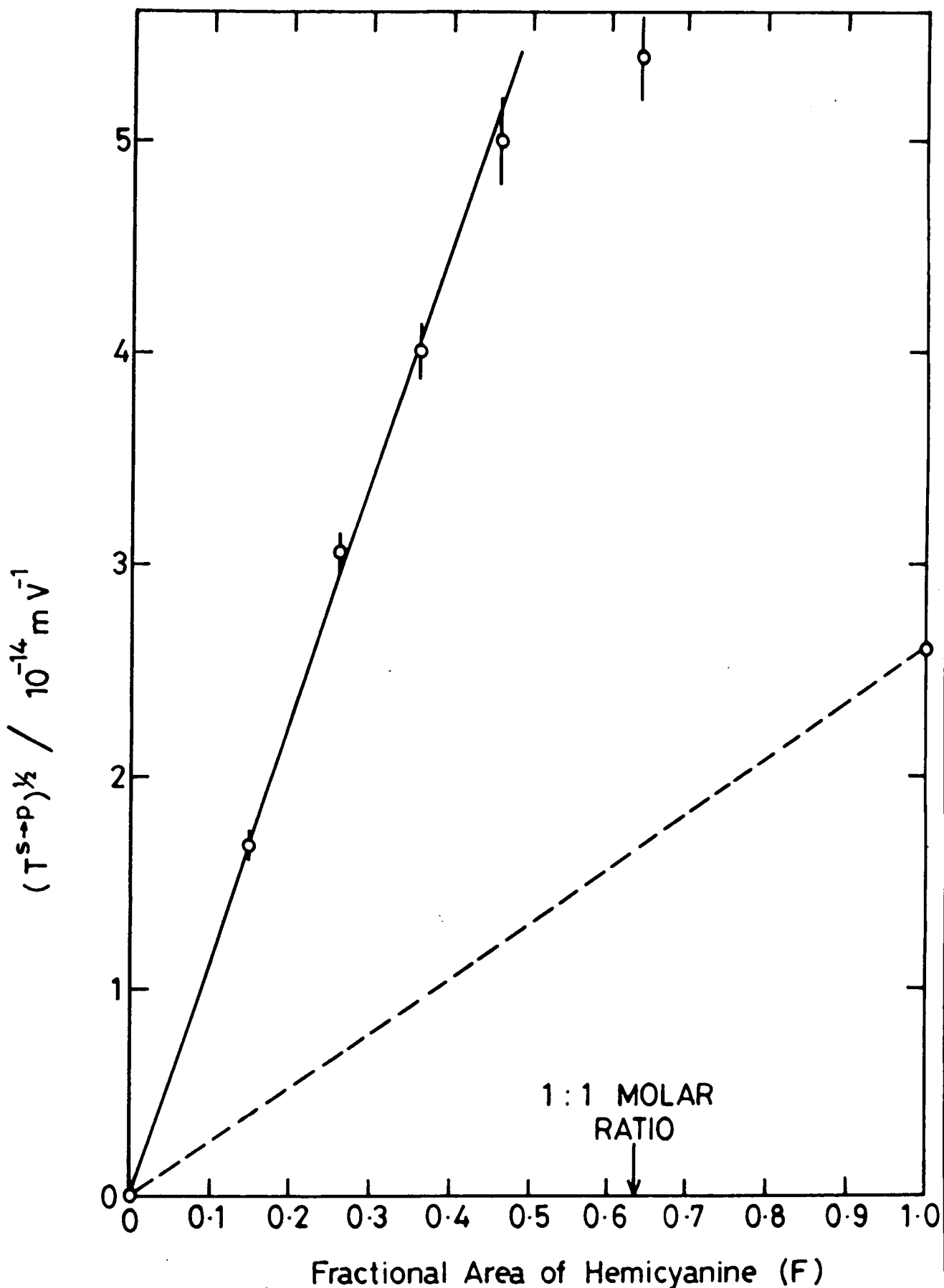


Figure 8.8

Plot of the square root of the $T^{S \rightarrow P}$ second harmonic signal strength versus the fractional area constituted by the dye in hemicyanine/cadmium arachidate mixed monolayers.

TABLE 8.5

Comparison of the gradient, $(dS^{1/2}/dF)_m$, of the initial linear portion of the plots of the square root of the second harmonic signal strength versus the fractional area constituted by dye, with the theoretical slope, $(dS^{1/2}/dF)_t$, predicted if the signals were not enhanced by dilution.

<u>Signal (S)</u>	<u>$(dS^{1/2}/dF)_m / (dS^{1/2}/dF)_t$</u>
T ^{p→p}	3.83 ± 0.32
R ^{p→p}	2.58 ± 0.66
T ^{s→p}	4.33 ± 0.39
R ^{s→p}	4.06 ± 0.16
T ^{s→s}	2.87 ± 0.26
R ^{s→s}	3.32 ± 0.73
T ^{p→s}	2.30 ± 0.45
R ^{p→s}	2.00 ± 0.39

the 1:1 molar ratio point, where the dye molecules would cease to be coordinated solely by arachidate species (assuming an intimate mixture of dye and ionized arachidic acid molecules). In order to test this theory, the most convenient signal to use is $T^{S \rightarrow P}$, since if it is assumed that $\beta_{yxx} \sim 0$, then $(T^{S \rightarrow P})^2 = C \beta_{zyy} F/\epsilon_2$ (where C is the constant of proportionality, and only involves terms which will be the same for both mixed and homogeneous monolayers; see equations 8.26c and 8.29a). Taking the limiting case for the mixed monolayers, in which the only contribution to ϵ_2 is from cadmium arachidate (i.e. assuming the pertinent ϵ_2 is that of the local environment of an active molecule and is not that of the molecule itself), then the ratio of the gradients for the full and dashed lines in figure 8.8 should be equal to $\epsilon_2(\text{hemicyanine})/\epsilon_2(\text{cadmium arachidate})$. Now, ϵ (cadmium arachidate) will not be resonantly enhanced at 532 nm, and its value (2.5 ± 0.1) is known quite accurately⁽⁹⁾. However, ϵ_2 (hemicyanine) has not been determined precisely, the best estimate available being 5.1 ± 0.4 as determined in section 8.4. Using these values the ratio of the slopes is predicted to be 2.0 ± 0.2 , which is far smaller than the measured value of 4.33 ± 0.39 given in table 8.5.

A second factor which might be operating is a change in packing of the dye molecules upon forming a significantly diluted monolayer, resulting in a better alignment relative to the electric fields of the incident and second harmonic light. This would contribute to the observed fact that the enhancement is not perfectly uniform for all geometries and polarizations, although to a certain extent the dielectric constant argument would do the same, since different factors of ϵ_1 and ϵ_2 appear in the various terms in equations 8.26.

One further mechanism which could explain the superior second harmonic signals from the mixed monolayers is the enhancement of β itself. In section 6.1.7 the bathochromic shift and increase in absorbance of the first absorption band of the dye upon forming a mixed monolayer was reported. This was interpreted in terms of the reduction of dipolar interactions in the heterogeneous layer, the molecules behaving more as they would do in a solution. The changes in the charge transfer characteristics of the molecules which give rise to these spectral shifts are also likely to have a great influence on β . Indeed, the larger value of β which could be associated with hemicyanine molecules in mixed monolayers would be closer to the theoretical value predicted in section 6.5 for the "free" molecule than the figure calculated for a pure monolayer in section 8.4. This effect is analogous to the solvent dependent hyperpolarizability of the merocyanine (D1) discussed in section 6.1.1.

In conclusion, it is likely that all three of the mechanisms discussed above will contribute, in varying degrees, to the enhanced SHG observed from mixed monolayers of hemicyanine. These findings may have important implications for improving the efficiencies of any non-linear optical device which utilises LB films.

8.5.2 Other heterogeneous monolayer systems

Compounds D7 and D8 could not be deposited as homogeneous layers (see chapter 5), therefore systems in which the dyes were mixed with cadmium arachidate were investigated. A further monolayer of interest was formed by mixing the two active dyes D2 and D5. SHG investigations of pure D2 monolayers alternated with pure D5 monolayers were reported in section 8.4; it was hoped that $\underline{\mu}_g$ would have the same direction (with respect to the hydrocarbon tails) for both molecules, so that $\underline{\beta}$ would be

oppositely directed and therefore additive in the multilayer arrays. By studying a mixed D2/D5 monolayer it was anticipated that the situation might become a little clearer. A monolayer in which D5 was mixed with cadmium arachidate was also investigated, in order to see whether the second harmonic generation was enhanced in the same manner as that observed with D2 in section 8.5.1.

D7/cadmium arachidate monolayers with molar ratios of ionized arachidic acid to dye of 1:1, 2:1, 3:1 and 5:1 were studied. Out of all these concentrations and all the possible combinations of polarization and detection geometry, the only detectable signal was the extremely low $T^{P \rightarrow P} = (0.04 \pm 0.02) \times 10^{-27} \text{ m}^2 \text{ V}^{-2}$ obtained for the 2:1 mixture. In view of the fact that the theoretical β for D7 (chapter 6) is greater than that for D5 (from which significant SHG has been observed), this would imply that the molecules of D7 are arranged in antiparallel aggregates within the layers. Such a process was postulated in chapter 5 to explain the low values of area per molecule observed in pressure-area isotherms of the homogeneous monolayer; clearly the use of heterogeneous monolayers does not overcome the problem, indicating that the dye does not form an intimate mixture with the cadmium arachidate.

Negligible SHG was observed from a monolayer containing arachidate ions and D5 in a 2:1 molar ratio. It seems, therefore, that the dilution of the active dye has resulted in a corresponding reduction in non-linearity, unlike the case of D2 where enhancement was observed. This would appear to give more weight to the argument that a change in β itself was responsible for the effects in hemicyanine, since the other mechanisms could be equally well applied to D5 (although alignment might also be significant, in view of the highly ordered structure exhibited

by even homogeneous monolayers of D5 -- see chapter 7). In chapter 6 the absorption spectrum of D5 was seen to be unchanged in profile as a result of dilution (which was not the case with D2), indicating that the charge-transfer process had not been greatly affected, and therefore little change in β would have been expected.

A summary of the second harmonic signals obtained from monolayers containing 5 moles of ionized arachidic acid to one mole of D8, and 1.02 moles of D5 to one mole of D2 (corresponding to a fractional area of hemicyanine of 0.57), is given in table 8.6.

The signal strengths given by the D8/cadmium arachidate monolayer were larger than those exhibited by a pure monolayer of D5 (section 8.2), although not as great as those from D2. It is not possible to say whether the dilution process has effectively enhanced or reduced the signal strengths from what they would have been in a homogeneous monolayer of D8, since such a film could not be deposited. However, the production of a high quality LB layer in which the dye molecules are not aligned in an antiparallel manner has clearly been demonstrated. It should be noted that compound D8 is the same as that used by Aktsipetrov et al⁽¹⁰⁾ in their letter on "second-harmonic generation on reflection from a monomolecular Langmuir layer", although the authors make no reference to the need for employing a heterogeneous system.

Temporarily neglecting the non-linearity of D5 (since it is significantly smaller than that of D2), the D2/D5 system gave signals which were enhanced (for example, by a factor of ~ 2 in the case of $(T^{P \rightarrow P})^{\frac{1}{2}}$) relative to those expected by simply allowing for the reduction in the surface density of D2 molecules. However, the signals were smaller than those obtained for the corresponding dye density in the D2/cadmium arachidate system (where the enhancement in $(T^{P \rightarrow P})^{\frac{1}{2}}$ was by a

TABLE 8.6 Calibrated signal strengths ($10^{-27} \text{ m}^2 \text{ V}^{-2}$) obtained for the D8/cadmium arachidate and D2/D5 systems of mixed monolayers.

System	Detection Geometry	$S^{p \rightarrow p}$	$S^{s \rightarrow p}$	$S^{s \rightarrow s}$	$S^{p \rightarrow s}$
D8 /cadmium arachidate	T	1.10 ± 0.03	0.10 ± 0.02	-	0.09 ± 0.05
	R	0.26 ± 0.03	0.14 ± 0.02	-	0.12 ± 0.02
D2/D5	T	12.6 ± 0.4	0.98 ± 0.09	0.16 ± 0.02	0.04 ± 0.01
	R	1.3 ± 0.1	0.97 ± 0.09	0.10 ± 0.02	0.07 ± 0.01

factor of ~ 3.8). This could be due partially to the polar nature of D5 (if $\underline{\mu}_g$ is in the same direction for both dyes), the higher value of ϵ_2 for D5 compared to cadmium arachidate (but lower than that for D2), and the partial cancellation of the β 's of the hemicyanine molecules by those of the amidonitrostilbene. Had $\underline{\mu}_g$ been in opposite directions for D2 and D5, then the favourable influence on charge transfer would probably have resulted in greater enhancement than was in fact observed; furthermore, the β 's of the two species would have had the same direction and therefore been additive. However, the uncertainty surrounding the level of importance to attach to ϵ_2 for the diluting material means that this interpretation is only tentative.

8.6 Summary

Second harmonic generation has been observed from a variety of different monolayer and alternating multilayer LB films. Of the materials studied in homogeneous monolayer form, compounds D1 and D2 gave particularly large signals, whilst those obtained from D5 and D6 were not insignificant. The absence of any signal from monolayers of A8 and A9 is indicative that the anthracene nucleus is less suitable as a conjugated system than, for example, a stilbene bridge. In general, the effects of any in-plane anisotropy in the films were found to be negligible. When the non-linear material was deposited on both sides of a glass slide, varying the angle of incidence of the fundamental was found to produce maxima and minima in the second harmonic signal strength, arising from interference effects. For thin alternating layer films, in which coherent addition of the signals produced by each bilayer can be assumed, the square root of the second harmonic signal strength would be expected to increase linearly with the number of bilayers, and in practice this was approximately the case.

Noncentrosymmetric arrays were produced in which an active material was alternated with an inert spacer material or a second active material (whose donor and acceptor groups were reversed with respect to the hydrophobic tails, so that the second-order molecular hyperpolarizabilities of the molecules in adjacent layers added constructively). One such doubly active system consisted of the hemicyanine (D2) and amidonitrostilbene (D5) dyes; in fact the bilayer was found to be a much superior second harmonic material than is predicted by a simple addition of the β coefficients of the separate layers. The signal strengths obtained from this structure were analysed in terms of second harmonic surface susceptibilities, and the value of β obtained was $(410 \pm 140) \times 10^{-50} \text{ C}^3 \text{ m}^3 \text{ J}^{-2}$ for the first bilayer.

On diluting a monolayer of hemicyanine with cadmium arachidate, the second harmonic signals were found to be significantly enhanced. This change was attributed to changes in the charge-transfer characteristics of the dye, as well as to a more favourable film dielectric constant and possible changes in the packing of the molecules. LB monolayers of the amidonitrostilbene did not display the same effects. However, the significant SHG displayed by another material (D8) in highly diluted form suggests that heterogeneous layers may have an important role to play in improving the non-linear efficiency of LB films; a further discussion of this point is given briefly in the "suggestions for further work" section of chapter 9.

CHAPTER 9

CONCLUSIONS AND SUGGESTIONS FOR FURTHER WORK

Many organic materials are composed of molecules possessing large second-order hyperpolarizabilities (β), yet this inherent non-linearity is frequently not manifested at a macroscopic level due to a tendency for these molecules to pack in centrosymmetric crystalline structures. The Langmuir-Blodgett technique is an elegant method of assembling amphiphilic organic molecules into layers of a well defined thickness and alignment. Moreover, non-centrosymmetric supermolecular arrays may be fabricated by alternating layers of different materials; hence the method provides a means to exploit the non-linear optical properties of the individual molecules.

In general, large values of β are exhibited by molecules which contain a conjugated system of bonds, polarized by the addition of electron donor and acceptor groups. A series of such compounds has been adapted for LB film formation by the incorporation of hydrophobic tails into the molecules. The materials fall into three categories: (i) modified commercially available substances; (ii) 9,10 disubstituted anthracenes; (iii) dipolar chromophores. The water-surface monolayer and, where appropriate, LB deposition properties of all of these materials have been characterized. None of the group (i) compounds were found to give films of a satisfactory quality, and most of the anthracene derivatives were found to be too soluble in the subphase; however, several of the dipolar chromophores and two of the anthracenes could be deposited in high quality homogeneous or heterogeneous LB films.

Once the deposition of a new material had been successfully accomplished, the films were extensively characterized by a variety of techniques. Optical absorption spectra of LB films and solutions were used to determine the wavelength range over which the material could usefully be applied, and to gain an insight into the charge transfer processes occurring in the molecules. Studies of absorbance and capacitance as a function of film thickness were used to check the uniformity of deposition from one monolayer to the next, whilst surface plasmon resonance techniques were employed to estimate the relative permittivity of amidonitrostilbene layers. Several materials were assessed for bulk second-order optical non-linearity using the Kurtz powder technique, but this method proved to be inappropriate for LB film materials and was subsequently replaced by theoretical determinations of β .

The physical properties of LB films are strongly influenced by their structural order. In order to investigate this phenomenon, extensive reflection high energy and transmission electron diffraction studies have been performed on a variety of different films. C4 anthracene multilayers exhibited a high degree of crystalline order, and a detailed structural analysis of them was performed. Similarly, amidonitrostilbene monolayers displayed an exceptional level of structural order (probably stabilized by hydrogen bonding), although this was not propagated through to thicker films. By comparing the RHEED patterns obtained from various different monolayers of amidonitrostilbene, the effects of changes in the deposition conditions on the quality of the layers was shown.

The optical non-linearity of several different LB film systems was demonstrated by the observation of second harmonic generation on both

reflection from, and transmission through, the layers. Homogeneous monolayers of hemicyanine (D2) and merocyanine (D1) gave particularly large signals, whilst those obtained from the nitrostilbenes (D5 and D6) were not insignificant. Although the β of merocyanine is nearly three times that of hemicyanine (calculated as $(134 \pm 26) \times 10^{-50} \text{ C}^3 \text{ m}^3 \text{ J}^{-2}$ in Chapter 8), the dielectric constant of the former is strongly resonantly enhanced at the frequency of the second harmonic, thereby reducing the efficiency of the conversion; furthermore, the merocyanine readily undergoes protonation to a form with lower β , thereby restricting its use to basic environments. The absence of a signal from two of the anthracene derivatives was taken as an indication that, as a conjugated system intended to give rise to a large value of β , the anthracene nucleus is inferior to many other candidates, such as a stilbene bridge.

Non-centrosymmetric arrays were produced in which an active material was alternated either with an inert spacer material, such as a fatty acid, or with a second active material. In the latter case, the positions of the donor and acceptor groups in the two species were reversed, with respect to the hydrocarbon chains, so that the hyperpolarizabilities of the molecules in adjacent layers would be additive. Optical non-linearity was demonstrated in such a system for the first time by alternating the hemicyanine (D2) and amidonitrostilbene (D5) dyes. The signal strengths obtained from this structure were analysed in terms of second harmonic surface susceptibilities, and the value of β obtained for the first bilayer $[(410 \pm 140) \times 10^{-50} \text{ C}^3 \text{ m}^3 \text{ J}^{-2}]$ was much superior to that expected by the simple addition of the β coefficients of the separate layers.

Heterogeneous monolayers of hemicyanine and cadmium arachidate were found to give rise to enhanced second harmonic generation, relative to a homogeneous monolayer of the dye. This phenomenon was attributed to changes in the charge-transfer characteristics of the dye (also reflected in its absorption spectrum), accompanied by a reduction in the dielectric constant of the film and possible changes in the packing of the molecules. These findings may have important implications for improving the efficiencies of any non-linear optical device which utilises LB films.

Suggestions for further work

LB films displaying large second-order optical non-linearities should exhibit the Pockels effect (as described in chapter 2), in which the refractive index at the optical frequency is dependent on an electric field applied across the film. This phenomenon could be used in conjunction with surface plasmon resonance to produce an optical modulator.

Figure 9.1 shows a schematic diagram of such a device. An electrical contact should not be evaporated directly onto the LB film, since a metallic layer so close to the silver would be likely to interact with the evanescent field associated with the surface plasmons. One possible way of overcoming this problem is illustrated in the diagram; a Mylar washer ($\sim 10\mu\text{m}$ thick) can be used as a spacer between the LB film and an aluminium block. Electrical contact is made to the block and a region of the silver layer remote from the point of incidence of the laser beam; if a voltage is then applied, some of the field will be dropped across the air-gap, and the rest across the film. This electric field should cause a change in refractive index, which in

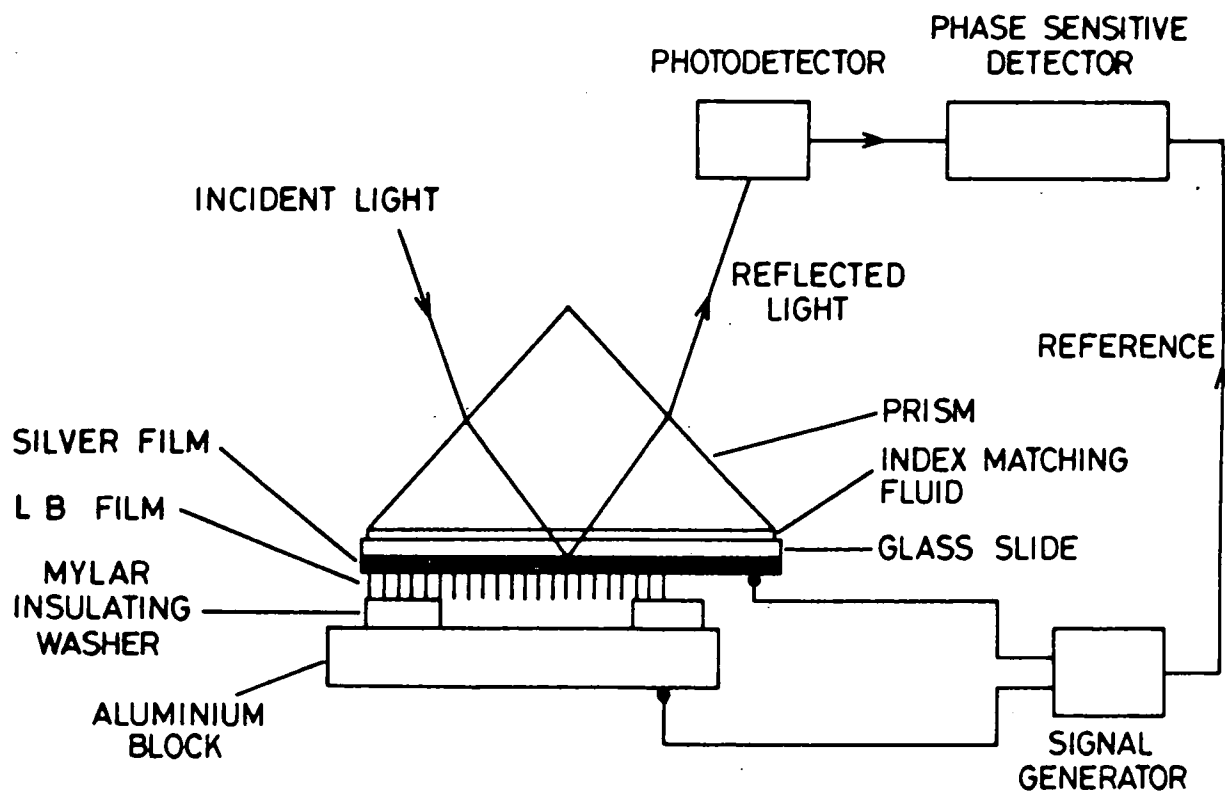
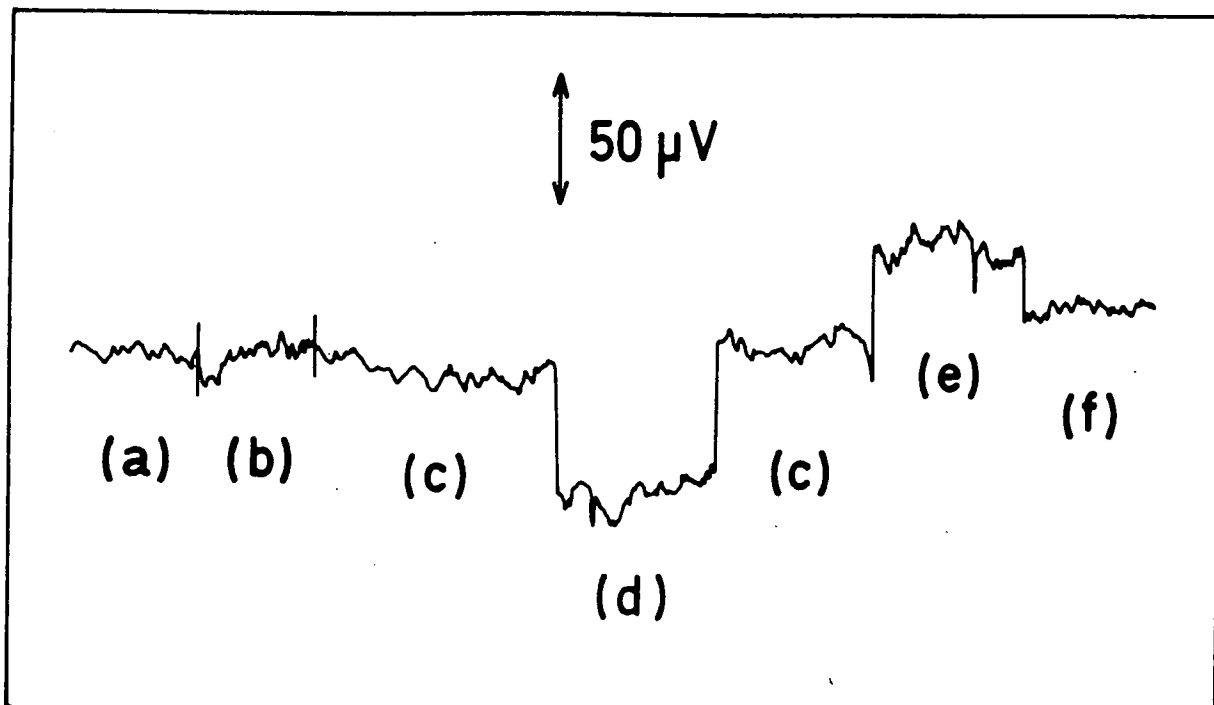


Figure 9.1

Experimental configuration for a Pockels effect modulator based on surface plasmon resonance. Inset: Phase sensitive detector output for the system (a) off resonance, incident light blocked; (b) off resonance, incident light unblocked; (c) halfway up low internal angle side of resonance curve, incident light blocked; (d) halfway up low internal angle side of resonance curve, incident light unblocked; (e) halfway up high internal angle side of resonance curve, incident light unblocked; (f) halfway up high internal angle side of resonance curve, incident light blocked.

turn will produce a shift in the resonance angle (cf. figure 6.17 in chapter 6); if the laser beam is directed at an angle corresponding to the initial resonance position, then this angle of incidence will no longer correspond to a reflectance minimum. The electric field therefore gives rise to a change in reflectance which will modulate the signal reaching the photodetector. In practice the changes in refractive index are extremely small, and therefore an a.c. voltage has to be employed, with a lock-in amplifier used as a phase sensitive detector to monitor the changes in the photodetector output occurring in phase with the applied field. A further improvement in the sensitivity can be made by positioning the laser at an angle corresponding to a point halfway up the resonance minimum, since the change in reflectance for a given shift in resonance angle will be greater at this point than at the minimum itself.

Preliminary investigations of such a modulator, incorporating three bilayers of a doubly active LB film of hemicyanine and amidonitrostilbene, are currently being undertaken in collaboration with Drs. M. C. Petty and J. P. Lloyd. A small degree of modulation has already been observed, and has been shown to be a function of the electric field applied across the film. When the angle of incidence of the laser was changed so that it corresponded to a point halfway up the other side of the resonance minimum, the output from the phase sensitive detector was reversed in sign and altered in magnitude (relative to the level with the laser light blocked off), as illustrated in figure 9.1. This was to be expected in view of the asymmetrical nature of the reflectance curve. Further experiments are required, and in particular the optimum thickness of the LB film needs to be determined; thicker films should produce a greater resonance angle shift for a given change

in refractive index (see figure 6.17), but will give rise to the deleterious effect of a broadening of the reflectance curve. Cross et al⁽¹⁾ have used a similar technique to demonstrate the linear Pockels effect in a monolayer of hemicyanine.

It is suggested that some effort be placed into the development of a computer program for the accurate curve-fitting of experimental SPR data, in order that accurate estimates of refractive index (and hence dielectric constant) can be obtained. The measurements themselves should be performed using sources of the appropriate wavelength, in case any resonance enhancement of the dielectric constants occurs at optical frequencies.

Further work is also required on the behaviour of heterogeneous LB films, following the observation of enhanced second harmonic generation from monolayers of hemicyanine in which the active dye was mixed with passive cadmium arachidate. As well as studying the effects of dilution on the non-linearity of other dyes, experiments are required in related fields; for example, to determine whether multilayers of such systems will cause greater or less scattering of light propagating in the plane of the film, compared to that which occurs in conventional, homogeneous assemblies.

The materials studied in this thesis represent a minute fraction of the interesting structures which can be envisaged, and it is anticipated that a continuation of the programme of screening will reveal many more highly efficient non-linear materials suitable for deposition in LB films. Theoretical modelling of molecules, to predict values of β prior to lengthy chemical synthesis and characterization, is likely to play an ever more important role in this process. The general requirements for a large molecular hyperpolarizability (i.e. a polarized conjugated

system) should be remembered, and some specific ideas are as follows:

- (i) Increase the conjugation length, e.g. by introducing an extra styrene unit into a stilbene bridge.
- (ii) Investigate novel strong donor and acceptor groups, such as pyrrolidine and $-\text{SO}_2\text{CF}_3$, and try to produce pairs of compounds in which the hydrocarbon tails are attached to opposite ends of the chromophore, in anticipation of forming doubly active superlattices.
- (iii) Investigate the use of more than one hydrocarbon tail per molecule, in order to bring about a better match of the cross-sectional areas of the hydrophobic and chromophore regions, and thereby improve the structural order of the films. Adjusting the positions and lengths of these substituents could also engender a degree of control over the orientation of the chromogen in the film^(2,3).

One further point on the subject of materials concerns the already characterized merocyanine (D1). The main drawback to this highly non-linear material lies in its great susceptibility to protonation (see chapter 6), a process which reduces its efficiency so greatly that it can only be used in an atmosphere of ammonia vapour. Any procedure which could render the dye stable in air would therefore be of interest. One possible way might be to deposit layers in which the material is mixed with a long chain amine (in the light of section 8.5 this is a process which might not be deleterious to its non-linearity), so that the latter component will react preferentially with any acid adsorbed by the film. Y-type multilayers of D1 mixed with docosylamine have been deposited and the dye did, indeed, display an increased lifetime in its unprotonated form, although this improvement was by only a factor of

two. A structure in which mixed layers of docosylamine and D1 were alternated with layers of pure docosylamine exhibited a further increase in stability, but the dye still became protonated eventually. Another step which may be taken is to deposit many Y-type layers of the amine on top of the alternate layer structure in the hope that any carbonic acid from the air will not penetrate through to the dye. One possible doubly active alternate layer structure could be formed by hemicyanine (D2) and mixed layers of D1/docosylamine; the dimethylamino donor group of D2 might help to stabilize the molecules of D1 (although it is uncertain whether the directions of the β 's of the two species are such as to add constructively or destructively).

In conclusion, much work remains to be performed in this field, and the future holds great promise.

CHAPTER 1- REFERENCES

1. Williams, D. J., *Angew. Chem. Int. Ed. Engl.*, 23, 690 (1984).
2. Zyss, J., *J. Molec. Electron.*, 1, 25 (1985).
3. Roberts, G. G., *Contemp. Phys.*, 23, 109 (1984).

CHAPTER 2 - REFERENCES

1. Harper, P. G., Wherrett, B. S. (Eds.), "Non-linear Optics", Proceedings of the 16th Scottish Universities Summer School in Physics (1975), Academic Press.
2. Hecht, E., Zajac, A. "Optics", Addison-Wesley (1974).
3. Yariv, A., "Introduction to Optical Electronics", 2nd Edition, Holt, Rinehart and Winston (1976).
4. Butcher, P. N., "N. L. O. Phenomena", Ohio State University (1965).
5. Garito, A. F., Singer, K. D., *Laser Focus*, 80, 59 (1982).
6. Garito, A. F., Singer, K. D., Teng, C. C., in "Non-linear optical properties of organic and polymeric materials", Ed. Williams, D. J., ACS Symposium Series 233, Washington (1983).
7. Williams, D. J., *Angew. Chem. Int. Ed. Engl.*, 23, 690 (1984).
8. Zyss, J., Chemla, D. S., Nicoud, J. F., *J. Chem. Phys.*, 74 (9), 4800 (1981).
9. Oudar, J. L., Zyss, J., *Phys. Rev. A*, 26 (4), 2016 (1982).
10. Zyss, J., Oudar, J. L., *Phys. Rev. A*, 26 (4), 2028 (1982).
11. Badan, J., Hierle, R., Périgaud, A., Zyss, J., in "Non-linear optical properties of organic and polymeric materials", Ed. Williams, D. J., ACS Symposium Series 233, Washington (1983).
12. Twieg, R. J., Jain, K., in "Non-linear optical properties of organic and polymeric materials", Ed. Williams, D. J., ACS Symposium Series 233, Washington (1983).
13. Oudar, J. L., Chemla, D. S., *Opt. Commun.*, 13, 164 (1975).
14. Oudar, J. L., Le Person, H., *Opt. Commun.*, 15, 258 (1975).
15. Fabian, J., Hartmann, H., "Light absorption of organic colorants", Springer-Verlag, New York (1980).
16. Griffiths, J., "Colour and constitution of organic molecules", Academic Press (1976).
17. Kitaigorodsky, A. I., "Molecular crystals and molecules", Academic Press, New York (1973).

18. Nayar, B. K., in "Non-linear optical properties of organic and polymeric materials", Ed. Williams, D.J., ACS Symposium Series 233, Washington (1983).
19. Meredith, G. R., in "Non-linear optical properties of organic and polymeric materials", Ed. Williams, D. J., ACS Symposium Series 233, Washington (1983).
20. Zyss, J., J. Non-Crystalline Solids, 47 (2), 211 (1982).
21. Oudar, J. L., Hierle, R., J. App. Phys., 48 (7), 2699 (1977).
22. Sigelle, M., Zyss, J., Hierle, R., J. Non-Crystalline Solids, 47 (2), 287 (1982).
23. Bass, M., Bua, D., Mozzi, R., Monchamp, R. R., Appl. Phys. Lett., 15, 393 (1969).
24. Smith, P. W., Tomlinson, W. J., IEEE Spectrum, June 1981, 26.

CHAPTER 3 - REFERENCES

1. Gaines, G. L., Insoluble monolayers at liquid-gas interfaces, Wiley (1966).
2. Barraud, A., Rosilio, C., Raudel-Textier, A., J. Coll. Int. Sci., 62, 509 (1977).
3. Barraud, A., Thin Solid Films, 99, 317 (1983).
4. Veale, G., Peterson, I. R., J. Coll. Int. Sci., 103, 178 (1985).
5. Tieke, B., Wegner, G., Naegele, D., Rinsdorf, H., Angew. Chem. Int. Ed. Engl., 15, 764 (1976).
6. Simpson, W. H., Reucroft, P. J., Thin Solid Films, 6, 167 (1970).
7. Procarione, W. L., Kaufman, J. W., Chem. Phys. Lipids, 12, 251 (1974).
8. Wei, L. Y., Woo, B. Y., Biophys. J., 13, 215 (1973).
9. Vincett, P. S., Barlow, W. A., Boyle, F. T., Finney, J. A., Roberts, G. G., Thin Solid Films, 60, 265 (1979).
10. Baker, S., Petty, M. C., Roberts, G. G., Twigg, M. V., Thin Solid Films, 99, 53 (1983).
11. Baker, S., Roberts, G. G., Petty, M. C., IEE Proc., 130-I, 260 (1983).
12. Hua, Y. L., Roberts, G. G., Ahmad, M. M., Petty, M. C., Hanack, M., Rein, M., Phil. Mag. B, 53, 105 (1986).
13. Sugi, M., Saito, M., Fukui, T., Iizima, S., Thin Solid Films, 88, L15 (1982).

14. Girling, I. R., Cade, N. A., Kolinsky, P. V., Earls, J. D., Cross, G. H., Peterson, I. R., *Thin Solid Films*, 132, 101 (1985).
15. Holcroft, B., Petty, M. C., Roberts, G. G., Russell, G. J., *Proc. 2nd International Conference on LB Films, Thin Solid Films*, 134, 83 (1985).
16. Fukuda, K., Nakahara, H., Kato, T., *J. Coll. Int. Sci.*, 54, 430 (1976).
17. Ahmad, M. M., Feast, W. J., Neal, D. B., Petty, M. C., Roberts, G. G., *J. Molec. Elec.*, in press.
18. Heesemann, J., *J.A.C.S.*, 102, 2167 (1980).
19. Gaines, G. L., *Anal. Chem.*, 48; 450 (1976).
20. Blodgett, K. B., Langmuir, I., *Phys. Rev.*, 51, 964 (1937).
21. Möbius, D., Blücher, H., 'Physical methods of chemistry', Weissberger, A., Rossiter, B. (Eds.), Wiley.
22. Fromherz, P., *Rev. Sci. Inst.*, 46, 1380 (1975).
23. Roberts, G. G., Vincett, P. S., Barlow, W. A., *Phys. Technol.*, 12, 69 (1981).
24. Langmuir, I., *J.A.C.S.*, 39, 1848 (1917).
25. Blodgett, K. B., *J.A.C.S.*, 57, 1007 (1935).
26. Allara, D., Swalen, J. D., *J. Phys. Chem.*, 86, 2700 (1982).
27. Brundle, C. R., Hopster, H., Swalen, J. D., *J. Chem. Phys.*, 70, 5190 (1979).
28. Mori, C., Noguchi, H., Mizuno, M., Watanabe, T., *Jap. J. Appl. Phys.*, 19, 725 (1980).
29. Peterson, I. R., Russell, G. J., Roberts, G. G., *Thin Solid Films*, 109, 371 (1983).
30. Peterson, I. R., Russell, G. J., Neal, D. B., Petty, M. C., Roberts, G. G., Ginnai, T., *Phil. Mag. B*, 54, 71 (1986).
31. Vincett, P. S., Barlow, W. A., *Thin Solid Films*, 71, 305 (1980).
32. Matsuda, A., Sugi, M., Fukui, T., Iizima, S., *J. App. Phys.*, 48, 771 (1977).
33. Nicklow, R. M., Pomerantz, M., Segmuller, A., *Phys. Rev.*, B23, 1081 (1981).
34. Russell, G. J., Petty, M. C., Peterson, I. R., Roberts, G. G., Lloyd, J. P., Kan, K. K., *J. Mat. Sci. Letts.*, 3, 25 (1984).

35. Roberts, G. G., Vincett, P. S., Barlow, W. A., J. Phys. C, 11, 2077 (1978).
36. Peterson, I. R., Thin Solid Films, 116, 357 (1984).
37. Roberts, G. G., Pande, K. P., Barlow, W. A., Solid State Electron. Dev., 2, 169 (1978).
38. Roberts, G. G., Petty, M. C., Caplan, P. J., Poindexter, E. H., Proc. INFOS Conf. Eindhoven, North-Holland, 20 (1983).
39. Peterson, I. R., IEE Proc., 130-I, 252 (1983).
40. Pitt, C. W., Walpita, L. M., Electrocomponent Sci. and Tech., 3, 191 (1977).
41. Roberts, G. G., McGinnity, T. M., Barlow, W. A., Vincett, P. S., Solid State Commun., 32, 683 (1979).
42. Kuhn, H., Thin Solid Films, 99, 1 (1983).
43. Franks, N. P., Snook, K. A., Thin Solid Films, 99, 139 (1983).
44. Roberts, G. G., Advances in Physics, 34, (1985).
45. Nayar, B. K., in "Non-linear optical properties of organic and polymeric materials", Ed. Williams, D. J., ACS Symposium Series 233, Washington (1983).
46. Zyss, J., J. Molec. Electron., 1, 25 (1985).
47. Pitt, C. W., Walpita, L. M., Electron. Lett., 12, 479 (1976).
48. Pitt, C. W., J. Non-Crystalline Solids, 47, 159 (1982).
49. Vickers, A. J., Tredgold, R. H., Hodge, P., Khoshdel, E., Girling, I. R., Thin Solid Films, 134, 43 (1985).
50. Kajzar, F., Messier, J., Thin Solid Films, in press.
51. Kajzar, F., Messier, J., Zyss, J., Ledoux, I., Optics Commun., 45, 133 (1983).
52. Carter, G. M., Chen, Y. J., Tripathy, S. K., Appl. Phys. Lett., 43, 891 (1983).
53. Carter, G. M., Chen, Y. J., Tripathy, S. K., in "Non-linear optical properties of organic and polymeric materials", Ed. Williams, D. J., ACS Symposium Series 233, Washington (1983).
54. Girling, I. R., Cade, N. A., Kolinsky, P. V., Montgomery, C. M., Electron. Lett., 21, 169 (1985).
55. Girling, I. R., Kolinsky, P. V., Cade, N. A., Earls, J. D., Peterson, I. R., Optics Commun., 55, 289 (1985).

56. Aktsipetrov, O. A., Akhmediev, N. N., Mishina, E. D., Novak, V. R., JETP Lett., 37, 207 (1983).
57. Aktsipetrov, O. A., Akhmediev, N. N., Baranova, I. M., Mishina, E. D., Novak, V. R., Pis'ma Zh. Tekh. Fiz., 11, 599 (1985).
58. Aktsipetrov, O. A., Akhmediev, N. N., Baranova, I. M., Mishina, E. D., Novak, V. R., Sov. Phys. JETP, 62, 524 (1985).
59. Chen, Z., Chen, W., Zheng, J., Wang, W., Zhang, Z., Optics Commun., 54, 305 (1985).
60. Rasing, T., Shen, Y. R., Kim, M. W., Valint, P., Bock, J., Phys. Rev. A, 31, 537 (1985).
61. Chollet, P. A., Kajzar, F., Messier, J., Thin Solid Films, 132, 1 (1985).
62. Blinov, L. M., Davydova, N. N., Lazarev, V. V., Yudin, S. G., Sov. Phys. Solid State, 24, 1523 (1982).
63. Blinov, L. M., Dubinin, N. V., Mikhnev, L. V., Yudin, S. G., Thin Solid Films, 120, 161 (1984).

CHAPTER 4 - REFERENCES

1. Batey, J., Ph.D. Thesis, Durham University (1983).
2. Pockrand, I., Swalen, J. D., Gordon II, J. G., Philpott, M. R., Surface Science, 74, 237 (1977).
3. See for example, Pockrand, I., Swalen, J. D., Santo, R., Brillante, A., Philpott, M. R., J. Chem. Phys., 69 (9), 4001 (1978).
4. Raether, H., Physics of Thin Films, 9, 145 (1977).
5. Walkenhorst, W., Nature, 34, 373 (1947).
6. Zingsheim, H. P., Scanning Electron Microscopy, 1, 357 (1977).
7. Kurtz, S.K., Perry, T. T., J. Appl. Phys., 39, 3798 (1968).
8. Williams, D. J., Angew. Chem. Int. Ed. Engl., 23, 690 (1984).
9. See for example, Williams, D.J. (Ed.), "Non-linear Optical Properties of Organic and Polymeric Materials", ACS Symposium Series 233, Washington, D.C. (1983).
10. Presley, R. J. (Ed.) : "Handbook of Lasers", Chemical Rubber Co., Cleveland Ohio, 493 (1971).

CHAPTER 5 - REFERENCES

1. Roberts, G. G., McGinnity, T. M., Barlow, W. A., Vincett, P. S., Thin Solid Films, 68, 223 (1980).

2. Gaines, G. L., "Insoluble monolayers at liquid-gas interfaces", Wiley (1966).
3. Kuhn, H., Möbius, D., Blücher, H., "Spectroscopy of monolayer assemblies", in Physical Methods of Chemistry, Weissberger, A., Rossiter, B. (Eds.), 1, Part 3b, Wiley (1972).
4. Vincett, P. S., Barlow, W. A., Boyle, F. T., Finney, J. A., Roberts, G. G., Thin Solid Films, 60, 265 (1979).
5. Levine, B. F., Bethea, C. G., Wasserman, E., Leenders, L., J. Chem. Phys., 68 (11), 5042 (1978).
6. Dulcic, A., Flytzanis, C., Optics Commun., 25, 402 (1978).
7. Gaines, G. L., Anal. Chem., 48, 450 (1976).
8. Daniel, M. F., Smith, G. W., Mol. Cryst. Liq. Cryst., 102 (6-7), 193 (1984).

CHAPTER 6 - REFERENCES

1. Williams, D. J., Angew. Chem. Int. Ed. Engl. 23, 690 (1984).
2. Twieg, R. J., Jain, K., in "Non-linear optical properties of organic and polymeric materials", Ed. Williams, D. J., ACS Symposium Series 233, Washington, D.C. (1983).
3. Griffiths, J., "Colour and constitution of organic molecules", Academic Press (1976).
4. Baker, S., Ph.D. Thesis, University of Durham (1985).
5. Penner, T. L., Möbius, D., Thin Solid Films, 132, 185 (1985).
6. Gaines, G. L., Anal. Chem., 48, 450 (1976).
7. Levine, B. F., Bethea, C. G., Wasserman, E., Leenders, L., J. Chem. Phys., 68, 5042 (1978).
8. Dulcic, A., Chem. Phys., 37, 57 (1979).
9. Davidson, S. J., Jencks, W. P., J.A.C.S., 91, 225 (1969).
10. Daniel, M. F., Smith, G. W., Mol. Cryst. Liq. Cryst., 102 (6-7), 193 (1984).
11. Mooney, W. F., Brown, P. E., Russell, J. C., Costa, S. B., Pedersen, L. G., Whitten, D. G., J.A.C.S., 106, 5659 (1984).
12. For example: Kuhn, H., Möbius, D., Bucher, H., "Spectroscopy of monolayer assemblies", in A. Weissberger and B. Rossiter (Eds.), Physical Methods of Chemistry, 1, Part 3b, Wiley (1972).
13. Zernike, F., Midwinter, J. E., "Applied Non-linear Optics", Wiley (1973).
14. Oudar, J. L., Zyss, J., Phys. Rev. A, 26, 2016 (1982).

CHAPTER 7 - REFERENCES

1. Peterson, I. R., Russell, G. J., *British Polymer Journal*, 17, 364 (1985).
2. Peterson, I. R., *Thin Solid Films*, 116, 357 (1984).
3. Vincett, P. S., Barlow, W. A., *Thin Solid Films*, 71, 305 (1980).
4. For example: Fukuda, K., Shiozawa, T., *Thin Solid Films*, 68, 55 (1980).
5. Bonnerot, A., Chollet, P. A., Frisby, H., Hoclet, M., *Chem. Phys.*, 97, 365 (1985).
6. Fryer, J. R., Hann, R. A., Eyres, B. L., *Nature*, 313, 382 (1985).
7. Russell, G. J., Petty, M. C., Peterson, I. R., Roberts, G. G., Lloyd, J. P., Kan, K. K., *J. Mat. Sci. Letts.*, 3, 25 (1984).
8. Peterson, I. R., Russell, G. J., *Phil. Mag. A*, 49, 463 (1984).
9. Barrett, C. S., Massalski, T. B., "Structure of Metals", 3rd Ed., Pergamon (1980).
10. Cullity, B. D., "Elements of X-ray Diffraction", 2nd Ed., Addison-Wesley (1978).
11. For example: Tredgold, R. H., Vickers, A. J., Hoorfar, A., Hodge, P., Khoshdel, E., *J. Phys. D*, 18, 1139 (1985).
12. Earls, J. D., Peterson, I. R., Russell, G. J., Girling, I. R., Cade, N. A., *J. Molec. Electron.*, in press.
13. Daniel, M. F., Hart, J. T. T., *J. Molec. Electron.*, 1, 97 (1985).

CHAPTER 8 - REFERENCES

1. Presley, R. J. (Ed.): "Handbook of Lasers", Chemical Rubber Co., Cleveland Ohio, 493 (1971).
2. Kraus, J. D., Carver, K. R., "Electromagnetics", 2nd Ed., McGraw-Hill Kogakusha, 393 (1973).
3. Girling, I. R., Cade, N. A., Kolinsky, P. V., Montgomery, C. M., *Electron. Letts.*, 21, 169 (1985).
4. Neal, D. B., Petty, M. C., Roberts, G. G., Ahmad, M. M., Feast, W. J., Girling, I. R., Cade, N. A., Kolinsky, P. V., Peterson, I. R., *Electron. Letts.*, 22, 460 (1986) - see appendix 4.
5. Girling, I. R., Cade, N. A., Kolinsky, P. V., Earls, J. D., Cross, G. H., Peterson, I. R., *Thin Solid Films*, 132, 101 (1985).
6. Girling, I. R., Kolinsky, P. V., Cade, N. A., Earls, J. D., Peterson, I. R., *Optics Commun.*, 55, 289 (1985).

7. Zyss, J., J. Molec. Electron., 1, 25 (1985).
8. Hecht, E., Zajac, A., "Optics", Addison-Wesley (1974).
9. Petty, M. C., in "Langmuir-Blodgett Films", Ed. Roberts, G. G., Plenum Press.
10. Aktsipetrov, O. A., Akhmediev, N. N., Mishina, E. D., Novak, V. R., JETP Lett., 37, 207 (1983).

CHAPTER 9 - REFERENCES

1. Cross, G. H., Girling, I. R., Peterson, I. R., Cade, N. A., submitted to Electron. Letts.
2. Fukuda, K., Nakahara, H., Kato, T., J. Coll. Int. Sci., 54, 430 (1976).
3. Nakahara, H., Fukuda, K., Thin Solid Films, 99, 45 (1983).

APPENDICES

Publications

- A1. Peterson, I. R., Russell, G. J., Neal, D. B., Petty, M. C., Roberts, G. G., Ginnai, T., Hann, R. A., "An electron diffraction study of LB films prepared from a lightly substituted anthracene derivative", *Phil. Mag. B*, 54, 71 (1986).
- A2. Ahmad, M. M., Feast, W. J., Neal, D. B., Petty, M. C., Roberts, G. G., "4-n-heptadecylamido-4'-nitrostilbene, a new LB film material for non-linear optics", *J. Molec. Electron.*, in press.
- A3. Neal, D. B., Russell, G. J., Petty, M. C., Roberts, G. G., Ahmad, M. M., Feast, W. J., "A highly ordered Langmuir-Blodgett monolayer of an amidonitrostilbene", *J. Molec. Electron.*, in press.
- A4. Neal, D. B., Petty, M. C., Roberts, G. G., Ahmad, M. M., Feast, W. J., Girling, I. R., Cade, N. A., Kolinsky, P. V., Peterson, I. R., "Second harmonic generation from LB superlattices containing two active components", *Electron. Letts.*, 22, 460 (1986).
- A5. Neal, D. B., Petty, M. C., Roberts, G. G., Ahmad, M. M., Feast, W. J., Girling, I. R., Cade, N. A., Kolinsky, P. V., Peterson, I. R., "Langmuir-Blodgett films for non-linear optics", *Proc. IEEE Int. Symp. Appl. Ferroelectrics*, Lehigh University, 1986.

An electron diffraction study of LB films prepared from a lightly substituted anthracene derivative

By I. R. PETERSON†, G. J. RUSSELL, D. B. NEAL, M. C. PETTY, G. G. ROBERTS‡
and T. GINNAI§

Department of Applied Physics and Electronics, University of Durham,
South Road, Durham DH1 3LE, England

and R. A. HANN

Imperial Chemical Industries plc, Electronics Group,
P.O. Box 11, Runcorn, Cheshire WA7 4QE, England

[Received 27 January 1986 and accepted 20 March 1986]

ABSTRACT

Both reflection and transmission high-energy electron diffraction patterns obtained from Langmuir-Blodgett (LB) films of a lightly substituted anthracene derivative are interpreted in terms of a quasi-crystalline molecular packing, or secondary structure, which is consistent with the known primary structure of the molecule. The unit cell is orthorhombic, contains four molecules and probably has space group *Pba*2. The long axis of the aromatic nucleus lies at an angle of $60 \pm 1^\circ$ to the substrate normal in the LB film.

§ 1. INTRODUCTION

1.1. *Molecular electronic applications of LB films*

Many proposed applications of organic molecules in high-performance information-processing technologies involve conjugated molecules arranged into a stable organized structure with nanometre precision (Aviram and Ratner 1974, Carter 1983, Kuhn 1983, Williams 1984). The LB technique (Gaines 1966, Roberts 1985) is one of the few methods for fabricating such a structure. However the molecules of most existing LB film materials are not of the required type, being dominated by a large saturated moiety. In some applications, such as non-linear optics (Kajzar, Messier and Zyss 1983, Girling, Kolinsky, Cade, Earls and Peterson 1985), this merely results in a dilution of the active part of the molecule without completely destroying the desired effect. However in applications involving the transport of charge or excitations, it has a drastic and deleterious effect on the exchange integral for hopping between active centres. This accounts for the great interest shown recently in LB films of lightly substituted porphyrins (Jones, Tredgold and Hoorfar 1984) and phthalocyanines

† Present address: GEC Research Laboratories, Hirst Research Centre, East Lane, Wembley, Middlesex HA9 7PP, England.

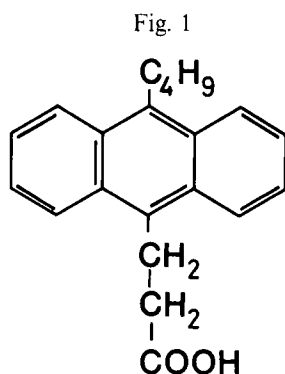
‡ Present address: Department of Engineering Science, University of Oxford, Oxford OX1 3PJ, England.

§ Present address: Molecular Electronics Corp., 4030 Spencer Street, MS 108, Torrance, California 90503-2417, U.S.A.

(Batey, Petty, Roberts and Wright 1984, Baker, Petty, Roberts and Twigg 1983). Unfortunately, several structural studies (Vickers 1984, Tredgold, Vickers, Hoorfar, Hodge and Khoshdel 1985) have revealed that thick films of porphyrins recrystallize rapidly after deposition and display little trace of the organized anisotropic layer structure required. One LB film material which is known to exhibit significant conductivity and, in addition, to retain its as-deposited layer structure is 9-butyl-10-anthrylpropionic acid, otherwise known as C4 anthracene (Roberts, McGinnity, Barlow and Vincett 1980, Roberts and McGinnity 1979) the molecular form of which is shown in fig. 1. In addition to these desirable properties its films have long-range orientational order (M. F. Daniel, 1985, personal communication) and good electrical properties (Roberts *et al.* 1980). Furthermore, the water surface monolayer is much more fluid than typical aromatic LB film materials and is capable of deposition rates of $80 \mu\text{m s}^{-1}$ (Vincett, Barlow, Boyle, Finney and Roberts 1979) without the addition of the 'lubricants' necessary with other lightly substituted aromatics (Baker *et al.* 1983, Schoeler, Tews and Kuhn 1974).

These benefits of C4 anthracene are to some extent offset by slight solubility of the monolayer on the water surface, and by its tendency to oxidize to anthraquinone. The latter fact makes it desirable to exclude ultraviolet radiation during the deposition procedure, and means that devices such as electroluminescent displays (Roberts *et al.* 1980) and novel, inexpensive thin-film switches (Roberts 1985) must be hermetically sealed. An understanding of the relationships between its structure and properties might lead to the development of an alternative material with similar electronic and water-surface behaviour but with greater stability under ambient conditions. A study of some aspects of the film structure has been published (Vincett and Barlow 1980). However the techniques employed in that investigation were not capable of determining the molecular orientation within the film to a high degree of precision or of distinguishing between different possible space groups. In the model proposed by Vincett and Barlow, the unit cell combined two molecules located in adjacent monolayers and the long axis of the anthracene nucleus was tilted at $55 \rightarrow 65^\circ$ to the substrate normal.

The present study is based on high-energy electron diffraction patterns obtained from LB films of C4 anthracene. These were recorded both in transmission (TED) and reflection (RHEED) and they provide significantly more information about the film structure than has been reported previously. Firstly, they enable the crystalline



Primary structure of C4 anthracene molecule.

symmetry to be determined and, secondly, they can be used to establish the orientation of the rigid moieties with respect to the crystalline axes (Earls, Peterson, Russell, Girling and Cade 1986).

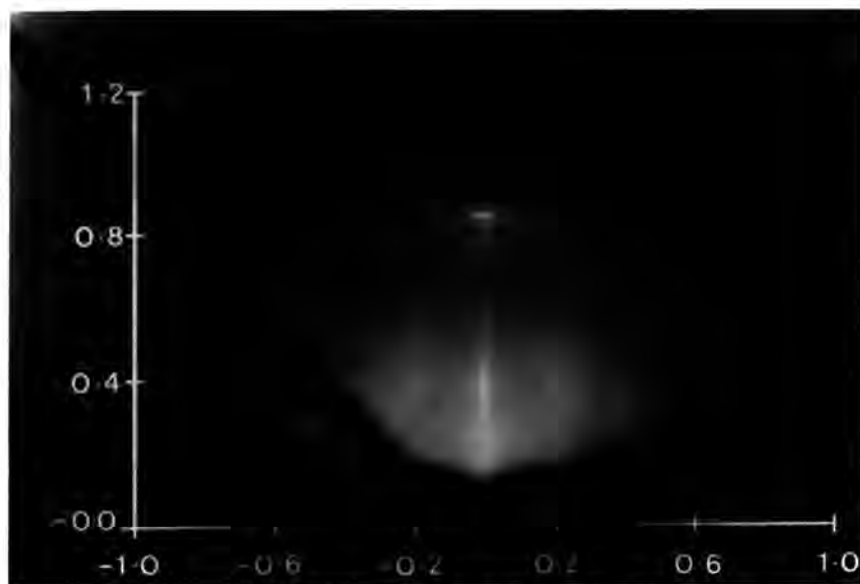
§2. EXPERIMENTAL

The C4 anthracene LB films were deposited in the manner described by Roberts *et al.* (1980). For the RHEED studies, single-crystal silicon substrates were used after refluxing in propan-2-ol over a period of several hours and LB films of 11 layers thickness were examined. Films for TED investigation were deposited on alumina substrates prepared by the Walkenhorst-Zingsheim technique (Walkenhorst 1947, Zingsheim 1977). Both the TED and RHEED studies were made using a JEM 120 transmission electron microscope operated at either 80 or 100 kV. Ealing CPK molecular models were used in the packing simulations.

§3. RESULTS

Figure 2 shows the RHEED pattern of an 11-layer film of C4 anthracene on a silicon substrate. (The labelled axes have been added to facilitate the subsequent discussion.) The diffraction spots on the central normal to the substrate lie on rings of lower intensity. Parallel to this central row of spots and symmetrically displaced to either side of it is a series of diffracted streaks of intensity. Figure 2 differs from RHEED patterns of other LB film materials (Bonnerot, Chollet, Frisby and Hoclet 1985, Garoff, Deckman, Dunsmuir and Alvarez 1986, Peterson and Russell 1984) in that the spots are unusually well defined and the central row of spots displays the fine splitting expected from the bilayer periodicity.

Fig. 2



80 kV RHEED pattern of an 11-layer LB film of C4 anthracene on silicon (labelled axes with scale identical to that in fig. 4).

The TED pattern recorded from a 25-layer LB film on a thin alumina substrate is shown in fig. 3. This displays well-defined spots which may be ascribed to a single crystalline grain as it exhibits rectangular in-plane symmetry. There appear to be systematic absences along both of the main axes and the positions of two of these are indicated by the arrows labelled S. The pattern can be indexed as arising from an orthorhombic structure with the beam incident along the [001] axis and Miller indices are applied to two of the spots in accordance with this assignment.

§4. DISCUSSION

4.1. Unit cell determination

On the assumption that the diffraction streaks seen in the RHEED pattern extend to the shadow edge of the sample, the distance of each streak from the centre of the pattern should correspond to the radius of one of the spots in the TED pattern. This comparison is given in the table, in which the Miller indices have been assigned on the basis of the rectangular symmetry exhibited by the TED pattern and where $a < b < c$. Inspection of this table confirms the very good agreement between the results obtained using the two different modes of diffraction and the film structure is similar on both Al_2O_3 and SiO_2 substrates.

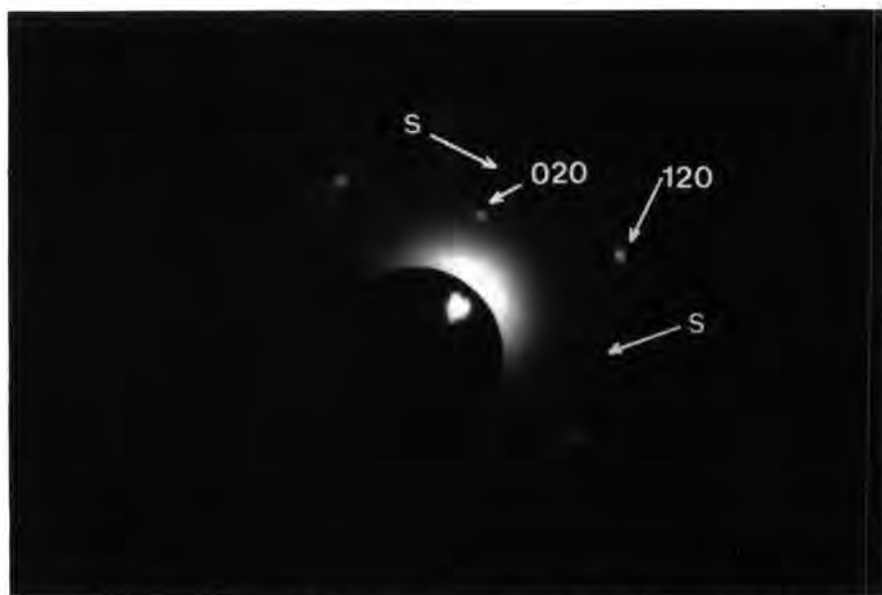
The unit cell can be deduced from the data given in the table together with the additional d -spacings obtained from the diffraction spots lying on the central normal in the RHEED pattern (fig. 2). This cell is orthorhombic and has the following lattice parameters:

$$a = 0.51 \text{ nm}$$

$$b = 1.54 \text{ nm} \quad \alpha = \beta = \gamma = 90^\circ.$$

$$c = 2.45 \text{ nm}$$

Fig. 3



100 kV TED pattern of a 25-layer LB film of C4 anthracene. (The arrows labelled S indicate the positions of systematic absences on the [100] and [010] axes.)

Comparison of TED and RHEED data for $(hk0)$ d -spacings.

Miller indices	d -spacings (nm) (TED pattern)	d -spacings (nm) (RHEED pattern)
(020)	0.775	—
(100)	0.500†	0.505
(110)	0.490	0.485
(120)	0.430	0.420
(040)	0.385	0.390
(130)	0.365	0.360
(140)	0.295‡	0.295
(200)	0.250‡	0.245

† Systematic absence—inferred value.

‡ Value deduced from extrapolation.

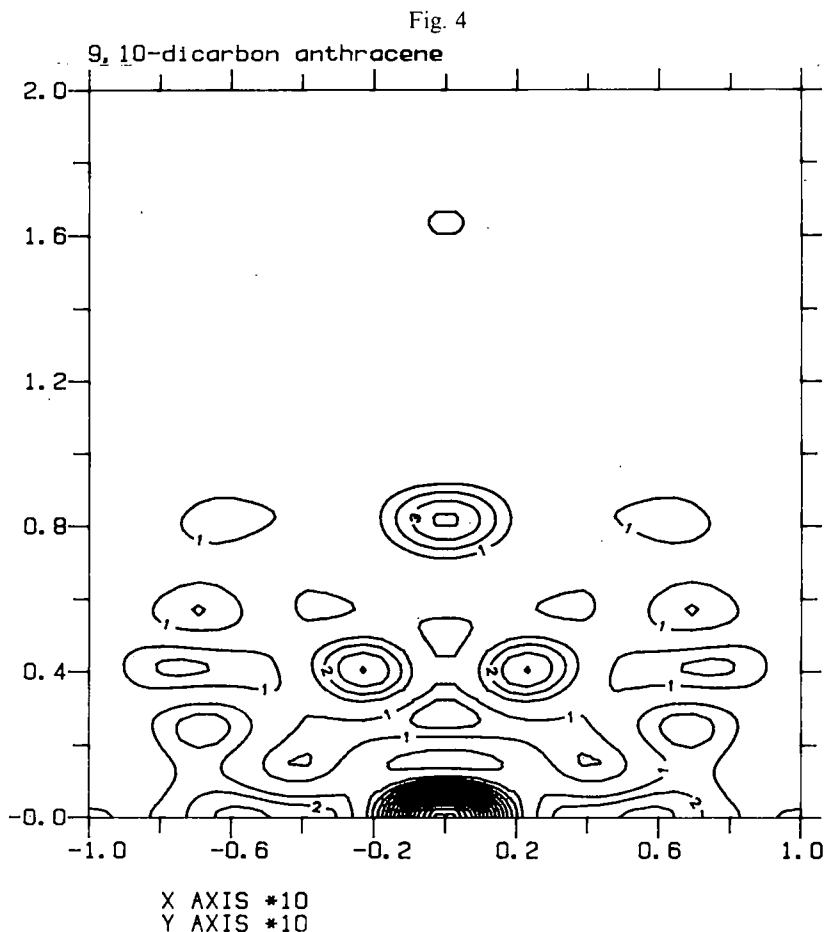
The area per unit cell in the substrate plane (ab) is 0.78 nm^2 . Comparison with the area per molecule of $\sim 0.40 \text{ nm}^2$ in the monolayer at the collapse point (Vincett *et al.* 1979) indicates that the unit cell contains two molecules in any cross-section and, since it extends over two layers, it consists of a total of four molecules.

4.2. Molecular orientation within the unit cell

In a previous paper we have shown that it is possible to deduce the orientation of rigid moieties in an LB film without carrying out a complete structure determination (Earls *et al.* 1986). The method involves comparison of the experimentally determined RHEED pattern (fig. 2 in this case) with a computer-generated intensity distribution of the diffraction pattern of a single moiety. Reasonable values for bond lengths, angles and atomic scattering factors for this moiety were chosen (Kitaigorodskii 1961, West and Astle 1980, Vainshtein 1964) and were used to compute the intensity distribution shown in fig. 4. This distribution is plotted on the same scale as fig. 2 to facilitate comparison. It is important to note that not all of the atoms in the molecule have been included in the computation, but the combined low-angle scattering factor for the moiety considered in this particular case is more than 1.4 times that of the remaining ones. Further the moiety is expected to display more spatial periodicity so that the features of the pattern will be dominated by it.

There are two possible matches between the experimental pattern and the computed distribution. In the first of these, the computed peak in intensity near $(0, 8)$ is identified with the bright spot in the experimental pattern at $(0, 8.2)$ and the computed peaks near $(\pm 2, 4)$ with the patches of intensity centred on coordinates $(\pm 2.4, 4)$ in fig. 2. This match is consistent with tilt angles ψ of the anthracene long axis to the substrate normal in the range $0 \rightarrow 13^\circ$. The broad nature of the computed peaks, the fourfold degeneracy of most of the streaks in the RHEED pattern and the presence of four molecules within the unit cell make it difficult to deduce any other details about the molecular orientation or to determine ψ more accurately.

There is a second good match at $\psi = 60 \pm 1^\circ$. This arises from the hexagonal symmetry of graphite from which the anthracene molecule may be considered to be derived. This match corresponds to the range of ψ from $55 \rightarrow 65^\circ$ which was previously reported for C4 anthracene by Vincett and Barlow (1980). Again it is difficult to determine other aspects of the molecular orientation.



Computer-generated diffracted intensity distribution for the beam incident normal to the anthracene nucleus with its long axis vertical (compare with fig. 2).

4.3. Stereochemistry and symmetry considerations

On the basis of Kitaigorodskii's theory of packing of molecular crystals (Kitaigorodskii 1973), it is possible to exclude the presence of mirror planes as, in all practical situations, these may be replaced by glide planes to achieve denser packing. In addition, the known orientation of amphiphilic molecules by dispersion, dipolar and hydrogen bonding forces in LB films, leads to the exclusion of certain symmetry elements which would imply the presence of oppositely oriented molecules within the same monolayer. These include n -type glide planes in the (100) and (010) orientations and 2_1 screw axes in the [001] orientation.

Further information may be obtained from a consideration of systematic absences such as those indicated by arrows labelled S in the TED pattern of fig. 3. The condition for allowed reflections along the $[h00]$ axis is $h = 2n$ and along the $[0k0]$ axis is $k = 2n$, where n is an integer. There are no systematic absences apparent along the $[00l]$ axis (the central normal row of spots) in the RHEED pattern of fig. 2. On its own this observation is inconclusive because of the greater likelihood of double diffraction in this case. However it is consistent with the result of earlier shallow-angle X-ray scattering studies of this material (Vincett and Barlow 1980).

The relationship between the observed systematic absences and the translational symmetry operators giving rise to them has been tabulated for the orthorhombic system crystal by Henry, Lipson and Wooster (1960). Taken in conjunction with the experimental observations, this implies the presence of only *a*- and *b*-type glide planes in the (010) and (001) orientations respectively and excludes the possibility of the presence of screw axes. Considering all of these restrictions, only one acceptable space group remains and this is *Pba2* (Henry and Lonsdale 1952).

Having determined the space group, it is now possible to return to much more specific stereochemical considerations in order to establish which of the two previously mentioned ranges of molecular tilt is valid. As the 0.34 nm van der Waals thickness of the aromatic nucleus is the only molecular dimension smaller than the 0.51 nm *a* lattice parameter, the one-dimensional 'chains' of molecules separated by this distance must be in close, face-to-face contact with no intervening molecules. A 'chain' with 0.51 nm spacing and a molecular tilt angle ψ in the range $0 \rightarrow 13^\circ$ is possible if the projection of **a** onto the aromatic plane is parallel to its short axis. However, consideration of three-dimensional models shows that there is no obvious correspondence of 'bumps' and 'hollows' as is required for a stable packing (Kitaigorodskii 1961). To fit the resulting molecular chains into the observed unit-cell dimensions requires *n*-type glide planes in the (100) orientation so that the two non-equivalent sets of molecules in the monolayer are at different distances from the water or substrate surface. Hence, for these reasons, it is possible to reject the structure with a value of ψ in the range $0 \rightarrow 13^\circ$.

Only one possible range of molecular tilt remains, namely $\psi \cong 60^\circ$. Models of such 'chains' can be built with the projection of the unit-cell vector **a** onto the aromatic plane lying almost parallel to its long axis. With a repeat spacing of 0.51 nm, the alkyl sidechains of adjacent molecules are in van der Waals contact, so that this corresponds to a local energy minimum. These chain models have been stacked to form a bulk packing with *Pba2* orthorhombic symmetry and it has been shown that the unit-cell parameters can be adjusted to correspond to the observed values. Hence this packing provides a unique fit to the experimental results.

Close inspection of the bulk-packing model revealed that there is a considerable range of possible values for the **b** lattice vector spacing. Changes in **b** are readily effected by contrarotating the **a**-axis 'chains' around their axes. Taken in conjunction with the dense packing in the **a** direction, it follows that on the water surface, dislocations must be highly mobile along the associated glide planes (Friedel 1964).

4.4. Structure—property relationships

The LB film materials that are most well behaved on a water surface are the long-chain fatty acids. It is believed that their fluidity is largely due to the fact that they form two-dimensional rotator phases (Lösche, Rabe, Fischer, Rucha, Knoll and Möhwalld 1984, Peterson and Russell 1985). These are analogous to three-dimensional plastic crystal phases (Sherwood 1979) which are readily deformed. However, because of the face-to-face contact of the anthracene nuclei, free rotation of molecules is clearly not possible in monolayers of this material. It is therefore proposed that their fluidity is related to the high mobility of dislocations along the (100) orientation glide plane.

It has recently been shown (Peterson 1986) that the defects responsible for conduction in LB films of fatty acids are associated with disclinations of the hexagonal symmetry water-surface structure. The present study indicates that the packing of C4 anthracene has only twofold rotational symmetry, so that the lowest energy

disclination has a 'Burgers angle' of 180° . It is suggested that disclinations in C4 anthracene monolayers are too energetic to be created during spreading thereby explaining the observed low incidence of defect conduction in the resulting films.

§ 5. CONCLUSIONS

Both the RHEED and TED patterns obtained from LB films of C4 anthracene are in good agreement with each other and with the accepted multilayer model of Y-type films. The consistency of the results of the two different electron diffraction techniques indicates that the structure of C4 anthracene LB films is the same on both Al_2O_3 and SiO_2 substrates. The present study confirms the conclusion of Vincett and Barlow (1980) concerning the molecular orientation in these films and narrows the probable range of long-axis molecular tilt to $60 \pm 1^\circ$. It supersedes their investigation by demonstrating that there are four molecules per unit cell, and extends it by defining the unit-cell parameters and space-group symmetry.

It is considered that the proposed connections between film structure and properties, both in relation to monolayer water-surface fluidity and metal-LB-metal conduction will be of great importance in guiding the design of molecular assemblies to perform electronic functions.

REFERENCES

- AVIRAM, A., and RATNER, M. A., 1974, *Chem. Phys. Lett.*, **29**, 277.
 BAKER, S., PETTY, M. C., ROBERTS, G. G., and TWIGG, M. V., 1983, *Thin Solid Films*, **99**, 53.
 BATEY, J., PETTY, M. C., ROBERTS, G. G., and WRIGHT, D. R., 1984, *Electron. Lett.*, **20**, 489.
 BONNEROT, A., CHOLLET, P. A., FRISBY, H., and HOCLET, M., 1985, *Chem. Phys.*, **97**, 365.
 CARTER, F. L. (editor), 1982, *Molecular Electronic Devices* (New York: Marcel Dekker).
 COUCH, N. R., MONTGOMERY, C. M., and JONES, R., *Thin Solid Films* (to be published).
 EARLS, J. D., PETERSON, I. R., RUSSELL, G. J., GIRLING, I. R., and CADE, N. A., 1986, *J. molec. Electron.* (to be published).
 FRIEDEL, J., 1964, *Dislocations* (Oxford: Pergamon).
 GAINES, G. L., 1966, *Insoluble Monolayers at Liquid-Gas Interfaces* (New York: Interscience).
 GAROFF, S., DECKMAN, H. W., DUNSMUIR, J. H., and ALVAREZ, M. S., 1986, *J. Phys., Paris*, **47**, 701.
 GIRLING, I. R., KOLINSKY, P. V., CADE, N. A., EARLS, J. D., and PETERSON, I. R., 1985, *Opt. Comm.*, **55**, 289.
 HENRY, N. F. M., LIPSON, H., and WOOSTER, W. A., 1960, *The Interpretation of X-Ray Diffraction Photographs* (London: Macmillan), p. 236.
 HENRY, N. F. M., and LONSDALE, K., 1952, *International Tables for X-ray Crystallography*, Vol. I (Birmingham: Kynoch).
 JONES, R., TREDGOLD, R. H., and HOORFAR, A., 1984, *Thin Solid Films*, **113**, 115.
 KAJZAR, F., MESSIER, J., and ZYSS, J., 1983, *J. Phys., Paris*, **44**, C3-709.
 KITAIGORODSKII, A. I., 1961, *Organic Chemical Crystallography* (New York: Consultants Bureau); 1973, *Molecular Crystals and Molecules* (New York: Academic Press).
 KUHN, H., 1983, *Thin Solid Films*, **99**, 1.
 LÖSCHE, M., RABE, J., FISCHER, A., RUCHA, B. U., KNOLL, W., and MÖHWALD, H., 1984, *Thin Solid Films*, **117**, 269.
 PETERSON, I. R., 1986, *J. Molec. Electron.* (submitted).
 PETERSON, I. R., and RUSSELL, G. J., 1984, *Phil. Mag. A*, **49**, 463; 1985, *Br. Polym. J.*, **17**, 364.
 ROBERTS, G. G., 1985, *Adv. Phys.*, **34**, 475.
 ROBERTS, G. G., and MCGINNITY, T. M., 1979, *Solid. St. Commun.*, **32**, 683.
 ROBERTS, G. G., MCGINNITY, T. M., BARLOW, W. A., and VINCETT, P. S., 1980, *Thin Solid Films*, **68**, 223.
 SCHOELER, U., TEWS, K. H., and KUHN, H., 1974, *J. Chem. Phys.*, **61**, 5009.

- SHERWOOD, J. N., 1979, *The Plastically Crystalline State: Orientationally Disordered Crystals* (New York: Wiley Interscience).
- TREGOLD, R. H., VICKERS, A. J., HOORFAR, A., HODGE, P., and KHOSHDEL, E., 1985, *J. Phys. D*, **18**, 1139.
- VAINSHTEIN, B. K., 1964, *Structure Analysis by Electron Diffraction*, translation edited by E. Feigel and J. A. Spink (New York: Macmillan).
- VICKERS, A. J., 1984, Ph.D. Thesis, Lancaster University.
- VINCETT, P. S., and BARLOW, W. A., 1980, *Thin Solid Films*, **71**, 305.
- VINCETT, P. S., BARLOW, W. A., BOYLE, F. T., FINNEY, J. A., and ROBERTS, G. G., 1979, *Thin Solid Films*, **60**, 265.
- WALKENHORST, W., 1947, *Naturwissenschaften*, **34**, 373.
- WEAST, R. C., and ASTLE, M. J. (editors), 1980, *CRC Handbook of Chemistry and Physics*, sixtieth edition (Boca Raton: CRC Press), p. F-216.
- WILLIAMS, D. J., 1984, *Angew Chem. Int. Ed. Engl.*, **23**, 690.
- ZINGSHEIM, H. P., 1977, *Scanning Electron Microsc.*, **1**, 357.

4-N-HEPTADECYLAMIDO-4'-NITROSTILBENE, A NEW LB FILM
MATERIAL FOR NON-LINEAR OPTICS

M. M. Ahmad and W. J. Feast
Department of Chemistry, University of Durham,
South Road, Durham, DH1 3LE.

D. B. Neal, M. C. Petty and G. G. Roberts^{*}
Department of Applied Physics and Electronics,
University of Durham, South Road, Durham, DH1 3LE.

ABSTRACT

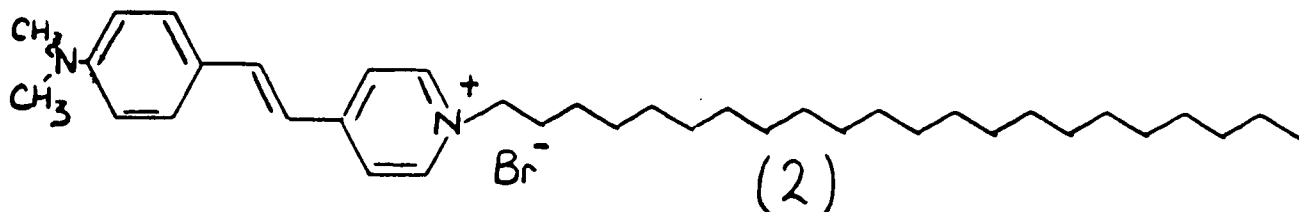
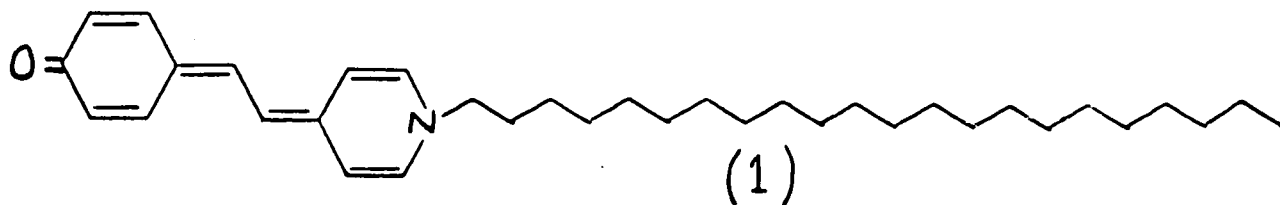
The synthesis of a new amphiphilic molecule, 4-heptadecylamido-4'-nitrostilbene, is described together with the formation of stable, high quality Langmuir-Blodgett multilayers. The material is suitable for the investigation of non-linear optical effects in organic superlattices.

* Present Address: Department of Engineering Science, University of Oxford, Parks Road, Oxford, OX1 3PJ.

Introduction

Devices processing optical signals require a range of materials with well defined properties; both conventional linear low loss materials and those exhibiting various kinds of non-linear behaviour are necessary. If such devices are to be realized in a useful form the purity specifications will have to be stringently defined so as to ensure absolute reproducibility; furthermore, the materials will need to be sufficiently stable to ensure consistent performance during a long device lifetime. It has been known for some time that inorganic dielectrics such as lithium niobate and potassium dihydrogen phosphate exhibit non-linear optical effects and are stable. More recently it has been shown that certain organic materials also display non-linear behaviour and it has been demonstrated that their non-linear coefficients can be much larger than those of inorganics⁽¹⁾. These organics generally consist of a polarizable delocalized π -electron system with donor and acceptor substituent groups at its extremities; 4-dimethylamino-4'-nitrostilbene is a good example of the genre. A necessary condition for the observation of a finite second order non-linear susceptibility is that the environment of the molecule in the solid state does not possess a centre of symmetry; this condition is not guaranteed in a molecular crystal. The Langmuir-Blodgett (LB) technique provides an elegant method for fabricating multilayers of amphiphilic molecules⁽²⁾. Multilayers of different materials can be constructed in a predetermined sequence allowing superlattices to be prepared in which the overall thickness, the symmetry properties, and the direction of the molecular dipoles are precisely defined. In order to investigate the properties of such superlattices it would be desirable to have a range of amphiphilic molecules available which form stable well ordered LB

multilayers and display appropriate non-linear optical behaviour. Examples of molecules which have been reported to fulfil these requirements are the merocyanine dye⁽³⁾ (1) and the hemicyanine dye⁽⁴⁾ (2).



In this paper we describe the synthesis of a new compound having nitro acceptor and alkylamido donor groups, and report its LB multilayer forming characteristics.

Experimental

4-N-heptadecylamido-4'-nitrostilbene (4HANS) was synthesised via a three step route from 4-nitrobenzylchloride. 4,4'-Dinitrostilbene was prepared and reduced to give 4-amino-4'-nitrostilbene following established procedures⁽⁵⁾. Acylation with octadecanoyl chloride in pyridine and CH_2Cl_2 gave the target compound in 50% overall yield after purification. 4-N-heptadecylamido-4'-nitrostilbene, an orange/red compound, was purified by recrystallization from chloroform followed by column chromatography (neutral alumina/chloroform); it was essential to shield the material from light during these manipulations. 4HANS was shown to

be a single component by hplc. The infrared spectrum was recorded as a KBr disc and displayed absorptions at 3280cm^{-1} (N-H stretch in trans secondary amide), $2960\text{-}2820\text{cm}^{-1}$ (aliphatic C-H stretch), 1660 and 1590cm^{-1} (secondary amide I and II bands), and 1510 and 1345cm^{-1} (respectively asymmetrical and symmetrical stretching bands of aromatic nitro group). Monolayer studies were conducted using a constant perimeter trough which has been described previously⁽²⁾. The material (4HANS) was spread from an approximately 2×10^{-3} M solution in chloroform ("Aristar" grade) onto a water subphase at a temperature of approximately 20°C . The water was purified by reverse osmosis, followed by deionization through a Millipore Milli-Q system; the subphase pH was adjusted by addition of HCl or NH_4OH , and where appropriate "Analar" grade CdCl_2 was added to give an approximately 2×10^{-4} M solution. Surface pressure/area isotherms were obtained by compressing the monolayer at a constant rate and simultaneously recording the surface area and pressure. Monolayer stability studies were performed by maintaining the surface pressure at a constant value and monitoring the surface area as a function of time. During LB film deposition the substrates were raised and lowered through the floating monolayer of 4HANS at a speed of approximately 2mm min^{-1} , whilst the surface pressure was maintained at a value of 32mN m^{-1} . A variety of different substrates were used with different surface properties; silicon wafers and glass slides (Corning 7059) were thoroughly cleaned to provide hydrophilic surfaces and in some cases they were further treated with dichlorodimethylsilane to provide hydrophobic surfaces; a layer of aluminium approximately 100nm thick was evaporated onto hydrophilic glass slides to provide an aluminium oxide surface.

Results and Discussion

A typical surface pressure versus surface area isotherm for 4HANS is shown in Figure 1, which also shows the molecular structure of the material. The isotherm was reproducible in the pH range 3.7 to 9.3 and was unaffected by the presence or absence of Cd^{2+} ions. Repeated cycles of compression at rates of approximately $7\text{cm}^2\text{s}^{-1}$ to a surface pressure of 30mN m^{-1} followed by expansion did not give any appreciable change in the isotherm. The surface area of a monolayer compressed to a surface pressure of 32mN m^{-1} was observed to decrease with time, see Figure 2. The effect of the nature of the subphase on the rate of decrease in area was studied by monitoring the change in area over a period of several hours for a variety of different subphase conditions. It was observed that the most stable monolayers were obtained in the pH range 5.5 to 9.0. These decay curves could not be fitted to standard decay models, such as $\text{Area} = C e^{-kt}$ (where C, k are constants, and t = time) for simple dissolution, since the t=0 position could not be accurately defined. The general appearance of the curve is typical of a good LB film forming material and monolayers were sufficiently stable for transfer to a substrate. LB multilayers were readily produced on a variety of surfaces: hydrophilic and hydrophobic glass and silicon, and aluminium oxide. Film transfer was Y-type with a deposition ratio very close to unity. Absorption spectra were recorded using a Cary 2300 spectrophotometer for multilayers of different thickness, see Figure 3. The spectra were recorded in transmission so that layers on both sides of the glass slide contributed to the absorption. The spectrum of 4HANS is shown as an inset in Figure 3; the material is essentially transparent above 500nm, which is appropriate for signal processing applications for most of the visible spectrum. The straight line fit to the plot of

absorbance at 370nm versus number of layers is indicative of good LB multilayer formation; the fact that the points derived from hydrophilic and hydrophobic substrates lie on the same line indicates that 4HANS has wide applicability. The absorption spectrum of a sample containing 46 layers of 4HANS was unchanged in profile or intensity over a period of several months indicating the stability of the dye in the LB multilayer form; in dilute chloroform solution 4HANS is bleached within a few weeks.

The donor capacity of the alkylamido group in 4HANS is lower than that of the tertiary amine group present in the hemicyanine dye(2) and consequently it might be anticipated that 4HANS would display a somewhat reduced capacity for second harmonic generation; nevertheless, it was hoped that the secondary amide function might convey a measure of stability to the ordered films via intermolecular hydrogen bonding and that this might offset the reduced non-linear effect. Second harmonic generation has now been demonstrated from monolayers and from multilayer structures produced by alternating 4HANS with layers of an "inert" fatty acid spacer (cadmium arachidate). A structure has also been produced in which the 4HANS is alternated with the hemicyanine dye. In the latter material the donor and acceptor groups are positioned in the opposite sense with respect to the hydrocarbon chain, see (2) above. Thus the second order non-linear molecular polarizabilities should be additive; the results of this investigation will be described elsewhere⁽⁶⁾.

Conclusions

4-N-Heptadecylamido-4'-nitrostilbene is a new LB film forming material which shows excellent multilayer forming properties. The molecule contains a delocalized π -electron system substituted with donor and acceptor groups and displays non-linear optical behaviour. Detailed studies of supermolecular arrays containing 4HANS are proceeding.

Acknowledgements

One of us (DEN) wishes to thank the SERC and Plessey Research Ltd. for the provision of a studentship. The work was funded under a Joint Opto-Electronics Research Scheme (JOERS) programme. The measurements of the non-linear optical properties were undertaken in collaboration with Drs. I. R. Girling and P. V. Kolinsky of GEC Research Laboratories, Wembley.

References

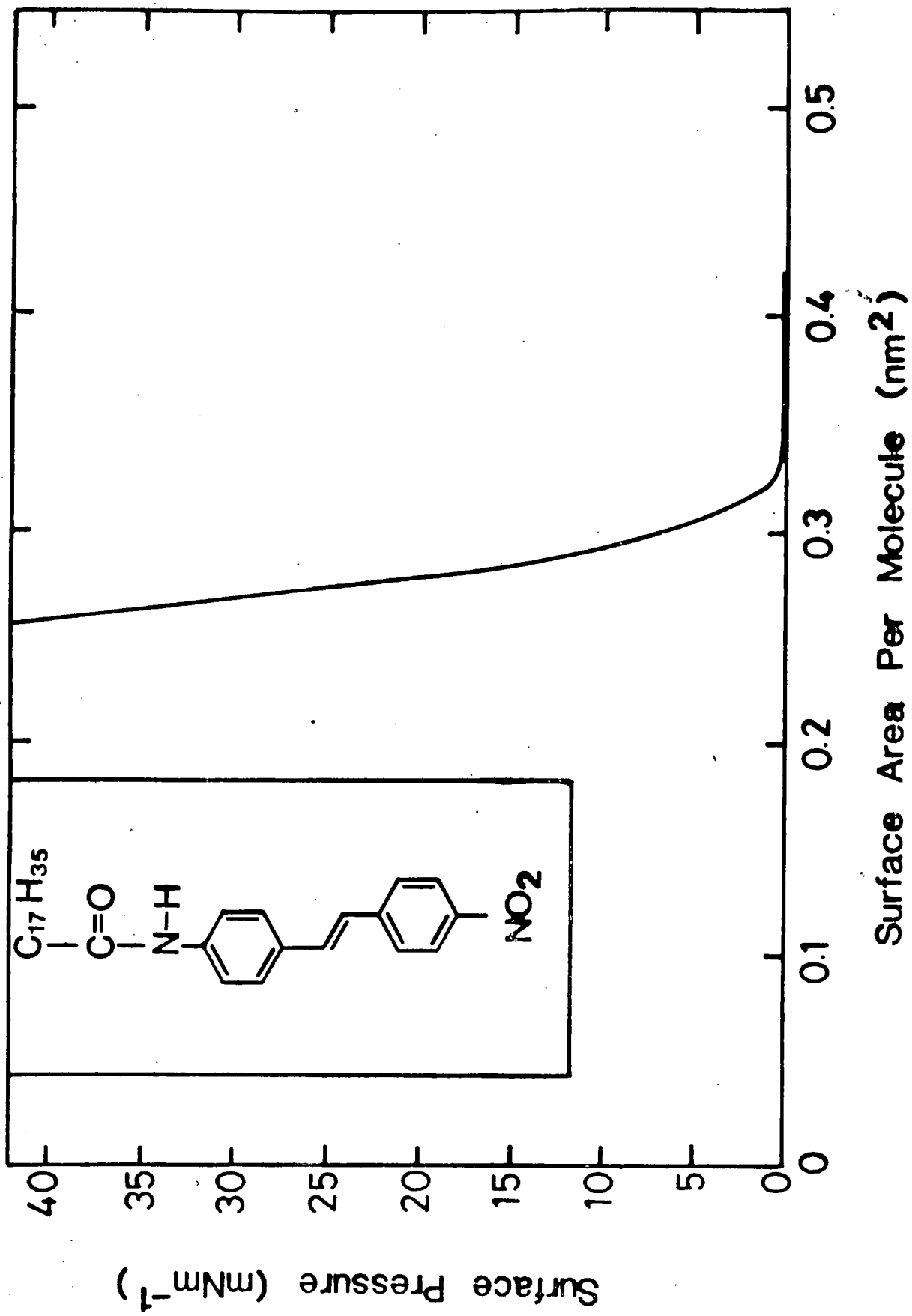
1. Williams, D. J., "Organic polymeric and non-polymeric materials with large optical non-linearities", *Angew. Chem. Int. Ed. Engl.*, 1984, 23, 690.
2. Roberts, G. G., "Langmuir-Blodgett Films", *Contemp. Phys.*, 1984, 25, 109.
3. Girling, I. R., Kolinsky, P. V., Cade, N. A., Earls, J. D., and Peterson, I. R., "Second harmonic generation from alternating Langmuir-Blodgett films", *Opt. Comm.*, 1985, 55, 289.
4. Girling, I. R., Cade, N. A., Kolinsky, P. V., Earls, J. D., Cross, G. H. and Peterson, I. R., "Observation of second harmonic generation from Langmuir-Blodgett multilayers of a hemicyanine dye", *Thin Solid Films*, in press.
5. Calvin, M. and Buckles, R. E., "The freedom of rotation about the carbon-carbon double bond. Certain substituted stilbenes", *J. Amer. Chem. Soc.*, 1940, 62, 3324.
6. Neal, D. B., Petty, M. C., Roberts, G. G., Ahmad, M. M., Feast, W. J., Girling, I. R., Cade, N. A., Kolinsky, P. V. and Peterson, I. R., "Second harmonic generation from LB superlattices containing two active components", *Electronics Letters*, submitted.

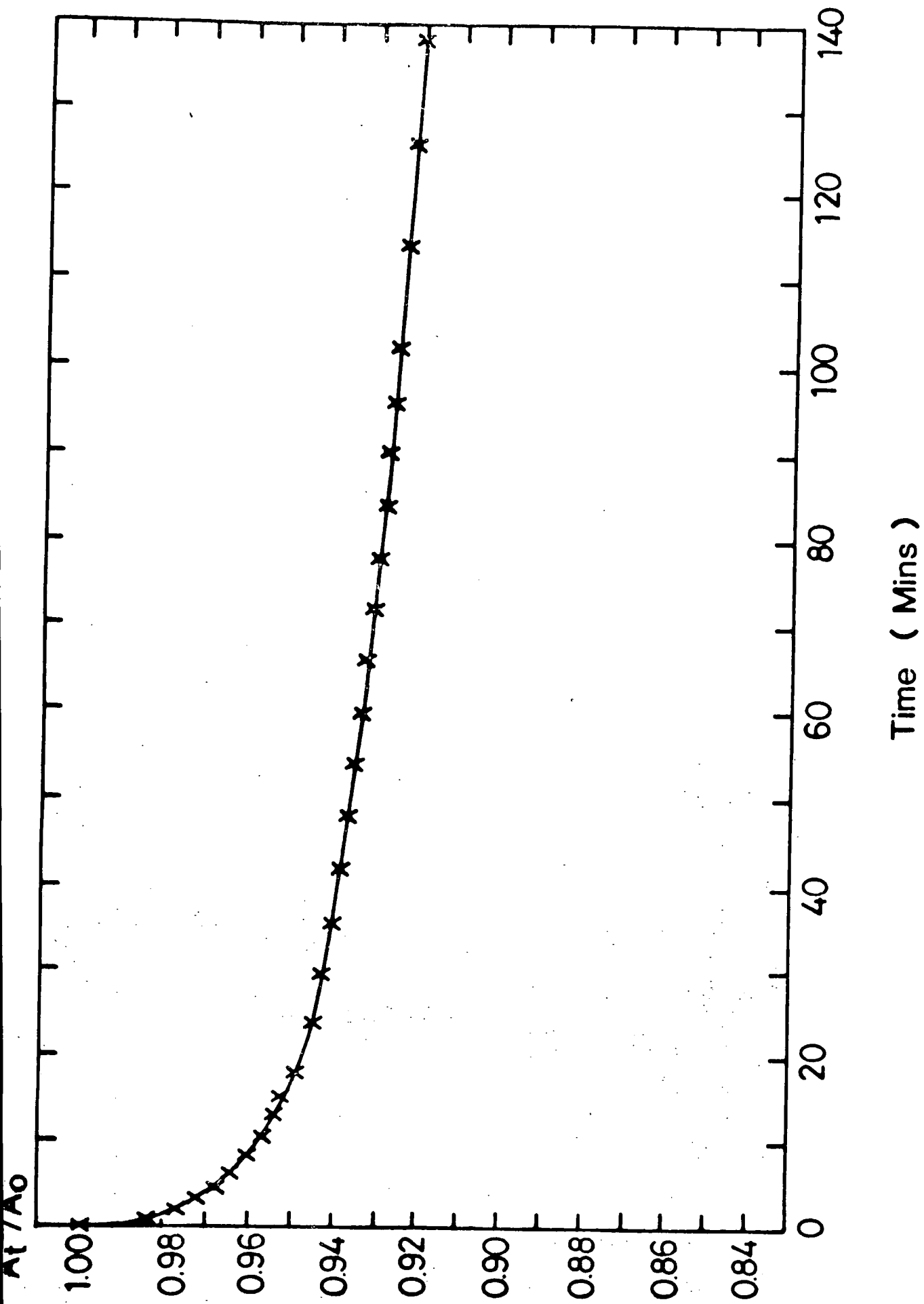
Figure Captions

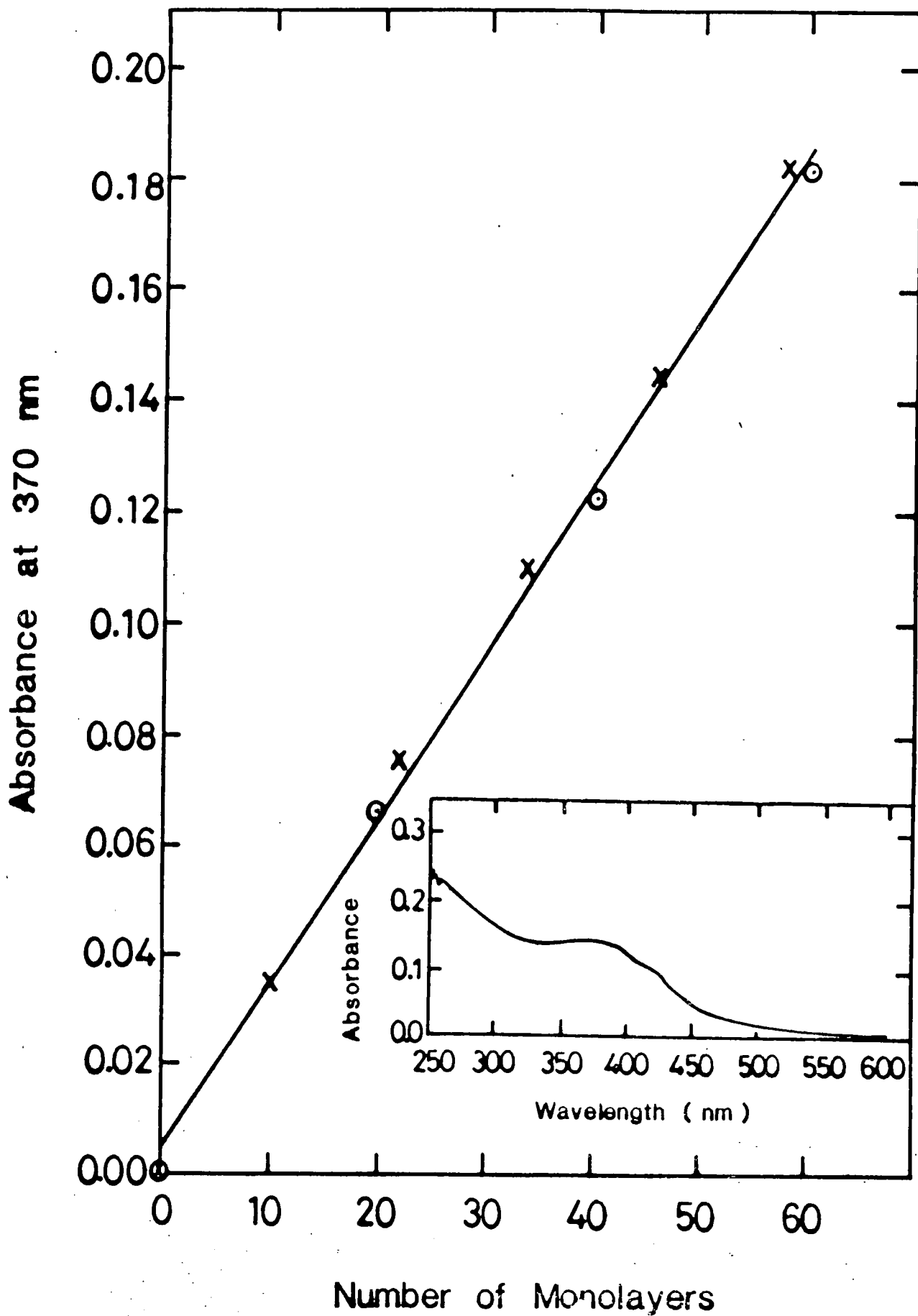
Figure 1 Surface pressure-area isotherm for 4HANS on a subphase of aqueous $\text{CdCl}_2, 2 \times 10^{-4} \text{ M}$ at pH 5.8 and a temperature of 23°C . Inset, the molecular formula of 4HANS

Figure 2 Plot of area (relative to initial value) versus time for a 4HANS monolayer maintained at a surface pressure of 32 mN m^{-1} on a subphase of aqueous $\text{CdCl}_2, 2 \times 10^{-4} \text{ M}$ at pH 5.7-5.8 and a temperature of 23°C .

Figure 3 Absorbance at 370nm versus number of monolayers for LB films of 4HANS on glass substrates; x-hydrophilic glass, o-hydrophobic glass. Inset, absorption spectrum for a 46 layer specimen.







A HIGHLY ORDERED LANGMUIR BLODGETT
MONOLAYER OF AN AMIDO NITROSTILBENE

D. B. Neal, G. J. Russell, M. C. Petty and G. G. Roberts^{*}
Department of Applied Physics and Electronics,
University of Durham, South Road, Durham, DH1 3LE.

M. M. Ahmad and W. J. Feast,
Department of Chemistry, University of Durham,
South Road, Durham, DH1 3LE.

There is an increasing interest in the exploitation of thin films of organic non-linear optical materials for signal processing applications⁽¹⁾. Such layers may be produced in a variety of ways; one particularly elegant technique is the method pioneered by Langmuir and Blodgett⁽²⁾. This allows amphiphilic organic molecules to be assembled into layers of a very precisely defined symmetry and thickness. Langmuir-Blodgett (LB) multilayer films of a wide range of materials can now be easily produced, with thicknesses up to a few micrometres. However, the success of the deposition and the quality of the films depend critically on the structure of the first monolayer⁽³⁾. Recently, it has been shown that monolayers of certain materials can be imaged directly by transmission electron microscopy⁽⁴⁾. In this work we report on the exceptional degree of structural order revealed by reflection high energy electron diffraction (RHEED) studies of monolayer films of 4-N-heptadecylamido-4'-nitrostilbene (4HANS), a material with potential non-linear optical applications^(5,6). Similar studies showed that monolayers of an amine analogue of 4HANS were noticeably less well ordered. It is inferred that, in the case of 4HANS, the monolayer structure is predominantly stabilised by hydrogen bonding.

A typical 80kV RHEED pattern obtained from an LB monolayer of 4 HANS (molecular formula shown in figure 1a), deposited with the

^{*} Present Address: Department of Engineering Science, University of Oxford, Parks Road, Oxford, OX1 3PJ.

chromophore adjacent to the {111} Si substrate, is shown in figure 2. The high degree of structural order is remarkable for an LB film and significantly better than has been observed for simple fatty-acid assemblies⁽⁷⁻⁹⁾. Identical patterns were recorded over a range of subphase conditions and also when {100} Si substrates were used. Further, it is important to note that the pattern obtained was independent of the direction of the incident electron beam in the plane of the film. The latter observation indicates that the layer is comprised of a mosaic structure of grains in which the long axes of all the chromophores have a common tilt angle away from the substrate normal, but in which the tilt azimuth varies from grain to grain. The pattern contains a rectangular matrix of reflections in which the diffraction spots located along the substrate normal and parallel to the shadow edge of the substrate correspond to interplanar spacings of 1.24nm and 1.28nm, and sub-multiples of these, respectively. However, due to systematic absences, it should be noted that the largest d-spacing measured in the direction along the substrate normal is 0.62nm. The d-spacings for planes lying parallel to the substrate should correspond to some intramolecular periodicity, whereas the spacings for planes perpendicular to it should correspond to intermolecular distances. It seems likely that the monolayer structure will be stabilized by hydrogen bonding between the hydrogens and carbonyl oxygens of amide groups in adjacent molecules.

During the course of this investigation, monolayers of an analogue (molecular formula given in figure 1b) of 4HANS were also studied using RHEED; a typical diffraction pattern, also recorded at 80kV, is shown in figure 3. Although this pattern is similar to that of figure 2 (indicating the same basic packing arrangement), most of the diffraction

spots are of a significantly lower intensity than are the corresponding reflections obtained from monolayers of 4HANS. The essential difference in the molecular structure of 4HANS and the analogue is that the amide group in the former material has been replaced by a simple amine. Thus the possibility of hydrogen bonding between the adjacent chromophores in the monolayer is substantially reduced. We therefore conclude that such interactions play a dominant role in the in-plane ordering of the molecules in monolayers of 4HANS.

The diffraction pattern in figure 2 indicates that the chromophores are extremely well-ordered; however, the reverse is true of the hydrocarbon tails. RHEED patterns from LB films of fatty acids display clear arcs due to the ordering of the hydrocarbon chains⁽⁷⁾; in corresponding positions, diffraction patterns of 4HANS show at best only faint diffuse rings. This is to be expected when considering the difference in cross-section between the chromophore and the tail; even when the chromophores are close-packed, there is still room for motion of the tails, thereby reducing their order. In contrast to this behaviour, the RHEED patterns from monolayers of the analogue of 4HANS display clear arcs (as at A in figure 3) corresponding to ordering of the hydrocarbon tails. This suggests that the removal of the carbonyl group reduces the effective size of the chromophore and enables the closer approach of the tails. Thus, although the molecules may be slightly closer packed in monolayers of the analogue, in 4HANS the order of the chromophore section of the molecule is more regular due to the stabilizing influence of intermolecular hydrogen bonding.

Multilayer films of 4HANS can be built up using the conventional Langmuir-Blodgett technique, the bonding between the first and second layers being tail-to-tail, and that between the second and third layers

being head-to-head, etc.⁽⁵⁾ From previous work on the epitaxial deposition of LB layers⁽³⁾, it might be expected that the exceptional degree of order in the first monolayer of 4HANS would give rise to a very high quality multilayer structure. Therefore RHEED studies were performed on a number of LB films of 4HANS (over the thickness range 3 to 15 monomolecular layers). However, the resulting diffraction patterns were indicative of progressively poorer crystalline order with increasing thickness. This effect is perhaps not surprising when one considers the relatively poor order of the hydrocarbon tails in the 4HANS monolayer. Molecules with a more uniform cross section would probably be more desirable for high quality multilayer formation.

In conclusion, we have reported on the excellent crystallinity of an LB monolayer of a substituted amido nitrostilbene. The RHEED pattern obtained from it can be explained in terms of a structure which is highly stabilized by hydrogen bonding. A more rigorous analysis of the diffraction patterns is currently being undertaken to deduce the orientation of the rigid chromophores by matching the RHEED patterns to a computer generated intensity distribution of the diffraction pattern of a single moiety^(10,11), and to explain the origin of the very large d-spacings both normal and parallel to the substrate plane.

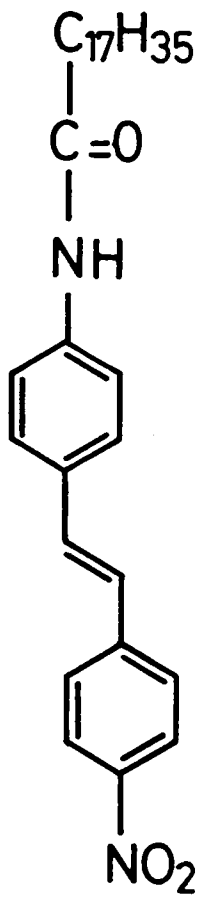
The authors wish to thank Dr. I. R. Peterson of GEC Hirst Research Laboratories for useful discussions and for critically reading the manuscript. One of us (DBN) would like to acknowledge the SERC and Plessey Research Ltd. for the provision of a studentship. The work was partly funded under a Joint Opto-Electronics Research Scheme (JOERS).

REFERENCES

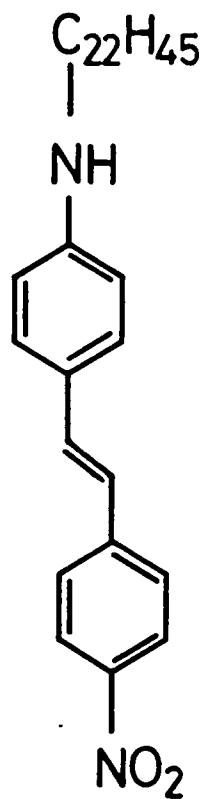
1. Williams, D. J., "Organic polymeric and non-polymeric materials with large optical non-linearities", *Angew. Chem. Int. Ed. Engl.*, 1984, 23, 690-703.
2. Roberts, G. G., "Langmuir-Blodgett films", *Contemp. Phys.*, 1984, 25, 109-128.
3. Peterson, I. R. and Russell, G. J., "Deposition mechanisms in Langmuir-Blodgett films", *British Polymer Journal*, 1985, 17, 364-367.
4. Fryer, J. R., Hann, R. A. and Eyres, B. L., "Single organic monolayer imaging by electron microscopy", *Nature*, 1985, 313 (6001), 382-384.
5. Ahmad, M. M., Feast, W. J., Neal, D. B., Petty, M. C. and Roberts G. G., "4-N-Heptadecylamido-4'-nitrostilbene, a new LB film material for non-linear optics", *J. Molec. Elec.*, in press.
6. Neal, D. B., Petty, M. C., Roberts, G. G., Ahmad, M. M., Feast, W. J., Girling, I. R., Cade, N. A., Kolinsky, P. V. and Peterson, I. R., "Second harmonic generation from LB superlattices containing two active components", *Elec. Letts.*, 1986, 22(9), 460-462.
7. Russell, G. J., Petty, M. C., Peterson, I. R., Roberts, G. G., Lloyd, J. P. and Kan, K. K., "A RHEED study of cadmium stearate Langmuir-Blodgett films", *J. Mat. Sci. Letts.*, 1984, 3, 25-28.
8. Peterson, I. R. and Russell, G. J., "An electron diffraction study of ω -tricosenoic acid Langmuir-Blodgett films", *Phil. Mag. A*, 1984, 49(3), 463-473.
9. Bonnerot, A., Chollet, P. A., Frisby, H. and Hoclet, M., "Infrared and electron diffraction studies of transient stages in very thin Langmuir-Blodgett films", *Chem. Phys.*, 1985, 97, 365-377.
10. Peterson, I. R., Russell, G. J., Neal, D. B., Petty, M. C., Roberts, G. G., Ginnai, T. and Hann, R. A., "An electron diffraction study of LB films from a lightly substituted anthracene derivative", *Phil. Mag.*, in press.
11. Earls, J. D., Peterson, I. R., Russell, G. J., Girling, I. R. and Cade, N. A., "An electron diffraction study of optically-nonlinear hemicyanine LB films", *J. Molec. Elec.*, in press.

FIGURE CAPTIONS

1. Molecular formulae of
 - (a) 4HANS
 - (b) Amine analogue of 4HANS
2. 80kV RHEED pattern obtained from a monolayer of 4HANS deposited on a {111} Si substrate.
3. 80kV RHEED pattern obtained from a monolayer of the amine analogue of 4HANS deposited on a {111} Si substrate.



4 HANS
(a)



4 HANS Analogue
(b)

Figure 1

SECOND HARMONIC GENERATION FROM LB SUPERLATTICES CONTAINING TWO ACTIVE COMPONENTS

Indexing terms: Semiconductor devices and materials, Langmuir-Blodgett films

Second harmonic generation has been observed from Langmuir-Blodgett multilayer arrays containing two active components. Both materials were based on long chain donor-acceptor dye compounds, but were designed with the donor-acceptor groups in opposite senses with respect to the hydrocarbon chain. Preliminary results indicate a significant enhancement of the second-order polarisability for this type of supermolecular array.

The Langmuir-Blodgett (LB) technique provides a means to exploit the nonlinear optical properties of certain organic materials. In previous publications second harmonic generation from monolayers and multilayers of merocyanine^{1,2} and hemicyanine³ dyes has been described. Whereas these studies involved the dye layers spaced by inert fatty acid layers in order to produce noncentrosymmetric structures, in this letter we report on second harmonic generation from a multilayer system in which two different dyes are alternated. One of the materials is the hemicyanine³ (Fig. 1a); the other, a long chain nitrostilbene (Fig. 1b), has been engineered with its donor-acceptor groups in the opposite sense, with respect to the hydrocarbon chain, to those of the hemicyanine. Thus, when the two dyes are alternately transferred to a substrate using the LB process, the individual second-order nonlinear molecular polarisabilities should be additive.

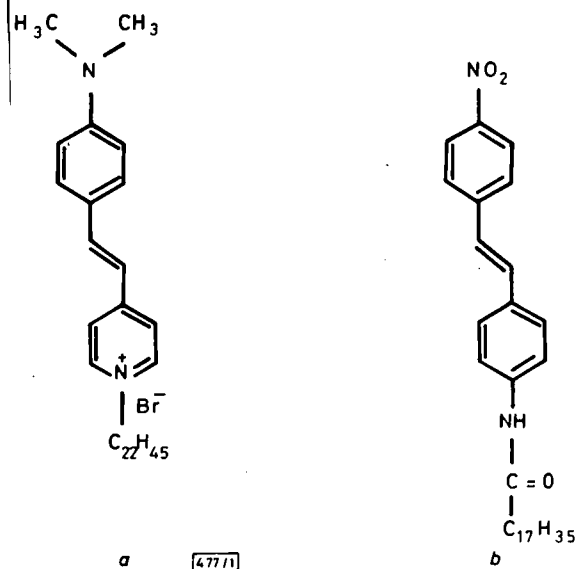


Fig. 1

- a Hemicyanine dye
b Nitrostilbene dye

The 4-heptadecylamido-4'-nitrostilbene was synthesised following the method of Calvin and Buckles⁴ and derivatised by reacting with the appropriate acid chloride. LB films were prepared using a constant-perimeter-type trough, and using procedures that have been discussed previously.¹⁻³ Fig. 2 shows the sample configurations that were used in this investigation. To prepare the alternating structures (Fig. 2b), the hemicyanine dye was spread as a 4.2×10^{-3} M solution in chloroform on to an aqueous subphase (temperature $\sim 20^\circ\text{C}$, pH ~ 9.0); the film was compressed to a surface pressure of 35 mN m^{-1} and subsequently transferred to the substrate at 2 mm min^{-1} on each upstroke. The nitrostilbene material was spread as a 2×10^{-3} M solution in chloroform (subphase condition as for the hemicyanine), compressed to a surface pressure of 32 mN m^{-1} , and then deposited at 2 mm min^{-1} on each downstroke of the substrate. Monolayers of the nitrostilbene (Fig. 2a) were deposited at 2 mm s^{-1} on withdrawal of the substrate from the subphase (at pH ~ 5.5). All films were built up on hydrophilic Corning 7059 glass microscope slides.

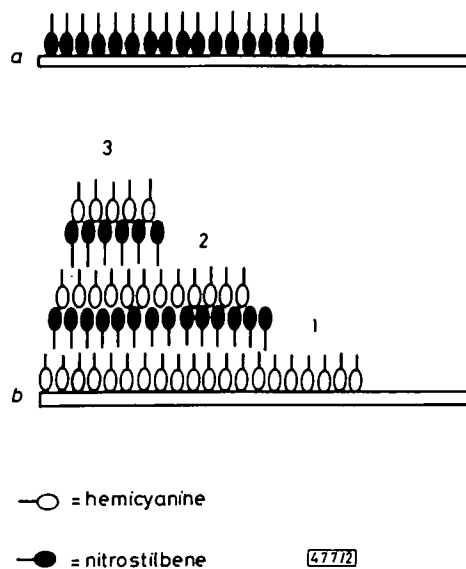


Fig. 2 Schematic diagrams of sample configurations used in experiments described in text

For the second harmonic measurements, light (*Q*-switched Nd YAG, $1.064 \mu\text{m}$, 25 ns FWHM), polarised either parallel (*p*) or perpendicular (*s*) to the plane of incidence, was directed at a 45° angle of incidence on to the sample.³ The second harmonic radiation (532 nm) was detected in both reflection (*R*) and transmission (*T*) geometries. Pulse energies of up to 2 mJ with a beam diameter of approximately $200 \mu\text{m}$ were used for all the measurements on the LB films. Absolute values of the electric field at 532 nm [$E(2\omega)$] were obtained by calibrating the system against the d_{11} nonlinear coefficient of a *y*-cut quartz wedge.⁵

All the LB film samples studied in this work exhibited second harmonic generation. Regions of the substrates free of film gave no detectable signal, confirming that the observed radiation was a property of the organic layer. The second harmonic signals, being quadratic in incident laser energy, were normalised by dividing by the square of the incident laser energy. These are summarised in Table 1 in terms of the incident [$E(\omega)$] and signal [$E(2\omega)$] electric field strengths. Thus $T^{p \rightarrow p} = |E^p(2\omega)|^2 / |E^p(\omega)|^4$ represents *p*-polarised incident and signal intensities in the transmission geometry; a corresponding notation is used for the other polarisation and geometry. It should be noted that the $T^{s \rightarrow p}$ and $R^{s \rightarrow p}$ intensities were of the same order.

Table 1 CALIBRATED SIGNAL STRENGTHS ($10^{-27} \text{ m}^2 \text{ V}^{-2} \pm 10\%$) OBTAINED FOR SAMPLES SHOWN IN FIG. 2

Sample	$T^{p \rightarrow p}$	$R^{p \rightarrow p}$	$T^{s \rightarrow p} \sim R^{s \rightarrow p}$	$\tilde{\chi}_{zzz}^{(2)} / \epsilon_2 \epsilon_1^2$	$\tilde{\chi}_{zyy}^{(2)} / \epsilon_2$	$\tilde{\chi}_{yyz}^{(2)} / \epsilon_1$
Fig. 2a	0.7	0.1	0.1	3.0	2.0	4.7
Fig. 2b	7.3	1.0	0.3	11.0	4.4	16.0
(region 1)						
Fig. 2b (2)	79.6	11.1	4.3	38.0	15.0	52.0
Fig. 2b (3)	350.5	24.7	16.1	91.0	30.0	98.0

Derived second harmonic surface susceptibilities ($\tilde{\chi}^{(2)}$) ($10^{-32} \text{ Cm V}^{-2}$), which still include the dielectric constants normal to the film, were obtained using the analysis of Girling *et al.*⁶

In all cases the *p*-polarised transmission signals were approximately ten times greater than those measured in reflection. This is consistent with an almost perfect vertical alignment of the dyes, which is also suggested by the weaker signals obtained for the *s*-polarised incident radiation. The absence of significant ($< 0.1 \text{ m}^2 \text{ V}^{-2}$) *s*-polarised second harmonic radiation indicates that the tilt of the dye molecules relative to the substrate normal is averaged out within a second harmonic wavelength, resulting in no observable macroscopic anisotropy.

The data have been analysed in terms of the second harmonic surface susceptibilities ($\tilde{\chi}^{(2)}$) for the thin organic layers using the approach of Girling *et al.*³ This requires knowledge of the linear dielectric constant components normal to the

substrate in each of the films; the values are required at frequencies of both ω (ϵ_1) and 2ω (ϵ_2). Because of the sensitivity of the results to the dielectric properties, the susceptibilities given in Table 1 include these quantities. On the assumption that the underlying molecular polarisabilities are dominated by single components along the long molecular axis, then the $\tilde{\chi}_{ijk}^{(2)}$ coefficients should be symmetric to permutation of the subscripts. A comparison of the last two columns of Table 1 therefore leads to $\epsilon_2 \sim 3\epsilon_1$, not inconsistent with the second harmonic energy being close to the lowest electronic molecular excitation.⁶ Taking a reasonable, nonresonant value $\epsilon_1 = 2$ for both dyes, the above symmetry condition gives $\epsilon_2 = 4.7$ and $\epsilon_2 = 7.8$ for the nitrostilbene and hemicyanine, respectively. These values are similar to those deduced from an observation of shifts in the surface plasmon resonance curves for the dyes deposited on to silver. Using an approximate surface density of $4 \times 10^{18} \text{ cm}^{-2}$ for both molecules, the second-order microscopic polarisabilities β and their average polar angle relative to the substrate normal, $\bar{\psi}$, could be calculated;³ these are shown in Table 2. The values for the nitrostilbene/hemicyanine bilayers were obtained by subtracting the figures given in the last two rows of Table 1.

Table 2 DERIVED POLARISABILITIES β AND AVERAGE POLAR ANGLE $\bar{\psi}$ DEDUCED FROM DATA IN TABLE 1 AND ASSUMING $\epsilon_1 = 2$

	β	$\bar{\psi}$
	$10^{-50} \text{ C}^3 \text{ m}^3 \text{ J}^{-2}$	
Nitrostilbene	21.5 ± 5	30°
Hemicyanine	116 ± 20	24°
Bilayer	316 ± 60	23°

The figure obtained for the hemicyanine dye is in good agreement with that obtained previously.³ The β coefficient for the nitrostilbene is slightly smaller than the value obtained for the parent (unsubstituted) molecule.⁶ This may well be explained by the decreased strength of the donor group in our material (being an amide rather than an amine). It is clear that the bilayer is a much superior second harmonic material than is predicted by a simple addition of the β coefficients of the separate layers. In the measurements reported here the second harmonic intensity is expected to increase quadratically with the number of bilayers; ignoring the effect of the first hemicyanine layer, Table 1 reveals that this is approximately the case. However, data for a much larger thickness range are clearly required before a detailed discussion on this aspect of the work is undertaken.

For the first time optical nonlinearity in an alternating donor-acceptor:inverted donor-acceptor dye multilayer has been demonstrated. The second-order polarisability for the bilayer is found to be much greater than that expected by simply adding the polarisabilities for the individual dye monolayers.

Acknowledgments: We should like to thank Dr. M. F. Daniel for useful discussions. One of us (DBN) wishes to thank the UK SERC and Plessey Research Ltd. for the provision of a studentship. The work was funded under a Joint Opto-Electronics Research Scheme (JOERS) programme.

D. B. NEAL
M. C. PETTY
G. G. ROBERTS*
M. M. AHMAD†
W. J. FEAST†

21st February 1986

Department of Applied Physics & Electronics
† Department of Chemistry
University of Durham
South Road, Durham DH1 3LE, United Kingdom

I. R. GIRLING
N. A. CADE
P. V. KOLINSKY
I. R. PETERSON

GEC Hirst Research Laboratories
East Lane, Wembley, Middlesex HA9 7PP, United Kingdom

* Present address: Department of Engineering Science, University of Oxford, Parks Road, Oxford OX1 3PJ, United Kingdom

References

- GIRLING, I. R., CADE, N. A., KOLINSKY, P. V., and MONTGOMERY, C. M.: 'Observation of second-harmonic generation from a Langmuir-Blodgett monolayer of a merocyanine dye', *Electron. Lett.*, 1985, **21**, pp. 169-170
- GIRLING, I. R., KOLINSKY, P. V., CADE, N. A., EARLS, J. D., and PETERSON, I. R.: 'Second harmonic generation from alternating Langmuir-Blodgett films', *Opt. Commun.*, 1985, **55**, pp. 289-292
- GIRLING, I. R., CADE, N. A., KOLINSKY, P. V., EARLS, J. D., CROSS, G. H., and PETERSON, I. R.: 'Observation of second harmonic generation from Langmuir-Blodgett multilayers of a hemicyanine dye', *Thin Solid Films* (in press)
- CALVIN, M., and BUCKLES, R. E.: 'The freedom of rotation about the carbon-carbon double bond. Certain substituted stilbenes', *J. Am. Chem. Soc.*, 1940, **62**, pp. 3324-3329
- PRESLEY, R. J. (Ed.): 'Handbook of lasers' (Chemical Rubber Co., Cleveland, OH, 1971), p. 493
- OUJAR, J. L.: 'Optical nonlinearities of conjugated molecules. Stilbene derivatives and highly polar aromatic compounds', *J. Chem. Phys.*, 1977, **67**, pp. 446-457

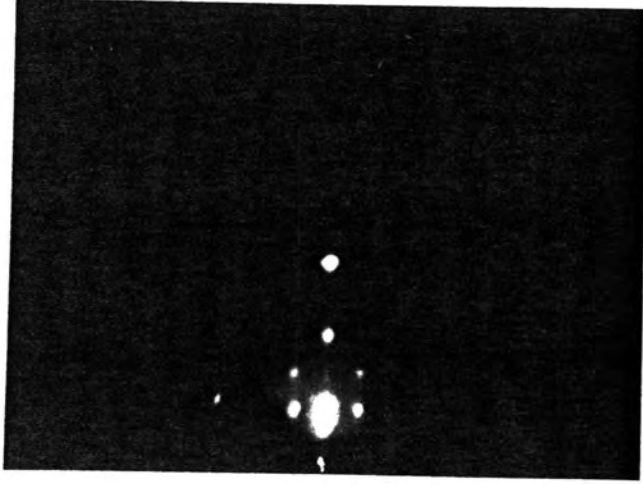


Figure 2

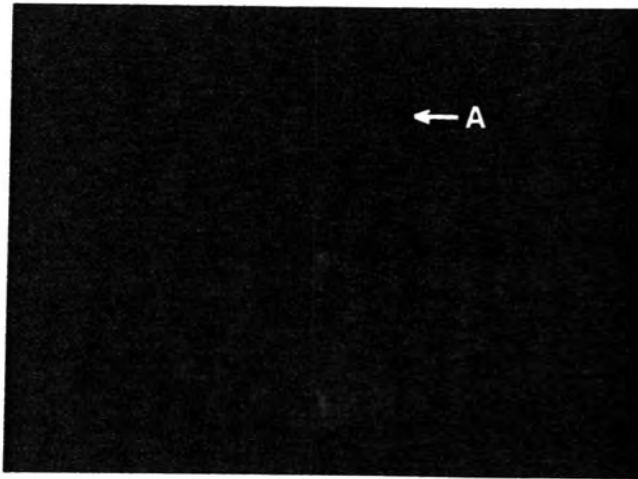


Figure 3

LANGMUIR-BLODGETT FILMS FOR NONLINEAR OPTICS

D. B. Neal, M. C. Petty, G. G. Roberts[†], M. M. Ahmad^{*}, W. J. Feast^{*},
I. R. Girling[†], N. A. Cade[†], P. V. Kolinsky[†], I. R. Peterson[†]

Department of Applied Physics and Electronics, University of Durham,
South Road, Durham, DH1 3LE, U.K.

[†]Department of Engineering Science, University of Oxford, Parks Road,
Oxford, OX1 3PJ, U.K.

^{*}Department of Chemistry, University of Durham, South Road, Durham, DH1 3LE, U.K.

[†]GEC Hirst Research Laboratories, East Lane, Wembley, Middlesex, HA9 7PP, U.K.

Abstract

Second harmonic generation has been observed from Langmuir-Blodgett monolayers and alternating multilayers of a hemicyanine and each of two nitrostilbene dyes. The non-linear response of a hemicyanine/nitrostilbene bilayer is shown to be greater than that expected from the simple addition of contributions arising from the individual (separated) monolayers. The unexpected enhancement of the second harmonic intensity upon diluting a monolayer of an active dye with a passive fatty acid material is also described.

1. Introduction

Certain organic materials exhibit large non-linear optical coefficients, often considerably larger than displayed by "conventional" inorganic dielectrics such as lithium niobate or potassium dihydrogen phosphate [1]. The second-order non-linearities displayed by bulk organic crystals can be traced back to the second-order hyperpolarizabilities (β) of their constituent molecules, which usually contain donor and acceptor groups separated by a conjugated system. However, in organic single crystals the inherent molecular non-linearity is often not manifested at a macroscopic level due to a tendency to crystallize centrosymmetrically and thereby cancel the β 's (β is a third rank tensor and therefore has properties similar to a vector). The Langmuir-Blodgett (LB) technique is an elegant method of assembling amphiphilic organic molecules into layers of a well defined thickness [2] and alignment; it thus provides a means to exploit the non-linear optical properties of the individual molecules. Moreover, by alternating layers of different materials, supermolecular arrays may be fabricated possessing the requisite non-centrosymmetric crystal structure.

Previous publications [3,4] have detailed studies of second harmonic generation (SHG) from alternate layer structures in which the active dye layers are spaced by inert layers of a fatty acid. Recently [5] we have reported on SHG from structures in which the fatty acid was replaced by a second active dye material; the two dyes used were a hemicyanine (I, figure 1) and an amidonitrostilbene (II, Figure 1). Dyes I and II were engineered with their donor-acceptor groups in

opposite senses with respect to their hydrocarbon chains so that when the two dyes are alternately transferred to a substrate using the LB process, the individual second order molecular hyperpolarizabilities should be additive. Preliminary results on very small numbers of layers seemed to indicate that the effective β for a pair of molecules of I and II in a bilayer was much greater than that expected by simply adding the β 's for the individual molecules [5]; in this paper the investigation has been extended to greater numbers of layers.

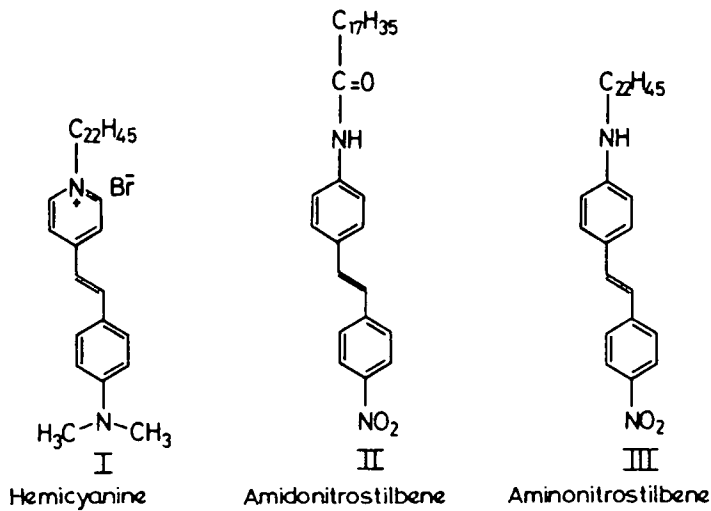


Figure 1 Molecular formulae of the dyes employed in this study

The strength of the donor group in II is likely to be reduced by the presence of the adjacent carbonyl group; compound III (figure 1) was therefore synthesized in which the amide group of II is replaced by an amine group. Studies of SHG from monolayers of III, and also from multilayers in which III is alternated with I, were performed and the results are contrasted with those from II.

Not all substituted dye materials will form homogeneous LB films; some have to be diluted with a fatty acid by up to a factor of ten in order to render them suitable for deposition by the LB technique. It was therefore of interest to use the hemicyanine dye (which could be deposited in homogeneous films and which also had a particularly

high value of β) as a model system to study the effects of dilution on nonlinear behaviour. We have therefore undertaken SHG investigations of mixed monolayers of hemicyanine and cadmium arachidate with mole fractions of hemicyanine ranging from 0.1 - 1.0.

2. Experimental

The syntheses of dyes I and II have been described elsewhere [4,6]. The LB films were prepared using a constant perimeter type trough of the form described in reference 2. The dyes were dissolved in a volatile solvent (chloroform) and spread onto the surface of the ultrapure water subphase in the trough using a microsyringe. At this stage the dye molecules should be held at the air-water interface, in a rather disordered manner, by the balance of forces between the attraction of the subphase for the polar chromophore end of the molecule and the hydrophobic nature of the tail. After allowing the solvent to evaporate, the area enclosed by the barriers was slowly reduced by driving the barriers with a motor. The surface pressure of the monolayer was monitored using a Wilhelmy plate connected to a microbalance, the output of which was taken to the barrier drive via a feedback loop. This arrangement allowed a preset surface pressure to be achieved and subsequently maintained as monolayer was removed and deposited onto the substrate. As the water-surface monolayer is compressed, the area occupied by each molecule is reduced and they begin to pack together in a more ordered fashion, until they eventually form a condensed phase analogous to a two-dimensional solid. Care has to be taken at this stage not to compress the monolayer too much, or else it will buckle and collapse. A monolayer of the material can now be transferred to a solid substrate each time the air-water interface is traversed. In order to do this, the substrate is mounted on a motor-driven micrometer screw which drives it at a constant speed in a vertical direction.

A summary of the structures produced is shown in figure 2, and the deposition conditions are summarized in table 1. All of the films were transferred at a rate of 2 mm min^{-1} from a 10^{-4} M

Cd^{2+} (aq) subphase (temperature $\sim 20^\circ\text{C}$). The spreading solutions for the mixed monolayers of I and cadmium arachidate (figure 2e) were prepared by mixing appropriate volumes of $4.57 \times 10^{-3} \text{ M}$ hemicyanine and $4.07 \times 10^{-3} \text{ M}$ arachidic acid solutions.

The substrates used for all of these experiments were hydrophilic Corning 7059 glass microscope slides. In the investigations described here, the alternating layer structures were fabricated by alternately spreading, compressing and removing the different monolayers from the subphase surface; a very time consuming procedure, even for small numbers of layers. In future work requiring greater thicknesses we would hope to use equipment that we have specially developed to produce alternate layer systems [7], since such considerations will be of importance for the eventual fabrication of optical devices based on such supermolecular arrays.

Structure	Dye	Surface pressure	Subphase pH
Fig. 2(a)	II	32	5.7
(b)	III	30	5.7
(c)	I	35	9.0
(c)	II	32	9.0
(d)	I	35	9.0
(d)	III	30	9.0
(e)	I/CdAr ₂	30	5.6

Table 1 : Deposition conditions for structures given in figure 2 (surface pressures in mN m^{-1})

The equipment used for the second harmonic measurements has been described, in some detail, in a previous publication [4]. Linearly polarized light (Q-switched Nd YAG, $1.064 \mu\text{m}$, 25ns FWHM), polarized either parallel (p) or perpendicular (s) to the plane of incidence, was directed at a 45° angle of incidence onto the vertically mounted sample. The second harmonic radiation (532 nm) resolved into s- and p-polarized components was detected in both reflection (R) and transmission (T) geometries using photomultiplier tubes at 90° and 180° respectively to the pumping direction. The total energy of each fundamental pulse was measured using a transmission type energy meter (GEC TF series). Infrared blocking filters and 532 nm interference filters were used to ensure that only second harmonic radiation was detected. Pulse energies of up to 2mJ with a beam diameter of approximately $200 \mu\text{m}$ were used for all the measurements on the LB films.

Results were obtained by averaging over several pulses taken on appropriate areas of the sample. Absolute values of the electric field at 532 nm ($E(2\omega)$) were obtained by calibrating the system against a y-cut quartz wedge and relating both the second harmonic signals and incident energy to the d_{11} non-linear coefficient of quartz [8].

3. Results and Discussion

There was no detectable signal from regions of the substrates which were free of film, confirming that the organic layer was responsible for the second harmonic radiation observed from all of the

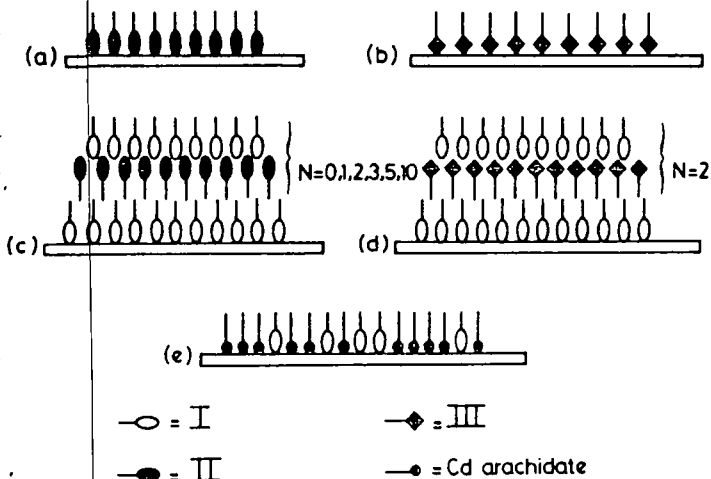


Figure 2 Schematic diagrams of sample configurations used in the experiments described in the text

LB film samples in this study. In addition, the radiation was clearly identified as second harmonic by its narrower bandwidth (using interference filters at 520 nm and 540 nm) and its narrow temporal profile. The second harmonic signals were normalised by dividing by the square of the incident laser energy. The notation employed when describing the signals can be exemplified as follows: $T^{s \rightarrow p} = |E^p(2\omega)|^2 / |E^s(\omega)|^4$ represents p-polarised signal intensity from s-polarised incident radiation in the transmission geometry; a corresponding notation is used for the other polarisations and geometry.

In all of the structures investigated, the $T^{p \rightarrow p}$ signals were approximately an order of magnitude greater than the $R^{p \rightarrow p}$ ones, which is consistent with the film being effectively isotropic within the plane. The much weaker signals obtained with s-polarized incident radiation provide further evidence for this deduction. The very small s-polarized second harmonic signals observed were indicative of the azimuth of the dye molecules relative to the substrate plane being averaged out within a second harmonic wavelength, resulting in negligible macroscopic anisotropy.

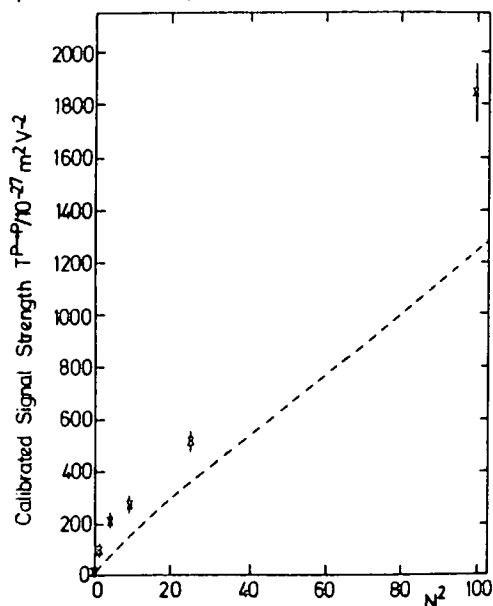


Figure 3 $T^{p \rightarrow p}$ second harmonic signal ($10^{-27} \text{ m}^2 \text{ V}^{-2}$) from structure shown in figure 2c plotted against the square of the number of bilayers. Dashed curve represents theoretical signal (see text)

In figure 3 the $T^{p \rightarrow p}$ signal observed from the various thickness regions of the structure shown in figure 2c is plotted against the square of the number of bilayers (N) of I and II deposited on a base layer of I. Also plotted on the same scale is a dashed curve which represents the theoretical response if the two dyes were to behave totally independently. This curve was calculated by summing the contributions from two hypothetical structures: one consisting of $N+1$ layers of I ($\beta=120 \times 10^{-30} \text{ C}^3 \text{ m}^3 \text{ J}^{-2}$ [5]), and the other consisting of N layers of II ($\beta=22 \times 10^{-50} \text{ C}^3 \text{ m}^3 \text{ J}^{-2}$ [5]), both alternated with an inert spacer material; the expected signal from each of these "substructures"

was calculated by multiplying the measured signal from a monolayer (figures 2a and 2c, $N=0$) by the square of the number of dye layers in the substructure. The theoretical curve assumes a perfect behaviour on increasing thickness, something which is rarely achieved in practice [3,4]. The measured second harmonic signals are clearly larger than even this ideal model would predict, which implies that there is some cooperative phenomenon occurring which renders the bilayer a much superior second harmonic material than would be predicted by the simple addition of the second order hyperpolarizabilities of the separate layers. The behaviour of a bilayer as a discrete unit is perhaps to be expected, since the chromophores within a bilayer are in close proximity and are therefore likely to interact strongly, whereas the active groups in the separate bilayers and in the initial hemicyanine monolayer are separated by "passive" alkyl chains. In addition, this strong interaction is also likely to result in some changes in packing.

Sample	$T^{p \rightarrow p}$	$R^{p \rightarrow p}$	$T^{s \rightarrow p}$	$R^{s \rightarrow p}$
2a	0.69 ± 0.05	0.07 ± 0.02	0.08 ± 0.02	0.08 ± 0.02
2b	0.42 ± 0.03	0.015 ± 0.01	0.11 ± 0.01	0.05 ± 0.01
2c (N=2)	209 ± 14	14.1 ± 0.8	7.7 ± 0.5	7.2 ± 0.6
2d	173 ± 11	8.2 ± 0.7	7.6 ± 0.8	5.9 ± 0.5

Table 2 : Calibrated signal strengths ($10^{-27} \text{ m}^2 \text{ V}^{-2}$) obtained for monolayers of II and III and for alternate multilayer structures containing three layers of I and two of II or III (see figure 2).

A summary of the second harmonic signals from monolayers of II and III and from alternate layer structures containing two layers of II or III alternated with three layers of hemicyanine (I) is given in table 2. From this comparison it is clear that the attempt to enhance the non-linear properties of the nitrostilbene by removing the carbonyl portion of the amide donor group in II has failed. In fact dyes II and III show very similar second harmonic generation efficiencies, with II being perhaps the slightly superior, possibly due to the better film quality (as revealed by reflection high energy electron diffraction studies).

Some typical results from the investigation of second harmonic generation from mixed monolayers of hemicyanine and cadmium arachidate are presented in figure 4. The fractional film area constituted by hemicyanine was calculated from the mole fraction of hemicyanine present in the spreading solution and assuming that a hemicyanine molecule occupies a surface area of approximately 0.35 nm^2 and an ionized arachidic acid molecule an area of 0.20 nm^2 (values measured from surface pressure-area isotherms of the materials) at the deposition surface pressure of 30 mN m^{-1} . It is very interesting to note that the $T^{p \rightarrow p}$ second harmonic signal is a factor of four times greater for a mixture containing equimolar quantities of hemicyanine and arachidic acid than for a pure hemicyanine monolayer. All of the other possible combinations of polarisation and detection geometry gave signals which were also a maximum (out of the

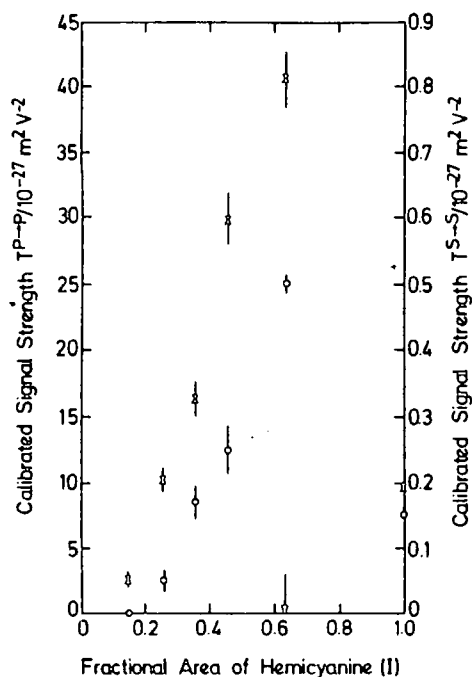


Figure 4 $T^{P+P}(x)$ and $T^{S+S}(o)$ second harmonic signal ($10^{-27} \text{ m}^2 \text{ V}^{-2}$) from mixed monolayers of I and cadmium arachidate (figure 2e) plotted against fraction of film area constituted by I (arrow indicates fractional area corresponding to an equimolar mixture).

range of concentrations studied) for the equimolar mixture, although the ratio of these signals to that for the pure hemicyanine were not always as great as with the T^{P+P} signal. This enhancement can be accounted for by two possible mechanisms: (i) a change in packing of the active hemicyanine dye, resulting in a better alignment relative to the electric fields of the incident and second harmonic light; or (ii) the local optical fields experienced by the active dye are enhanced by the decreased shielding provided by the more distant neighbouring dye moieties. Since enhancement with dilution is observed for all geometries and polarisations the second mechanism is perhaps favoured. Nevertheless, because this enhancement is not perfectly uniform for all geometries and polarizations, the first mechanism almost certainly makes some contribution. These findings may have important implications for improving the efficiencies of any non-linear optical device which utilises LB films. Further investigation of this phenomenon is currently underway.

4. Conclusions

In this paper we have discussed the possible application of LB film technology in the field of non-linear optics. Second harmonic generation from monolayer and alternating multilayer LB film structures has been employed to characterize a number of materials which may be suitable for device fabrication.

Alternating donor-acceptor : Inverted donor-acceptor dye assemblies have been shown to possess a greater optical non-linearity than that expected by simply adding the non-linearities of

the individual dye layers. An attempt to improve the contribution made by one of the components by increasing its donor capacity was unsuccessful, possibly due to poorer film quality in the modified material.

A study was made of the effect on second harmonic generation intensity from a monolayer of an active dye material of diluting the dye with a passive fatty acid. It was found that an equimolar mixture of dye and acid led to enhancement of the second harmonic signal for all combinations of incident and signal polarisations, and for both transmission and reflection detection geometries. In the case of p-polarised incident and signal radiation in transmission, this enhancement over the pure dye monolayer was by better than a factor of four. The origin of this phenomenon is probably in the local fields experienced by the dye molecules, although some change in molecular orientation may also be a contributory factor.

Acknowledgements

One of us (DBN) wishes to thank the SERC and Plessey Research Ltd. for the provision of a studentship. The work was funded under a Joint Opto-Electronics Research Scheme (JOERS) programme.

References

- [1] Williams, D. J., "Organic polymeric and non-polymeric materials with large optical non-linearities", *Angew. Chem. Int. Ed. Engl.*, **23**, pp. 690-703 (1984).
- [2] Roberts, G. G., "Langmuir-Blodgett films", *Contemp. Phys.*, **23**, pp. 109-128 (1984).
- [3] Girling, I. R., Kolinsky, P. V., Cade, N. A., Earls, J. D. and Peterson, I. R., "Second harmonic generation from alternating Langmuir-Blodgett films", *Opt. Commun.*, **55**, pp. 289-292 (1985).
- [4] Girling, I. R., Cade, N. A., Kolinsky, P. V., Earls, J. D., Cross, G. H. and Peterson, I. R., "Observation of second harmonic generation from Langmuir-Blodgett multilayers of a hemicyanine dye", *Thin Solid Films*, in press.
- [5] Neal, D. B., Petty, M. C., Roberts, G. G., Ahmad, M. M., Feast, W. J., Girling, I. R., Cade, N. A., Kolinsky, P. V. and Peterson, I. R., "Second harmonic generation from LB superlattices containing two active components", *Electronics Letters*, **22** (9), pp. 460-462 (1986).
- [6] Ahmad, M. M., Feast, W. J., Neal, D. B., Petty, M. C. and Roberts, G. G., "4-N-heptadecylamido-4'-nitrostilbene, a new LB film material for non-linear optics", *J. Molec. Elec.*, in press.
- [7] Holcroft, B., Petty, M. C., Roberts, G. G. and Russell, G. J., "A Langmuir trough for the production of organic superlattices", *Thin Solid Films*, in press.
- [8] Presley, R. J. (ed.), "Handbook of lasers", Chemical Rubber Co., Cleveland Ohio, p. 493 (1971).

